UNIVERSIDADE DE SÃO PAULO
Escola de Engenharia de São Carlos

Risk-based optimization of reinforced concrete frames under progressive collapse

Otimização baseada em riscos de pórticos de concreto armado sob colapso progressivo

Lucas da Rosa Ribeiro

Tese de Doutorado do Programa de Pós-Graduação em Engenharia Civil (Engenharia de Estruturas) da Escola de Engenharia de São Carlos, Universidade de São Paulo.

EESC · USP

UNIVERSITY OF SÃO PAULO
SÃO CARLOS SCHOOL OF ENGINEERING
STRUCTURAL ENGINEERING DEPARTMENT

Lucas da Rosa Ribeiro

Risk-based optimization of reinforced concrete frames under progressive collapse

Otimização baseada em riscos de pórticos de concreto armado sob colapso progressivo

São Carlos
2024

Lucas da Rosa Ribeiro

Risk-based optimization of reinforced concrete frames under progressive collapse

Otimização baseada em riscos de pórticos de concreto armado sob colapso progressivo

Corrected version

The original version can be found at Escola de Engenharia de São Carlos

Ph. D. Thesis presented to the Department of Structural Engineering of São Carlos School of Engineering, University of São Paulo, Brazil, to obtain the title of Doctor in Civil Engineering (Structures).

Advisor: Prof. Dr. André Teófilo Beck

São Carlos

2024

Ficha catalográfica elaborada pela Biblioteca Prof. Dr. Sérgio Rodrigues Fontes da EESC/USP com os dados inseridos pelo(a) autor(a).

Ribeiro, Lucas da Rosa
R484r Risk-based optimization of reinforced concrete frames under progressive collapse / Lucas da Rosa Ribeiro; orientador André Teófilo Beck. São Carlos, 2024.

Tese (Doutorado) - Programa de Pós-Graduação em Engenharia Civil (Engenharia de Estruturas) e Área de Concentração em Estruturas -- Escola de Engenharia de São Carlos da Universidade de São Paulo, 2024.

1. frames. 2. progressive collapse. 3. reinforced concrete. 4. risks. 5. structural optimization. 6. uncertainties. I. Título.

Eduardo Graziosi Silva - CRB - 8/8907

FOLHA DE JULGAMENTO

Candidato: Engenheiro **LUCAS DA ROSA RIBEIRO.**

Título da tese: "Otimização baseada em riscos de pórticos de concreto armado sob colapso progressivo.".

Data da defesa: 25/09/2024.

Comissão Julgadora	**Resultado**
Prof. Associado André Teófilo Beck (Orientador) (Escola de Engenharia de São Carlos/EESC-USP)	APROVADO
Prof. Dr. Daniel Carlos Taissum Cardoso (Pontifícia Universidade Católica do Rio de Janeiro/PUC-RIO)	APROVADO
Prof. Guilherme Sales Soares de Azevedo Melo (Universidade de Brasilia/UnB)	APROVADO
Prof. Dr. Gustavo Henrique Siqueira (Universidade Estadual de Campinas/UNICAMP)	APROVADO
Prof. Dr. Wellison José de Santana Gomes (Universidade Federal de Santa Catarina/UFSC)	APROVADO

Coordenador do Programa de Pós-Graduação em Engenharia Civil (Engenharia de Estruturas):
Prof Associado **Ricardo Carrazedo**

Presidente da Comissão de Pós-Graduação:
Prof. Titular **Carlos De Marqui Junior**

“Who would Sisyphus be without the boulder?” (own authorship).

ACKNOWLEDGEMENTS

I thank God, whatever or whoever He may be. His presence has been a constant companion throughout this journey—replenishing my strength when defeat seemed inevitable and filling me with profound gratitude during those rare moments when everything flowed seamlessly. As above, so below, His guidance has been the quiet force behind every step.

To my beloved Pâmela (Pitchulinha ☺), whom God put in my life just as I embarked on this journey—starting as a cherry on top and becoming my greatest source of resilience and strength. Her courage inspired me to dig deeper, and her love motivated me to strive for my best, continually earning the life we share. She is the main reason I resisted the urge to abandon everything and wander the world as a hobo during my toughest moments.

To my parents, who not only provided me with education, affection, and discipline but also taught me the strength of character to endure life's trials, each one in their own way. Through their unwavering example, they showed me how to persevere in the face of adversity and to always choose the path of integrity, no matter how painful it might be.

I am deeply grateful to my advisor, André Beck, whose patience and guidance have been invaluable. He gave me the freedom to explore the paths I found intriguing, gently steering me back when needed but always allowing me to follow my instincts. His prompt assistance, warmth, and boundless energy have been a source of constant encouragement. His exceptional competence and remarkable ability to link a multitude of different topics have broadened my understanding and appreciation for the complexity of our field. With a vast reservoir of knowledge, he has been not just a mentor in research, but a permanent reminder to embrace life fully, making every moment count.

To my abroad advisor during my time in Naples, Fulvio Parisi, whose enormous patience and kindness have left a lasting impression. He always granted me the freedom to explore my ideas and allowed me the time I needed to delve into them. Even though my overseas period ended two years ago, he continues to support me with unwavering dedication. His warmth and reassurance were a steady anchor when all felt lost. Despite his youth, Fulvio's patience and competence are remarkable, and I am deeply grateful for his guidance.

To my closest friends during this research journey: Felipe Johanns, Danilo Pereira, Matheus Rocha, and Lucas Araújo. Each one stood by me, in their own unique way, during my darkest moments, pushing me back to all out life after periods suspended in dusk. With teary eyes I dedicate a special thanks to Danilo, for reigniting my faith and showing me a way out of the nihilism I once felt.

To Isabela Durci and Henrique Kroetz, whom continuously inspired me and even taught me key techniques that saved my research. Isabela, who is a fellow PhD candidate friend pushing over a similar boulder uphill, is a source of determination that always renovates my will to keep moving. Henrique was my sole source of inspiration when I first began this journey. It always intrigued me how could a PhD candidate be so capable, sure of himself, and full of positive attitude. Seeing him stirred me to think that "maybe I can too".

A warm acknowledgement to the Murillo family—Alex, Rejane, Matheus, and Gabriel—for their kindness, warmth, laughter and all the wisdom they've shared. Special thanks to Alex, whose encouragement was a key factor in my decision to come to São Carlos. To Ricardo as well. Our paths have diverged, but valuable lessons are not forgotten.

I gratefully acknowledge the financial support provided by Fundação de Amparo à Pesquisa do Estado de São Paulo (FAPESP) under grant n. 2019/23531-8 and grant n. 2021/12884-7 (BEPE). This research would not have been possible without their generous funding and commitment to advancing scientific knowledge. I am deeply thankful for their invaluable contribution to my academic journey.

ABSTRACT

RIBEIRO, L. R. **Risk-based optimization of reinforced concrete frames under progressive collapse**. 2024. Thesis (PhD in Civil Engineering – Structures) – School of Engineering of São Carlos, University of São Paulo, São Carlos, Brazil, 2024.

Structural design has traditionally focused on individual elements, using calibrated safety factors to meet target reliability against conventional demands. However, this method often overlooks overall robustness. Recent incidents of partial and total progressive collapses have encouraged designers to adopt a more systemic approach, such as discretionary element removal to evaluate structural robustness. Although research on this topic has advanced significantly in the last decades, a gap exists between deterministic studies on realistic progressive collapse behavior and structural optimization studies that addresses uncertainties, risks, and systemic behavior. Hence, this thesis aims to bridge this gap by employing a risk-based optimization framework to examine the cost-effectiveness of strengthening reinforced concrete framed buildings against progressive collapse, balancing safety and economy while considering realistic collapse features. Cost-effective mitigation strategies for progressive collapse in reinforced concrete frames are shown to depend significantly on threat probabilities and the balance between beam and column flexural capacities. When column cross-sections are squared, enhancing beam moment of inertia to activate Compressive Arch Action proves more cost-effective than increasing column flexural strength to allow Catenary Action, regardless of the frame's aspect ratio. Conversely, frames with beams of lower moment of inertia (squared cross-sections) can be cost-effective for the Alternative Path Method if columns possess high flexural capacity to support the increased bending moments induced by Catenary Action. Furthermore, the primary design for abnormal lateral loading events, such as tornadoes and earthquakes, typically follows a strong-column, weak-beam approach, as evidenced in recent studies. It is highlighted the novel potential for achieving optimal, cost-effective configurations that are resilient to both progressive collapse and abnormal lateral loadings over the lifespan. Thus, designs with weak beams and adequately strong adjacent columns may serve as multi-hazard solutions. While squared columns may not be the most economical option for column-loss scenarios, they could be optimal if additional hazards, such as earthquakes or tornadoes, are considered—a topic that warrants further investigation.

Keywords: frames; progressive collapse; reinforced concrete; risks; structural optimization; uncertainties.

RESUMO

RIBEIRO, L. R. **Otimização baseada em riscos de pórticos de concreto armado sob colapso progressivo**. 2024. Tese (Doutorado em Engenharia Civil – Estruturas) – Escola de Engenharia de São Carlos, Universidade de São Paulo, São Carlos 2024.

O projeto estrutural tem tradicionalmente se concentrado em elementos individuais, utilizando fatores de segurança calibrados para atender à meta de confiabilidade em relação às demandas convencionais. No entanto, esse método muitas vezes negligencia a robustez geral da estrutura. Incidentes recentes de colapsos progressivos parciais e totais incentivaram os projetistas a adotar uma abordagem mais sistêmica, como a remoção controlada de elementos para avaliar a robustez estrutural. Embora a pesquisa sobre esse tema tenha avançado significativamente nas últimas décadas, ainda há uma lacuna entre os estudos determinísticos sobre o comportamento realista do colapso progressivo e os estudos de otimização estrutural que abordam incertezas, riscos e comportamento sistêmico. Assim, esta tese visa preencher essa lacuna, empregando uma metodologia de otimização baseada em risco para examinar a relação custo-benefício do reforço de edifícios aporticados em concreto armado contra o colapso progressivo, equilibrando segurança e economia ao mesmo tempo em que considera características realistas do colapso. Estratégias de mitigação custo-efetivas para colapso progressivo em estruturas de concreto armado dependem significativamente das probabilidades de ameaça e do equilíbrio entre as capacidades de flexão de vigas e pilares. Quando as seções transversais dos pilares são quadradas, aumentar o momento de inércia das vigas para ativar a Ação de Arco Comprimido se mostra mais econômico do que aumentar a resistência à flexão dos pilares para suportar a Ação Catenária, independentemente da relação de aspecto da estrutura. Por outro lado, estruturas com vigas de menor momento de inércia (seções quadradas) pode ser custo-efetivas pelo Método de Caminho Alternativo se os pilares tiverem alta capacidade de flexão para suportar os momentos fletores aumentados induzidos pela Ação de Catenária. Além disso, o projeto para eventos de carregamento lateral extremo, como tornados e terremotos, tipicamente segue uma abordagem de pilares fortes e vigas fracas. Destaca-se o potencial inédito para alcançar configurações otimizadas e econômicas que sejam resilientes tanto ao colapso progressivo quanto a carregamentos laterais anômalos ao longo da vida útil. Assim, projetos com vigas fracas e pilares adjacentes adequadamente fortes podem servir como soluções para múltiplos tipos de risco. Embora pilares quadrados possam não ser a opção mais econômica para cenários de perda de pilar, eles podem ser ideais se ameaças adicionais, como terremotos ou tornados, forem consideradas — um tópico que merece futuras investigações.

Palavras-chave: colapso progressivo; concreto armado; incertezas; otimização estrutural; pórticos; riscos.

SUMMARY

1 INTRODUCTION’

Structural design is typically done element by element, using calibrated partial safety factors to achieve a target reliability against expected conventional demands. Hence, overall robustness is not objectively addressed in this usual framework. Recent occurrences of partial and total progressive collapses have prompted designers to consider systemic behavior more objectively, e.g. addressing discretionary element removal to verify the structural robustness. System integrity depends on the capacity of its components to act together for ensuring overall resistance. Hence, a localized failure leads to a force redistribution to the remaining elements. If this force rearrangement is unsuccessful, the initial failure may propagate into progressive collapse (also referred to as disproportionate collapse).

1.1 OVERVIEW

Progressive collapse is a Low-Probability High-Consequence (LPHC) event that relates to a high level of uncertainty, justifying probabilistic analyses and risk assessments to address it. From a mathematical standpoint, great progress can be observed in structural optimization under uncertainties, but not so much in terms of systemic behavior under abnormal loadings. There is a gap between deterministic studies on realistic progressive collapse behavior, and structural optimization studies addressing uncertainties and systemic behavior.

Numerous studies in the literature investigate progressive collapse, particularly its numerical modeling (Adam et al., 2018). However, not so many studies consider uncertainties when investigating this phenomenon, e.g. Hartmann et al. (2008); Arshian et al. (2015); Arshian and Morgenthal (2015); Brunesi et al. (2015); Brunesi and Parisi (2017); Felipe et al. (2018); Felipe et al. (2019); Parisi et al. (2019); Scalvenzi et al. (2023). Similarly, few works on structural optimization under uncertainties address progressive collapse, e.g., Beyer and Sendhoff (2007); Schuëller and Jensen (2009); Aoues and Chateauneuf (2010); Lopez and Beck (2012); Beck et al. (2018); Luiz (2020). In terms of failure consequences (or risks), investigations addressing the optimal compromise between safety and economy for systems prone to progressive collapse are very recent, e.g. Beck et al. (2020); Beck et al. (2022); Praxedes and Yuan (2022); da Silva et al. (2023); Beck and Stewart (2023); Ribeiro et al. (2024); da Silva et al. (2024). It is evident that risk-based optimization of structures prone to progressive collapse is a broad open field of research, especially in terms of realistic progressive collapse simulation.

This research seeks to bridge this gap by using a risk-based optimization framework to investigate the cost-effectiveness of strengthening reinforced concrete framed buildings against progressive collapse, regarding the compromise between safety and economy (Figure 1.1). In this proposed framework, progressive collapse is realistically addressed in structural analysis stage, so that reliability and risk-based stages take into account the ultimate plastic reserve of the structure. Yet, this work is inherently conceptual, albeit utilizing advanced nonlinear numerical models. The study focuses on reinforced concrete framed buildings, but overall findings are also relevant for other structural alternatives and overall civil infrastructure.

Figure 1.1 – Brief framework depiction.

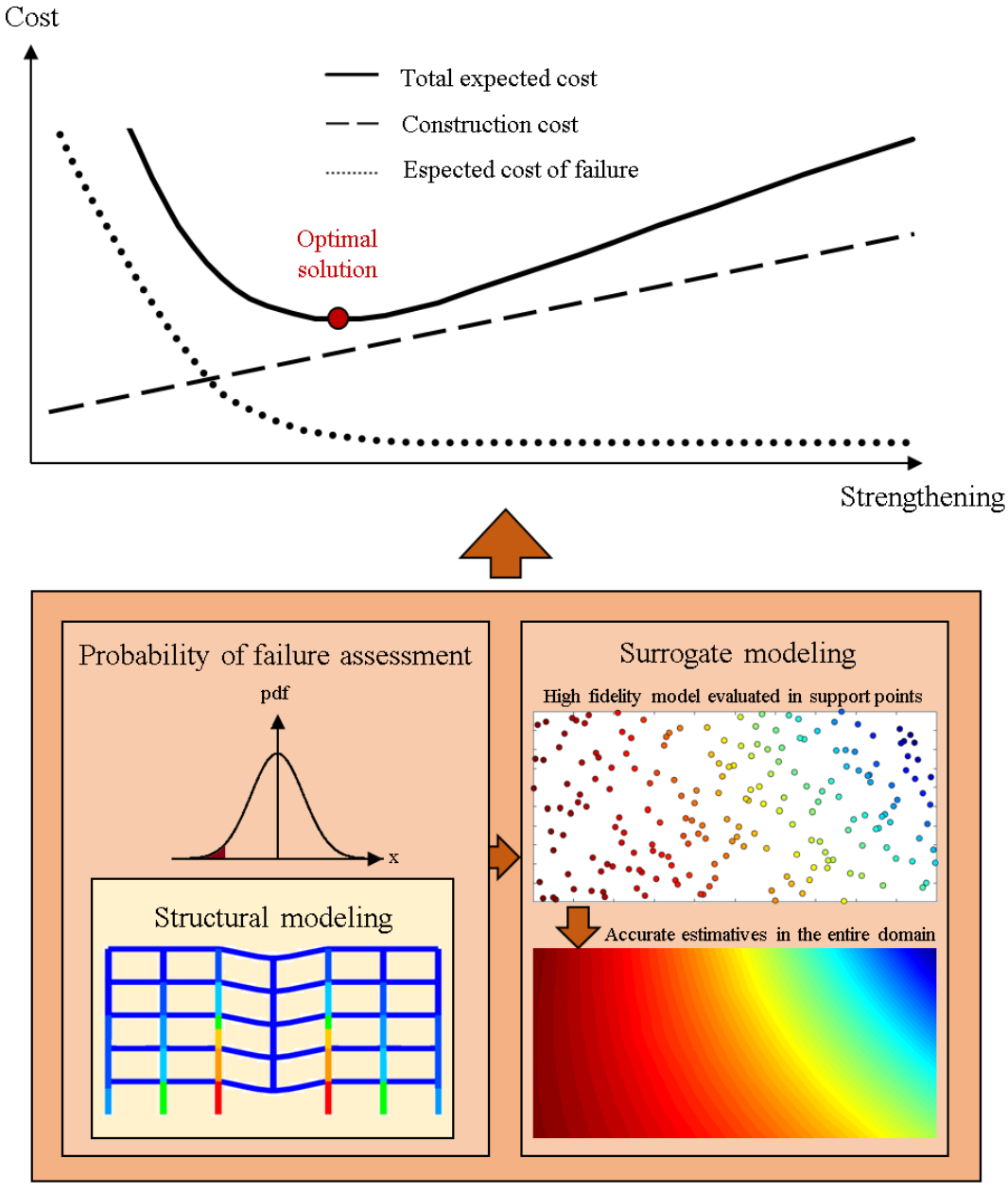

Source: own authorship.

As shown in Figure 1.1, advanced numerical tools for structural analysis, probabilistic approaches, risk-based optimization techniques, and metamodeling alternatives are integrated to comprehend how the optimal design of reinforced concrete frames behaves under progressive collapse threats. Reliability assessment is done in terms of nonlinear finite element analysis to address a realistic structural behavior, with surrogate modeling being used to attenuate the high computational cost in both stages.

Following Beck et al. (2020), the total expected cost C_{TE} for a given strengthening level can be generally addressed in terms of manufacturing cost C_M and expected cost of failure C_{EF}:

$$C_{TE}(\boldsymbol{d}) = C_M(\boldsymbol{d}) + \sum_{i=1}^{NIF} C_{ef,i}(\boldsymbol{X}, \boldsymbol{d}) + \sum_{j=1}^{NLDF} C_{ef,kj}(\boldsymbol{X}, \boldsymbol{d}, P_{LD}) \tag{1.1}$$

where *NIF* and *NLDF* represent the number of failure modes for intact structure and local damage scenario, respectively; $\boldsymbol{X}$ relates to the random variable vector; $\boldsymbol{d}$ corresponds to the design variable vector; and P_{LD} is the local damage probability.

1.2 OBJECTIVES

The objective of this work is to understand how the simultaneous consideration of progressive collapse and uncertainties influences the optimal risk-based design of reinforced concrete framed structures. Additionally, the following specific objectives are defined:

(a) Development and application of numerical tools for simulating progressive collapse in 2-dimensional framed structures, including physical and geometrical nonlinearities;
(b) Conceptual development of a framework and specific formulations for addressing optimal risk-based structural design, considering systemic behavior, progressive collapse, and uncertainties;
(c) Investigation of various cases of reinforced concrete frames prone to progressive collapse, addressing alternatives for robustness enhancement, different scenarios of triggering event, and distinct threat probabilities;
(d) Comparison of optimal designs with current guideline standards;
(e) Investigation on how resources are optimally allocated within the reinforced concrete frame to mitigate progressive collapse occurrences.

1.3 CONTRIBUTIONS AND SIGNIFICANCE OF THE STUDY

Although the literature contains several works on the aforementioned topics, only a few recent studies consider them simultaneously. Yet, they are mostly related to conceptual and simplified structures in order to provide an (essential) initial basis on how optimal risk-based design behaves when progressive collapse is addressed.

In terms of reinforced concrete (RC) frames, numerical progressive collapse investigations usually address structural robustness in terms of the ultimate capacity of the beam spans directly above a lost column. Remaining adjacent columns are usually designed to withstand expected axial loads and to provide enough lateral restraint for the beams. Hence, ultimate structural resistance against progressive collapse is typically related to the ultimate capacity of the beam spans directly above a suddenly lost column.

In terms of optimal risk-based design and realistic nonlinear structural modeling, this work reveals non-obvious compromises between beam and column capacities for progressive collapse mitigation. Thus, all optimal design solutions have enough safety margins against all addressed failure modes, and also are shown to be in accordance with current code provisions, evidencing reasonable, realistic, and feasible results.

Overall findings in this thesis comprise some of the initial contributions aimed to fill the previously mentioned knowledge gap between realistic progressive collapse behavior and risk-based optimization.

1.4 LIMITATIONS

This study provides valuable insights into the risk-based optimization of progressive collapse mitigation in reinforced concrete frames. However, several limitations must be acknowledged, primarily related to simplifications made for computational feasibility and focus on the main resisting mechanisms and failure modes. Yet, these limitations offer opportunities for future research, where more complex scenarios and phenomena could be considered to enhance the understanding and practical applications of the results. The limitations include:

(a) Only planar reinforced concrete frames are investigated, excluding the influence of walls, slabs, secondary beams, and other 3-dimensional features;
(b) Soil-structure interaction is neglected, so columns are assumed fully restrained at ground floor;

(c) The study disregards column shear forces, addressing column failure just in terms of axial vs bending demands for the sake of simplification;
(d) The risk-based optimization process does not rely on target reliability indexes; instead, the algorithm determines optimal reliability values for each failure mode depending on the severity of their consequences;
(e) Localized phenomena such as rebar debonding, cracking patterns, and member separation are disregarded in the structural models due to the need for computational efficiency for large samples;
(f) Localized failure mechanisms at the beam-column joints are not addressed;
(g) Axial forces are not considered when addressing shear capacity;
(h) Surrogate techniques are employed for structural modeling and reliability analysis to manage computational costs;
(i) The developed framework has several stages in series, inevitably leading to an accumulating amount of errors; yet, they are reduced as much as possible until accurate enough predictions are obtained for the purposes of this research;
(j) Only gravitational loads are considered, focusing on progressive collapse due to amplified vertical loads, while lateral loads and other hazards are not addressed;
(k) The analysis considers local damage due to the sudden loss of a single ground-floor column, without exploring more complex failure scenarios;
(l) Total expected costs focus solely on construction and expected failure costs, disregarding additional life-cycle costs e.g. maintenance, operation, and disposal;
(m) Only progressive collapse related to a lack of redistribution capacity after local damage is considered, excluding other collapse mechanisms e.g. impact and loss of stability;
(n) Mitigation techniques are limited to reinforcing beams and columns to ensure activation of intrinsic resisting mechanisms, without exploring alternative approaches such as those in Section 2.5;
(o) Hazards that induce abnormal lateral loadings are not addressed;
(p) Column failure is defined by comparing axial force vs bending moment demands with the resisting envelope, without considering post-yielding or buckling behavior in the structural modeling.

1.5 ORGANIZATION OF THE THESIS

Chapter 1 (Introduction) aims to present the work developed, contextualize the topic, list the objectives of the research, as well as identify the motivations for carrying it out.

Chapter 2 (Progressive collapse) explores mechanisms, causes, probabilistic approaches, and mitigation strategies of progressive collapse, emphasizing structural robustness via Alternative Load Paths and enhancement of the intrinsic resisting mechanisms.

Chapter 3 (Proposed framework) presents a comprehensive framework used for risk-based optimization of reinforced concrete structures under progressive collapse, integrating risk optimization, reliability analysis via simulation, nonlinear structural modeling via finite element method, and surrogate techniques for reducing the computational cost.

Chapter 4 (Results) presents the results of the risk-based optimization framework applied to usual 2-dimensional reinforced concrete structures, highlighting the trade-offs between safety and economy in progressive collapse mitigation.

2 PROGRESSIVE COLLAPSE

Progressive collapse is a chain reaction mechanism characterized by a significant disproportion between the area affected by an initial failure and the total area affected by its propagation (Parisi and Augenti, 2012). A local failure initiates the collapse of nearby elements, which progressively triggers further failures, culminating in a large-scale, global collapse (Allen and Schriever, 1972). Thus, loss of load-bearing capacity in a small part of the structure due to abnormal loads can trigger a domino effect of subsequent failures able to affect a disproportionately larger portion of the structure (Gross and Mcguire, 1983).

2.1 HISTORICAL CONTEXT

Safety against progressive collapse was highlighted after the partial collapse of the 22-story Ronan Point Apartment Tower, in London, 1968. A gas explosion in a kitchen of the 18th floor dislodged a facade panel that supported the slab above. The lack of support and reinforcement continuity between structural elements led to the upward collapse from the 19th floor up to the roof, and their impact caused the floors below to collapse from the 18th floor down to the ground floor (Griffiths et al., 1968).

Prefabricated RC panels built with the Larsen-Nielsen system formed the Ronan Point structure. Each floor slab was connected to load-bearing walls through dowel bars filled with dry mortar. Although this system reduced manufacturing costs, it compromised structural continuity and the ability of force redistribution. In addition, existing building codes were found to be inadequate for ensuring safety and integrity for high-rise precast concrete apartment buildings (Pearson and Delatte, 2005). Better ties between panels started to be proposed for progressive collapse prevention due to new requirements in the fifth amendment of the UK building regulations (Hendry, 1979; Elkady et al. 2024).

Worldwide concern increased at each new occurrence of progressive collapse, particularly those with greater number of victims and/or caused by malicious intents. For instance, in April 1995, a truck bomb detonation near the Alfred P. Murrah Federal Building in Oklahoma, USA, resulted in 168 deaths and in the partial collapse of the structure (FEMA 277, 1996). The facade facing the explosion had a transfer girder beam supported by four columns, with three of them collapsing in the detonation. This triggered a collapse propagation that ended damaging a third of the building. As the building integrity strongly relied on the transfer girder, this collapse event highlighted the need for Alternative Load Paths (ALPs).

The Sampoong Department Store collapse in Seoul, South Korea, 1995, caused over 500 deaths due to poor construction quality control, inappropriate design decisions, and lack of supervision. Neglected problems, such as reduced column cross-sections, reduced slab depth, concrete strength below specified, and increased dead load due to change in use of the 5th floor, contributed to the collapse (Gardner et al. 2002).

In June 1996, a detonation happened in front of the Khobar Towers residential complex, in Saudi Arabia. The most damaged building had 8 stories and was constructed using prefabricated reinforced concrete walls and slabs. Connections between slabs and walls followed progressive collapse prevention requirements from the British standard CP 110-1 (1972). Hence, collapse did not propagate much beyond the initial damage, being contained to the targeted facade and part of the internal walls and slabs (NISTIR 7396, 2017).

The collapse of the World Trade Center (WTC) Twin Towers in Manhattan NY, USA, 2001, resulted in almost 3000 deaths, several injured and many with long-term health aftereffects (9/11 Memorial & Museum, 2006; Alper et al. 2017). According to NIST (2005) final report, the collapse of both towers was triggered by a multi-floor fire caused by impact of highjacked aircrafts. Despite the towers being hit at high speed and key structural components being lost, such as core columns, perimeter columns, and floors, the towers initially withstood the impacts due to the robust perimeter frame-tube system and the buildings' large size. However, overall loss of fireproofing insulation followed by multi-floor fires led to a mix of impact damage and heat-weakened structural components causing the final abrupt collapse (NIST, 2005). As the fires progressed, sagging floors pulled the perimeter columns inward, and their viscoplastic buckling ultimately led to loss of their load-carrying capacity. This resulted in the entire upper section to fall on the floors below, triggering a cascading effect of falling floors all the way down (Bažant et al. 2009). This multi-hazard collapse (collision, explosion and fire) highlighted the dependency between distinct threats, justifying cost-effective solutions to simultaneously ensure safety against multiple hazards (Mattos, 2024; Carneiro, 2024).

In view of the above, there has been a significant increase in progressive collapse related studies over the past decades (Elkady et al. 2024). Until 2001, most studies on this topic were conducted in USA and UK, largely motivated by the Alfred P. Murrah Federal Building (Oklahoma, 1995) and Ronan Point (London, 1968) collapses. The WTC attack boosted the worldwide concern for progressive collapse mitigation, causing a substantial increase in studies about it. Although USA and UK remain among the most active countries in this research field, Asia took the lead from 2009 onwards, with China currently being the most prominent country addressing this topic (Adam et al., 2018).

Progressive collapse is often triggered by abnormal loads, resulting from threats like fires, natural disasters, human error, accidental impact and terrorist attacks. Hence, progressive collapse is a Low Probability-High Consequence (LPHC) event. These hazards introduce enhanced dynamic loads due to a sudden initial local damage, which can severely compromise structural integrity and force redistribution capacity (Starossek, 2010). Thus, construction, material, and design flaws are contributing factors for collapse propagation (Byfield et al. 2014). For instance, corrosion can lead to component overloading, causing the premature collapse of nearby elements (Lu et al. 2021). Caredda et al. (2023) demonstrated that design and construction errors contributed to 48% and 29% of the forty collapse cases studied by these authors, respectively. Hence, preventing progressive collapse relies on the strength of individual members and on the overall interaction capacity between structural elements, with redundancy and ductility enhancing progressive collapse resistance (Li et al. 2014).

2.2 TYPES OF PROGRESSIVE COLLAPSE

Starossek (2007) classifies progressive collapse into six categories regarding the structural response after an initial failure: pancake, zipper, domino, section, instability and mixed. A broader classification is also proposed, grouping the original six categories into four classes regarding similarities in their causes and in collapse propagation: redistribution-type, impact-type, instability, and mixed-type collapses.

Redistribution-type collapses include zipper and section, occurring due to inefficient force redistribution. Zipper collapses are one of the most common types, occurring when ALPs fail to bridge over an initial damage in the structure. Hence, it relates to the system inadequate dynamic response to impulsive loadings caused by sudden failure, e.g. overload of adjacent beams and columns in a framed structure under column loss scenarios. Zipper collapse typically propagates transversally, e.g. lateral column failure propagation in frames and bridges; upward vertical propagation in case of beam failure over a lost column. Current building guidelines address ALPs enhancement as mitigation strategy for zipper-type progressive collapse.

Section collapse relates to an inadequate force redistribution capacity in cross-sectional level, typically happening as a quick fracture instead of a progressive fashion. Hence, Section-type is appropriate to address individual members, such as cables and membranes. Starossek (2007) addressed section-type just to point out analogies between cross-section failure and system failure, with “cross section” relating to the overall structure, and “cross section part” to individual elements.

Impact type-collapses include pancake and domino, occurring due to potential energy being converted into kinetic energy as the structure falls down on itself. Falling parts abruptly impact the remaining structure, causing a significant dynamic overloading able to trigger new parts to fall and/or overturn. Pancake collapse relates to a downward collapse propagation due to member separation and vertical falling, being common in high-rise frame buildings. A notorious example is the ultimate collapse stage of the WTC Twin Towers, where the building section above the initial impacted area fell on the floor below as in a rigid body motion. The amplified dynamic impact forces were beyond the floor's ultimate capacity, so a cascading downward collapse was triggered all the way to the ground floor (La Malva et al, 2009; Kotsovinos and Usmani, 2013).

In Domino impact-type collapses, the conversion from potential to kinetic energy causes the overturning of the separated parts, causing them to fall with an angular rigid-body motion. Domino type is more common in bridge structures (Khoey et al. 2019). In framed structures, it may happen when an initial column loss leads to excessive horizontal forces in the beam spans above it, pulling the entire frame inwards and potentially overturning the adjacent elements. Although similar to Pancake collapses, collapse propagates in the overturning direction, as in a domino-effect. Besides, the impact forces that trigger failure in the next element act toward a direction other than the main forces originally transmitted by it. Unlike other types of collapse, progressive collapse-resistant design in terms of enhanced ALPs usually is not effective against impact-type collapses, as the energy of falling structural elements can be far beyond the structural capacity (Kiakojouri et al. 2022).

Instability collapses relate to failure in compressed stabilizing components, followed by a potentially abrupt failure in the destabilized components, and causing collapse propagation. In this type, potential energy converts into strain energy. For instance, failure in bracing components of pinned steel frames can trigger instability collapse, as they stabilize the structure against lateral loadings (Starosek, 2017). If a primary stabilizing component fails, it can cause an immediate collapse with severe disproportion between initial and final damaged areas. Therefore, the sudden collapse of the entire Block 7 of the 13-story Lotus Riverside residential building in Shangai, China, 2009, may be classified as an Instability collapse. An ongoing excavation was happening in one side of this building, and the excavated soil was being dumped at the other side of the building. The weight of the 10 m high stock-pilled soil, combined with an excavated area without lateral supports, caused the soft soil to move below the building and toward the excavation. This severely compromised the foundation piles, causing the immediate overturning of the entire building and one death (Wang et al. 2017).

Alternatively, instability collapse can progress consecutively through destabilized elements, as seen in propagating buckles of deep-water pipelines (Starosek, 2007). Thus, small perturbations in compressed members able to cause a disproportionate final damage strongly resembles the main definition of progressive collapse. Hence, progressive collapse can also be addressed as a type of instability. This is especially convenient when addressing it via nonlinear dynamic procedures, as the ultimate structural capacity corresponds to loss of dynamic stability (Ding et al. 2024).

Mixed-type collapses relate to features of two or more types being present, covering the majority of progressive collapse occurrences. The Alfred P. Murrah collapse, for example, happened with Pancake and Domino-like characteristics. Although Pancake collapse was the prevalent type, lateral forces may have developed in the transfer girder causing column overturn. In addition, the Sampoong Department Store collapse had characteristics of a Pancake and Zipper types. Failure began via column punching shear mechanism, inducing Zipper-type collapse as the structure failed to promote force redistribution. This ultimately triggered Pancake collapse due to loss of load-bearing capacity in the slabs (Elkady et al. 2024).

2.3 RESISTING MECHANISMS IN FRAMED STRUCTURES

When addressing RC framed structures, progressive collapse typically has features of Pancake-type, Zipper-type, and Domino-type, the latter being less common. As shown in Kiakojouri et al. (2022), mitigation techniques that are appropriate for one type of collapse may be ineffective against other collapse types, which is a main issue when addressing realistic Mixed-types. Nonetheless, resistant mechanisms thoroughly described in this Section relate to Redistribution-type Zipper collapses, following current guidelines for promoting progressive collapse capacity by means of enhancing the structure’s ALPs. Sudden loss of a supporting element initially mobilizes the structural capacity of force redistribution, so Zipper-type has a major relevance soon after the initial damage. Regarding RC frames, assuming ALPs able to efficiently bridge over a lost column imply in no further member separation, avoiding later stages of Impact-type collapse (as verified in the Sampoong Department Store collapse).

Alternative Path Method (APM) is a design framework for progressive collapse mitigation, in which ALPs are enhanced by increasing the structural robustness. Robustness refers to a structure's ability to withstand local failures caused by abnormal loadings without triggering collapse propagation and a disproportionately larger final damaged extension (CEN, 2006). Hence, it relates to the structural resistance against damage imposed by a given threat.

Although robustness relies on several system characteristics, such as overall strength, ductility, redundancy and continuity, it strongly depends on the type of abnormal loading. For instance, the WTC Twin Towers had enough robustness to withstand direct aircraft impacts that removed almost 60% of the perimeter columns of the walls they hit. However, they lacked robustness against the subsequent high temperatures and Impact-type collapse (Eagar and Musso, 2001). Hence, for the results shown in this thesis, robustness always relates to the sudden loss of a single column caused by an unspecified hazard (threat-independent approach), following the usual APM guideline framework.

There are other relevant properties that describe how a structure behaves after being struck by an abnormal loading. For instance, fragility relates to how prone to failure a structure is, in terms of probabilities, for a prescribed hazard intensity and damage state. This property is more commonly addressed in risk-analysis frameworks, especially for performance-based seismic analysis (Singhal e Kiremidjiian, 1998). However, recent studies address it for progressive collapse, aiming to quantify its probability and to allow its performance-based assessment (Brunesi et al. 2015; Parisi et al. 2019; Scalvenzi et al. 2023). Vulnerability also addresses how prone to failure a structure is relative to a prescribed hazard intensity and damage state, but in terms of loss/risk. Additionally, some critical infrastructure buildings may require resilience, i.e. capacity to withstand and recover its functionality after an extreme event. This encompasses the robustness property and adds a broader spectrum for progressive collapse mitigation. Nevertheless, only robustness is addressed in this thesis.

Several deterministic and reliability/risk-based methods have been proposed for quantifying robustness (Adam et al. 2018; Beck et al. 2023). In general, by addressing robustness R_X as the system insensitivity to small changes (Eq. 2.1), Brett and Lu (2013) show that robustness ranges from zero (infinite structural sensitivity S_X) to one (insensitive structure).

$$R_X = \frac{1}{1 + S_X} \tag{2.1}$$

Aiming to increase a RC frame robustness, ensuring load redistribution capacity via ALPs is an efficient approach to reduce the overall sensitivity to a column loss scenario. When an abnormal loading causes a sudden column removal in an RC frame, the ALPs rely on a series of resisting mechanisms whose activation depend on the capacity of the remaining beams and columns. Beam spans directly above the lost column are the most critical part in the remaining structure, especially in the floor immediately above the local damage. Hence, as shown in Figure 2.1, all resisting mechanisms can be directly associated to the frame's overall behavior.

Figure 2.1 – Progressive collapse resisting mechanisms for an inner column loss.

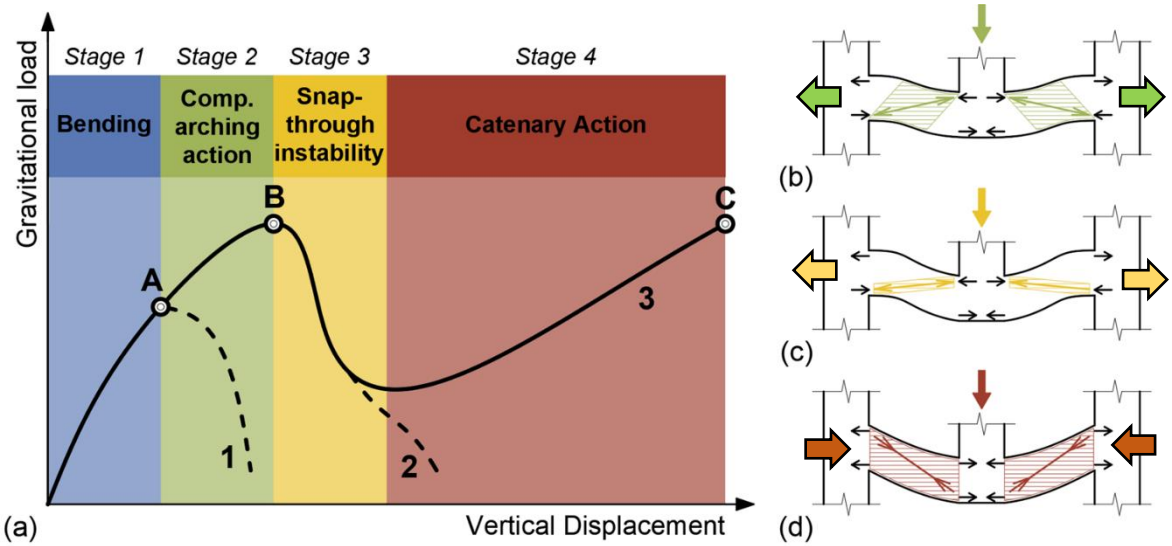

Source: Praxedes (2020).

The first mechanism corresponds to Bending or Flexural Action, being related to elastic behavior, beam cracking, and ultimately on the onset of cross-section plastification (point A in Figure 2.1a). Hence, beam behavior in this stage corresponds to what would be expected for a conventional scenario, with small displacements and all materials in their elastic phases. Small rotations are observed at beam ends fixed to adjacent columns, so axial forces are negligible in the beams. Since bending is mobilized right after the loss of a column, it is the first line of defense against the sudden transition in stress signs in the beam sections above the missing column. Originally, the cross-section top at beam ends is in tension while the bottom is in compression, but this flips when the column is removed. Flexural Action ends as the cross-section leaves the elastic behavior, with concrete reaching its peak strength and/or steel rebars starting to yield. The exact characteristics of the plastification onset relies on the rebar ratio: only rebar yielding occurs for under reinforced sections; concrete reaches its peak strength for over reinforced sections; and both happen in conventionally designed cross-sections.

If the adjacent columns fail to provide anchorage and lateral restraint to the beams, the peak of the force vs displacement curve in Figure 2.1a is Point A. In this case, Curve 1 represents a post-peak behavior clearly indicating a premature failure of the load redistribution via ALPs. From this point, all resisting mechanisms depicted in Figure 2.1 relate to loss of an inner column. Since further mechanisms rely on the available lateral restraint provided by adjacent supports, Figure 2.1 does not apply for scenarios of external column loss. Hence, loss of outer columns solely relies on Flexural Action and Vierendeel Action, which will be addressed later.

Greater rotations start to develop in the beam-column connections due to triggering of plastic stage, causing the beam ends to be pushed outwards as they rotate. If the adjacent columns provide anchorage and adequate horizontal confinement to the beams, this causes compressive axial forces to develop resembling an arch-shape in the critical double-span beam (Figure 2.1b). This additional resistance to the downward drift of the double-span beam characterizes Compressive Arch Action (CAA). As the beam ends are pushed outwards as they rotate, columns supporting the deflecting beams are pushed outwards in this mechanism. Flexural damage starts to propagate through the entire depth in beam end sections, and a relevant bending effort starts to propagate to the adjacent columns (Long et al. 2021). Thus, since the additional vertical resistance comes from beam ends being pushed outward, beams with greater depths have greater CAA capacity (Yu and Tan, 2013).

Load-bearing capacity reaches a peak during CAA due to advanced rebar yielding and concrete crushing at beam ends (Point B in Figure 2.1a), forming plastic hinges in these regions. The structure may not go further in case of insufficient horizontal restraint, anchorage failure, or rebar rupture, with Curve 2 in Figure 2.1a representing the final structural response in this case. However, if lateral restraint is still available, a snap-through instability occurs (Figure 2.1c), with its intensity relying on how strong the lateral confinement is. Stronger columns allow a well evidenced instability stage such as the one depicted in Figure 2.1a (Yu and Tan, 2013). However, this instability stage is much shorter for weaker columns, with the characteristic downhill slope of the snap-through instability being substituted by a brief plateau after CAA peak (Yi et al. 2007). Intermediate columns lead to intermediate instability behavior (Lew et al. 2014). This instability stage is not a proper resisting mechanism, but rather a transition stage between two effective mechanisms.

If the structure survived all the previous stages, beams enter the Catenary Action (CA) stage when their axial load turns to tension, with the double span beam vertical drift typically exceeding the beam section depth (Figure 2.1d). In this stage, the entire double-span beam is damaged and in tension, resulting in additional load capacity due to rebars being used up to their limit. Since it uses the final plastic reserve of the double-span beam, CA is one of the most investigated resisting mechanisms, as it is the last line of defense against redistribution-type collapse (Elkady et al. 2024). Just as CAA, CA relies on the lateral column confinement to be mobilized, but now they are pulled inwards due to beams being in tension. Yu and Tan (2013) show that a reduced beam depth enhances CA capacity and mobilize it earlier, although at the expense of reducing CAA capacity. Ultimate load-carrying capacity in CA is related to rebar rupture in the adjacent beam column joints, being indicated by Point C in Figure 2.1a.

If the vertical load related to Point C in Figure 2.1a is below Point B, then the frame never actually recovers from the instability stage. In this case, the frame ultimate capacity relates to the CAA peak capacity, and reaching Point C is as ineffective as the failure Curve 2. Hence, significantly strong lateral confinement may cause brittle rebar rupture before the beam being able to recover from the instability stage.

Yet, shear failure may also happen at any point of the described force vs displacement curve, causing a premature and brittle structural collapse in case of insufficient transversal reinforcement. Lateral confinement provided by columns adjacent to the lost one is not equivalent to the concrete confinement provided by proper stirrup detailing at cross-sectional level. In this text, the horizontal restraint provided by adjacent columns is mentioned as lateral, horizontal, or column confinement, whereas the cross-sectional feature is addressed as concrete, cross-section, or core confinement.

Rebar detailing significantly influences the mobilization of these resistance mechanisms. Afefy (2012) shows that beams with discontinuous lap spliced rebars reach their flexural capacity right after the column loss. Thus, it is shown that conventional design leads to lower Flexural capacity, highlighting the importance of APM design. Additionally, an increase in load capacity was noticed when beams had more column supports, vouching for redundancy effectiveness in providing ALPs.

Continuous reinforcement along all the spans of beams and columns is often impractical, so design strategies are essential to mitigate progressive collapse when using spliced rebars. Mechanical splices, such as couplers, provide direct load transfer and improve structural robustness compared to traditional lap splices. When lap splices are used, ensuring adequate lap lengths and enhancing transverse reinforcement at splice locations improves bond performance and reduces the propensity of brittle debonding failure. Additionally, splices should be strategically placed in lower-stress regions to avoid critical tension zones. However, in the examples presented in this thesis, perfect anchorage and continuous rebars are assumed for simplification. As shown in the structural analysis validation of Section 3.4.1, results with adequate accuracy are obtained with this approach given the purposes of this research.

Abdelwahed (2019) found that greater rebar reinforcement can increase ultimate load-bearing capacity up to 50%. Conversely, Long et al. (2021) observed that increased rebar reinforcement enhances and triggers CA earlier. Ren et al. (2016) added that over-reinforcement can accelerate bending failure and hasten the CA onset. Greater top reinforcement is preferable as it is shown to reduce both rotations and tensile forces, effectively increasing ultimate CA capacity (Yu and Tan, 2013b; Praxedes and Yuan, 2022)

Resistance mechanisms covered in Figure 2.1 occur in sequence. However, an additional mechanism not implicitly related to this sequence has major relevance: Vierendeel Action (VA). As vertical drifts increase due to column loss, VA develops particularly in the adjacent columns and upper beam spans. When mobilized, (ideally) rigid beam-column connections transfer axial and shear forces, as well as bending moments, across all members encompassed by the VA mechanism. Thus, each beam and column span within the VA system experience combined axial, shear and bending demands. Hence, increased axial forces in the first story (critical) double-span beam cause extra shear and bending demands in the adjacent columns, which are redistributed (mostly) to all beam and column spans up to the last floor.

To ensure equilibrium for the VA subsystem, axial forces in the beam spans above a lost column show a sign transition from the lower floor to the upper floor. For instance, if a 1st floor double-span beam is in compression (CAA), beams immediately above show lower compressive forces, gradually changing to tension at each floor up the last one. Similarly, if the 1st floor spans are in tension (CA), a gradual transition to compression happens at each floor until the last one. Vierendeel Action starts typically after Flexural Action and together with CAA, as axial forces in the critical beams start to get relevant.

Sasani et al. (2007) show that VA dominates the load redistribution capacity when perimeter frame columns are removed, being the main provider of ALPs for external column loss scenarios. A visual indication of this VA synergy is a double curvature in all beam spans above a lost column, regardless of the column loss scenario (Figure 2.2).

Figure 2.2 – Double curvature due to Vierendeel Action.

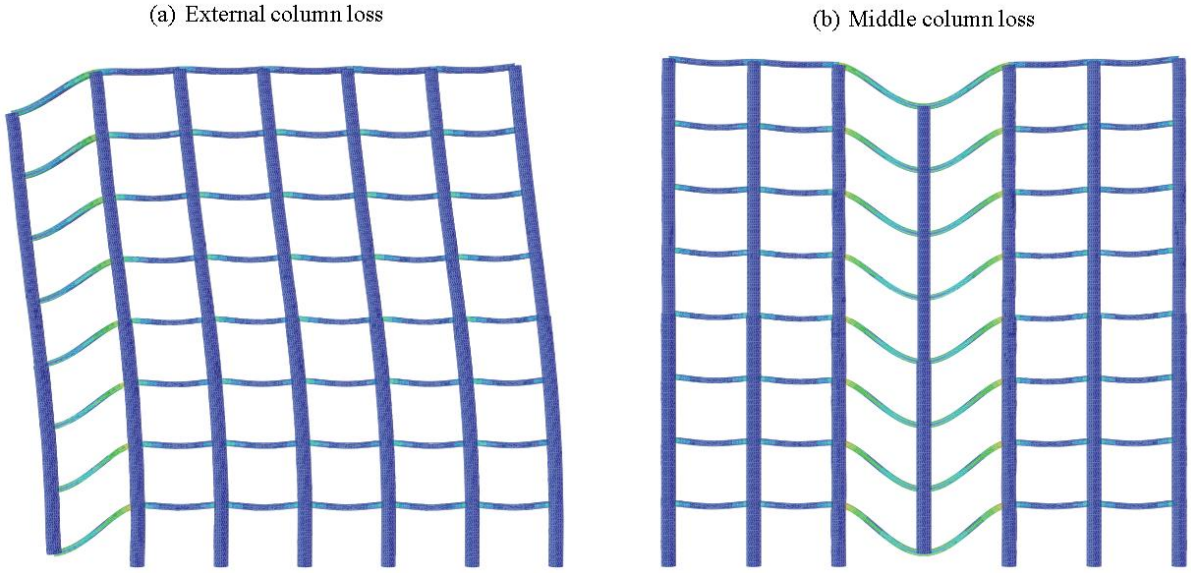

Source: Shu et al. (2017)

Hence, VA provides additional resistance due to moment transfer between beams and columns. This also prevents adjacent beams from acting as if they were simply supported, allowing all beam spans above a lost column to act together, further resisting collapse propagation. When addressing an entire building, additional resistance is also provided due to non-structural components and systemic tridimensional features. Infill walls may enhance the load-carrying capacity, especially for Flexural and CAA stages, as result of additional ALPs provided by them. Such gain in early stages is due to the infill walls behaving as compressed braces within each cell of the frame. However, infill walls may reduce overall frame ductility and ultimate CA capacity (Kiakojouri et al. 2022; Shan et al. 2023).

For the sake of simplicity and to focus on the system's primary elements, infill walls are not considered in the analyses presented in this thesis. Their behavior and interaction with the structural frame introduce complexities that are outside the scope of this initial study, though it is acknowledged that they are physically present in the building. While infill walls can enhance the overall robustness of the structure, this work concentrates on beams and columns due to their greater significance in the structural performance and load-carrying mechanisms.

Tridimensional features able to assist in progressive collapse mitigation are mostly expanded versions of the main mechanisms previously discussed. Floor slabs have a major role in force redistribution due to their diaphragm and membrane effects. Bidimensional resisting mechanisms analogous to CAA and CA can be developed in floor spans above a lost column, namely Compressive Membrane Action (CMA) and Tensile Membrane Action (TMA). For instance, Alshaikh et al. (2020) show that TMA can increase the ultimate tensile capacity by 2.5 times. In addition, floor slabs may contribute up to 34% on the overall progressive collapse resistance (Elkady et al. 2024). Shear walls have shown to reduce the potential for progressive collapse in flat slab buildings due to greater overall stability and more uniform load redistribution (Garg et al. 2021).

Moreover, progressive collapse triggered by punching failure in RC flat slab buildings is inherently a 3-dimensional problem, so regarding all the 3D features involved is mandatory to realistically address such cases (Melo and Regan, 1998; Oliveira, Melo and Regan, 2004; Santos et al. 2022; Galdino and Melo, 2023).

Nonetheless, only planar RC frames are investigated in this thesis, disregarding the influence of walls and slabs. This work dealt with the complex task of combining nonlinear structural analysis, reliability analysis, metamodeling approaches, and risk-based optimization to address one goal: comprehend how progressive collapse influences the optimal configuration of RC frames.

As shown in this Section, all major resisting mechanisms are able to develop in planar frames. Hence, delineating the objects of study to 2-dimensional frames is justifiable for the initial approach proposed herein. Yet, to minimize inaccuracies and oversights due to 3D features not being addressed, only primary RC frames related to unidirectional floor slabs are considered in this work.

2.4 PROBABILISTIC APPROACHES

Progressive collapse is associated with high uncertainties regarding extreme events and structural response, so a growing interest in addressing it by probabilistic thinking can be observed in the community. For instance, Ellingwood and Leyendecker (1978) pioneered a probabilistic approach to the vulnerability of structural systems for specific damage scenarios, advocating the APM design as framework for robustness assessment.

Bennett (1988) developed models and conceptual formulations to estimate the progressive collapse probability due to high local damage caused by exceptional loading. It was found that even if the progressive collapse probability is relatively high for a given local damage, overall safety margins can be acceptable if the probability of initial damage is low.

Agarwal et al. (2003) assessed the vulnerability of three-dimensional structures by analyzing their shapes and connectivity, regardless of their responses to specific actions. This methodology proved capable of providing sufficient information regarding structural vulnerability to unpredictable events (England et al., 2008).

Ellingwood (2006) proposed a framework for risk-analysis related to progressive collapse, discarding trivial threats and focusing on those that most contribute to overall risk. Probabilistic risk analysis, which relies on quantitative risk measures, is shown to be a rational approach for decision-making in terms of disaster mitigation. Thus, progressive collapse probability can be computed in terms of two conditional probabilities: local damage for a given extreme event, and disproportionate collapse for a given local damage:

$$P[C] = P[C|LD]\, P[LD|H]\, \lambda_H \tag{2.2}$$

where LD is the local damage resulting from event H; C is the progressive collapse induced by LD; λ_H is the average annual rate of occurrence of H; and H is the threat or extreme LPHC event able to trigger progressive collapse. By assuming multiple threats and damage states, Eq. (2.2) can be rewritten as:

$$P[C] = \sum_{H} \sum_{LD} P[C|LD]\, P[LD|H]\, \lambda_H \tag{2.3}$$

Parisi (2015) presents blast fragility curves and probabilistic pressure-impulse diagrams for addressing multiple damage levels in RC columns of a rectangular section. Fragility curves allow to obtain the conditional failure probability for a given damage state and combination of overpressure and impulse. From these curves, probabilistic overpressure-impulse diagrams are obtained, which can assist in quantitative risk analysis, performance-based assessment, and progressive collapse risk studies for blast events.

Based on concepts and methodologies applied in Earthquake Engineering, Brunesi et al. (2015) developed fragility functions for multiple damage stages to address the risk of progressive collapse for low-rise RC buildings. An increase in robustness from 20% to 40% was found for the earthquake-resistant design. Incremental dynamic analysis is shown to be more conservative compared to static pushdown analysis in terms of structural response prediction. Thus, secondary beams are also shown to contribute to ALPs and overall robustness.

Fragility models are well-established tools in earthquake engineering, offering critical estimates of collapse probability as a function of earthquake intensity parameters, such as peak ground acceleration (PGA) or spectral acceleration (Sa). Hence, these curves correlate the probability of exceeding specific damage states with the intensity of ground motion, making them essential for assessing the physical vulnerability of buildings and bridges (Siqueira, Tavares and Paultre, 2014; Siqueira et al. 2014).

Yu et al. (2017) show, through reliability and sensitivity analysis, that uncertainties have great influence on the residual capacity of RC frames under column loss, especially those related to gravitational actions and rebar reinforcement. Thus, quasi-static pushdown analysis was performed on a 2D co-rotational macromodel to define the residual load capacity in terms of two damage criteria: DC-I to represent the yielding onset, and DC-II to represent ultimate capacity. DC-II capacity was found to be 1.5 to 2.0 times higher than DC-I capacity.

Parisi et al. (2019) performed a multilevel sensitivity analysis to characterize progressive collapse for modern European RC buildings. The sensitivity of the ultimate load capacity, variability in terms of the ultimate steel strain, and location of the lost column are investigated. Thus, five performance-based limit states related to increasing damage levels are obtained. It was found that ultimate load capacity is significantly sensitive to the ultimate steel strain, being 141% greater than design load for ultimate strain of 20%. Ultimate capacity was shown to be more sensitive to the column loss location in plan than in elevation.

Parisi et al. (2019) also found that the most severe column removal scenarios are those referring to the removal of corner columns on the first floor, in line with previous researches. Regarding the sensitivity of the maximum dynamic displacement, it was found that the compressive strength of the concrete is not significant when compared to the steel yield strength, reinforcement ratio, beam span and ceiling height. Concrete strength was shown to be relevant only when CAA was mobilized in the double-span beams.

Beck (2020) presented a pioneering conceptual study on risk-based optimization for structures subject to progressive collapse, exploring the optimal design of redundant systems. It is shown that uncertainties related to non-structural factors have great influence on the optimal design, being the primary driver to redundant optimal systems. These non-structural uncertainties are addressed by the latent failure probability P_L, including workmanship, failure due to unanticipated loads, accidental loads, terrorist attacks, and connection capacity. Hence, there is a latent background probability of failure regardless of the actual structural strength.

Considering the above, Beck et al. (2020) rewrote the Ellingwood (2006) equation (Eq. 2.3) considering the probability of collapse in terms of the conditional probability of collapse given column loss $P[C \mid CL]$, and a probability of column loss P_{CL}:

$$P[C] = \sum_{H} \sum_{LD} P[C|CL]\, P_{CL} \tag{2.4}$$

In Eq. 2.4, $P_{CL} = \sum_H P[CL|H]P[H]$ is an independent parameter related to non-structural uncertainties, similarly to P_L in Beck (2020); $P[CL|H]$ is the column loss probability for a given hazard H; $P[H]$ is the hazard probability during the lifespan and the sum $\sum_{LD}(.)$ refers to different column loss scenarios. This expression addresses the risk-based optimization of common structures, such as continuous beams, regular floor spans, and regular frames, all subject to column loss. Thus, progressive collapse behavior for each case is addressed via analytical approaches. Beck et al. (2020) show that P_{CL} has major influence on the optimal design, and stregthening the frame to produce alternate load paths only has positive cost-benefit if this probability exceeds a threshold column loss probability P_{CL}^{th}. In case $P_{CL} \approx P_{CL}^{th}$, optimal design is indifferent to stregthening or not, which is characterized by a plateau or by multiple similar local minima in the objective function. For $P_{CL} < P_{CL}^{th}$, conventional design is cost-effective, with expected costs of progressive collapse being smaller than strengthening costs.

Beck et al. (2022) used the concepts and formulation in Beck et al. (2020) to study the optimal design of regular RC frames subject to the loss of columns and beams, now in terms of a probability of local damage P_{LD}, instead of P_{CL}. Progressive collapse behavior is addressed by analytical formulations proposed by Masoero et al. (2013). It is shown that optimal APM strengthening strongly depends on P_{LD}, as it only pays off after a threshold local damage probability P_{LD}^{th}. Moreover, P_{LD}^{th} is shown to be dependent on frame aspect ratio, consequences of failure, and strengthening strategies (which parts of the structure should be strengthened). It is also found that APM design is more cost-effective for taller frames; for greater sizes of the local damage; and for cheaper and/or partial strengthening strategies.

Optimal risk-based designs found in Beck et al. (2022) relate to the best resource allocation when simultaneously dealing with beam bending, column crushing and global pancake failures. For wider and shorter frames, optimal design is often related to smaller beam safety margins and greater reinforcement of the columns. This happens due to upward collapse propagation being much less severe than horizontal propagation due to column crushing. In contrast, tall frames require both beams and columns to be strong, as both vertical and horizontal propagation become almost equally severe. This contrasts with the seismic design principle of weak beam - strong column, which prioritizes beam plastification over column failure, as briefly discussed in the end of Section 4.5.

Praxedes et al. (2021) proposed a Damage Evolution Curve (DEC) to address the disproportionality and cascading failure related to progressive collapse. Based on the DEC, the authors propose a risk-based robustness index. The DEC shows how prone an initial damage is to propagate throughout the system, and how quickly it happens. When it comes to the pushdown analysis of a framed structure (Khandelwal and El-Tawil, 2011), the vertical drift of the joint related to the missing column is used as measure for the evolution of structural damage, enabling to obtain the DEC and its respective risk curve.

The expected value of losses is defined as the total area under the risk curve, which is used to estimate a vulnerability index and a robustness index. Praxedes et al. (2021) presented examples involving trusses and framed structures to compare the proposed index with previously existing indices. Yet, Praxedes and Yuan (2021) show an evaluation framework for the aforementioned robustness index in RC framed structures. Praxedes and Yuan (2022) find that the probability threshold for justifying investment against progressive collapse aligns with the lower values of the empirical incidence rate of extreme events. Optimal strengthening is also found to strongly rely on cost parameters, such as relative costs between concrete and steel.

Beck and Stewart (2023) address the risk-based cost-benefit analysis of strengthening RC frames to mitigate progressive collapse due to terrorist blast loading. A break-even point related to an annual threat probability leading to both conventional and APM design having the same total expected costs is identified. Thus, a break-even point related to strengthening against one or two column losses is obtained. For buildings susceptible to blast threats, the authors suggest slightly increased strengthening for columns prone to brittle failure, and reduced strengthening for beams with ductile failure.

2.5 MITIGATION STRATEGIES

Load redistribution capacity due to ALPs implies in greater robustness. However, there are additional strategies to deal with progressive collapse, e.g. segmentation and key element design. Alternative strategies not only enhance the overall robustness, but also serve as new lines of defense in case of the intrinsic ALPs not being enough. Hence, mitigating measures beyond the frame inherent ALPs may be justifiable from a risk analysis perspective.

Risk analysis aims to ensure that materials and resources are being efficiently allocated, considering the many potential initial damage and damage propagation scenarios. This decision relies on the type of occupation, potential number of victims, size of the structure, building relevance to society, and others. Therefore, reinforcements beyond necessary are avoided in less relevant buildings, related to low occupancy and lower threat probabilities, whereas lack of robustness is avoided in higher risk buildings (Stewart and Melchers, 1997). Strategies against progressive collapse consists of preventing initial damage, containing its propagation, or limiting the final damaged area (Kiakojouri et al. 2022). Thus, they are closely related to overall guideline requirements of continuity, redundancy and ductility (ASCE 7, 2005; UFC 4-023-03, 2009; GSA, 2016; NISTIR 7396, 2017).

In structural mechanics, a structure is considered statically indeterminate when the equilibrium equations alone are insufficient to determine the internal forces and reactions. The degree of static indeterminacy (g_h) is defined as the number of additional equations needed to solve for the static unknowns in the structure. For typical reinforced concrete (RC) frame buildings, g_h can be in the order of hundreds or even thousands. Redundancy, on the other hand, refers to the availability of ALPs that can be activated in the event of localized failure of one or more structural elements. This redundancy depends on both the location and extent of the initial damage. Generally, the degree of redundancy (g_r) is associated with the number of columns that can be removed from an RC frame without triggering a disproportionate collapse. In RC frames, it is typical for g_h to be significantly greater than g_r.

Redundant elements make hyperstatic structures, enabling greater number of ALPs and greater force redistribution capacity after a localized failure. In a redundant structure with degree g_r, failure of $g_r + 1$ elements need to occur to cause global system failure (Melchers and Beck, 2018). Thus, more redundant systems mean more paths for force redistribution. However, force redistribution only occurs if there is continuity between elements.

Continuous rebar reinforcement and anchorage as perfect as possible along beams and columns ensures continuity in RC frames. Additionally, it is desirable that failures happen in a ductile manner if they are inevitable, allowing large displacements that provide visual warning and evacuation time (Dimas, 2014). In RC frame structures, the same reinforcements that ensure systemic continuity also promote ductile failure through CA mechanism.

Additional strategies against progressive collapse can be added to both new and existing structures. As stated by Kiakojouri et al. (2022) it is not always possible to classify a reinforcement or strenghtening measure, as they may have dual effects and their performance depends on the initial triggering event, loading level and size of initial failure. For instance, measures targeted to mitigate initial damage may also ensure more effective ALPs. Thus, some reinforcement measures, such as inactive cables under usual loading conditions, only contribute after mobilization of intrinsic resisting mechanisms, especially Catenary Action.

2.5.1 Initial damage

Strategies to reduce the magnitude of initial damage are mostly focused on individual elements and for specific threats, e.g. fire, impacts, and blasts. Yet, few studies address strengthening to prevent initial damage of seismic origin (Tavakoli and Hasani, 2017; Maghroon et al. 2022).

Progressive collapse caused by fire is typically addressed for steel structures (Zhou et al. 2021), as RC frames have intrinsic protection due to aggregates (Gedam, 2021) and cover layers (Murugam and Srinivasan, 2021). However, significant strength reduction over time and potentially irreversible physical-chemical changes (Khoury, 1992) may trigger an earlier onset of progressive collapse. Mattos (2024) and Carneiro (2024) propose an alloy-based cellular protection device enclosing column spans as mitigating strategy against both fire and impact threats in existing RC flat slab buildings. Its cost-effectiveness is estimated by means of risk-based optimization, addressing cost of device implementation, expected costs of load redistribution failure and device failure, and the occurrence probability of each threat.

Reinforcement strategies against impact can be grouped in: (a) ensuring additional resistance by adding material; and (b) using sacrificial elements to protect key members. Damage from impact can result from external elements like cars and planes, or from failed structural elements within the structure itself. In the first case, columns are typically the critical elements to be reinforced, while in the second case, slabs and floor beams are the focus. To mitigate impact loads, large deformations can assist in dissipating the kinetic energy. Lu et al. (2020) and Xu et al. (2021) suggest wrapping structural elements with aluminum foam, which absorbs kinetic energy from small impacts and confines concrete for higher impacts. Although expensive, Mattos, Carneiro and Beck (2024) shows that this approach has positive cost-benefit for greater threat probabilities of impact and fire. Fan et al. (2020) recommend using corrugated steel tubes to encase ultra-high-strength fiber-reinforced concrete columns in bridge structures. Another common protective measure is using fiber-reinforced polymers (FRP), as noted by Kadhim et al. (2018) and Alam et al. (2020), especially for bridge columns. Sandwich structures also reduce impact (Ma et al. 2021; Wang et al. 2021).

Motivated by recent terrorist attacks, the literature has extensively studied blasting as triggers for progressive collapse, both at member level and system level. Due to the similarities between triggering events, some impact mitigating strategies can also be used for blast scenarios, either ensuring additional resistance or using sacrificial elements.

Adding material to increase element resistance includes jacketing concrete elements with steel (Thai et al. 2020; Hanifehzadeh et al. 2021), using sandwich structures (Vatani and Kiakojouri, 2015; Yang et al. 2021), and using fiber-reinforced polymers (Buchan and Chen, 2003; Vapper and Lasn, 2020).

However, strengthening for blast scenarios can have negative effects. Increased resistance, especially in columns, can redistribute explosion forces to the rest of the structure, expanding the area subject to overpressure and potentially leading to greater initial failure (Kiakojouri et al. 2022; Beck and Stewart, 2023).

2.5.2 Collapse propagation

Design measures that aim to mitigate the spread of collapse consist of either adding new ALPs or improving the efficiency of existing ones. In case of incorporating new paths, the additional structural elements typically involve struts, cables (relaxed or not), and trusses. The inclusion of new load-bearing walls or pillars is usually economically disadvantageous, although it can be effective (Kiakojouri et al. 2022).

As shown in the WTC Twin Towers collapse, additional columns along the perimeter improve the system's rigidity, ductility and energy dissipation, also acting as direct protection against impacts and explosions (Ezoddin et al. 2021). Load paths are guided by stiffness distribution. Therefore, if a new element does not provide additional stiffness to the system, its inclusion does not provide a new load path (De Biagi and Chihaia, 2016). Furthermore, new load paths depend on the type of load generated by the initial failure, so the same structural element may behave differently depending on the beginning of propagation. Additional beams are not usually an adequate strategy to ensure ALPs, but there are exceptions. In case of RC flat slab structures, for instance, beams along the perimeter are proposed as an effective measure against progressive collapse (Garg et al. 2021a; 2021b; 2021c).

Another strategy to combat collapse spread is by using truss structures between beam spans. This measure is known to be effective against seismic actions, and has recently been proposed to also mitigate collapse spread, mostly for steel structures and independent of the threat (Khandewal et al. 2009; Qian et al. 2019; Yu et al. 2020; Qian et al. 2021).

Reinforcement trusses can also be applied on the top floor of the structure, being an effective alternative for low to medium height buildings (Zahrai and Ezoddin; 2018; Naji and Ommetalab, 2019; among others). However, as the height of the building increases, the ability to control the propagation of collapse decreases for initial damage occurring on the first floors.

Such reinforcement substructures can also act in conjunction with cables (Izadi and Ranjbaran, 2012) and other floor substructures along the height of the building (Sun et al. 2012). Such a strengthening strategy allows for a more uniform distribution of axial loads on the columns after an initial failure, as well as a reduction in dynamic amplification related effects (Freddi et al. 2022).

Cables and ropes are effective elements in reinforcing against progressive collapse, and can be applied to both steel and concrete structures without interfering with seismic performance. Another reinforcement measure is the use of shock absorbers, although studies of these applications are still scarce. Such devices act to absorb energy, therefore generating new ALPs (Kim et al. 2011; Kim et al. 2014).

However, this alternative is complex and interferes with the architectural design in existing structures. Strengthening the original columns is rarely efficient, but is usually necessary to ensure integrity for the combined use with reinforcement cables, or to use them as energy absorbers (Horr and Safi, 2003). Meanwhile, strengthening beams is the main strategy for improving the original ALPs (Galal and El-Sawy, 2010).

Additional beam reinforcement is a classic strategy to improve structural performance against progressive collapse. In order to make progressive collapse reinforcement independent of the seismic reinforcement, Alogla et al. (2016) propose additional longitudinal rebars in the middle of the cross-section to assist CA. Yet, in the case of tall buildings, contribution of each structural element may vary along the height, so the need for reinforcement for the first floors may be far beyond the necessary for upper floors (Shan et al. 2019).

2.5.3 Extent of final failure

If initial failure cannot be avoided and collapse propagation is difficult to control, the final emergency alternative is to limit the extent of progressive collapse propagation. This strategy is commonly applied to prevent Impact-type collapses, most notably Pancake type. Yankelevsky et al. (2021) show that design based on current regulations is not enough to ensure robustness to flat slab connections under Pancake collapse.

As the dynamic impact forces can reach three to four times the total weight of the floors during free fall, usual strategies against progressive collapse are shown not to be enough. Hence, to overcome this scenario, two alternatives are shown to be efficient: (a) using energy absorption devices and (b) compartmentalization.

Energy absorption devices are common to provide lateral dynamic stabilization, but their use in mitigating Impact-type collapse is promising. Zhou and Yu (2004), for instance, propose a high-efficiency device to mitigate progressive collapse propagation in tall structures. Yet, little is known about how the collapse behavior is influenced by the additional weight that such devices add on the structure, as well as interactions between frame and device.

Compartmentalization, also addressed as segmentation, is a much simpler alternative. It consists on limiting the final damage extent by dividing the structure into smaller sections, so that the failure in one portion does not physically propagate to the others. Starossek (2017) suggested this technique for skyscrapers and bridges. Horizontal segmentation is commonly introduced by construction joints and structural fuses. As verified in the Alfred P. Murrah collapse, reinforcement discontinuities are favorable for horizontal compartmentalization (Starossek, 2017). Hence, reducing the flexural capacity in key parts of beams and slabs act in favor of arresting collapse propagation, as well as the use of fuse (sacrificial) elements.

Vertical segmentation in high-rise buildings is possible by using sections of different energy dissipation capabilities, in which reinforced floors are designed to withstand the impact of the upper floors (Lalkovsky and Starossek, 2014; Yang and Zhang, 2021).

RELEVANT DESIGN FACTORS

All different mitigation strategies shown previously have the main purpose of increasing overall robustness, and the cost-effectiveness of each should be addressed via risk analysis. Since a given alternative can be more or less efficient depending on structural topology and type of triggering event, these and other key factors are mandatory in risk analysis. When seismic threats are relevant, mitigation strategies that separate seismic and progressive collapse reinforcements should be considered to avoid unwanted effects from their interaction. Thus, dual effects shown by some strategies should be carefully investigated.

2.5.4 Structural topology

Size and arrangement of the structural system can influence the possible failure modes to be triggered and, consequently, the most adequate reinforcement strategy. Collapse in tall and slender buildings tend to propagate downwards, so Pancake collapse is the critical type, whereas in large low-rise buildings the collapse can propagate both vertically and horizontally (Beck et al. 2022; Beck and Stewart, 2023).

Member length is another relevant factor in framed buildings: for a similar column loss scenario and frame length, short and rigid beams (more columns) provide better force redistribution when compared to long beams (less columns).

This goes in line with the redundancy concept, as a continuous beam having more supports is clearly more robust. Yet, the plastic hinges formed earlier in longer beams may also act as a structural fuse, limiting the collapse spread to the beam spans above the lost column.

Building irregularities are another major factor. When comparing regular buildings with inclined and twisted buildings, Kim et al. (2011; 2013; 2014) show that beam plastic hinges can lead to further collapse propagation in irregular buildings. In regular frames, beam plastic hinges tend to limit the propagation within the damaged span.

2.5.5 Triggering event and initial failure

Guideline standards usually recommend discretionary removal of a single ground floor column to address robustness. However, the initial failure may be much greater in real cases. Although there are no limits to the extent of initial failure, there are technical and economic limitations in terms of structural strengthening.

Few studies consider beam loss as the initial failure (Fang et al. 2013; Rezvani et al. 2017; Behnam et al. 2019), as this is more common in earthquake and fire scenarios. Yet, this is considered the most likely cause of initial failure in the Plasco building collapse (Yarlagadda et al. 2018).

Each type of triggering event can lead to different types of progressive collapse depending on the available resistance mechanisms and the topological system configuration. While the proportion of initial damage tends to be limited to a single structural element in the event of a vehicular impact, it is possible for an entire floor to be affected by fire.

Figure 2.3 illustrates a comparison between increasing pre-existing ALPs and providing compartmentalization in terms of initial failure magnitude. As the proportion of initial damage increases, it becomes more difficult to provide ALPs via APM, reaching the point where it becomes economically and technically unfeasible to use this methodology. On the other hand, compartmentalization is not as cost-effective for smaller initial damages. Considering that size of initial failure depends on an unknown threat, Starossek (2012) suggests a hybrid methodology, with ALP enhancement being more adequate for vertically-alligned frames, and segmentation being more suitable for horizontally-aligned buildings.

Figure 2.3 – Impact of initial failure size on reinforcement strategy.

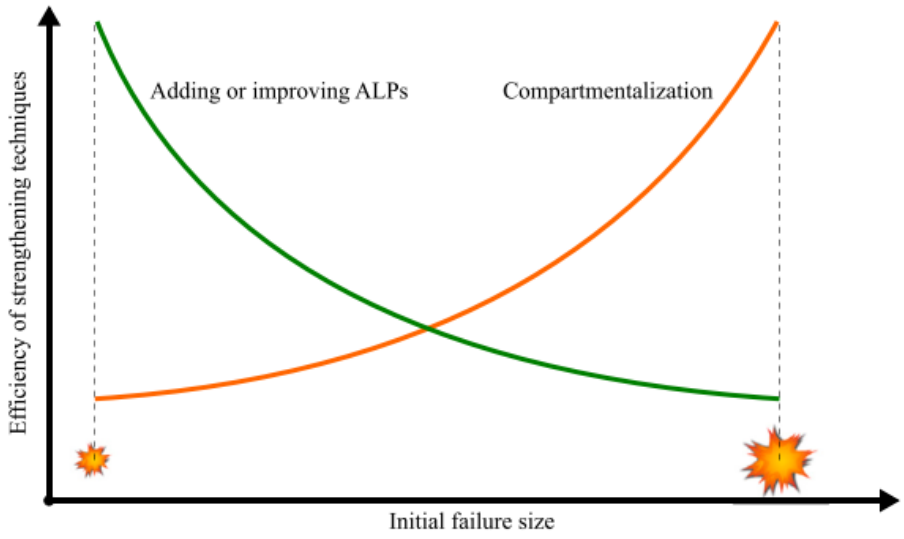

Source: Kiakojouri et al. (2022), based on Starosek (2012).

Strengthening measures at the structural element level aimed at mitigating initial damage are generally useful for smaller triggering events, such as a vehicular collision or small nearby explosion. Nevertheless, the focus of the structural reinforcement must address global systemic performance.

2.5.6 Interaction between seismic and progressive collapse design

Seismic-resistant designs aim to resist predominantly horizontal loadings, whilst a progressive collapse-resistant design aims to resist predominantly vertical loadings. Musavi and Sheidaii (2021) discuss the influence of earthquake-resistant design on progressive collapse. Earthquake-resistant designs tend to use “strong pillars – weak beams” or “strong connections – weak elements” frameworks, which can intensify the propagation of certain types of progressive collapse. This is further addressed at the end of Chapter 4.

As mentioned in the previous Section, there are some proposals to make additional progressive collapse resisting mechanisms independent of seismic-oriented mechanisms. These strategies can be grouped in: (a) inactive load-bearing systems under usual and seismic loading conditions, but active in progressive collapse related scenarios (large vertical drifts); and (b) providing additional reinforcement in a way which causes little interference in seismic performance. Among the alternatives in the first strategy, techniques involving relaxed cables and/or ropes stand out, while the second strategy highlights ALP enhancement through additional strategically positioned reinforcement elements (Kiakojouri et al. 2022).

For instance, Lin et al. (2019) and Yang et al. (2021) propose an additional rebar reinforcement in the middle of the beam depth. Since it is close to the beam neutral axis, this extra rebar layer only influences the intrinsic CA mechanism. Qiu et al. (2020) propose relaxed external cables below the beam spans, while Feng et al. (2017) and Qiang et al. (2020) study kinked rebar reinforcements (rebar folds close to beam-column joints). The two later alternatives also activate extra ALPs only at greater values of vertical drifts, thus relating solely to progressive collapse mitigation.

2.5.7 Collateral effects

Some mitigating strategies can lead to undesirable effects on the overall system performance, which is little understood. In fact, Chapter 4 shows that addressing just the intrinsic resisting mechanisms is able to cause dual effects in beam and column strengthening.

Depending on the reinforcement strategy, significant differences may arise in the force redistribution in mobilization of CAA, CA, and VA mechanisms. Reinforcement using high-resistance cables and tie rods can have the adverse effect of transmitting the dynamic overloading of the initial failure to the rest of the structure through these elements (Sarti et al. 2016). Similarly, blast strengthening can increase the loading surface and promote further spread of initial damage (Kiakojouri et al. 2022; Beck and Stewart, 2023).

Although continuity is commonly seen as a favorable feature in terms of robustness, it can have adverse effects, e.g. propagating horizontal Domino-type collapse by means of pulling mechanisms (Starossek, 2017). Besides, some mitigation strategies against progressive collapse are undesirable from an aesthetic and architectural point of view, such as the addition of trusses between spans, truss subsystems on the roof, and large energy absorption devices.

2.6 DESIGN STANDARDS

Given the severity of progressive collapse consequences, various international regulations have been proposed to prescribe minimum safety margin against it and to establish efficient frameworks on how to address it. These guidelines outline acceptable damage limits after an initial failure, specific reinforcement frameworks, and risk classes for buildings. Hence, in terms of the building's risk level, different robustness requirements are prescribed for government buildings and residential buildings, for instance.

Guideline approaches for preventing progressive collapse are categorized into direct and indirect methods. Direct methods address increase in robustness by designing key structural elements to withstand abnormal loadings, and also by ensuring enough ALPs (Dimas, 2014). When addressing ALPs via APM design, dynamic effects related to a sudden column loss need to be addressed. GSA (2016) proposes Dynamic Amplification Factors (DAF) up to 2.0, which must be included in the abnormal load combinations regardless on the type of structural analysis performed (linear static, nonlinear static, or nonlinear dynamic).

Indirect methods rely on implicit strategies for robustness, such as imposing minimum values of resistance, ductility and continuity on the elements. As it does not resort to a complex analysis, it is simpler than direct methods, although more limited (Dimas, 2014). Tie requirements are an example of indirect method, in which overall robustness is enhanced by means of minimal requirements for the connections (UFC 4-023-03, 2009).

Acceptable limits for the final damage extent are also prescribed. The European standard EC2 1-7 (2006), for instance, suggests that damage to a building resulting from an exceptional action does not exceed 15% of the floor area or 100 m². In the vertical direction, damage must not exceed two floors adjacent to the origin of the damage.

Stewart (2017) shows that North American guidelines against progressive collapse led to a satisfactory cost-benefit only for very high threat probabilities, around 10^{-3}/building/year. Thus, the risk related to blast-induced progressive collapse in government buildings is very low. It should be noticed, however, that cost-benefit can become positive if the columns are subject to other threats, such as earthquakes and vehicular impacts.

Brazilian guidelines do not explicitly deal with progressive collapse caused by sudden column loss, but prescribe constructive standards to avoid its onset by brittle failure modes in flat slab RC structures (NBR 6118, 2023). No formal definition is presented for the phenomenon, possibly reflecting the low incidence of typical abnormal threats in Brazil, such as earthquakes and terrorist attacks. Yet, Pereira et al. (2024) argue that earthquake loads should not be dismissed in Brazil, particularly for important or critical buildings.

Brazil has its own notorious occurrences of progressive collapse. For instance, the partial collapse of Pallace II residential building, in Rio de Janeiro, 1998, happened in two instances due to failure in two columns, as result of several construction errors and poor choice of materials (Instability collapse). In 2001, in Ubatuba, SP, block B of Anêmona residential building collapsed due to failure in its foundation piles (also Instability collapse).

Dos Anjos (2016) found that designs based on Brazilian regulations did not satisfy the Demand-Capacity Ratio criteria established by GSA (2013) for a 12-story regular RC frame in terms of a linear static procedure. However, by increasing the longitudinal reinforcement ratio by up to 380% and transverse reinforcement ratio by up to 400%, it was possible to comply with the required limits for scenarios of internal column loss. While the reinforcement required to mitigate progressive collapse is ~400% higher than for intact scenario, rebar and stirrup detailing remain reasonable and within permissible limits. Thus, as shown in the linear procedure of Section 4.1, similar increases for rebars and stirrups are found.

2.7 STRUCTURAL ANALYSIS

Pushdown analysis, proposed by Khandelwal and El-Tawil (2013), is a framework for evaluating progressive collapse robustness due to loss of load-bearing elements, similar to the pushover analysis used in earthquake engineering. The technique consists of gradually increasing the gravitational load after the loss of one or more critical elements until collapse is verified. Besides, robustness can be quantified in terms of the Overload Factor (OF):

$$OF = \frac{\text{Ultimate capacity}}{\text{Nominal gravitational load}} \tag{2.5}$$

Following GSA (2016), pushdown analysis can be performed in three ways: Uniform Pushdown (UP), Bay pushdown (BP), and Incremental Dynamic Pushdown (IDP). In UP, gravitational loads are increased throughout the entire damaged structure via static nonlinear procedure until failure.

On the other hand, BP emphasizes the increasing loads only in the beam spans above the lost column. The more realistic IDP consists of a series of dynamic analyses, with each step having a vertical load over the critical spans greater than in the previous step, until failure occurs in one of the increments. Khandelwal and El-Tawil (2013) show that IDP is the alternative closer to reality, and results via BP closely resemble those via IDP, even without considering dynamic effects. Hence, BP is a simpler yet efficient approach able to replace IDP.

In this regard, Biagi et al. (2017) propose various techniques to address progressive collapse robustness of RC frames. They suggest three alternatives for column removal: (a) reducing mechanical properties; (b) complete column removal followed by incremental load application; (c) and incremental unloading of internal forces on the damaged column. Since external forces are always present during structural damage, the third alternative is considered the most realistic. However, its complexity makes it less preferable. The second approach, which resembles BP, is the simplest, but does not account for the presence of the damaged element. The first approach disregards external actions. In terms of structural efficiency and computational burden, the simple element removal for robustness assessment is justified.

According to Fascetti et al. (2015), BP associated with dynamic effects is an efficient alternative, since dynamic effects make up a large part of the progressive collapse behavior. Such effects can be represented by explicit dynamic analysis, DAFs (conservative approach), or by Energy Equivalent Method (EEM).

A pragmatic solution is enabled by EEM, as it relies on the nonlinear static pushdown curve and the principle of energy conservation (Izzudin et al. 2008; Xue and Ellingwood, 2011; Xue and Le, 2016; Bao et al. 2017). In a dynamic deformable body, the sum of kinetic energy, external work and internal deformation energy must remain constant for any time instant and for any deformation. For simplification, energy dissipation from other sources, such as heat and plastic strains, is neglected, leading to small discrepancies in the dynamic estimation.

Considering the oscillation of the affected frame bay as a single-degree-of-freedom system, the kinetic energy at peak dynamic displacement is zero. Hence, the relationship between force and peak dynamic displacement can be obtained by equating the external work to the internal strain energy:

$$\lambda_d(d) \cdot d = \int_0^d \lambda_s(u)\, du \tag{2.6}$$

where $\lambda_d\ (d)$ and $\lambda_s\ (d)$ represent the pseudo-static and static pushdown curves, respectively (Praxedes, 2020).

In this thesis, progressive collapse is addressed by a combination of Bay Pushdown Analysis and Energy Equivalence Method, unless stated otherwise. This approach is used by Praxedes (2020), and it has shown a good balance in terms of progressive collapse behavior prediction and computational burden for risk-optimization purposes.

Yet, metamodeling techniques had to be added in this thesis due to a broader range of systemic outputs addressed, significantly increasing the computational time for both structural and reliability analyses. In this work, robustness is addressed in terms of the overall frame systemic behavior, relying in more than just the RC beams. Further details regarding these aspects are shown in Section 3.3.

Several alternatives are available for the numerical modelling of progressive collapse (Adam et al.2018). Four approaches stand out: (a) Finite Element Method (FEM); (b) Discrete Element Method (DEM); (c) Applied Element Method (AEM); and (d) Cohesive Element Method (CEM). The main features for each of them are displayed in Figure 2.4.

Figure 2.4 – Main features of the most relevant progressive collapse numerical methods.

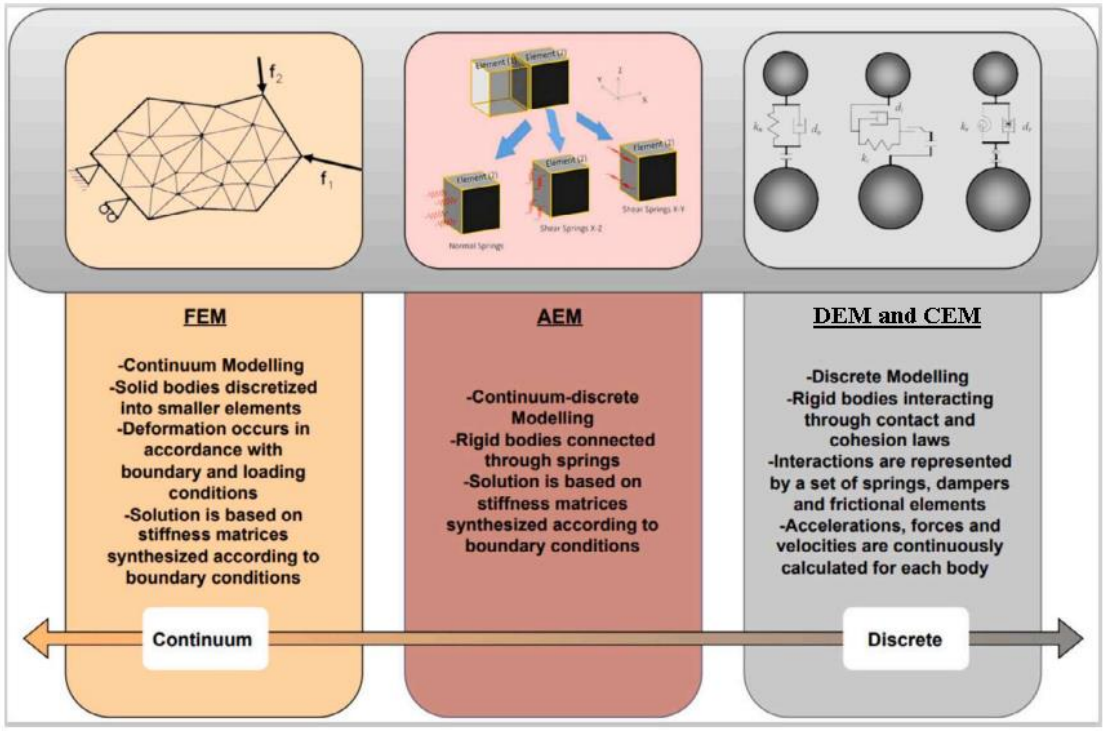

Source: Adapted from Elkady et al. (2024).

Herein, FEM approach is adopted by combining BP and EEM, due to its broad acceptance in the community, being the analysis method incorporated in several Software Packages. In fact, the widely accepted OpenSees Software (Mckenna et al. 2010), which relies on FEM, is used in this thesis in progressive collapse simulation, unless stated otherwise.

OpenSees is an open-source software framework developed at UC Berkeley, supported by renowned US research centers, and was designed for advanced analysis of non-linear structural responses to seismic events. However, over the past decades, it has grown into a powerful tool with capabilities in geotechnical modeling, reliability analysis, and structural simulation for earthquake, progressive collapse, fire, and explosions. As the platform of choice in many researches, OpenSees facilitates data sharing, remote experiments, and hybrid simulations, fostering a large, collaborative community of engineers dedicated to solving complex structural challenges (Usmani et al. 2010; Usmani et al. 2012).

Although FEM does not allow to directly address member separation, these other alternatives are fairly recent, time demanding, and rather complex for the purpose of this work. Yet, as shown in the validation examples of Section 3.4.1, FEM approach is able to accurately depict the entire static pushdown behavior for a broad-range of experimental tests. Nonetheless, future studies may address these alternative methods in order to simulate other collapse features better depicted by them.

3 PROPOSED FRAMEWORK

The objective of this thesis is to comprehend how progressive collapse influences the optimal risk-based configuration of reinforced concrete framed structures. To achieve this, a framework of several methods was adopted to address each desired feature.

3.1 OVERVIEW

As stated in the previous Chapter, redistribution-type progressive collapse due to single column loss is addressed. Only intrinsic resisting mechanisms are considered (Section 2.3), so the main strategy for progressive collapse mitigation consists on enhancing existing ALPs via APM design, as done in usual guideline framework. In this initial study, only primary RC frames related to unidirectional floor slabs are addressed, minimizing potential inaccuracies due to 3D features not being considered. Typical design variables are optimized to ensure enough safety margin against progressive collapse, such as cross-sectional depths, longitudinal and transversal reinforcement ratios, and concrete strength. Alternative strategies are addressed, but they also ensure robustness by means of enhancing existing ALPs.

Based on Beck et al. (2020; 2022), a threat-independent approach is adopted, combining hazard probability and column loss probability given hazard as probability of local damage $P_{LD} = \sum_H P[CL|H]P[H]$. To understand how progressive collapse influences the optimal design, P_{LD} is assumed to range between a lower value $P_{LD}^{min} = 5 \times 10^{-6}$ to 1. This allows to cover scenarios gradually changing from negligible to very significant threat of column loss. It is noteworthy to mention that P_{LD}^{min} relates to the 50-year lifespan equivalent to the "de minimis" annual probability $p = 10^{-7}$ (Pate-Cornel, 1987).

Given the above, the adopted framework relies generally on four pillars (Figure 3.1):

(a) risk-based optimization: total expected costs, given by cost of construction and expected costs of failure, are minimized for each P_{LD} (Section 3.2);
(b) reliability analysis: in order to compute the expected costs of failure, probability of occurrence for each failure mode is addressed (Section 3.3);
(c) structural modeling: at each sample point, structural response is addressed via nonlinear FEM for limit state evaluation (Section 3.4);
(d) metamodeling: as structural and reliability analyses have great computational burden, simplified yet accurate models are used to hasten these stages (Section 3.5).

Figure 3.1 – Simplified depiction of the proposed framework.

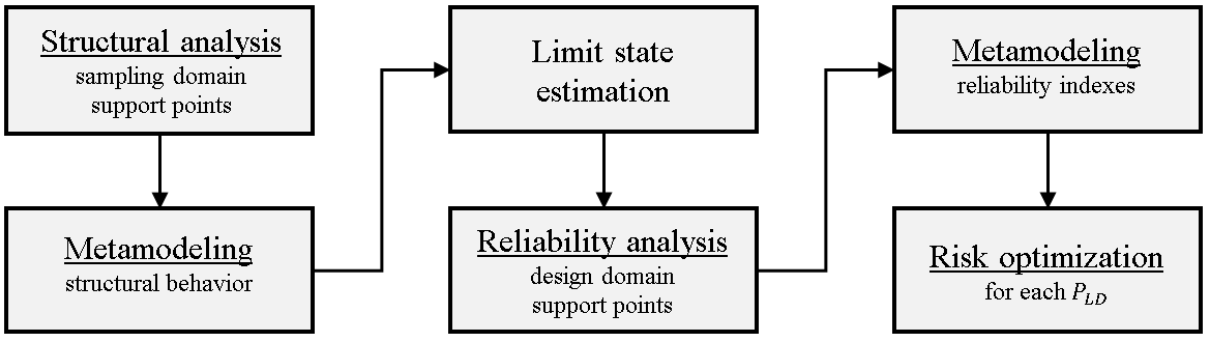

Source: own authorship.

Latin Hypercube Sampling (LHS) is used to create a uniform sample (1st) across the sampling domain $\boldsymbol{\mathcal{S}}$ containing the problem's random variables (McKay et al. 1979; Tang, 1993; Ye, 1998). These sample points are support points for the 1st metamodeling stage related to structural behavior (Section 3.5). Then, FEM is used to realistically address structural behavior for the intact structure and each column loss scenario.

A new and significantly bigger sample (2nd) is created via LHS across $\boldsymbol{\mathcal{S}}$, but structural behavior is now quickly (and accurately) estimated by metamodeling based on previously analyzed support points via FEM. To ensure convergence in reliability analysis, this larger sample may reach dozens of millions of sample points, so it would be highly unfeasible to get their structural behavior via FEM.

Each sample point in the bigger sample has its limit states computed accordingly to the addressed failure modes, but always in terms of a resistance term minus a demand term. Some failure modes have resistance terms estimated via metamodeling (FEM), such as ultimate capacities in CAA and CA. Others have demand terms obtained via metamodeling (FEM), such as shear demand in beams, force vs bending demand in columns, and material strains. Nevertheless, limit state estimation leads to outputs equal to 0 (safety, demand < resistance) or 1 (failure, demand ≥ resistance). More details related to each limit state function are described in the introduction of each example shown in Chapter 4.

A new sample (3rd) is created via LHS across the design domain $\boldsymbol{\mathcal{D}}$. Design domain $\boldsymbol{\mathcal{D}}$ contains the mean values of some of the random variables in $\boldsymbol{\mathcal{S}}$; hence, $\boldsymbol{\mathcal{D}} \subset \boldsymbol{\mathcal{S}}$. Vector $\boldsymbol{\mathcal{D}}$ has a smaller dimension than vector $\boldsymbol{\mathcal{S}}$, as some random variables are not considered as design variables, e.g. yielding strength, dead load, live loads, and model error. For each new sample point in the 3rd sample, the previous larger sample (2nd) and their limit state results are used to compute the probability of occurrence for all of its failure modes.

Design variables are conveniently considered as random design variables in order to: (a) ensure a more robust uncertainty modelling; and (b) allow usage of the most efficient reliability analysis method found for this framework (more details in Section 3.3).

A final sample (4th) is then created via LHS across $\boldsymbol{\mathcal{D}}$ and for risk-based optimization purposes. The reliability indexes are quickly (and accurately) estimated via metamodeling in terms of the support points previously evaluated in reliability analysis.

As the iterative optimization process advances, optimal candidates converge towards the optimum (most cost-effective solution), and for each candidate the failure probabilities are quickly (and accurately) estimated based on reliability index metamodels. These surrogates are related to specific failure modes of intact structure scenario and column loss scenarios. Although the probability of failure modes related to column loss scenarios is conditional on threat probability, the same reliability index metamodels can be used regardless of P_{LD}.

To briefly illustrate the efficiency of the proposed framework, in terms of the examples in Chapter 4 and which are mostly solved in a notebook (16 GB RAM, 64 bits OS, Intel® Core i7-11800H @ 2.30 GHz, 8 cores), the average computational times for each stage were:

(a) structural analysis (continuous RC beam example): 20 to 30 minutes for a column loss scenario and 2000 support points in $\boldsymbol{\mathcal{S}}$;
(b) structural analysis (RC frame examples): 3 to 8 hours for each column loss scenario and 2000 support points in $\boldsymbol{\mathcal{S}}$, with taller frames taking longer;
(c) limit state estimation: 2 to 6 hours for 30 million points in $\boldsymbol{\mathcal{S}}$ using FEM metamodels, with RC frames under several column loss scenarios taking longer;
(d) reliability analysis: 1 to 4 hours for 2000 support points in $\boldsymbol{\mathcal{D}}$, with RC frames under several column loss scenarios taking longer;
(e) risk optimization: less than a minute for each P_{LD}, 100 iterations, an initial extensive search for 10 thousand candidates in $\boldsymbol{\mathcal{D}}$, reliability indexes surrogates, and regardless of the structure.

This clearly shows how fundamental the metamodeling approaches were, being the key factors to link the stages of structural modeling, reliability analysis and risk optimization. If not for metamodeling, structural analysis for 30 million tall frame sample points would roughly take 13.7 years, which would be unfeasible. Yet, different metamodeling approaches were used for RC beam and RC frame examples, as the method used for beams was shown to be too complex and slow for RC frames with many more outputs (more details in Section 3.5).

Metamodeling enabled refined nonlinear FEM to be used (Section 3.4). Besides, reliability analysis relies on a simulation method that allows using the same large sample in $\boldsymbol{\mathcal{S}}$ for computing failure probabilities for all support points in $\boldsymbol{\mathcal{D}}$ (Section 3.3).

3.2 RISK OPTIMIZATION PROBLEM

For each P_{LD}, cost-effectiveness provided by a given configuration in design variable vector $\boldsymbol{d} \in \boldsymbol{\mathcal{D}}$ is measured in terms of the compromise between construction cost and expected costs of failure. Hence, risk-based optimization is chosen to describe the cost-benefit of an APM design against progressive collapse.

Risk optimization (RO) is currently the best alternative for addressing the optimal balance between economy and safety (in terms of probability of failure), leading to consistent results when system failure can be characterized and when costs of failure can be defined. Thus, only RO is able to result in optimal configurations in terms of uncertainty and monetary consequences of failure (Beck et al. 2012; 2015).

Reliability-based design optimization (RBDO) is historically the most studied method for optimization under uncertainties, but as results depend on admissible failure probabilities (constraints), optimal compromise between safety and economy is not necessarily achieved. Deterministic design optimization (DDO) does not account for failure probabilities at all, so minimal construction costs are related to increased expected costs of failure, even when using safety coefficients (Beck et al. 2012).

Robust optimization does not make use of probabilistic measures, often relying on arbitrary design constraints and normalizing constants to make a structure less sensitive to uncertainties. This lack of objectiveness leads to optimal results not necessarily related to the best compromise between safety and economy (Beck et al. 2015).

In this thesis, construction costs and expected costs of failure (cost of failure x probability of failure) compose the total expected cost $C_{TE}(\boldsymbol{X}, \boldsymbol{d})$, with $\boldsymbol{X}$ being the random variable vector, and $\boldsymbol{d}$ being the design vector.

Additional life-cycle costs could be included in C_{TE}, e.g. costs of maintenance, operation, inspection, demolition and disposal. However, only those related to construction and expected loss are used, solely addressing consequences of progressive collapse, following Beck et al. (2020; 2022) and Ribeiro et al. (2023). Hence, RO consists in solving the following optimization problem:

$$\begin{aligned} &\text{find } \boldsymbol{d}^* \\ &\text{which minimizes } C_{TE}(\boldsymbol{X}, \boldsymbol{d}) \\ &\text{subject to } \boldsymbol{d} \in \boldsymbol{\mathcal{D}} \end{aligned} \tag{3.1}$$

The objective function $C_{TE}(\boldsymbol{X}, \boldsymbol{d})$ is typically a non-convex function with multiple local minima; therefore, gradient-based mathematical programing methods cannot be used for RO. Herein, global heuristic algorithms are adopted for solving Eq. (3.1) (Beck et al. 2012).

Firefly algorithm (FA) is chosen for solving RO in this thesis. Introduced by Yang (2008), FA is a metaheuristic optimization algorithm inspired by firefly behavior. Hence, each optimal candidate in $\boldsymbol{\mathcal{D}}$ is assumed as a firefly, and C_{TE} landscape formed in $\boldsymbol{\mathcal{D}}$ is given in terms of the brightness of the fireflies. Convergence is then characterized by fireflies getting closer to the brightest ones. Three idealized rules define their behavior: (a) fireflies are attracted to each other regardless of sex; (b) attractiveness is proportional to brightness; and (c) brightness is given in terms of the landscape (C_{TE}).

As shown in Yang (2008), attractiveness relies on the coefficients γ^{FA} (related to sky light absorption) and β_0^{FA} (greatest possible attractiveness, as it decreases over distance). Thus, firefly movement relies on a randomization parameter α^{FA}. In a parametric study, Yuan-Bin et al. (2013) suggest $0.1 \leq \gamma^{FA} \leq 30$, $0.1 \leq \alpha^{FA} \leq 0.2$, and 20 to 50 fireflies across $\boldsymbol{\mathcal{D}}$. In this thesis, it is used $\gamma^{FA} = 0$ (no light absorption); α^{FA} is set for decreasing randomness; β_0^{FA} ranges from 0 to 1, in terms of its C_{TE} compared to the maximum; 40 fireflies; initial extensive search of 10 thousand fireflies; and 100 iterations. For each P_{LD}, 10 optimization runs are performed.

Heuristic algorithms with better probabilistic metrics could have been employed instead of FA (Gomes et al. 2018). However, thanks to metamodeling, optimization proved to be the fastest stage of the framework. Additionally, a quick extensive search was conducted before the iterative process, significantly reducing convergence issues.

3.3 RELIABILITY ANALYSIS

As C_{TE} needs to be computed at each optimal candidate, in each iteration and for each P_{LD}, several evaluations of probability of failure P_f are required for a single optimization run. Hence, reliability analysis is done in two stages: (a) an estimation via simulation method for a set of support points in $\boldsymbol{\mathcal{D}}$ for metamodeling purposes; and (b) estimations via metamodeling during optimization, based on the previously obtained support points (Figure 3.1).

Weighted Average Simulation Method (WASM) is used in the first stage of reliability analysis. Proposed by Rashki et al. (2012), WASM consists on estimating P_f from a sample of uniformly distributed points for all random variables, regardless of their real distribution. It is also able to estimate design point location, but this property is not addressed in this work.

The weight of each sample point i is defined by the product of the probability density function f_j of its NV random variables (Eq. 3.2), being greater or smaller as it is closer or farther from the mean value, as shown in Figure 3.2 ($W_1 > W_2 > W_3$).

$$W_i = \Pi_{j=1}^{NV} f_j(i) \tag{3.2}$$

Figure 3.2 – Weighting of sample points in sampling space.

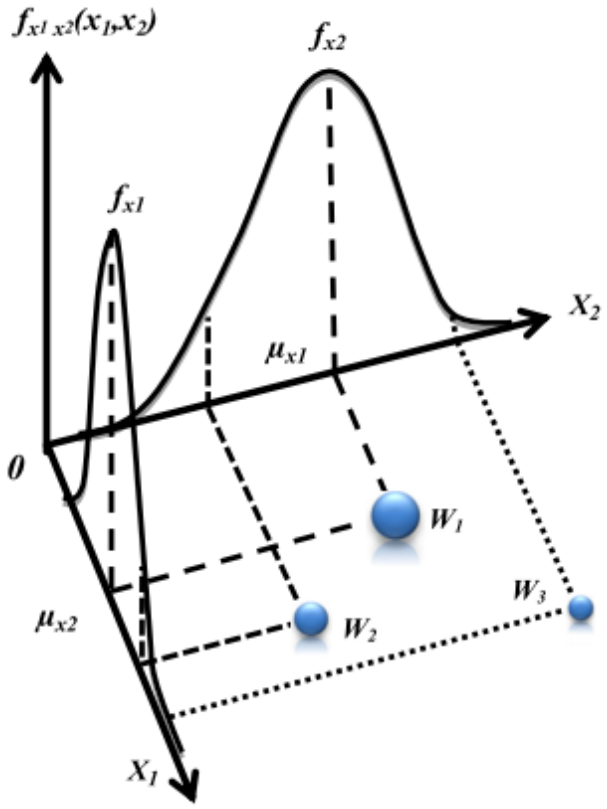

Source: Rashki et al. (2012)

From the weight of each sample point, P_f is estimated by:

$$P_f = \frac{\sum_{i=1}^{NS} W_i I(x_i)}{\sum_{i=1}^{NS} W_i} \tag{3.3}$$

where x_i is the i-th sample point; W_i is the sample point weight; $I(x_i)$ is the indicator function of x_i, worth 0 for survival and 1 for failure; and NS is the number of sample points. Two proofs attesting to the veracity of Eq. (3.3) are presented in Rashki et al (2014).

Rashki et al. (2012) show that this technique avoids classic drawbacks of crude Monte Carlo simulation, especially the need for a very large sample. By using low coefficients of variation, design variables typically addressed as deterministic can be adopted as random. However, its greatest advantage relates to a single sample being used regardless on $\boldsymbol{d} \in \boldsymbol{\mathcal{D}}$.

In optimization problems involving random design variables, only W_i is dependent on the optimal candidate configuration. As $I(x_i)$ depends on sampling, changing the optimal candidate design (mean value) only requires the reevaluation of the sampling weight W_i, enabling a single sample to be used throughout the entire process (Okasha, 2016).

Although WASM is not used within the iterative optimization processes, this property has great value in the 1st stage reliability analysis, as up to 2000 support points are used for metamodeling purposes. Hence, the same large sample across $\boldsymbol{S}$ is used for all support points.

3.3.1 Risk optimization and reliability analysis validation

This example relates to the continuous 6 span elastoplastic beam addressed in Beck et al. (2020). A uniform loading composed by dead load D_n and live load L_n acts over the spans, and the beam is subject to middle and external column loss scenarios (Figure 3.3). Cross-section is rectangular and constant along the length, with plastic modulus z_p, and all properties are assumed adimensional as in the reference.

Figure 3.3 – Object of study for validation.

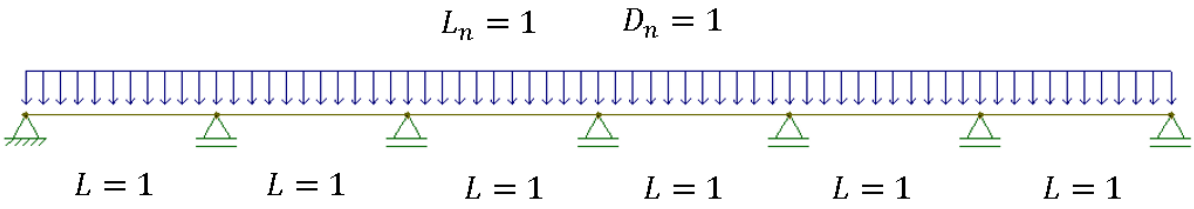

Source: adapted from Beck et al. (2020).

Figure 3.4 shows bending moment factors m for each support loss scenario in terms of a unitary uniform load. If optimal design is satisfactory for the maximum bending moment factors m, then it also is for the remaining sections. Table 3.1 lists the uncertainty modeling.

Figure 3.4 – Greatest bending moment factors m for each scenario.

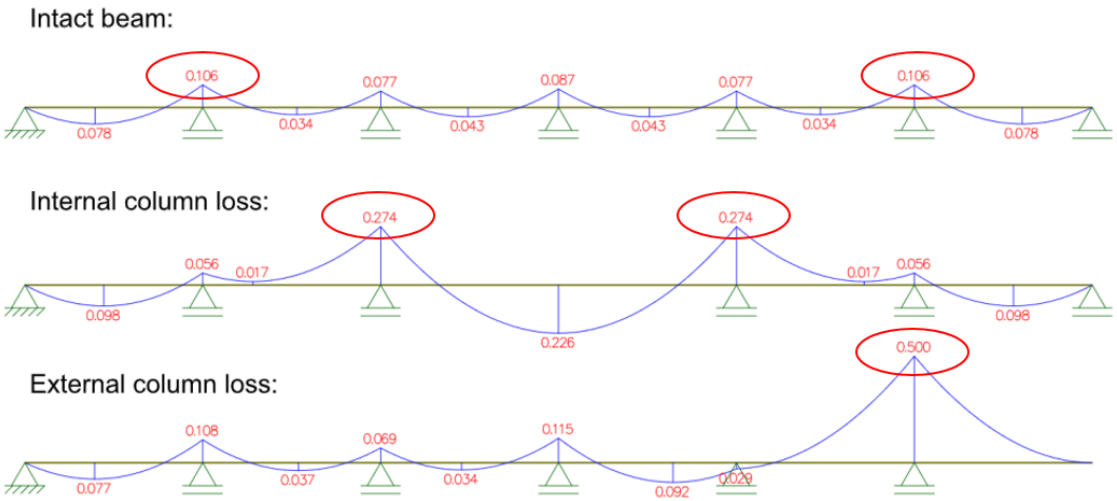

Source: adapted from Beck et al. (2020).

Table 3.1 – Uncertainty modeling.

Variable	Mean (μ)	COV (δ)	Distribution
Resisting plastic moment of steel beams (Z) - adimensional	1.30	0.12	Normal
Dead load (D)	1.05 D_n	0.10	Normal
Arbitrary point in time live load (L_{apt})	0.25 L_n	0.55	Gamma
50-year live load (L_{50})	1.0 L_n	0.25	Gumbel

Source: Beck et al. (2020).

Following the reference, design variable relates to the mean value of resisting plastic moment μ_Z, but in terms $\lambda_{PC} = \mu_Z^*/\mu_{Z0}$, with μ_Z^* being the optimal mean value of Z, and μ_{Z0} =1.30 the reference mean value of Z (Table 3.1). Thus, μ_{Z0} = 1.3 corresponds to the reinforcement required to meet the guideline abnormal load condition $R \geq 1.2D_n + 0.5L_n$, and design variable λ_{PC} corresponds to the additional strengthening required.

The objective function C_{TE} addresses construction cost C_C and expected costs of failure for each scenario $C_{EF|NLC}$, $C_{EF|ICL}$, e $C_{EF|ECL}$, with NLC being normal loading condition, ICL being internal column loss, and ECL is external column loss. Construction cost C_C is assumed equivalent to the beam resisting plastic moment, but non-dimensional in terms of $R(\lambda_{PC} = 1)$:

$$C_C = \frac{R(\lambda_{PC})}{R(\lambda_{PC} = 1)} = \frac{\lambda_{PC}\, z_p\, \mu_{Z0}}{z_p\, \mu_{Z0}} = \lambda_{PC} \tag{3.4}$$

Expected cost of failure C_{EF} is given by failure cost C_F multiplied by failure probability. Term C_F is assumed equivalent to a reference construction cost $\left(R(\lambda_{PC}=1)\right)$ multiplied by a cost factor k above 1.0. According to the Joint Committee on Structural Safety (JCSS, 2001), risk analyzes are not necessary in situations where $k < 10$. That said, $k = 20$ was considered, slightly higher than that found by Marchand and Stevens (2015) for steel frames ($\approx$ 16.7). Expected failure costs C_{EF} are made non-dimensional by dividing by R($\lambda_{PC}=1$):

$$C_{EF} = \frac{k\, R(\lambda_{PC}=1) P_f}{R(\lambda_{PC}=1)} = k\, P_f \tag{3.5}$$

$$P_f = \begin{cases} P_f[NLC] & \text{for } NLC \\ P_{ICL}\, P_f[ICL] & \text{for } ICL \\ P_{ECL}\, P_f[ECL] & \text{for } ECL \end{cases} \tag{3.6}$$

where $P_f[NLC]$ is the failure probability of the intact beam, under normal loading condition; P_{ICL} and P_{ECL} are probabilities of suddenly losing internal and external supports, respectively; and $P_f[ICL]$ and $P_f[ECL]$ are failure probabilities conditional to ICL and ECL, respectively.

Probabilities of sudden support removal are assumed equivalent ($P_{ICL} = P_{ECL} = P_{CL}$). According to Ellingwood (2006), column removal analysis is not necessary when the probability of the threat occurring is less than 10^{-7}/year. Considering a design life of 50 years, the lower limit $P_{CL}^{min} = 5 \times 10^{-6}$ is obtained. At the upper limit, P_{CL}^{max} = 1.0 is adopted. That said, total expected cost C_{TE} and optimization problem are given by:

$$\begin{aligned} C_{TE}(\boldsymbol{X}, \lambda_{PC}) &= \lambda_{PC} + k\, P[NLC(\boldsymbol{X}, \lambda_{PC})] + \\ &+ k\, P_{CL}\, P[ICL(\boldsymbol{X}, \lambda_{PC})] + k\, P_{CL}\, P[ECL(\boldsymbol{X}, \lambda_{PC})] \end{aligned} \tag{3.7}$$

$$\begin{aligned} &\text{find } \lambda_{PC}^{*} \\ &\text{which minimizes } C_{ET}(\boldsymbol{X}, \lambda_{PC}) \end{aligned} \tag{3.8}$$

As previously stated, FA is used to solve the RO problem and WASM is addressed for reliability analysis, as proposed by Okasha (2016). No metamodeling is employed in this validation, so WASM is used within each iterative optimization stage based on a sample of 70 thousand points in $\boldsymbol{S}$.

Yet, a new sample is created for each optimization run, no auxiliary extensive search is performed prior to optimization, and only 30 fireflies are adopted. Moreover, $\gamma^{FA} = 1$ (slight light absorption), so fireflies convergence is slower; α^{FA} starting equal to 0.7, but decreasing to 0 as the iterative process advances (decreasing randomness). Limit state functions are assumed linear in Gaussian random variables:

$$g_{NLC}(\boldsymbol{\lambda_{PC}}, \boldsymbol{X}) = z_p \, Z \, \boldsymbol{\lambda_{PC}} - m_{NLC}(D + L_{50}) \tag{3.9}$$

$$g_{ICL}(\boldsymbol{\lambda_{PC}}, \boldsymbol{X}) = z_p \, Z \, \boldsymbol{\lambda_{PC}} - m_{ICL}\left(D + L_{apt}\right) \tag{3.10}$$

$$g_{ECL}(\boldsymbol{\lambda_{PC}}, \boldsymbol{X}) = z_p \, Z \, \boldsymbol{\lambda_{PC}} - m_{ECL}\left(D + L_{apt}\right) \tag{3.11}$$

Figures 3.5, 3.6 and 3.7 show sampling results in terms of resisting and demand bending moments, indicating failure and survival domains. Figure 3.8 shows the convergence of 30 fireflies along the iterative process for P_{CL}^{min}.

Figure 3.5 – Sampling results for NLC.

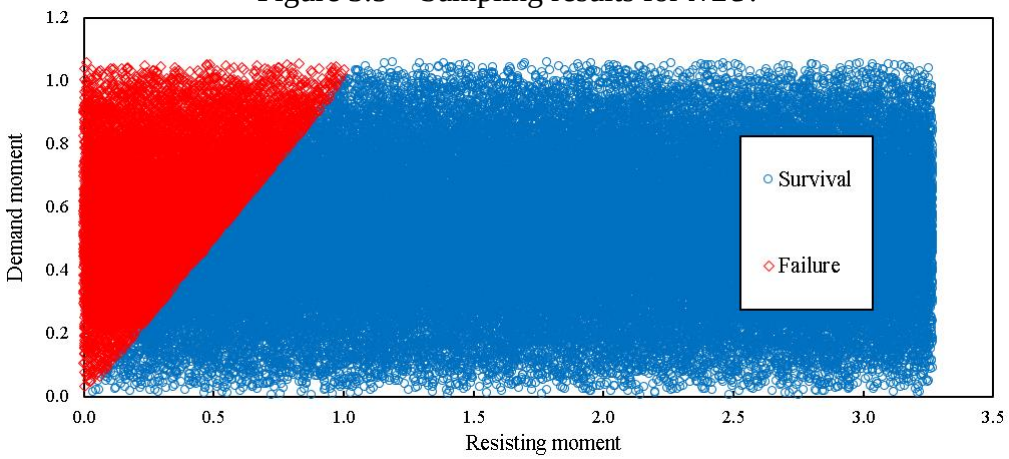

Source: own authorship.

Figure 3.6 – Sampling results for ICL.

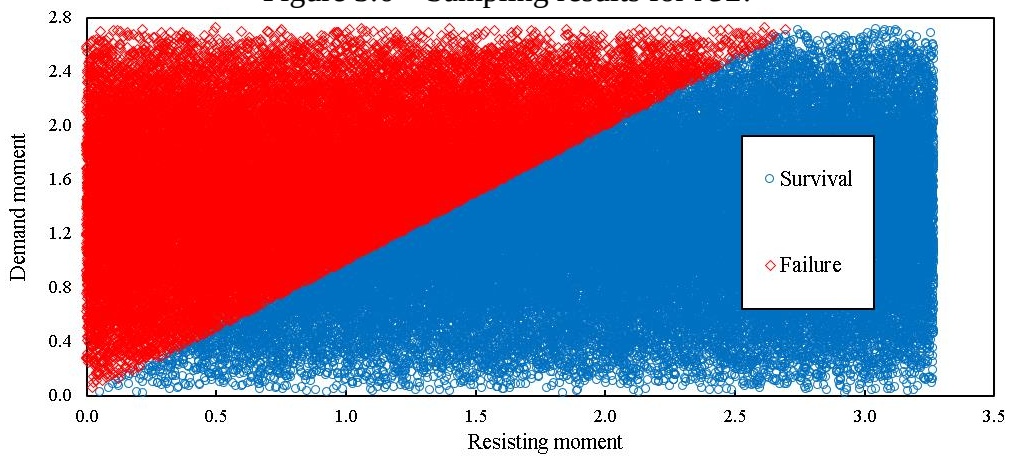

Source: own authorship.

Figure 3.7 – Sampling results for ECL.

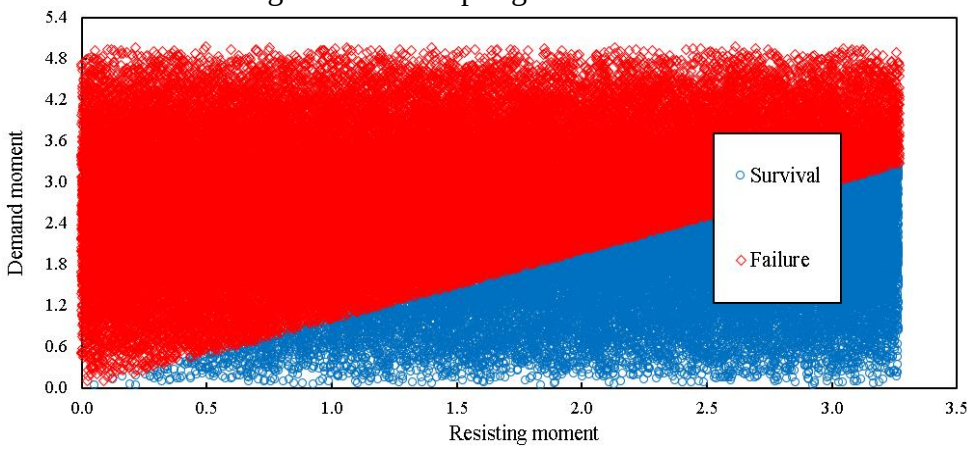

Source: own authorship.

Figure 3.8 – Firefly convergence for P_{LD}^{min}.

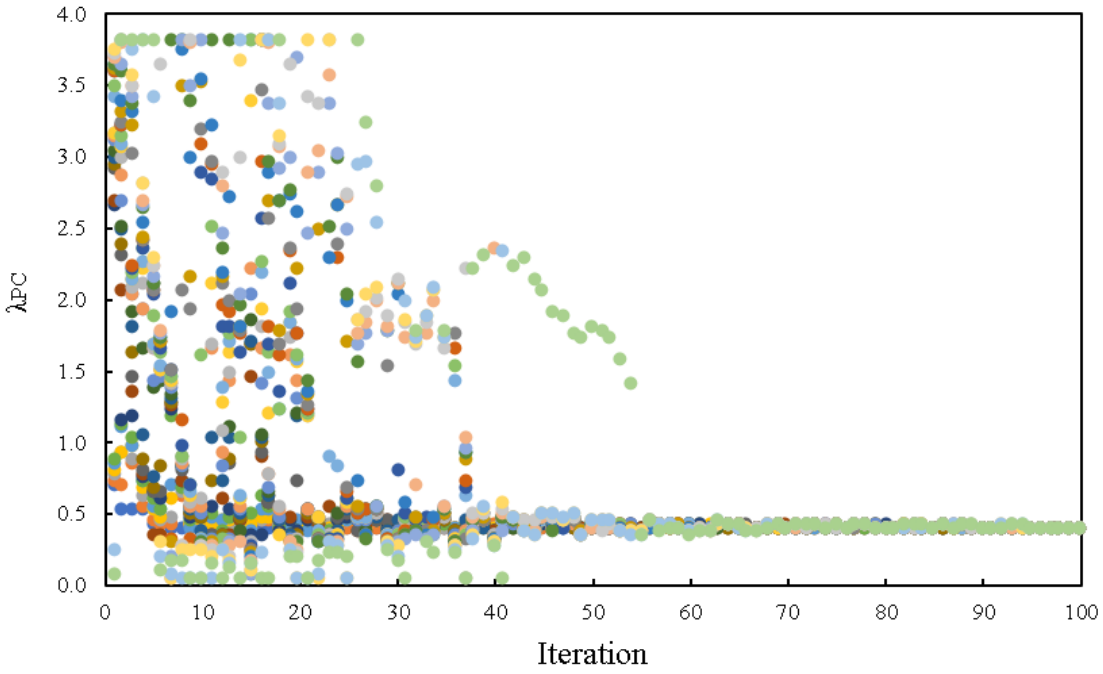

Source: own authorship.

Considering 20 optimization runs for each P_{CL} value, the result shown in Figure 3.9 is obtained. For each P_{CL}, all optimization runs converge to the same optimal. Yet, there is a slight variance in optimal designs due to a small number of sample points being used for WASM. For P_{CL} equal to 0.017 and 0.020, two optimal designs are found at $\lambda_{PC}^{*} = 0.5$ and $\lambda_{PC}^{*} = 0.8$.

Two optimal designs found for $P_{CL} \approx 0.02$ indicate two local minima. Beck et al. (2020) show that for $P_{CL} \approx 0.02$, C_{TE} has a flat behavior over a wide range of λ_{PC} values. This indicates an equivalence between considering or not the removal of columns in the structural design.

Figure 3.9 – Optimal designs for each P_{CL}.

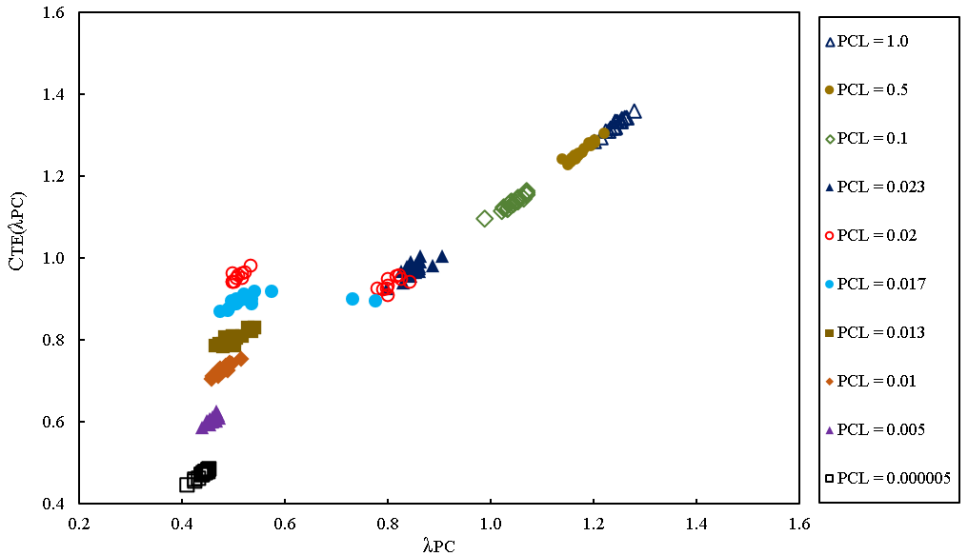

Source: own authorship.

Beck et al. (2020) call $P_{CL} \approx 0.02$ the Column Loss Probability Treshold P_{CL}^{th}, being the value above which there is positive cost-benefit in addressing APM design to mitigate progressive collapse. Figure 3.10 shows strong correspondence between the global optima of Beck et al. (2020) with those obtained via FA and WASM, confirming the framework accuracy and efficiency.

Figure 3.10 – Optimal design validation.

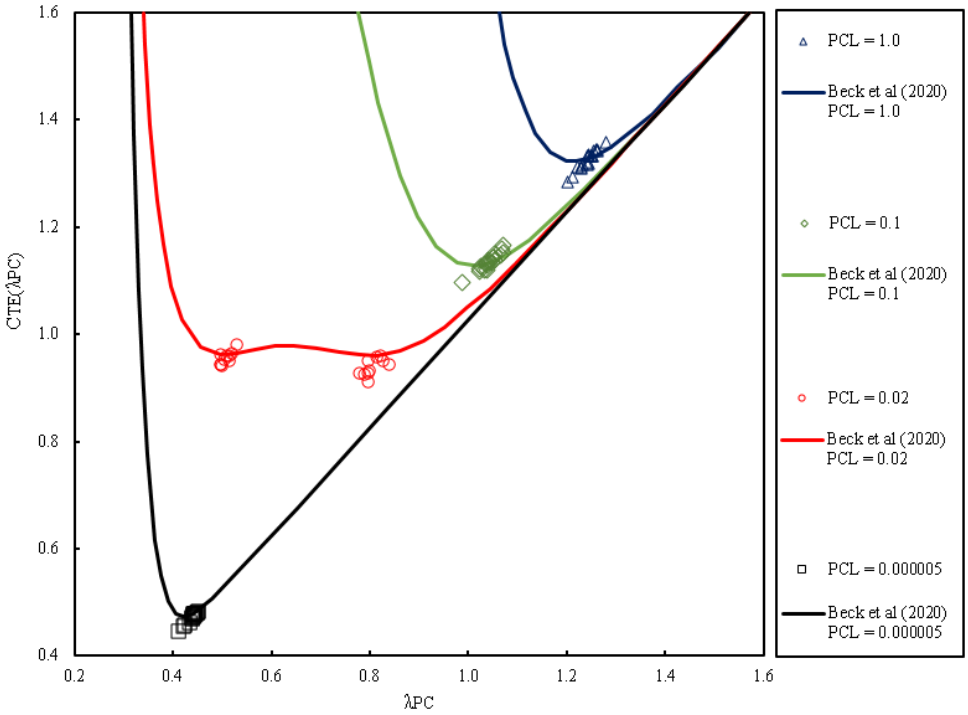

Source: own authorship, based on Beck et al. (2020).

3.4 STRUCTURAL ANALYSIS

Nonlinear FEM modeling is used to realistically address progressive collapse behavior due to a sudden column loss. As mentioned in the previous Chapter, BA is used to obtain the static pushdown curve, and EEM is used to get a pseudo-static pushdown curve. This allows to address dynamic effects in a simple, yet effective, manner. Only 2-dimensional frames are investigated in Chapter 4, so modeling relates only to beam and column spans.

Based on the mesh analysis made by Praxedes (2020), beam spans are discretized in 5 fiber displacement-based Finite Elements (FE), being 3 FEs for the beam itself and 1 at each beam end to represent the joint region. This is shown to be an efficient approach in terms of minimal refinement level and agreement with experimental data, even though beam-column joints are not explicitly modeled. Thus, each FE has 3 Gauss-Lobatto integration points. In terms of column discretization, Section 3.4.2 justifies a single linear element being used.

Corrotational transformation is used for all elements to account for large displacements due to geometrical nonlinearities. Cross-section layering consists of 200 fibers for confined concrete and 10 fibers for each face of unconfined concrete cover. This amount of fibers is used to avoid convergence issues along the entire set $\boldsymbol{S}$, especially for greater values of beam depth.

Static bay pushdown analysis is performed with a displacement-based integrator using Krylov-Newton method to solve the nonlinear problem (tolerance of 10^{-5}). An initial increment size of 1 mm is adopted, but an adaptive algorithm is used to enhance or decrease the step depending on lack or need of convergence improvement, respectively.

Two load steps are adopted for BA: a) nominal dead and live load are applied over the beam spans, also accounting for self-weight of all members on themselves; and b) if beam rebar rupture does not occur at the first stage (possible for weak beams), an increasing load is applied over the beam spans of interest until rebar rupture is verified. Parameters obtained as outputs include applied force, vertical drift, internal forces and rebar strains.

Details related to material constitutive relationship are addressed in the introduction of each example of Chapter 4, as different models were adopted in the examples. In general, a nonlinear model that accounts for elastoplastic behavior is adopted for the rebars, and uniaxial models that allows to consider confinement effects, softening, tensile strength and unilateral behavior are chosen for concrete. Although stirrups cannot be explicitly modeled, their effects over concrete core ductility can be addressed if the concrete model meets the previous requirements, with the amount of core confinement given in terms of stirrup detailing, concrete strength, and cross section geometry for each sample point.

A self-made algorithm based on Coda and Paccola (2014) was initially adopted. This nonlinear FE algorithm followed a total-Lagrangian position-based formulation, considering two translations and one rotation as degrees of freedom (DOFs) for each node. Newton-Raphson was used to find equilibrium at each loading step, and Arc-Length method was introduced to address instability stages. According to a mesh analysis, each RC beam was discretized into 14 FEs, which were layered 2D frame elements with fifth degree of approximation. A total of 20 layers with one integration point were used for transversal discretization, being 18 for concrete and one for each rebar layer.

Although proven to be accurate, the lack of advanced parallelization techniques led to tall frames requiring up to 45 min to be analyzed, making it an unfeasible tool. Hence, it was only used for the RC beam example in Section 4.2, being then replaced by OpenSees.

3.4.1 Structural analysis validation

Following Praxedes (2020), some experimental tests are chosen for a brief validation of the structural analysis model: two RC beam subassemblages from Yu and Tan (2013), one RC beam-column subassemblage from Lew et al. (2014), and one RC frame from Yi et al. (2009). Table 3.2 depicts material and geometrical parameters of each structure.

Table 3.2 – Input data for specimens used in model validation.

Parameter	RC beam non-seismic (Yu and Tan, 2013)	RC beam seismic (Yu and Tan, 2013)	Intermediate RC frame IMF (Lew et al. 2014)	RC frame (Yi et al. 2009)
Beam span (m)	2.75	2.75	6.09	2.667
Column span (m)	-	-	4.19	1.567 (1st floor) 1.100 (above)
Beam depth (mm) × width (mm)	250 × 150	250 × 150	508 × 712	200 × 100
Column depth (mm) × width (mm)	-	-	712 × 712	200 × 200
Concr. cover (mm)	20	20	50	25

continues.

conclusion.

Parameter	RC beam non-seismic (Yu and Tan, 2013)	RC beam seismic (Yu and Tan, 2013)	Intermediate RC frame IMF (Lew et al. 2014)	RC frame (Yi et al. 2009)
Top reinf. area (mm^2)	236	290	2027	226
Bottom reinf. area (mm^2)	157	157	1289	226
Column reinf. area (mm^2)	-	-	7736	452
f_c' (MPa)	31.20	31.20	32.00	20.83
f_{ctm} (MPa)	3.5	3.2	3.2	2.8
E_C (GPa)	27.60	27.60	25.57	22.82
f_y (MPa)	511	511	476	416
E_S (GPa)	200	200	200	200
ε_{su}	0.11	0.11	0.17	0.16
Stirrup diam.(mm)	6	6	12.70	6
Stirrup space (mm)	100	50	102	150
Stirrup f_{yt} (MPa)	310	310	524	370
Number of stirrup legs	2	2	2 in beams 4 in columns	2

Source: based on Yu and Tan (2013), Lew et al. (2014), and Yi et al. (2009).

As shown in Figure 3.11, the numerical force vs displacement curves show good agreement with experimental data for both the in-house FE algorithm based on Coda and Paccola (2014) and OpenSees, with slight discrepancies terms of CAA and CA stages. Both tools are appropriate in terms of structural modeling, but OpenSees is significantly faster.

Member discretization is done as previously mentioned, and nonlinear constitutive models used for each case are:

(a) in-house FE algorithm: μ Model (Mazars et al. 2015) for concrete, and bilinear elastoplastic model with isotropic hardening for rebars (Section 4.2);

(b) opensees: ConcretewBeta for concrete, and ReinforcingSteel for rebars (both in the software library, with more details in Section 4.3 and Figure 4.17).

Figure 3.11 – Model validation for progressive collapse analysis.

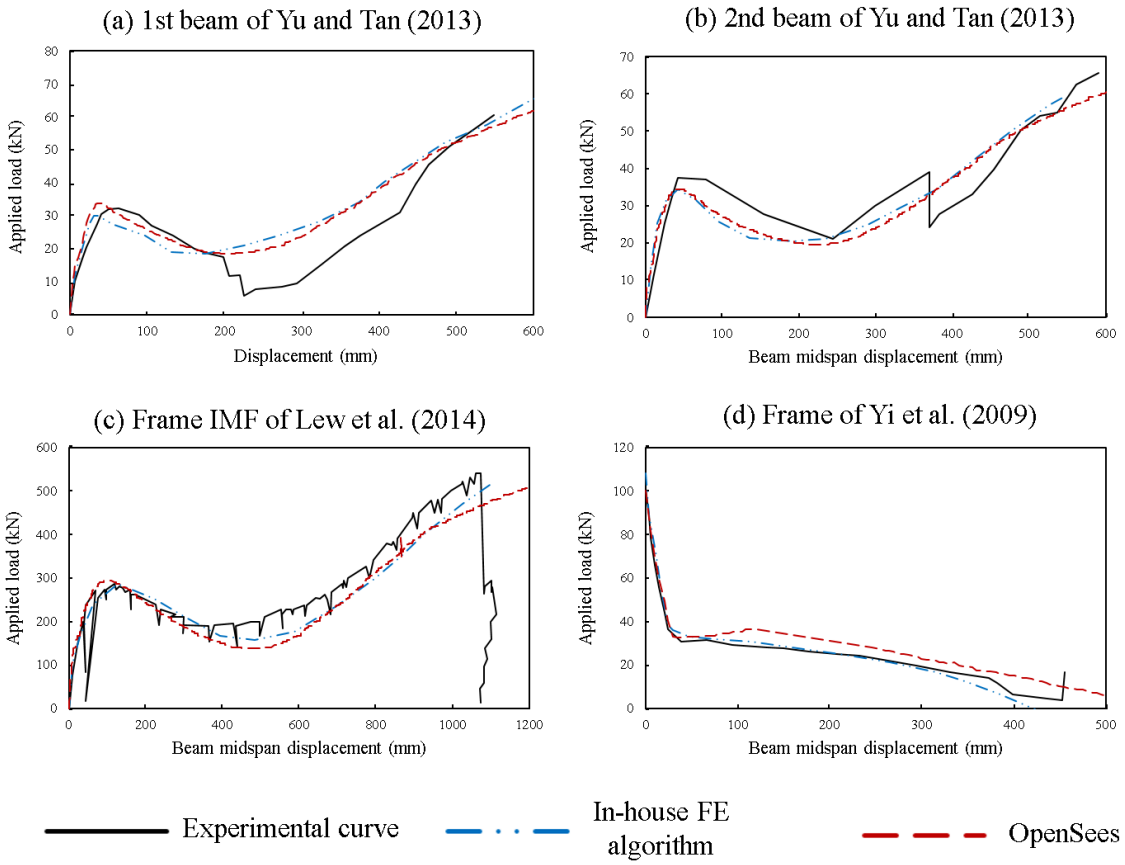

Source: own authorship.

Pushdown curves in Figure 3.11 closely match the experimental behavior for RC beams and RC frames for both structural analysis models, revealing the efficiency of the discretization approach and constitutive models for concrete and longitudinal rebars. As mentioned in Section 1.4, rebar debonding and member separation is not addressed in the analyses, justifying the continuity of the numerical pushdown curves while the experimental results show breaks due to localized fractures in rebars, stirrups, and concrete. Yet, estimation of structural capacity at CAA and CA is accurate enough for the purposes in this research, and fast enough to allow multiple structural analyses for each sample point of a large sample over $\boldsymbol{S}$ i.e. several analyses for each column loss scenario of a given structure.

3.4.2 Commentary on column discretization

Material nonlinear behavior is not addressed in column discretization to avoid sudden breaks in the pushdown curve. These disruptions are most common when addressing tall frames, but even for lower frames it can happen if columns are too weak. While the column rebars are not explicitly modeled in the linear discretization, they are accounted for when calculating the column's resistance envelope for each sample point.

Compressive rebar yielding, often related to column buckling, is the sole reason behind this tricky behavior. Tensile column rebar yielding also has an impact in the pushdown curve, but not as severe, especially in frame regions where columns are related to low axial forces.

To investigate this behavior, the primary RC frame from Scalvenzi et al. (2022) is used as reference (Figure 3.12). This structure was designed to gravity loads in accordance with EC2 1-1 (CEN, 2004), being representative of low-rise modern European RC buildings not strengthened against seismic activities. The RC frame is made of C20/25 concrete and B450C rebars, and $D_n = 3$ kN/m² and $L_n = 2$ kN/m² represent dead and live loads, respectively.

Figure 3.12 – Case-study structure.

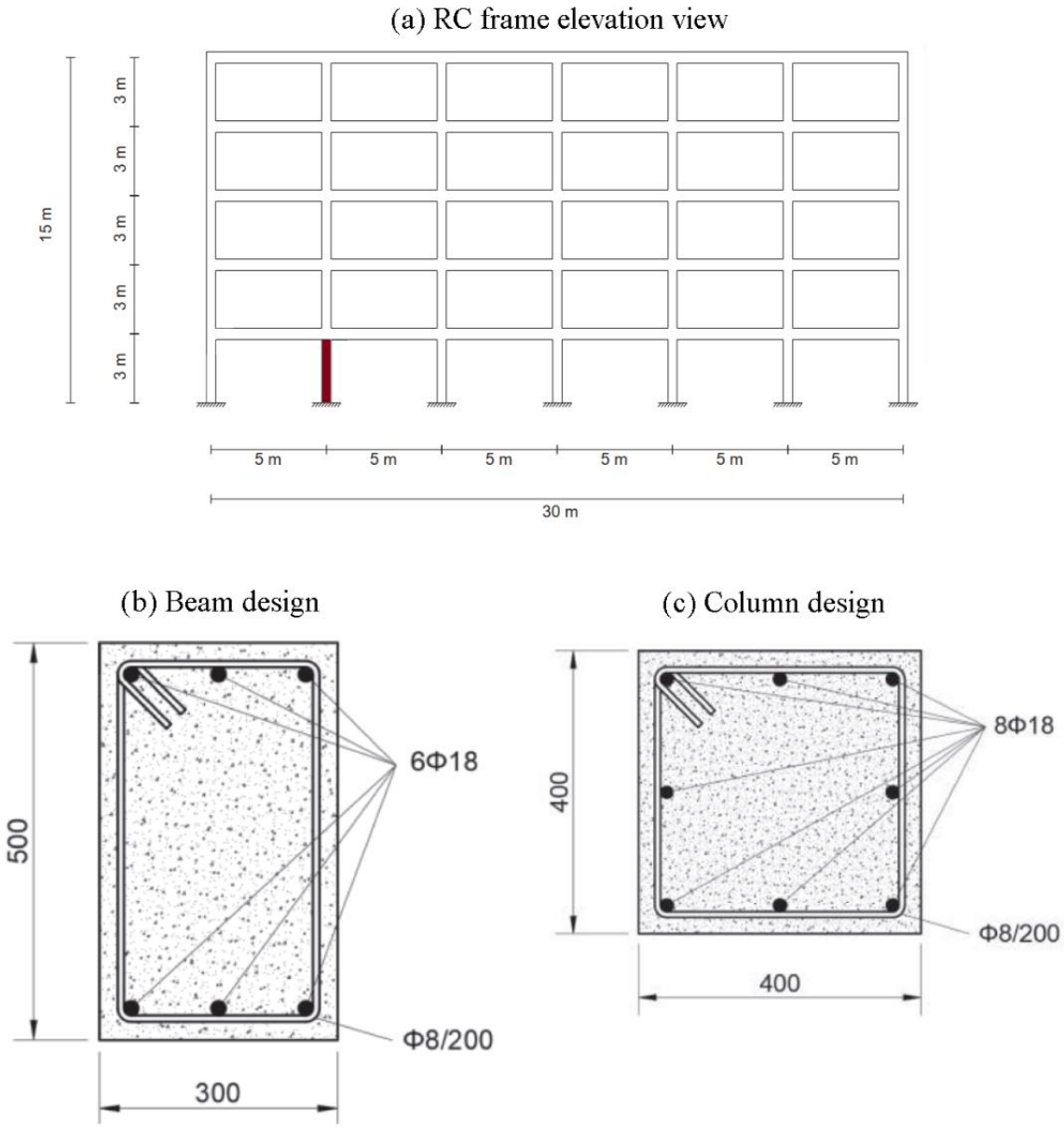

Source: adapted from Scalvenzi et al. (2022).

Only penultimate column loss is addressed. Figure 3.13 show a sensitivity analysis in terms of the beam depth h_B, ranging from 300 mm (weak beam, square cross-section) to 600 mm (strong beam), with “weak” and “strong” referring to its flexural capacity. Besides, two discretization approaches are used for the columns: (a) nonlinear columns discretized exactly as the beams (5FEs); and (b) linear columns discretized with a single FE.

Figure 3.13 shows that overall structural response is almost identical for both column modeling approaches before they reach their plastic capacity.

Figure 3.13 – Structural behavior in terms of beam depth and column capacity.

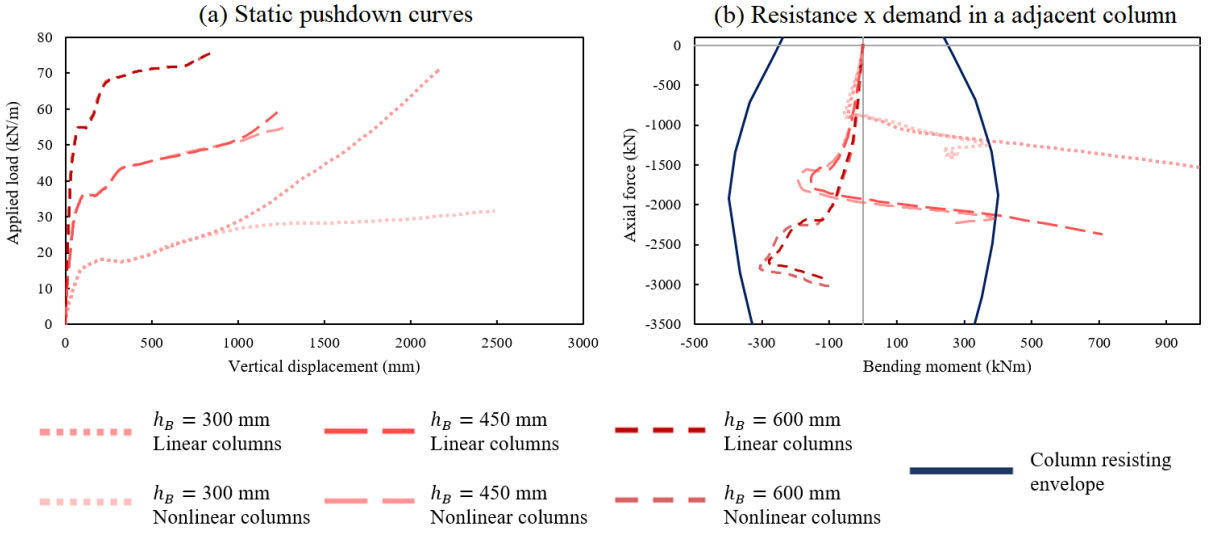

Source: own authorship.

Figure 3.13 illustrates a consistent column behavior in VA, with negative moments related to columns being pushed outwards (CAA) and positive moments referring to columns being pulled inwards (CA). Weaker beams have CA mobilized for smaller loadings, leading to severe bending moments in the adjacent columns. When force vs moment demand reaches the resisting column envelope for nonlinear column modeling, the cross-section enters a plastic stage. In the analysis shown in Figure 3.13, column rebar yielding happens in tension, so no sudden breaks are observed in the pushdown curve. Yet, the ricochet behavior observed in force vs bending diagrams is already enough to compromise surrogate efficacy.

Thus, column yielding in tension compromises the adjacent column's ability to provide sufficient lateral restraint, hindering the double-span beams from fully developing their resisting mechanisms, particularly catenary action. This relates to curve 2 in the illustrative pushdown curve of Figure 2.2.

Column yielding in tension was also shown to be common in frame regions related to lower axial forces, as depicted in the yield maps of Figure 3.14. However, these column sections entering a plastic phase have shown small influence over the pushdown behavior and over the most critical components of the VA subsystem.

Figure 3.14 – Typical mild column yielding locations.

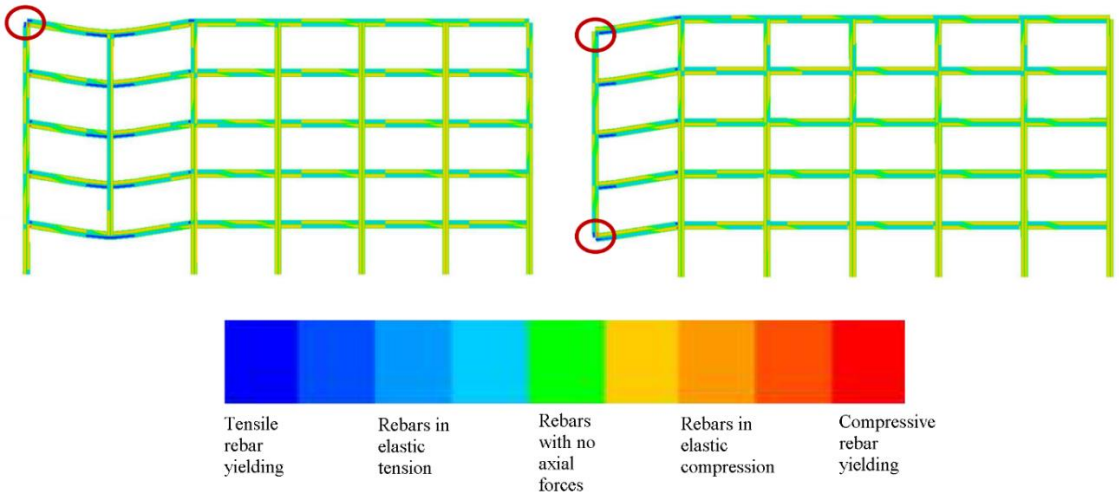

Source: own authorship.

However, when column rebar yielding happens in compression, the entire response becomes discontinuous, severely compromising further surrogate techniques. Even 30 thousand support points explicitly addressing column failure were not enough to ensure metamodeling effectiveness when columns are prone to compressive yielding and/or column buckling.

As structural disruptions are inherently related to material behavior, even the simplest nonlinear material models led to the aforementioned issues. Therefore, the most efficient solution found is to assume one linear FE for columns in structural analysis. This approach still ensures a realistic evolution of axial forces and bending moments until the resisting envelope of the column is reached (Figure 3.13).

This simplified approach allows the internal forces to go beyond the cross section resisting envelope, without a sudden force redistribution. Besides, this allows to estimate the frame load capacity at CA even though premature column failure may have happened, ensuring the needed smooth behavior across $\boldsymbol{S}$ and $\boldsymbol{\mathcal{D}}$ to enable both metamodeling stages.

The estimated pushdown curve may differ from the realistic behavior if a premature column failure is prone to occur. This, however, is not an issue for the risk-based framework. Figure 3.13 shows that column internal forces are realistically addressed until their respective resisting limit is reached.

Hence, as long as the internal forces are within these limits, the pushdown curve is realistic. Besides, when addressing expected costs of failure, premature failures have greater penalization factors when compared to ductile beam failure at CA. Hence, optimal risk-based design solutions are expected not to be prone to premature failure modes. Results in Chapter 4 confirm this.

The issues caused by compressive column rebar yielding were first noticed when investigating the taller frames of Section 4.4. Hence, the same structure from Scalvenzi et al. (2022) is addressed, but now with 20 stories. When addressing the same material and geometric parameters of the reference, Figure 3.15 shows that pushdown behavior is prematurely interrupted due to compressive yielding in both rebars located in the foot of the outermost adjacent column. The pushdown curve suddenly drops and then it increases again, leading to an ultimate beam capacity equivalent to the ultimate loading prior to the disruption. As shown in Figure 3.16, this is inherently related to plastic rebar behavior.

Figure 3.15 – Compressive rebar yielding in a frame with strong columns and respective static pushdown curve.

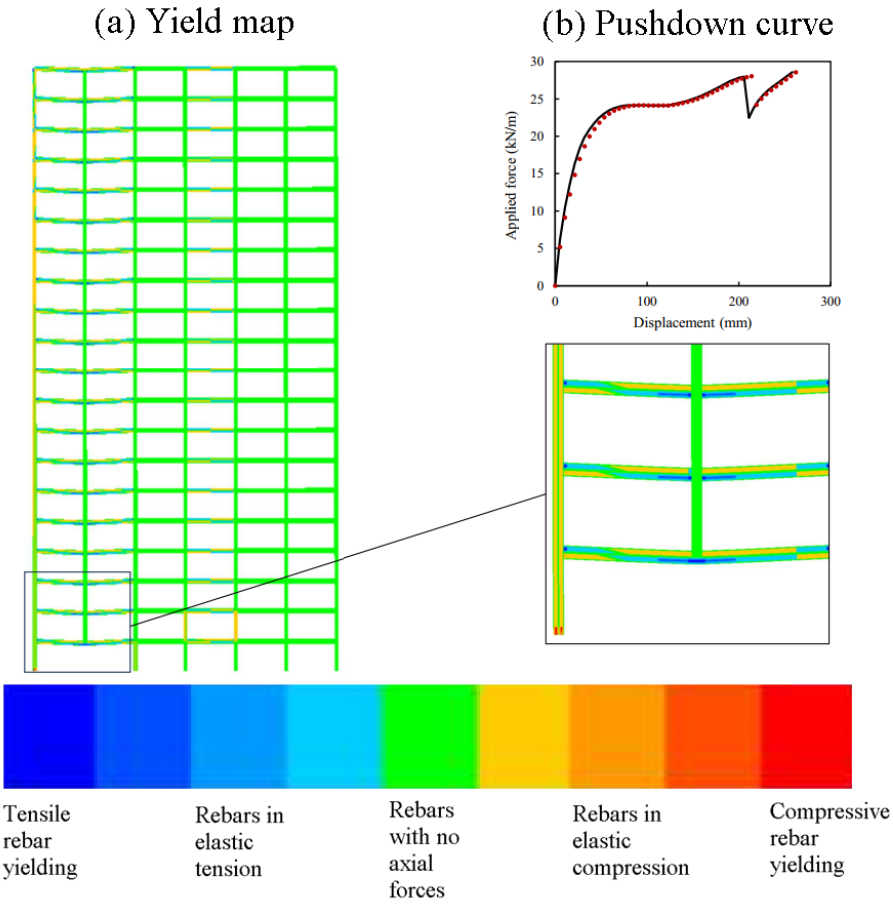

Source: own authorship.

Figure 3.16 – Rebar strains in the critical column at the instant of pushdown break.

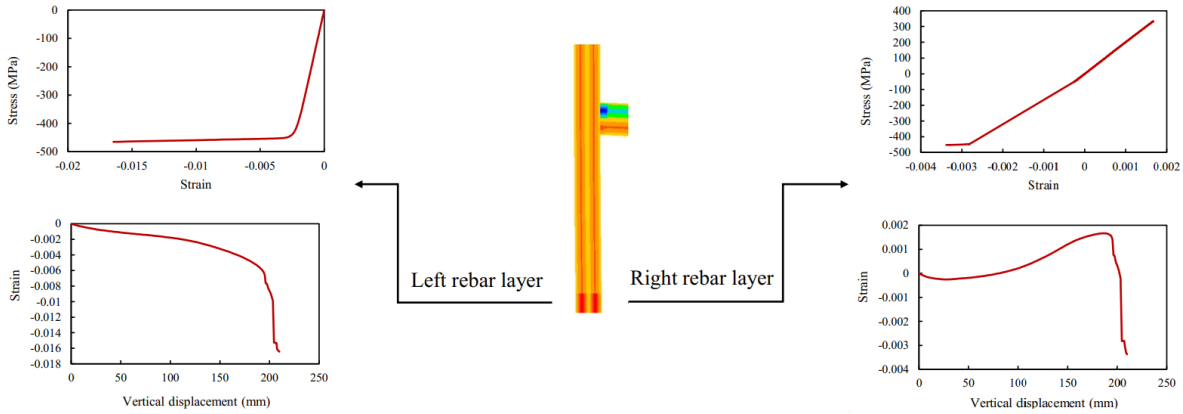

Source: own authorship.

The “break” in the pushdown curve coincides with the instant where both rebar layers reach compressive yielding (around a vertical drift of 200 mm). The pushdown curve “recovery” coincides with compressive strains in the outer-most rebar layer reaching values above ε_{sh} (adopted as 0.03), characterizing the hardening rebar phase.

Small load steps were needed after to accurately depict the buckling behavior (Baumgardt et al. 2023). Pushdown curves in Figures 3.15 and 3.17 show results for greater overall refinement level (continuous black lines) and greater refinement only for the critical frame regions (red dotted lines).

Figure 3.17 shows that weak column configurations (exaggerated low depth and width of 250 mm) have a severely worst behavior. Not only the adjacent columns are affected, but several other column spans in the vicinity also sustain buckling. Ultimate beam capacity is significantly below the peak capacity prior to the instability in pushdown behavior, and axial forces originally transmitted to the adjacent columns are redistributed to other columns.

Several attempts were made to enable metamodeling while realistically addressing the pushdown instability due to column compressive yielding. The breaks related to these events are not caused by mistakes in structural analysis, but due to intrinsic material properties. Hence, in an idealized scenario, it would be convenient to address this. Yet, only linear column modeling was found to allow further surrogate usage.

As previously stated, column internal forces realistically increase until their respective resisting envelope is reached, and structural configurations related to premature column failure (expected demands beyond resisting limits) are greatly penalized in RO. Hence, optimal risk-based design solutions are expected to not be prone to premature column failure.

Figure 3.17 – Pushdown curve with column buckling.

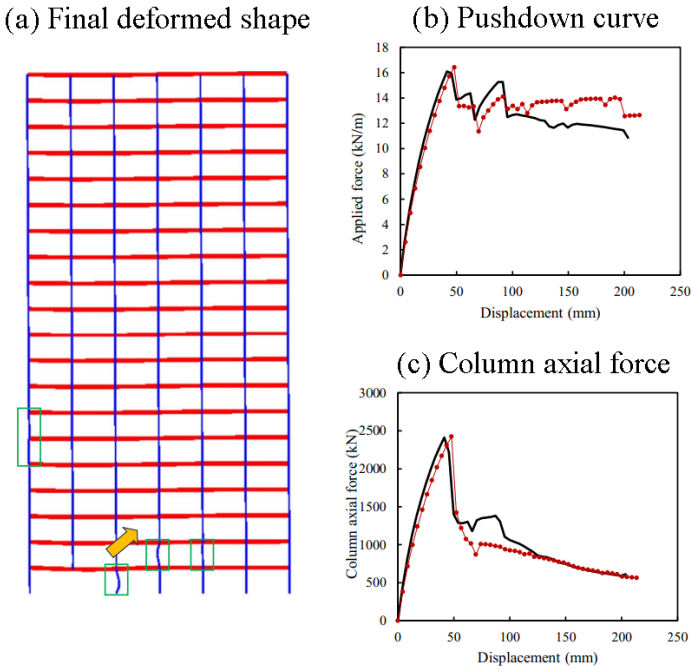

Source: own authorship.

3.5 METAMODELING STRATEGIES

If not for metamodeling, this research would not have been possible. Since a large sample is needed to ensure good P_f estimates via WASM, especially when random design variables with low uncertainty are addressed, simplified models based on support points accurately analyzed were shown to be key-factors in this framework.

Kriging was the first metamodeling technique to be addressed. It considers that a complex model of interest can be approximated by a stochastic process (Kroetz et al. 2020):

$$\tilde{Y}(\boldsymbol{x}) = f(\boldsymbol{x})^T \boldsymbol{A} + Z(\boldsymbol{x}) \tag{3.11}$$

where the first term relates to a deterministic mean value function and the second term is a Gaussian process with a constant mean equal to zero; $f(\boldsymbol{x})$, in this work, is a basis of polynomial functions; and $\boldsymbol{A}$ is a vector of coefficients associated to correlations between responses at different support points:

$$\boldsymbol{A} = (\boldsymbol{F}^T \boldsymbol{R}^{-1} \boldsymbol{F})^{-1} \boldsymbol{F}^T \boldsymbol{R}^{-1} \boldsymbol{B} \tag{3.12}$$

where $\boldsymbol{B}$ is the vector with the original responses of the high-fidelity model in the support points; $\boldsymbol{R}$ is the correlation matrix between pairs of support points; $\boldsymbol{F}$ is the regression matrix with the basis functions evaluated at the support points. The terms R_{jk} in the correlation matrix are obtained, in this work, by:

$$R_{jk}\left(x_j - x_k, \theta\right) = \Pi_{i=1}^{n} \exp\left(-\theta_i \, d_i^2\right) \tag{3.13}$$

with d_i being the distance between support points in the i direction, and $\boldsymbol{\theta}$ the hyperparameter vector that defines the correlation length of the stochastic field $\tilde{Y}(\boldsymbol{x})$. Both correlation matrix and coefficient vector $\boldsymbol{A}$ depend on $\boldsymbol{\theta}$. In this work, the hyperparameter vector is defined based on the minimization of the Maximum Likelihood Function in Dubourg (2011). As in RO, FA is also used for this purpose:

$$\boldsymbol{\theta} = \arg\min_{\vec{\theta} \in \mathbf{n}_{\boldsymbol{\theta}}} \mathcal{L}(\boldsymbol{\theta}) = \sigma_Z^2(\boldsymbol{\theta}) \, |\boldsymbol{R}(\boldsymbol{\theta})|^{1/n} \tag{3.14}$$

where the stochastic field variance σ_Z^2 is given by:

$$\sigma_Z^2 = \frac{1}{n_{sup}} \, (\boldsymbol{B} - \boldsymbol{F}\boldsymbol{A})^T \, \boldsymbol{R}^{-1} \, (\boldsymbol{B} - \boldsymbol{F}\boldsymbol{A}) \tag{3.15}$$

Given the hyperparameter vector $\boldsymbol{\theta}$, the coefficient vector $\boldsymbol{A}$ and stochastic field variance σ_Z^2, it is possible to estimate the high-fidelity model response by:

$$Z(\boldsymbol{x}) = r(\boldsymbol{x})^T \, \boldsymbol{R}^{-1} \, (\boldsymbol{B} - \boldsymbol{F}\boldsymbol{A}) \tag{3.16}$$

where $r(\boldsymbol{x})$ is a vector containing the correlation between the model response at point $\boldsymbol{x}$ and the responses in the support points.

One of the main advantages of kriging, in relation to other metamodeling techniques, such as neural networks and polynomial chaos expansions, is knowing the model variance at any point in the domain. This allows support point adaptability in regions of greater variance:

$$\sigma^2(\boldsymbol{x}) = \sigma_Z^2[1 - r^T(\boldsymbol{x}) \, \boldsymbol{R}^{-1} \, \boldsymbol{r}(\boldsymbol{x}) + \boldsymbol{u}^T(\boldsymbol{x}) \, (\boldsymbol{F}^T \, \boldsymbol{R}^{-1} \, \boldsymbol{F})^{-1} \, \boldsymbol{u}(\boldsymbol{x})] \tag{3.17}$$

with $\boldsymbol{u(x) = F^T R^{-1} r(x) - f(x)}$. Thus, kriging recovers the high-fidelity response at the support points (Beck, 2019; Kroetz, 2018; 2019; Kim and Boukouvala, 2020).

In this thesis, more specifically for continuous RC beams, kriging is used to estimate structural behavior and reliability indexes for larger samples based on a relatively small number of support points, always following the maximum local variances $\sigma^2(\boldsymbol{x})$ to ensure that no region of the domain is lacking support points.

Kriging was shown to be a key-feature when addressing risk-based optimization of RC beams. However, it became too slow and complex when advancing to planar RC frame analysis. Since more outputs need to be estimated, the number of $\boldsymbol{R}$ matrix inversions, hyperparameter calibrations and overall matrix operations were greatly increased.

Hence, Inverse Distance Weighting (IDW) was chosen to address the compromise between computational burden and accurate enough estimations when dealing with frames. It is not as accurate as kriging, but it is significantly faster and accurate enough in terms of the objectives of this work. As shown in Figure 3.18, IDW consists on estimating the behavior in given sample point in terms of the known answer in its closest support points by means of weighted average estimation (Shepard, 1968).

This technique is commonly used to map surfaces in several applied areas, such as geoprocessing (Figure 3.18), environmental modeling (air quality, temperature, rainfall), soil mapping, and others. Its formulation closely resembles the P_f estimation via WASM (Eq. 3.3), with weights given in terms of the inverse of the distance between points, and the known answers being used instead of an index function. Unlike kriging, IDW does not have a formulation that allows estimating the error and dispersion of estimates in any region of the domain. Its advantage is its low computational cost. This is the simplest efficient approach found, with its simplicity compensating its significant reduction in the computational burden.

Figure 3.18 – IDW concept

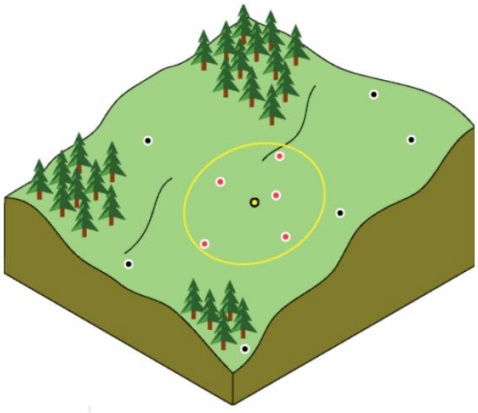

Source: ArcGIS Pro (2024).

In order to briefly address the efficiency of both metamodeling techniques, Figure 3.19 shows dispersion curves in terms of ultimate beam capacity for a small RC frame under middle and external column loss scenarios. A total of 1000 support points are analyzed via FEM in terms of changing values of beam depth, column size (square cross-section), beam reinforcement and column reinforcement. Then, 70 new sample points are estimated via FEM, kriging and IDW to build the dispersion curves. In this short example, only the 10 closest support points are used for IDW estimation.

As expected, kriging shows better accuracy than IDW, but overall results can be improved by using more support points. Hence, RC frame examples in Chapter 4 uses 2000 support points, and IDW is done considering all support points with non-dimensional weight greater than 0.1, leading to roughly 20 to 30 support points for each estimation.

More accurate surrogate approaches, such as Artificial Neural Networks or Adaptive Kriging, could have been used at least in the 2nd metamodeling stage to address P_f in RO (Gomes and Beck, 2013; Kroetz, 2019). However, as previously mentioned, the simplicity and faster computational time of IDW were deemed appropriate for the scope of this work and the large number of parameters requiring simultaneous estimation. Besides, there is no need for estimating probabilities of failure below 10^{-5} with great accuracy due to related expected costs of failure becoming negligible past this point.

Figure 3.19 – Brief metamodeling comparison.

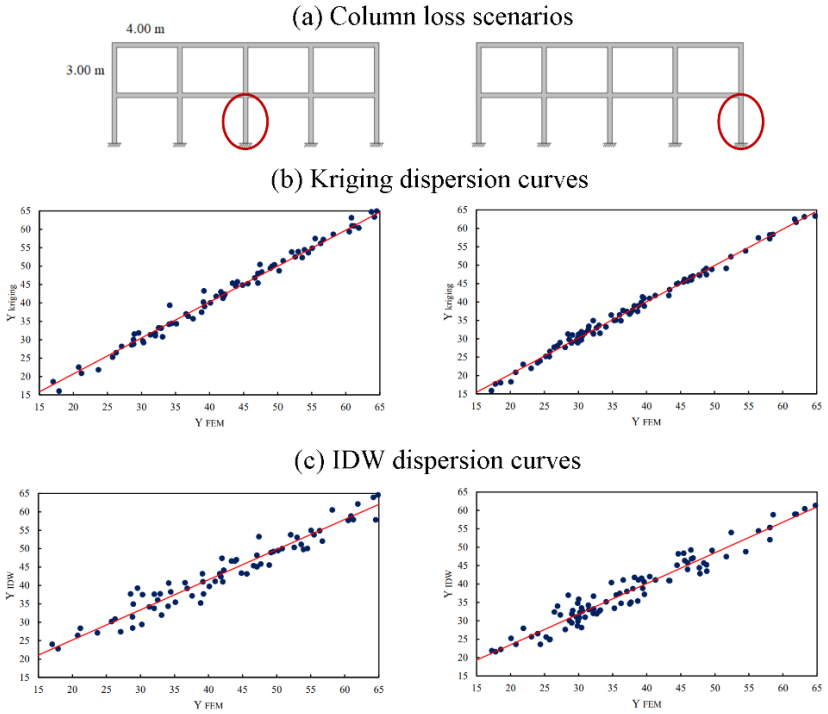

Source: own authorship.

3.6 FRAMEWORK LIMITATIONS AND CHALLENGES

The developed framework comprises a series of complex, sequential steps, where errors from early stages propagate and amplify through subsequent stages, resulting in a magnified final error. Nonetheless, as demonstrated in the validation examples, the framework achieved strong alignment between experimental and numerical results for structural analysis, as well as for risk optimization combined with reliability analysis.

The greatest challenge in implementing the framework lies in managing the computational burden associated with linking all sequential steps effectively. The later examples in Chapter 4 adopt strategies in structural analysis and surrogate modeling that prioritize time efficiency while maintaining the necessary accuracy and precision of estimates. Furthermore, the precision of small failure probability estimates due to WASM is less critical, as the corresponding expected failure cost will naturally approach zero in the optimization stage, ensuring minimal impact on overall results.

For surrogate modeling, kriging displayed the lowest error, requiring fewer support points to maintain accuracy, whereas IDW demanded more support points to achieve comparable error levels, albeit with a faster computation speed. Potential strategies to further reduce error in future research include adaptive kriging with optimized learning functions (Kroetz, 2019), advanced parallelization methods, and Latin hypercube sampling with iterative adjustments to improve sample uniformity (Sheikholeslami and Razavi, 2017).

Thus, each example in Chapter 4 presents slight adaptations from the general framework, which serves as an overarching methodology. The first example, due to its simplicity, omits the metamodeling stages. In contrast, the second example incorporates ordinary kriging as a surrogate, while the third and fourth examples employ IDW to meet the requirements of more complex scenarios.

The second example utilizes a self-developed finite element (FE) algorithm; however, due to the code’s limited parallelization and optimization, OpenSees was selected for the third and fourth examples to facilitate faster analysis of full reinforced concrete (RC) frames. While the examples from the second to fourth follow the general framework steps, they feature minor variations in the specific techniques applied for structural and reliability analysis.

4 RESULTS

Progressive collapse is a complex mechanism of cascading failures triggered by an initial local damage. Large displacements are expected, materials are stressed to their limits, and all members of the structural system may act together both in the resisting mechanism and in promoting collapse propagation. For instance, beam and column spans above and adjacent to a missing column create a Vierendeel Action mechanism that is essential in the frame load-bearing capacity. Even infill walls have been found to contribute in the frame load-carrying capacity. Yet, excessive horizontal forces in adjacent columns, which are transmitted by the double span beams in Catenary Action above a lost column, may trigger a zipper –type progressive collapse, or even domino-type, causing a greater final damaged extent.

Due to its natural complexity and the number of distinctive contributions provided by structural and nonstructural factors, results in this work are shown following an increasing amount of complexity in terms of progressive collapse simulation. This promotes the comprehension on how each random variable, modelling strategy, column loss scenario and systemic behavior intricacies influence over the optimal risk-based design, thus allowing a clear presentation for each factor.

Following Beck et al. (2020), the risk-based optimization consists on minimizing the total expected costs C_{TE}, given in Eq. 4.1, for all studied cases.

$$C_{TE}(\boldsymbol{d}) = C_M(\boldsymbol{d}) + \sum_{i=1}^{NIF} C_{ef,i}(\boldsymbol{X}, \boldsymbol{d}) + \sum_{k=1}^{NCL} \sum_{j=1}^{NCLF} C_{ef,kj}\left(\boldsymbol{X}, \boldsymbol{d}, P_{LD_k}\right) \tag{4.1}$$

where C_M is the construction cost; C_{ef} is the expected cost of failure; *NIF* and *NCLF* represent the number of failure modes for intact and each column loss scenario, respectively; and NCL stands for the number of column loss scenarios. Vector $\boldsymbol{X}$ relates to the random variables, while vector $\boldsymbol{d}$ corresponds to the mean value to be optimized for each random design variable.

As mentioned in section 3.1, the possibility of sudden column loss is addressed by the probability of local damage $P_{LD} = P[LD|H]P[H]$. This term allows to consider progressive collapse analysis independent of a series of subjective factors that could make a building prone to one or more kind of hazards.

Hence, for each example P_{LD} increases from a very small value up to a large value, ensuring that risk-based optimal designs encompass scenarios where progressive collapse may be neglected, scenarios where it is too relevant to be ignored, and intermediate situations.

In real life situations the main interest is to define if a building needs to be strengthened against collapse propagation. Threshold values of P_{LD} define when the strengthening cost against progressive collapse compensates the reduction of expected costs of failure. Hence, the decision to reinforce a particular building should take into account if $P[LD|H]P[H]$ is above or below the threshold P_{LD}^{th}, and this relies on a meticulous risk assessment that is out of the scope of this study. In this work, the reader must be aware that the objective is not to define if the studied structures must be strengthened against progressive collapse, but to comprehend how this LPHC event affects the optimal configuration of reinforced concrete frame structures.

4.1 RC BEAM SUBASSEMBLAGE – ANALYTICAL APPROACH

The first example deals with a double span RC beam subassemblage subjected to middle column loss, with progressive collapse being treated considering structural linear analysis. This allows an initial and basic comprehension on how the optimal reinforcement changes when the local damage probability changes from a negligible value to a significant figure.

Results in this subsection are based on the conference paper by Ribeiro and Beck (2020), but updated accordingly to the feedback given in the event. In this manuscript, this and all further examples uses Firefly Algorithm to solve the optimization problem since it is simpler, consolidated in the literature, suitable for highly nonlinear objective functions and do not rely on gradient quantification for the limit states.

Figure 4.1 illustrates the study object of this example, which is a RC beam subassemblage tested by Yu and Tan (2013) extracted from a perimeter RC frame. Each beam span has 6.00 m, rectangular cross section with depth of 500 mm and width of 300 mm, concrete strength f_c' of 32 MPa, and concrete cover of 40 mm.

Columns have length of 4 m at the first floor and 3.3 m at upper floors, squared cross sections of 500×500 mm^2, and were assumed to provide great lateral stiffness for the beams tested experimentally. This justified considering just the RC beam subassemblage in the reference paper, and the same is done in this example and the next one. The impact of this simplification is addressed in Section 4.5.

Following Yu and Tan (2013), a design dead load of 7.1 kN/m² and design live load of 4.8 kN/m² are considered. One-way floor systems lead to a nominal dead load $D_n = 23.3$ kN/m and live load $L_n = 14.4$ kN/m on the beams. The lost column is located at the first floor of a perimeter frame, in the middle of the continuous RC beam.

The reference beam is designed in accordance with ACI 318-05 (ACI, 2005) for both seismic and non-seismic detailing. Yu and Tan (2013) show the stirrup detailing for 50% scaled specimens, with Φ6 @100 mm (stirrups with 6 mm of diameter spaced by 100 mm) for non-seismic design and Φ6 @50 mm for seismic design. Considering the same transverse reinforcement ratio ρ_{st} for the full-scale structure leads to Φ10 @130 mm for non-seismic design ($\rho_{st} \approx 0.39\%$) and Φ10 @70 mm for seismic design ($\rho_{st} \approx 0.77\%$). Both designs have beam depth of 500 mm and stirrups with equal diameter, with differences relying on the longitudinal reinforcement ratio and stirrup spacing.

Figure 4.1 – Location of the reference RC beam (a and b) and structural model adopted for both scenarios (c and d), showing loadings, constraints, shear and bending diagrams.

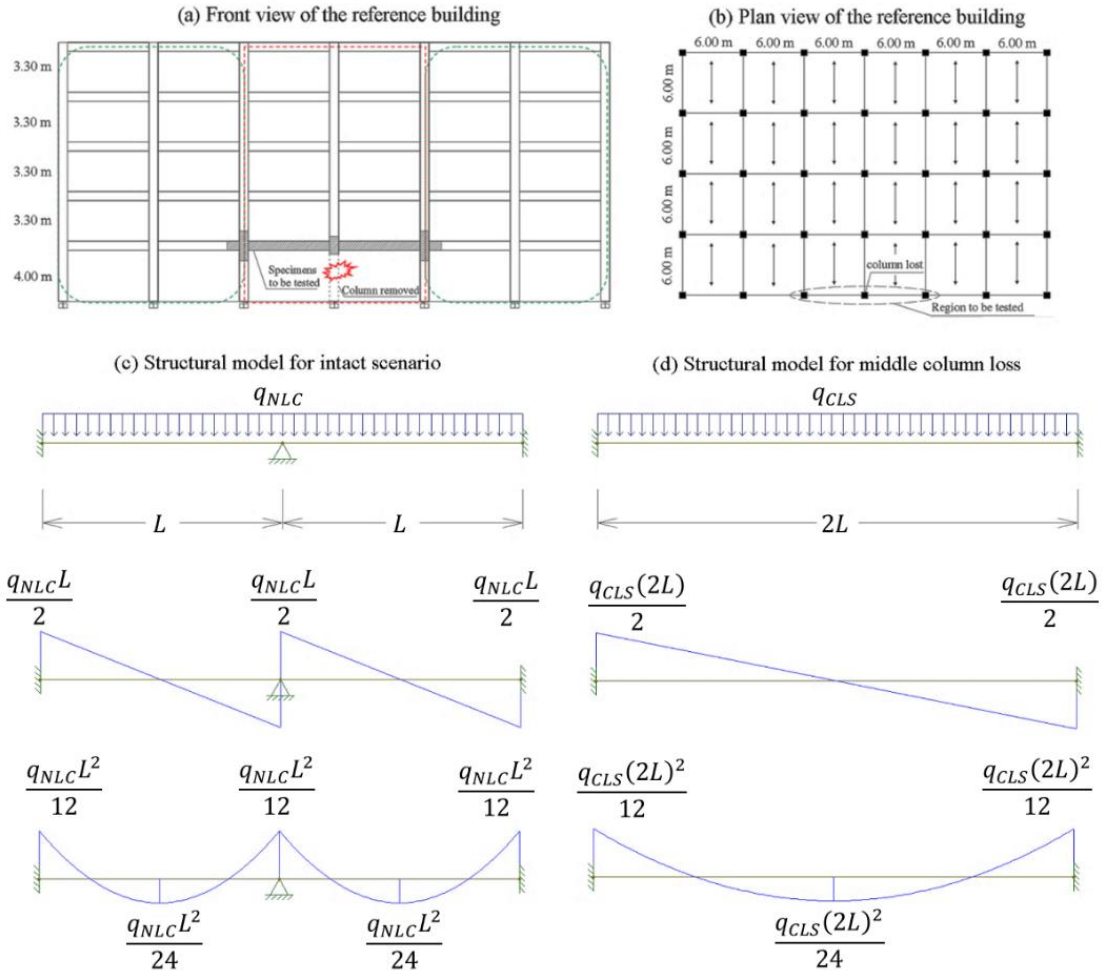

Source: adapted from Yu and Tan (2013).

The risk optimization problem is based on the formulation proposed by Beck et al. (2020), with total expected cost C_{TE} given in Eq. 4.1 adapted for this problem:

$$C_{TE}(\boldsymbol{d}) = C_M + \sum_{i=1}^{NIF} k_i P_{fi} C_M + P_{LD} \sum_{j=1}^{NCLF} k_j P_{fj} C_M \tag{4.2}$$

For both scenarios, ultimate failure modes of beam bending and shear are addressed. Construction cost C_M is given in terms of $(\boldsymbol{d})$, while the probabilities of failure in Eq. (4.2) are functions of $(\boldsymbol{X}, \boldsymbol{d})$, but this is omitted for notation convenience.

The design parameters to be optimized are the top and bottom longitudinal rebar areas (A_B and A_T) and stirrup spacing (s_t). Two cases of transversal reinforcement are addressed: 2- and 3-legged stirrup across the beam depth. Random design variables with low uncertainty are assumed in order to allow WASM for reliability analysis, so $\boldsymbol{d} = \{A_B, A_T, s_t\}$ is the mean value of a random variable in vector $\boldsymbol{X}$.

Brazilian SINAPI database is adopted to estimate C_M in Brazilian Reais (R$), where unencumbered costs for São Paulo regarding the period of April 2024 are considered. Later, C_M is converted to Euros (€) at a rate of € 1.00 equal to R$ 5.28 (as of April 9, 2024).

In this example, C_M is composed by cost of formwork, concrete and steel rebars, as well as corresponding workmanship. The cost-benefit analysis is done by solving the optimization problem given by:

$$\begin{gathered} \text{find } \boldsymbol{d}^* \\ \text{which minimizes } C_{TE}(\boldsymbol{d}) \\ \text{subject to } \boldsymbol{d} \in \boldsymbol{\mathcal{D}} \end{gathered} \tag{4.3}$$

where $\boldsymbol{\mathcal{D}}$ is a matrix of side constraints, and Eq. (4.3) is solved via firefly algorithm. The uncertainties considered in this example are shown in Table 4.1, and ultimate limit state functions are shown in Table 4.2.

Table 4.1. Uncertainty modeling.

Category	RV	Distribution	Mean	Standard deviation	Coefficient of variation
Geometry	Beam depth (h)	Normal	500 mm	1 mm	-
	Bottom rebar area (A_B)	Normal	To be optimized*	-	0.05
	Top rebar area (A_T)	Normal	To be optimized*	-	0.05
	Stirrup spacing (s_t)	Normal	To be optimized*	-	0.05 (assumed)
Material	Concrete compressive strength (f_c')	Lognormal	32 MPa	-	0.12
	Rebar yield strength (f_y)	Normal	510 MPa	-	0.05
Loads	Dead load (D)	Normal	$1.05D_n$	-	0.10
	50-year live load (L_{50})	Gumbel	$1.00L_n$	-	0.25
	Arbitrary point in time live load (L_{apt})	Gamma	$0.25L_n$	-	0.55

Source: Ellingwood and Galambos (1982), JCSS (2001), Real, Campos Filho and Maestrini (2003), Wisniewski et al. (2012), Santiago (2018), Santiago and Beck (2018), Parisi et al. (2018), Costa and Beck (2024a; 2024b).

Table 4.2. Failure mode assessment.

Scenario	Failure mode	Cost factor k	Limit state function
Intact structure (I)	Bending failure at the beam midspan	30	$g_{I,BM}(\boldsymbol{x}) = M_{RM} - \frac{q_{NLC}L^2}{24}$
	Bending failure at the beam ends	30	$g_{I,BE}(\boldsymbol{x}) = M_{RE} - \frac{q_{NLC}L^2}{12}$
	Shear failure	60	$g_{I,SH}(\boldsymbol{x}) = V_R - \frac{q_{NLC}L}{2}$
Column loss (CL)	Bending failure at the beam midspan	50	$g_{CL,BM}(\boldsymbol{x}) = M_{RM} - \frac{q_{CLS}(2L)^2}{24}$
	Bending failure at the beam ends	50	$g_{CL,BE}(\boldsymbol{x}) = M_{RE} - \frac{q_{CLS}(2L)^2}{12}$
	Shear failure	80	$g_{CL,SH}(\boldsymbol{x}) = V_R - \frac{q_{CLS}(2L)}{2}$

Source: own authorship.

where M_{RM} is the resisting midspan bending moment; M_{RE} is the resisting bending moment at the beam ends; and V_R is the shear strength.

All resistance terms are obtained according to ACI 318-19 (ACI, 2019), and demand terms in Table 4.2 are obtained for each sample point following shear and bending diagrams shown in Figure 4.1. Each scenario has its own loading condition, with $q_{NLC} = h_B b\gamma_c + D + L_{50}$ for the Normal Load Condition (NLC) of a intact structure, and $q_{CLS} = h_B b\gamma_c + D + L_{apt}$ for Column Loss Scenario (CLS). No Dynamic Amplification Factor is adopted for CLS in this initial approach.

4.1.1 Optimal design solutions

Figure 4.2 depicts the behavior of each optimal design variable for increasing values of column loss probabilities P_{LD}. For each P_{LD}, a total of 10 optimization runs are performed, each one with 40 fireflies, 100 iterations, and an initial iteration of 10000 fireflies to provide a fast auxiliary extensive search over $\boldsymbol{\mathcal{D}}$. In the following depiction, superscript $(\cdot)^*$ represents the optimal value of the given design variable.

Figure 4.2 - Optimal design for each P_{LD} and corresponding total expected cost C_{TE}.

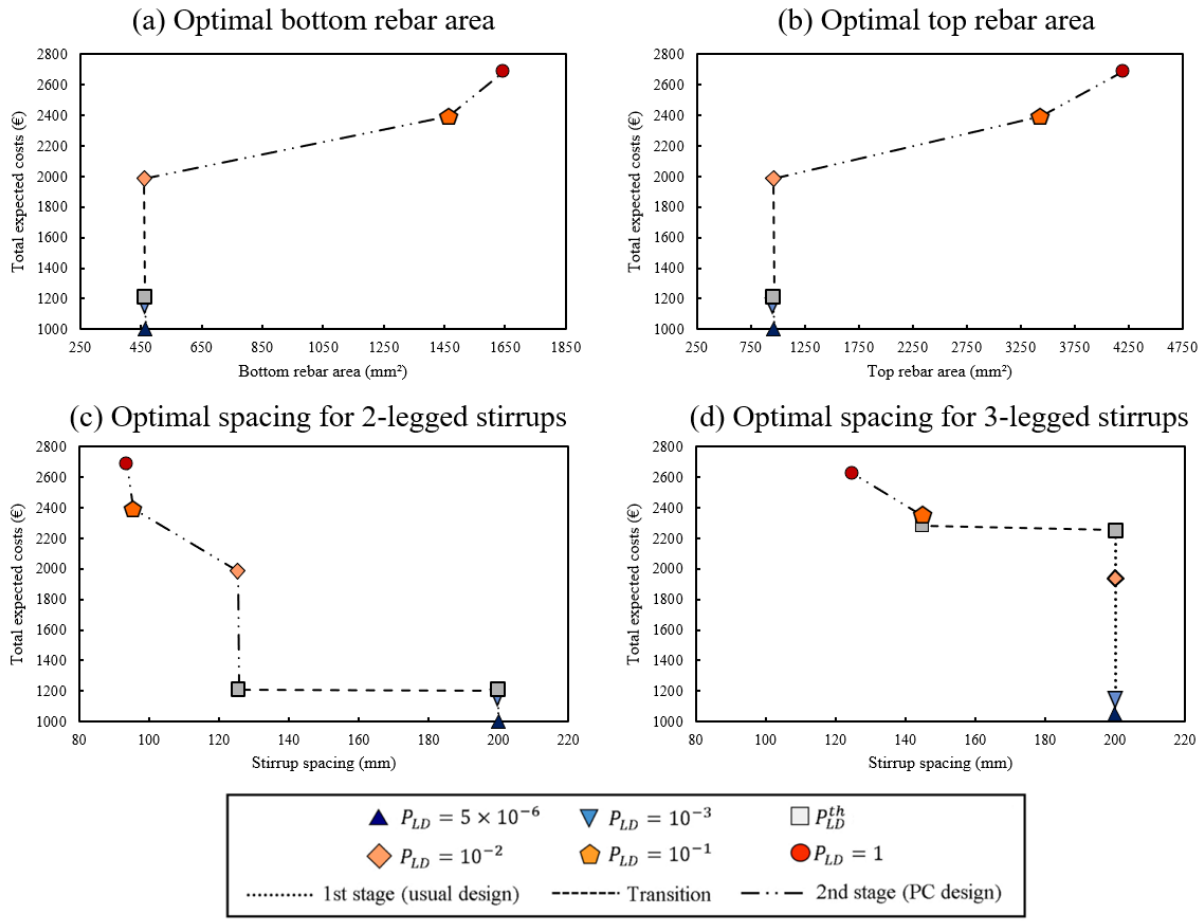

Source: own authorship.

Optimal design solutions show small variability for all values of P_{LD}, revealing an effective calibration of the optimization algorithm parameters and the effectiveness of combining it to an auxiliary extensive search. Optimal results for A_B and A_T are identical for both cases of stirrup detailing, justifying they being shown just once in Figure 4.2.

Multiple optimal configurations are observed for each stirrup configuration: at $P_{LD} \approx 1.5 \times 10^{-3}$ for 2-legged stirrups, and at $P_{LD} \approx 1.35 \times 10^{-2}$ for 3-legged stirrups. The optimal design remains constant until these threshold P_{LD}^{th} values are reached, but then two local optimal solutions are found at them: one identical to those previously found, and a strengthened new one. Beyond these values, the total reinforcement increases as P_{LD} rises.

This characterizes a transition in optimal design behavior, reflecting stages of negligible and significant threat of column loss before and after threshold, respectively. In the 1st stage the optimal configuration is controlled by the normal loading condition (NLC), hence a typical design for intact structure is obtained. Larger values of P_{LD} above threshold characterize the 2nd stage, with optimal designs adapting to resist progressive collapse threats.

Optimal results with an equivalent real-life detailing and reinforcement ratios are shown in Table 4.3. Figure 4.3 shows the evolution of manufacturing cost (C_M) and total expected cost (C_{TE}) with P_{LD}. Figure 4.4 shows the evolution of the optimal conditional reliability indexes β^* with P_{LD} for the different NLC and CLS failure modes. Figure 4.5 shows how the expected costs of each failure mode (C_{ef}) behaves as P_{LD} increases.

Table 4.3. Optimal reinforcement ratios.

Design variable	2 legged stirrups			3 legged stirrups		
	1st stage	Transition	2nd stage	1st stage	Transition	2nd stage
A_B^* (mm²)	465 (~3Φ14)	465 (~3Φ14)	1645 (~3Φ27)	465 (~3Φ14)	1492 (~3Φ25)	1763 (~3Φ27)
ρ_B (%)	0.31	0.31	1.10	0.31	0.99	1.18
A_T^* (mm²)	961 (~3Φ20)	961 (~3Φ20)	4194 (~5Φ32)	961 (~3Φ20)	3400 (~5Φ29)	3965 (~5Φ32)
ρ_T (%)	0.64	0.64	2.80	0.64	2.27	2.64
s_t^* (mm)	200	125	94	200	145	126
ρ_{st} (%)	0.17	0.26	0.36	0.25	0.35	0.40

Source: own authorship.

Figure 4.3 - Behavior of manufacturing cost C_M and total expected cost C_{TE} with P_{LD}.

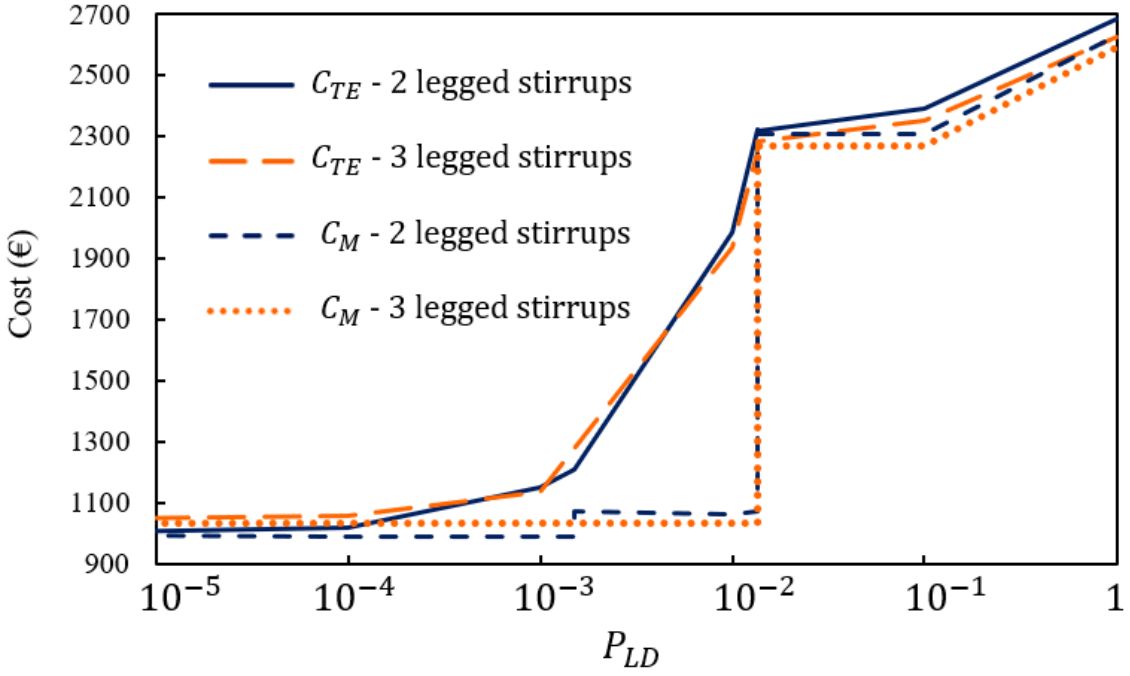

Source: own authorship.

Figure 4.4 - Behavior of each conditional β^* with P_{LD}.

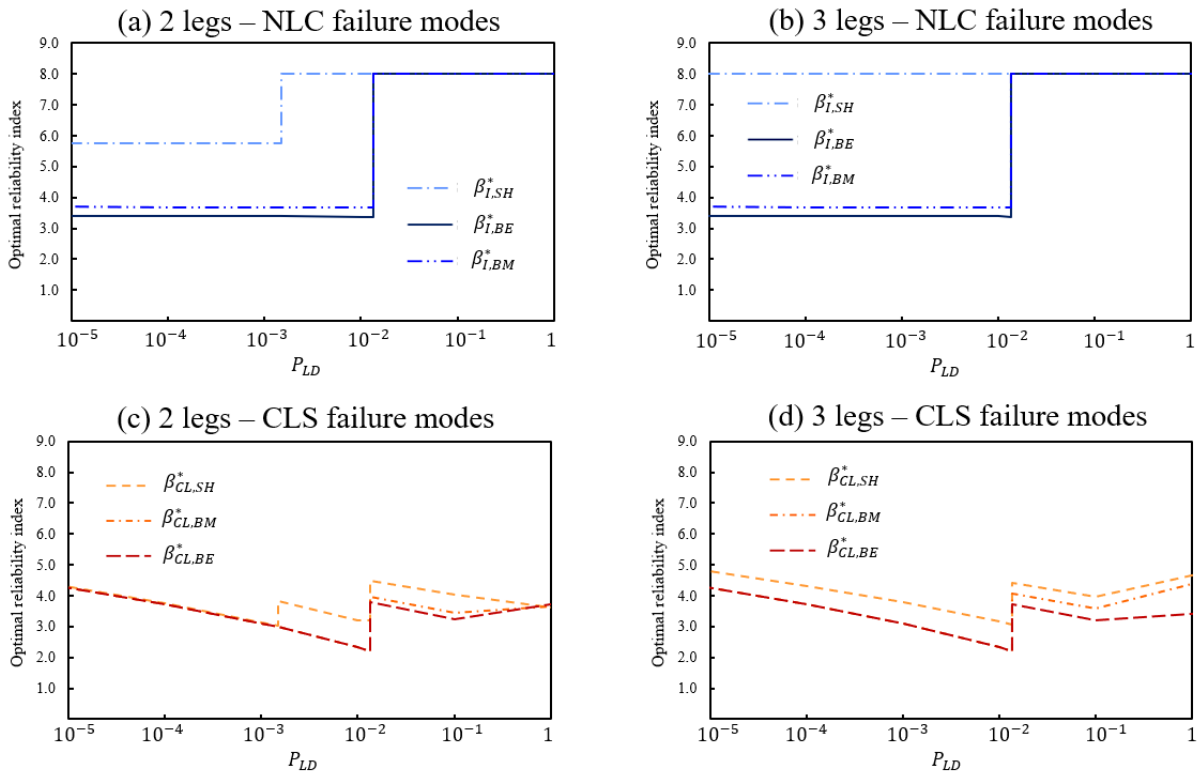

Source: own authorship.

Figure 4.5 - Behavior of each C^*_{ef} with P_{LD}.

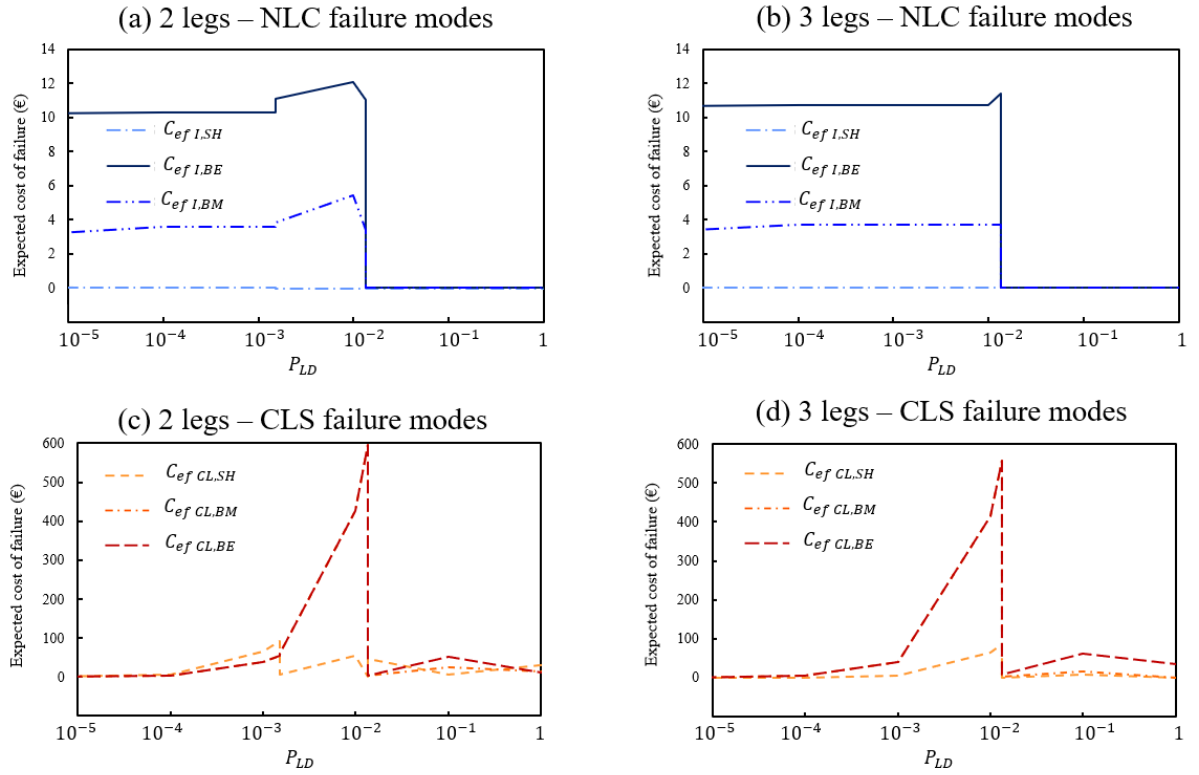

Source: own authorship.

The transitions identified in Figure 4.2 and the reinforcement increase beyond P_{LD}^{th} rely on the balance between manufacturing costs and expect costs of failure. Both optimal values at P_{LD}^{th} for 2-legged stirrups have identical total C_{TE}^{*} although their C_{M}^{*} are different due to the increased transversal reinforcement in the 2nd optimal. For the 3-legged stirrups the discrepancy between each C_{M}^{*} is significantly greater due to both longitudinal and transversal reinforcements being increased. Although C_{M}^{*} being distinct for each optimal at P_{LD}^{th}, C_{TE}^{*} is identical at both due to a similar balance between economy and safety for both solutions.

At P_{LD}^{th}, the optimal related to NLC has less C_{M}^{*} but greater $\sum C_{ef}^{*}$, while the optimal related to CLS has greater C_{M}^{*} but reduced $\sum C_{ef}^{*}$ (Figures 4.3 and 4.5). Nevertheless, their balance between C_{M}^{*} and $\sum C_{ef}^{*}$ is identical at P_{LD}^{th}, revealing an indifferent cost-benefit in reinforcing the structure to ensure load-bearing capacity in CLS. Hence, for $P_{LD} < P_{LD}^{th}$ strengthening the structure against progressive collapse leads to an increased C_{M} without beneficial reduction in $\sum C_{ef}$, so the optimal design for NLC has better cost-benefit. However, for $P_{LD} > P_{LD}^{th}$ strengthening against column loss pays off, with strengthening costs smaller than the reduction in expected costs of failure.

Figure 4.4 and 4.5 outlines that the most critical failure modes under NLC are bending at the beam ends (BE) and at the midspan (BM) for both 2- and 3-legged stirrups. Under CLS, bending failures are still critical, but collapse from a lacking shear resistance (SH) becomes much more significant, especially for the 2-legged stirrup detailing.

Although both stirrup cases allows minimal transverse reinforcement for NLC (ϕ8 @200), Figure 4.4 shows that shear capacity is greater for 3-legged stirrups due to its greater initial ρ_{st}^{*} ($\beta_{I,SH}^{*} \approx 5.8$ for 2 legs and $\beta_{I,SH}^{*} \approx 8.0$ for 3 legs). To ensure similar ρ_{st}^{*} for both cases at the 1st stage, s_t should be equal to 296 mm for the 3-legged option. The smaller shear capacity for 2 legged stirrups leads to a faster increase of $C_{ef\ CL,SH}$, justifying a smaller P_{LD}^{th} for this transversal detailing.

Besides, the material increase due to an additional stirrup leg is not compensated by an increase in s_t^{*} , which in turn leads to greater C_M and C_{TE} at the 1st stage (Figure 4.3). Transverse reinforcement with 2-legged stirrups is suitable, in terms of costs, for the 1st stage, while 3-legged stirrups are shown to be efficient, in terms of costs, for the 2nd stage. For $P_{LD} = 1.0$, both stirrup detailing have similar ρ_{st}^{*}, but the 3-legged option leads to a cheaper structure and is related to greater shear capacity at 2nd stage.

It should be noticed that increasing the longitudinal reinforcement to mitigate progressive collapse happens beyond $P_{LD} \approx 1.35\times10^{-2}$ for both cases of transversal detailing. Although this P_{LD} value is a threshold for longitudinal reinforcement, it leads to the first instance of positive-cost benefit of strengthening only for the 3-legged case. Hence, this P_{LD} value corresponds to the overall threshold P_{LD}^{th} only for the second option of stirrup detailing.

For the 1st stage, Figure 4.4 shows that optimal reliability indexes for bending at midspan and beam ends are constant and $\beta_{I,BM}^{*}$, $\beta_{I,BE}^{*}$ ~ 3.5. Figure 4.5 shows that all NLC failure modes have C_{ef} lower around 1% of C_M at the 1st stage, and zero at the second stage. Hence, strengthening against progressive collapse has shown no reduction in the intact structure safety margins. Optimal rebar ratios at the end of 2nd stage range from 1 to 3%, but this is better addressed in the next example.

4.1.2 Assessment of guideline-conforming design solutions

Load and Resistance Factor Design (LRFD) according to ACI 318-19 (ACI, 2019) is used to validate optimal configurations for NLC following load combination for usual design:

$$\phi R_n \geq 1.2D_n + 1.6L_n \tag{4.4}$$

where ϕ is the strength reduction factor set to 0.9 for beam bending and 0.75 for shear failure; and R_n is the resistance parameter of interest. For CLS, the LRFD approach is adopted following a load combination for extraordinary loading events (ASCE, 2022):

$$\phi R_n \geq 1.2D_n + 0.5L_n \tag{4.5}$$

Table 4.4 shows the overall guideline assessment via demand capacity (DCR) factors. Optimal design solutions for NLC and CLS meet ACI 318-19 (2022) and ASCE 7 (2010) provisions, respectively. Demand-capacity ratio (DCR) is very close to 1 for NLC, showing that the optimization algorithm ensured a minimal safety level against its failure modes. This reflects an adequate choice for the cost factors for bending failure, as $k = 30$ is enough to keep DCR around 0.91 ~ 0.92 ($\beta_{I,BM}^{*} \approx 3.6$ and $\beta_{I,BE}^{*} \approx 3.4$ for the optima with 2 and 3 legs). For shear failure, $k = 60$ leads to a DCR of 0.95 for 2-legged stirrups ($\beta_{I,SH}^{*} \approx 5.8$) and 0.79 for the 3-legged setup ($\beta_{I,SH}^{*} \approx 8.0$).

Table 4.4. DCR factors for intact structure and column loss scenario ($P_{LD} = 1$).

Scenario	Failure mode	Parameter	Optimal design	
			2-legged stirrups	3-legged stirrups
Intact structure	Bending at midspan	$0.9M_R$ (kNm)	91.20	91.20
		M_S (kNm)	83.25	83.25
		DCR	0.91	0.91
	Bending at beam ends	$0.9M_R$ (kNm)	181.89	181.89
		M_S (kNm)	166.50	166.50
		DCR	0.92	0.92
	Shear failure	$0.75V_R$ (kN)	175.40	210.26
		$V_{S,I}$ (kN)	166.50	166.50
		DCR	0.95	0.79
Column loss	Bending at midspan	$0.9M_R$ (kNm)	295.94	314.25
		M_S (kNm)	237.96	237.96
		DCR	0.80	0.76
	Bending at beam ends	$0.9M_R$ (kNm)	606.80	586.12
		M_S (kNm)	475.92	475.92
		DCR	0.78	0.81
	Shear failure	$0.75V_R$ (kN)	254.72	273.65
		$V_{S,I}$ (kN)	237.96	237.96
		DCR	0.93	0.87

Source: own authorship.

As previously stated, the transversal detailing with 3 legs requires a stirrup spacing of 296 mm (beyond the usual limit of 200 mm) in order to have a ρ_{st}^* (and potentially $\beta_{I,SH}^*$) equivalent to the 2-legged option. This is addressed once again in the next example.

For CLS, optimal DCRs at $P_{LD} = 1$ are around ~0.80 for bending at the ends of the double span beam and at its midspan (location of the lost support), revealing a slightly excess of safety margin against them in terms of DCR ($\beta_{CL,BE}^*$ and $\beta_{CL,BM}^* \approx 4.0$). As a cost multiplier $k = 30$ is adopted to penalize bending failure for NLC, k equal to 50 is adopted for bending at CLS, which seems to be too much for penalizing the cross-section plastification of the double span beam.

Shear failure at CLS shows DCRs of 0.93 for 2-legged stirrups and 0.87 for the 3-legged setup. This evidences once again the superiority of the second stirrup detailing in terms of providing shear capacity with reduced C_M and C_{TE}. Besides, as opposed to bending failures, an increased cost multiplier $k = 80$ does not lead to an excess in safety margin against shear failure in terms of DCR ($\beta^*_{CL,SH} \approx 4.5$).

Dynamic Amplification Factor (DAF) is not accounted for q_{CLS} due to exaggerated longitudinal reinforcements being required to mitigate bending failure at the double-span beam. Following GSA (2016), assuming DAF = 1.25 for a Linear Static Procedure leads to:

$$\phi R_n \geq 1.25\ (1.2D_n + 0.5L_n) \tag{4.6}$$

Hence, in order to meet GSA (2016) provision for CLS, ϕR_n for bending capacity needs to be at least 25% greater than the values shown in Table 4.4. Roughly assuming $1.25A^*_B$ and $1.25A^*_T$ as optimal bottom reinforcement for $P_{LD} = 1.0$ is able to ensure DCR < 1.0 for bending at the midspan and at the beam ends. However, $1.25A^*_T$ is equivalent to an unfeasible beam detailing of $8\phi30$ just at the top layers, above the maximum $\rho_{T,lim} = 2.5\%$.

In view of that, a conservative consideration of dynamic effects shows that an analytical approach addressing bending failure is not appropriate for realistically addressing optimal risk-based design for CLS under larger P_{LD} values. It is appropriate, however, to address NLC for intact structures.

4.2 RC BEAM SUBASSEMBLAGE – NONLINEAR APPROACH

The same double span RC beam subassemblage of the previous example is once again the object of study, but relying on a nonlinear approach for progressive collapse analysis (Figure 4.6). This allows to comprehend how the realistic material degradation and nonlinear evolution of load vs displacement and internal forces affect the optimal risk-based results, and how these optima change compared to those obtained from linear analysis. Besides, no interference between distinct failure modes happened in the previous example due to each design variable relating to a specific failure mode. In this example, altering a single design variable may reflect in several NLC and CLS failure modes. Results presented herein are from a journal paper by Ribeiro et al. (2023) published in Engineering Structures. Besides, these results are an expanded version from those in Ribeiro and Beck (2021).

Figure 4.6 – Object of study.

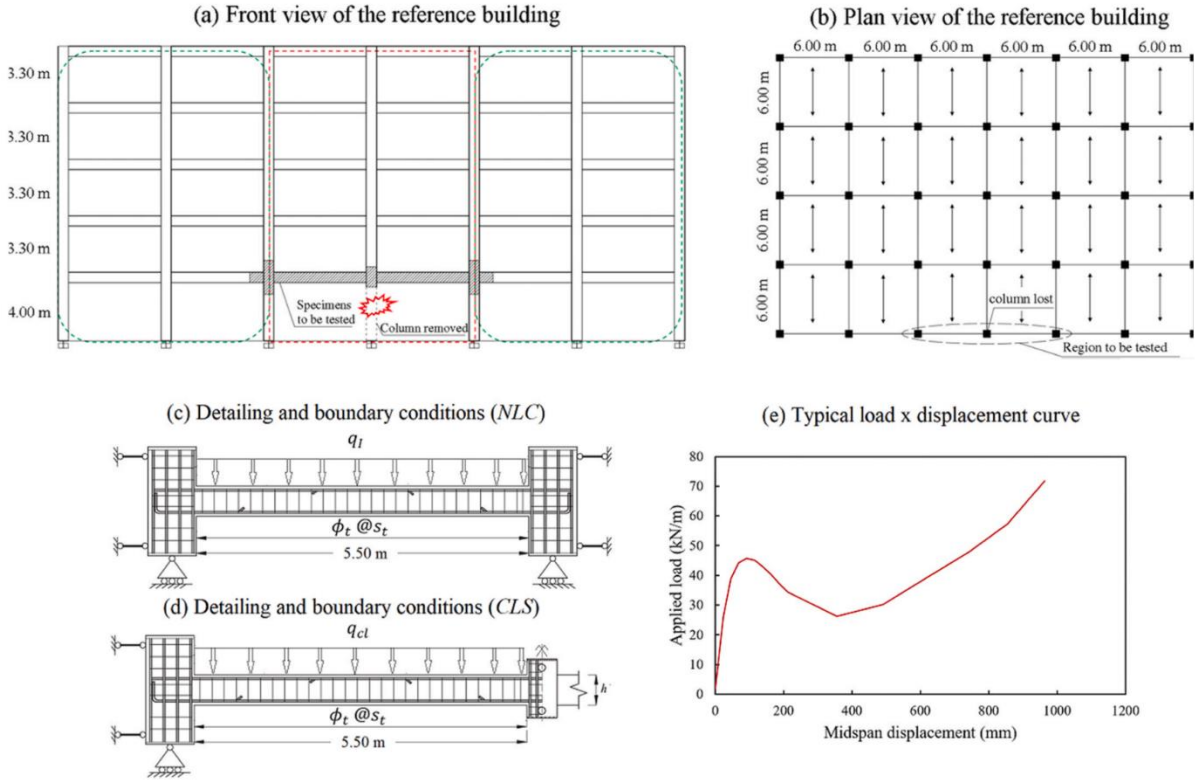

Source: own authorship.

As done in the previous example, columns are assumed to provide great lateral stiffness for the beam subassemblage, and the impact of this simplification is addressed in the next example. In order to reduce the analysis error due to a 2D capacity model being used, floors are once again assumed unidirectional to prioritize the structural load-bearing capacity over the perimeter primary frame of interest. Nevertheless, secondary beams are still able to increase overall robustness for this type of framed structure (Brunesi and Parisi, 2017; Parisi et al. 2018), but this is not addressed herein.

Only two local damage/hazard combinations are considered: intact structure under normal gravity load condition, and column loss under dynamically amplified gravity loads. The independent term P_{LD} is varied from $P_{LD}^{min} \approx 5 \times 10^{-6}$, which is the 50-year lifespan equivalent to the "de minimis" annual probability $p = 10^{-7}$ (Pate-Cornel, 1987), to $P_{LD} = 1.0$.

Quantitative risk analysis considering all collapse modes of the RC beam, with sectional dimensions and reinforcement ratios as design parameters, allows to verify the cost-effectiveness of APM design, specifically for a RC beam to form a load bridge' over a failed column. The uncertainties adopted are shown in Table 4.5, and the failure modes in Table 4.6.

Table 4.5. Uncertainty modeling.

Category	RV	Distribution	Mean	Standard deviation	Coef. of variation
Geometry	Beam depth (h)	Normal	To be optimized*	1 mm	-
	Bottom rebar area (A_B)	Normal	To be optimized*	-	0.05
	Top rebar area (A_T)	Normal	To be optimized*	-	0.05
	Stirrup cross section area (A_{st})	Normal	To be optimized*	-	0.05 (assumed)
	Stirrup spacing (s_t)	Normal	To be optimized*	-	0.05 (assumed)
Material	Concrete compressive strength (f_c')	Lognormal	32 MPa	-	0.12
	Rebar yield strength (f_y)	Normal	510 MPa	-	0.05
	Concrete unit weight (γ_c)	Normal	25 kN/m³	-	0.05 (assumed)
	Ultimate steel strain (ε_{su})	Normal	0.20	-	0.14
Loads	Dead load (D)	Normal	$1.05D_n$	-	0.10
	50-year live load (L_{50})	Gumbel	$1.00L_n$	-	0.25
	Arbitrary point in time live load (L_{apt})	Gamma	$0.25L_n$	-	0.55
Analysis	Model error (M_E)	Lognormal	1.107	0.255	-

Source: Ellingwood and Galambos (1982), JCSS (2001), Real, Campos Filho and Maestrini (2003), Wisniewski et al. (2012), Santiago (2018), Santiago and Beck (2018), Parisi et al. (2018), Costa and Beck (2024a; 2024b).

Design parameters to be optimized are the mean values of beam depth (h_B), top and bottom longitudinal rebar areas (A_B and A_T), stirrups cross section area (A_{st}) and stirrup spacing (s_t). Every design variable in vector $\boldsymbol{d} = \{h, A_B, A_T, A_{st}, s_t\}$ is the mean value of one random variable of vector $\boldsymbol{X}$. The previous example has shown that s_t^* should be near 300 mm in order to the 3-legged stirrup option have the same ρ_{st}^* as the 2-legged option, hence s_t now ranges from 50 mm to 300 mm in $\boldsymbol{\mathcal{D}}$ to allow this possible comparison.

Besides, C_{TE} is once again addressed by Eq. 4.2, but with an improved choice of failure modes which was made possible from the nonlinear approach. Risk-based optimization problem is once again given by Eq. 4.3. The Brazilian SINAPI database is adopted to estimate C_M in Brazilian Reais (R$), where unencumbered prices for São Paulo regarding the period of July 2022 are considered. Later, C_M is converted to Euros (€) at a rate of € 1.00 equal to R$ 5.28 (as of July 15, 2022, when the results were first submitted). As in the previous example, C_M is composed by cost of formwork, concrete, steel rebars, and corresponding workmanship.

Table 4.6. Failure mode depiction.

Condition	Limit state	Failure mode	Limit state function
Intact structure (I)	Serviceability	Large deflection	$g_{SE}(\boldsymbol{x}) = q_{I,SE} - q_I$
	Ultimate	Positive bending	$g_{BM}(\boldsymbol{x}) = q_{I,BM} - q_I$
		Negative bending	$g_{BE}(\boldsymbol{x}) = q_{I,BE} - q_I$
		Shear failure	$g_{I,SH2L}(\boldsymbol{x}) = V_R - V_I$
Column loss (CLS)	Ultimate	Steel rupture after instab.	$g_{SRCA}(\boldsymbol{x}) = M_E\, q_{CL,SRCA} - q_{CL}$
		Steel rupture at instab.	$g_{SRST}(\boldsymbol{x}) = \begin{cases} M_E\, q_{CL,CAA} - q_{CL} & \text{if } q_{CL,SRCA} < q_{CL,CAA} \\ 1 & \text{if } q_{CL,SRCA} \geq q_{CL,CAA} \end{cases}$
		Shear failure	$g_{CL,SH2L}(\boldsymbol{x}) = V_R - V_{CL}$

Source: own authorship.

In Table 4.6, $q_{I,SE}$ is the load intensity that produces a midspan deflection of L/400; L is the beam span of 6.00 m; $q_I = hb\gamma_c + D + L_{50}$ is the acting load for intact scenario; b is the cross-section width (300 mm); $q_{I,BM}$ is the load that leads to the resisting bending moment $M_{R,B}$ at the midspan; $q_{I,BE}$ is the load that leads to the resisting bending moment $M_{R,T}$ at the beam ends; V_R is the shear strength; V_I is the shear demand for I; $q_{CL,CAA}$ is the ultimate CAA capacity; $q_{CL,SRCA}$ is the ultimate CA capacity; $q_{CL} = 2(hb\gamma_c + D + L_{apt})$ is the acting uniform load for the CLS, with multiplier 2.0 representing a worst-case value of dynamic amplification factor; and V_{CL} is the shear demand for CLS.

The limit state functions rely on resistance and demand terms. Resistance thresholds for bending, shear and allowable displacements are estimated accordingly to ACI 318-19 (2019). Ultimate loads $q_{CL,CAA}$ and $q_{CL,SRCA}$ are obtained using an in-house static FE implementation, which addresses geometrical and material nonlinearities. Rebar failure is addressed in two situations: during or after snap-through instability, which is typical for strong lateral restraint (Figure 4.6e). Since this instability stage is sudden, a rebar rupture during its occurrence denies the positive ductility aspects of the longitudinal reinforcements, leading to a failure as brittle and severe as shear failure. A commentary on this instability stage is done in Chapter 2, and validation examples addressing this phenomenon is shown in Section 3.4.1.

To address the severity of each failure mode, cost factors k_i are chosen based on Beck et al. (2020; 2022; 2023). Therefore, k_i is assumed as 5 for serviceability failure, 30 for bending failure at beam ends and midspan, 40 for steel rupture at CA, and 60 for all brittle failure modes, namely, shear and steel rupture during instability stage. As done in Beck et al. (2020; 2022), these values range accordingly to the analysis by Marchand and Stevens (2015), which compares the cost of construction to the cost of collapse of the Alfred P. Murrah Federal Building, World Trade Center and Pentagon. Nevertheless, higher failure cost multipliers could be assumed for critical or strategic buildings. Yet, further verifications of optimal designs complying to guideline provisions attest a well choice for these parameters.

The nonlinear FE algorithm used in progressive collapse analysis follows the total-Lagrangian position-based method proposed by Coda (2014). Newton-Raphson algorithm is used at every loading step to find the equilibrium configuration, considering two translations and one rotation as degrees of freedom (DOFs) for each node. Thus, Arc-Length method is introduced in order to investigate the structural response even at instability stages. Each RC beam is discretized into 14 FEs, which are layered 2D frame elements with a fifth degree of approximation. A total of 20 layers with 1 integration point are used for transversal discretization, being 18 for concrete and one for each steel reinforcement.

This modelling allows implementation of distinct constitutive relations for concrete (confined or not) and steel layers. A uniaxial model of isotropic hardening is enough to represent the elastoplastic behavior of steel reinforcements. For concrete, μ-Model (Mazars et al. 2015) is used to represent the damage evolution and its unilateral behavior after stress reversals. The choice of accurately representing crack opening and closure (unilateral behavior) is to correctly simulate, in column loss scenarios, the transition of the RC beam from CAA to the CA stage, where locations originally in compression end up under tensile stresses.

Stirrups are not explicitly considered in the adopted FE modeling. However, their influence on concrete ductility is regarded by using the uniaxial curve from the modified Park-Kent model (Park et al. 1982) as basis to automatically calibrate the μ-Model compressive parameters. Concrete tensile behavior is defined via the uniaxial tensile curve from fib Model Code (2012), which is also used for the automatic calibration of tensile μ-Model parameters.

Two structural analyses are performed for each sample point, namely, the analysis of the intact structure under normal loading condition (NLC) and the analysis under column loss scenario (CLS). Analysis for NLC is done considering the beam built in in both ends (rotation and translations restrained), as shown in Figure 4.6c, while analysis for CLS is done considering the beam built in the left end, while on the right only free vertical translation is allowed as symmetry is considered (Figure 4.6d). Further details regarding the FE implementation and validation with experimental results are described in Appendix B of Ribeiro et al. (2023).

Hence, the overall framework shown in Chapter 3 is adopted. First, nonlinear static (pushdown) analysis is performed for limit state support points created via LHS. The outputs are then metamodeled via ordinary kriging to ensure a faster, yet accurate estimation of sample points for the uncertainty assessment via WASM for each failure mode. Additional ordinary kriging metamodels for the reliability indexes are then constructed for the design support points over the design domain $\boldsymbol{\mathcal{D}}$, ensuring a fast run for each optimization process.

4.2.1 Optimal design solutions

Figure 4.7 shows, for each design variable, the evolution of optimal designs $\boldsymbol{d}^*$ with P_{LD} ranging from 5×10^{-6} to 1, for cross sections with 2- and 3-legged stirrups. For each P_{LD}, a total of 10 optimization runs were performed, each one with 20 fireflies, 100 iterations, and an initial iteration of 6000 fireflies to provide a fast auxiliary extensive search over $\boldsymbol{\mathcal{D}}$.

The optimal design remains constant from P_{LD}^{min} to $P_{LD} \approx 10^{-3}$, but two local optimal solutions with similar C_{TE} are found at $P_{LD} \approx 3 \times 10^{-3}$. From this value until $P_{LD} = 1$, the optimal configurations follow the general characteristics of the new optima as P_{LD} increases. This clearly characterizes a transition in optimal design behavior. Smaller values of P_{LD} reflect situations with less relevant threat of column loss, characterizing a 1st stage where optimal configuration is controlled by the normal loading condition (NLC). Larger values of P_{LD} characterize the 2nd stage, with more significant column loss threat, where optimal design clearly adapts to resist progressive collapse under column loss conditions (CLS).

Figure 4.7 – Optimal design for each P_{LD} and corresponding total expected cost C_{TE}.

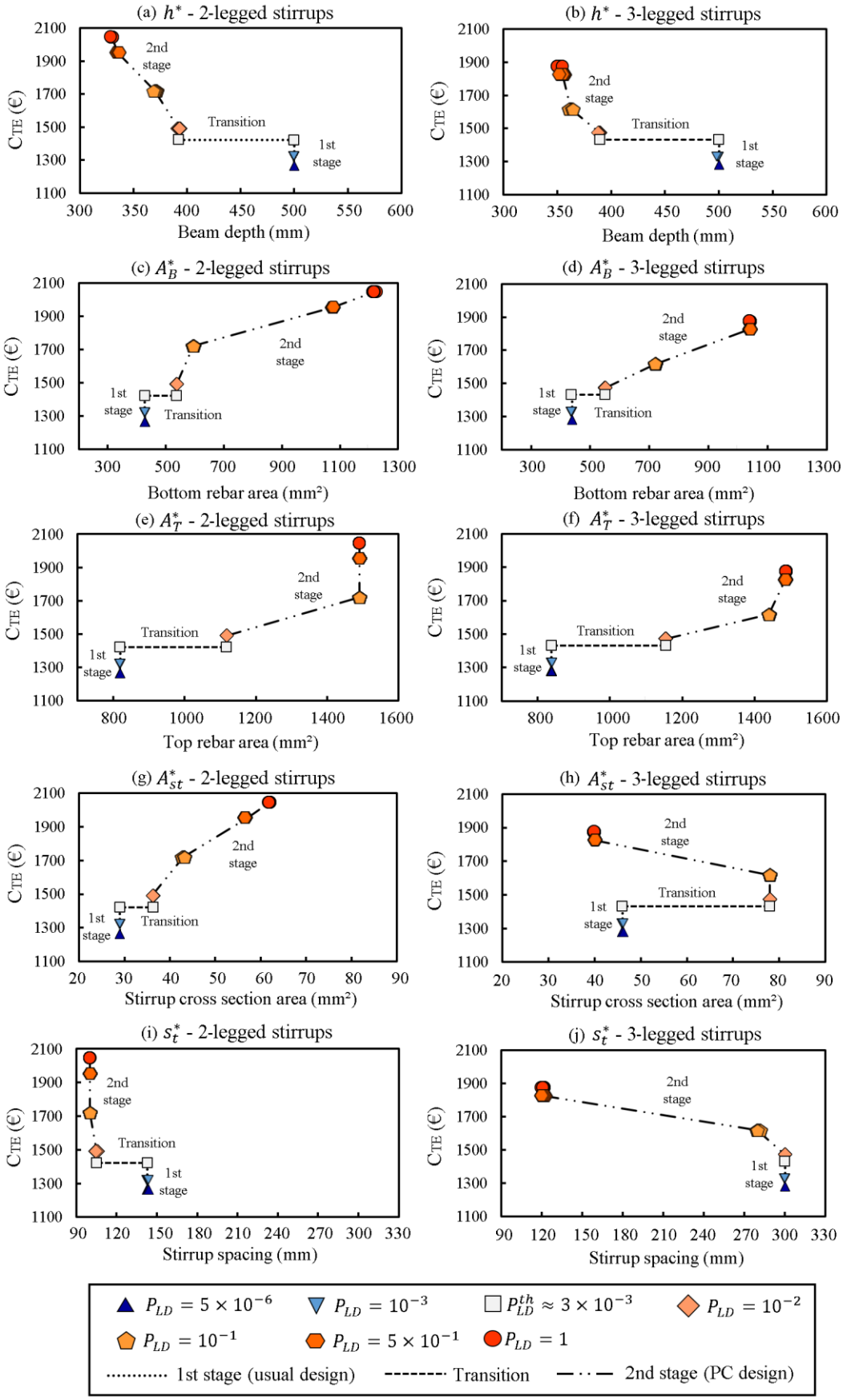

Source: own authorship.

In Fig. 4.7h, A_{st} for the 3-legged setup increases significantly at P_{LD}^{th} and then reduces after $P_{LD} = 10^{-1}$. This, however, is accompanied by an optimal gradual decrease in stirrup spacing, leading to an overall increase in transverse reinforcement after P_{LD}^{th}.

Figure 4.8 shows the behavior of C_M and C_{TE} in terms of P_{LD}. Figure 4.9 shows the evolution of the optimal conditional reliability indexes β^* with P_{LD} for the different NLC and CLS failure modes. Figure 4.10 shows the of expected costs of failure (C_{ef}) behavior with P_{LD}. The transition identified in Figure 4.7 is reflected in the optimal reliability indexes (Figure 4.9), and in the cost functions in Figure 4.10. Figure 4.9 outlines that the most critical failure modes under NLC are bending at beam ends (BE), bending at midspan (BM) and shear failure (SH) for both 2- and 3-legged stirrups. Under CLS, steel rupture at catenary action (SRCA) and shear failure (SH) are the most critical failure modes, especially for larger P_{LD} values.

Figure 4.8 – Evolution of manufacturing cost C_M and total expected cost C_{TE} with P_{LD}.

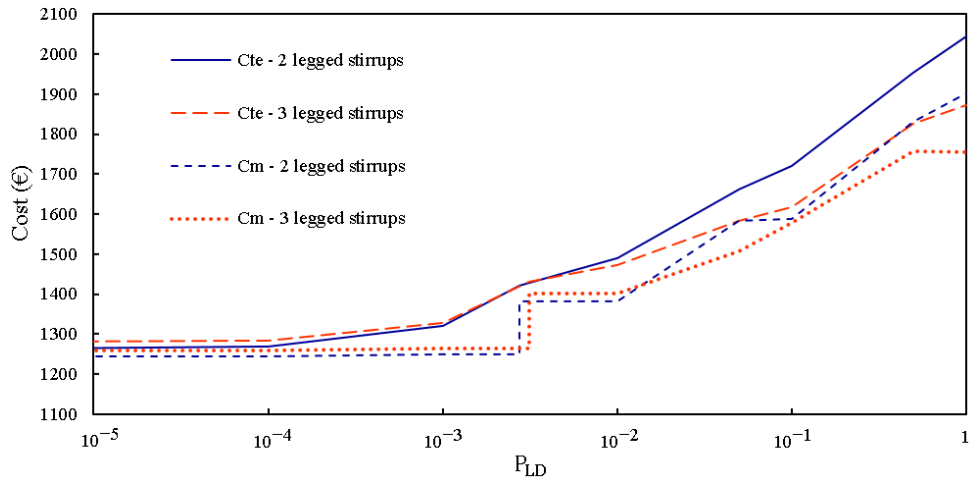

Source: own authorship.

Optimal cross section detailing is shown in Table 4.7, with an equivalent real-life detailing and reinforcement ratios being shown for A_B^*, A_T^* and A_{st}^*. At the 1st stage, optimal solutions for cross sections with 2-legged stirrups and 3-legged stirrups are quite similar. As shown in Figures 4.8 and 4.10, the increase in C_M and C_{TE} due to an additional stirrup leg is compensated by an increase in A_{st}^* and s_t^*, leading to a similar transverse reinforcement ratio ρ_{st} (Table 4.7) and similar safety margin against shear failure in NLC (Figure 4.9, $\beta_{I,SH}^* \approx 3.5$). Nonetheless, C_M and C_{TE} for 3-legged stirrup are slightly greater, making transverse reinforcement with 2-legged stirrups more suitable, in terms of costs, for the 1st stage. Although opposed to the verified in the previous example, in which similar ρ_{st}^* and $\beta_{I,SH}^*$ was not possible, 2-legged stirrups are still found to be the optimal choice for NLC.

Figure 4.9 – Behavior of optimal reliability indexes β^* with P_{LD}.

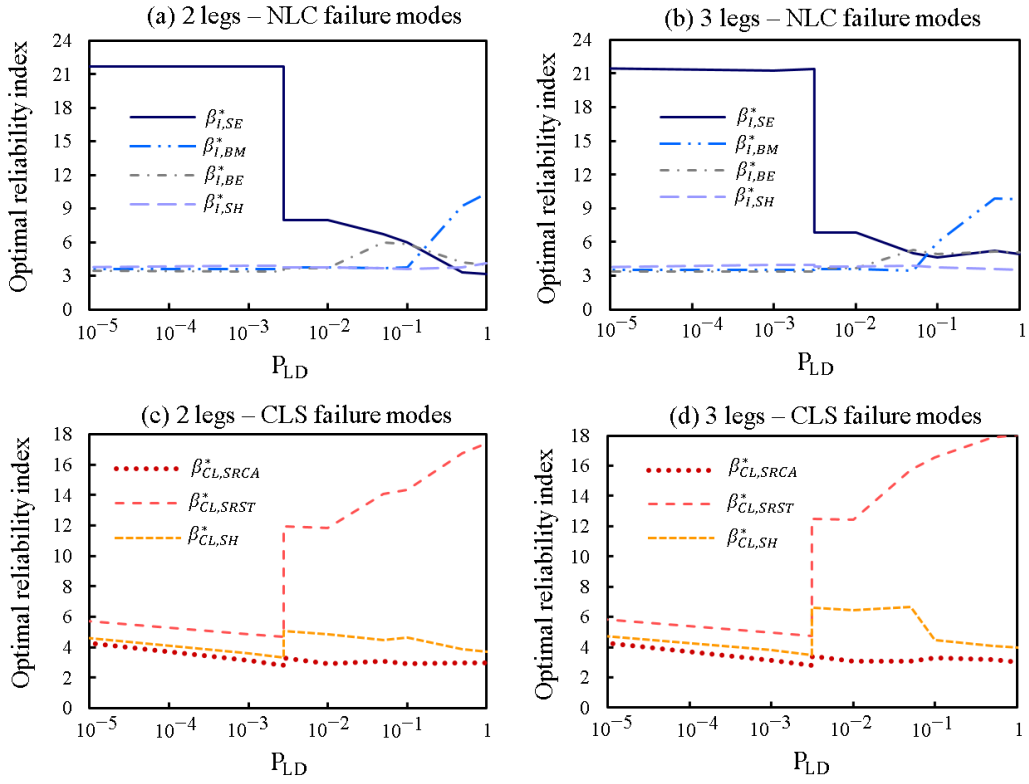

Source: own authorship.

Figure 4.10 – Behavior of each C^*_{ef} with P_{LD}.

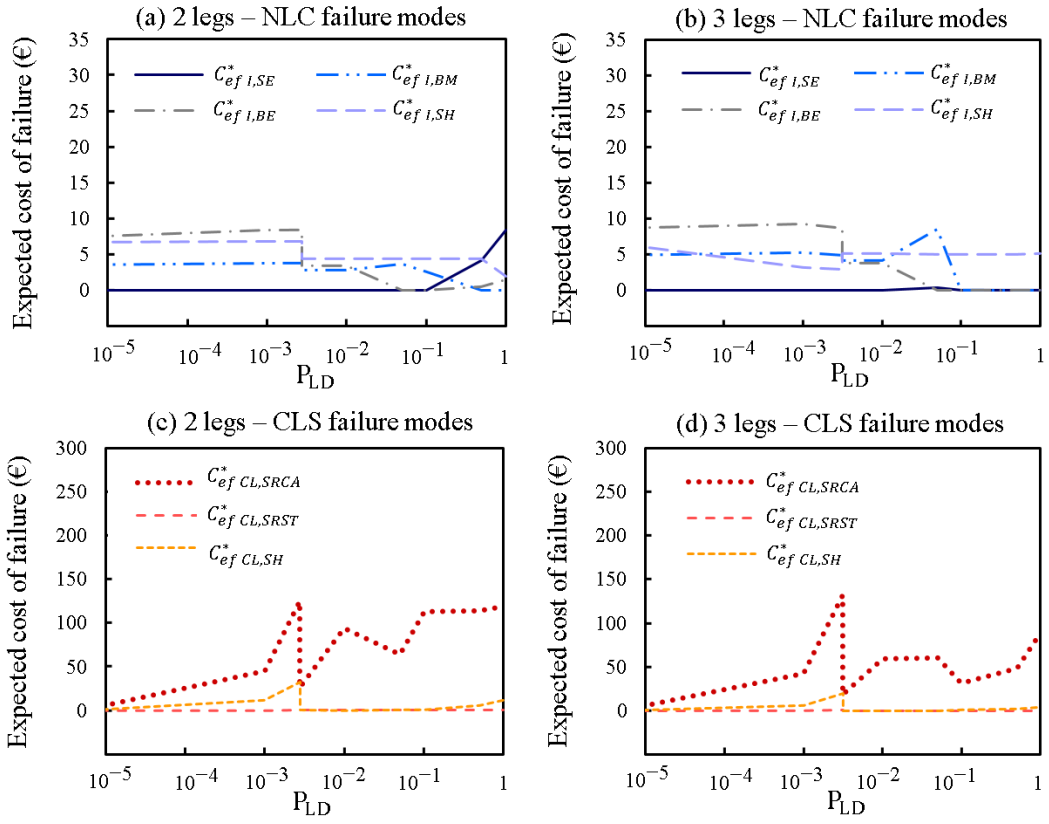

Source: own authorship.

Table 4.7. Optimal design solutions related to cross section detailing.

Design variable	2 legged stirrups			3 legged stirrups		
	$P_{LD} < P_{LD}^{th}$ (1st stage)	$P_{LD} \approx P_{LD}^{th}$ (transition)	$P_{LD} > P_{LD}^{th}$ (2nd stage)	$P_{LD} < P_{LD}^{th}$ (1st stage)	$P_{LD} \approx P_{LD}^{th}$ (transition)	$P_{LD} > P_{LD}^{th}$ (2nd stage)
h^* (mm)	500	390	330	500	390	350
A_B^* (mm²)	428 (~3Φ14)	538 (~3Φ16)	1219 (~3Φ22)	438 (~3Φ14)	550 (~3Φ16)	1041 (~3Φ22)
ρ_B^* (%)	0.29	0.60	1.23	0.29	0.47	0.99
A_T^* (mm²)	819 (~3Φ20)	1118 (~3Φ22)	1490 (~3Φ26)	838 (~3Φ20)	1155 (~3Φ22)	1488 (~3Φ26)
ρ_T^* (%)	0.56	0.96	1.51	0.56	0.98	1.42
A_{st}^* (mm²)	29 (~Φ6)	36 (~Φ8)	62 (~Φ10)	46 (~Φ8)	77 (~Φ10)	40 (~Φ8)
s_t^* (mm)	150	110	100	300	300	100
ρ_{st} (%)	0.13	0.23	0.41	0.15	0.26	0.33
C_M (€)	1245.00	1382.00	1903.00	1259.00	1401.00	1756.00
C_{TE} (€)	1263.00	1422.00	2045.00	1280.00	1432.00	1873.00

Source: own authorship.

When addressing the previous example, C_M is computed based on reference values with a 2-year gap: April 2024 in the previous approach, and July 2022 in this example. This explains why this example is ~200 € more expensive in terms of the 1st stage optimal, despite the similarity between optimal designs. Although the conversion from R$ to € was lower in 2022, construction costs were worldwide greater as an outcome of Covid-19 pandemic (Kisi and Sulbaran, 2022). Nonetheless, this does not compromise overall findings from the individual analysis of each example, or those from their comparison.

Albeit significantly more expensive, reference costs of 2022 lead to slightly inferior optimal rebar reinforcements for the 1st stage and similar optimal reliability indexes against bending failure for NLC (Figures 4.4 and 4.9). Lower stirrup ratios are found in this case, but this is due to stirrup cross-section area A_{st} also being a design variable and to a greater upper bound for s_t in $\mathcal{D}$ (300 mm). Hence, a better transversal detailing was enabled, ensuring a better balance between economy (reduced ρ_{st}^*) and safety (enough safety margins, as reflected by $\beta_{I,SH}^* \approx 3.5$) when compared to the previous analysis. This also prevented the discrepancy between P_{LD}^{th} values that was found in the previous analysis.

For the 1st stage, Figure 4.9 shows that optimal reliability indexes for bending at midspan and beam ends are constant and $\beta^*_{I,BM}$, $\beta^*_{I,BE} \approx 3.5$; for serviceability, probability of failure is negligible. Figure 4.10 shows that all failure modes for NLC have low expected costs of failure C_{ef} at the 1st stage (lower than 1% of C_M). Besides, the optimization leads to a detailing that meets multiple purposes: for instance, large beam depth not only provides safety against serviceability limit state (SE), bending (BM and BE), and shear failure (SH), but also allows a simultaneous reduction in both longitudinal and transversal reinforcements. Even though a reduced h with increased longitudinal reinforcement could ensure similar safety against SE, BE, and BM, an increased ρ_{st} is needed to compensate for reduced shear resistance, hence increasing C_M.

As the local damage probability increases approaching $P_{LD} \approx 3 \times 10^{-3}$, an additional optimal design with equivalent C_{TE} is obtained, as shown in Table 4.7. This additional optimum occurs due to the greater expected costs of rebar rupture at catenary action (SRCA) and shear failure at CLS as a function of increasing P_{LD} (Figure 4.10), with a concomitant reduction of $\beta^*_{CL,SRCA}$ and $\beta^*_{CL,SH}$ (Figure 4.9).

Since P_{LD} multiplies the failure probabilities of CLS, expected costs of failure C_{ef} increases if the optimal conventional design is not appropriate for CLS, which is the case of the stage 1 optimal design. Hence, $P_{LD} \approx 3 \times 10^{-3}$ marks a sudden transition, in which reliability against SRCA reaches a minimum ($\beta^*_{CL,SRCA} \approx 3$).

Before this point, there is no benefit in reinforcing the structure to ensure robustness against progressive collapse. By contrast, as P_{LD} increases, conventional design is no longer appropriate due to lack of robustness. This is directly in line with previous results found by Beck et al. (2020); hence, $P_{LD} \approx 3 \times 10^{-3}$ marks a threshold local damage probability P^{th}_{LD}. As stated by Beck et al. (2020), the threshold local damage probability is the value above which APM design under discretionary local damage has positive cost-benefit in comparison to usual design.

Herein, optimal design solutions leads to $P^{th}_{LD} \approx 2.75\times10^{-3}$ for 2-legged stirrups and $P^{th}_{LD} \approx 3.13\times10^{-3}$ for 3-legged stirrups. This means that strengthening the beam with 2-legged stirrup against column loss is justified for slightly smaller threat probabilities. As shown in Table 4.8, this difference relies on rather greater unconditional probability of CLS failure modes for the usual design setup with 2 legs, mainly for SRCA. Hence, as shown in Figure 4.10, the probability $P_{f\,CL,SRCA} \times P_{LD}$ and its corresponding C_{ef} grow slightly faster for the 2-legged stirrup option, justifying its earlier transition to optimal progressive collapse design.

Table 4.8. Optimal unconditional probability for each CLS failure mode.

Failure mode probability	2-legged stirrups			3-legged stirrups		
	$P_{LD} \approx P_{LD}^{th}$		$P_{LD} = 1$	$P_{LD} \approx P_{LD}^{th}$		$P_{LD} = 1$
	Usual design	PC design	PC design	Usual design	PC design	PC design
$P_{f\ CL,SRCA}$	9.04×10^{-1}	1.70×10^{-1}	1.56×10^{-3}	8.30×10^{-1}	6.39×10^{-2}	1.27×10^{-3}
$P_{f\ CL,SRST}$	4.74×10^{-4}	~0	~0	2.94×10^{-4}	~0	~0
$P_{f\ CL,SH}$	1.94×10^{-1}	6.55×10^{-5}	9.90×10^{-5}	1.25×10^{-1}	3.75×10^{-9}	3.70×10^{-5}

Source: own authorship.

In contrast with the previous example, the number of stirrup legs influences more than just the shear capacity. This is possible to be addressed due to the adopted nonlinear approach, which allows to represent the slightly increase in concrete strength and softening ductility that results from a greater core confinement provided by additional stirrup legs (Park et al. 1982). This leads to a minor enhancement in CAA and CA capacity, which in turn reflects in slightly smaller unconditional probabilities of rebar rupture for 3-legged stirrups and, consequently, in a slightly greater P_{LD}^{th} for this transversal setup. Yet, the biggest difference between setups is that, in terms of C_{TE}, 2-legs is more suitable for NLC and 3-legs is more appropriate for CLS due to its advantages regarding concrete confinement.

For $P_{LD} > P_{LD}^{th}$, optimal design is controlled by ductile steel rupture. Nonetheless, Figure 4.9 shows that safety margins against all other ultimate failure modes (including those related to the intact structure) increase as well. A decreasing trend is only observed for serviceability, yet ensuring a minimum $\beta_{I,SE}^{*} \approx 3.0$, which is enough to maintain $C_{EF\ I,SE}$ irrelevant in contrast with C_M and C_{TE}. This shows that greater robustness against progressive collapse is also beneficial, in terms of safety, for usual loading conditions. The reduction in $\beta_{I,SE}^{*}$ is due to smaller h^* for CLS, which ensures greater CA capacity for a RC beam subassemblage. Yet, this is better addressed in the next example.

In contrast to the 1st stage, Figure 4.7 shows that optimal design solutions do not remain constant for $P_{LD} > P_{LD}^{th}$, delineating an expected outcome. For the intact structure, failure probabilities do not depend on P_{LD}, the opposite occurring under local damage condition. Hence, as P_{LD} increases past P_{LD}^{th}, the optimal design has to become more and more robust. As shown in Figures 4.11 and 4.12, the increase in robustness is given by larger rebar reinforcement, greater transversal reinforcement, and smaller beam depth.

Figure 4.11 – Optimal design solutions for (a) usual and (b) progressive collapse conditions for option with 2-legged stirrups.

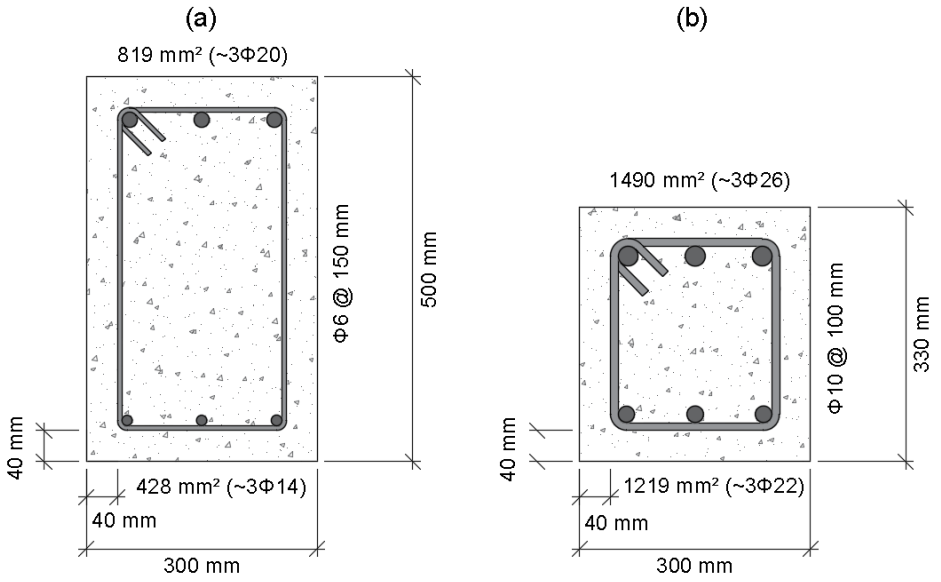

Source: own authorship.

Figure 4.12 – Optimal design solutions for (a) usual and (b) progressive collapse conditions for option with 3-legged stirrups.

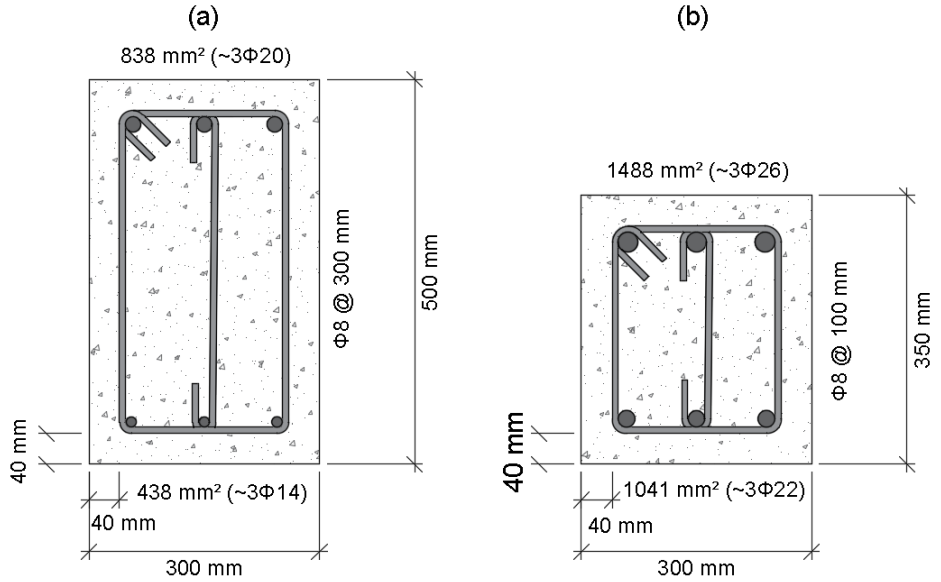

Source: own authorship.

The extra cross-section confinement observed for $P_{LD} > P_{LD}^{th}$ increases the actual concrete strength, yet shear resistance decreases for smaller h^*. Hence, transverse reinforcement has to increase in order to ensure shear resistance, which is mainly characterized by greater stirrup diameter and spacing reduction. Such a combination appears to be the most economical for the studied structure and adopted costs factors.

As mentioned earlier, increasing ρ_{st} provides greater shear resistance, but also greater ductility for the confined concrete, meaning that more stresses at cross sectional level will be shared between concrete and steel rebars after the CAA peak. This slightly helps the beam to postpone SRCA and to prevent SRST. As for steel rupture, a reduced beam depth allows rebars layers to be closer to each other, reducing stress discrepancies between bottom and top rebars, and enabling them to be used more efficiently at CA. However, as discussed in the next example, this is verified only for a RC beam subassemblage.

For $P_{LD} > P_{LD}^{th}$, optimal rebar ratios range from 0.47% to 1.23% for the bottom layer, and from 0.98% to 1.51% for the top layer. Bottom layer ratios are very similar to those found via analytical approach, but not the top layer ratio, which ranges from 0.64% to 2.80%. This is due to how CLS was previously addressed, as typical bending failures relates to cross-section plastification either by rebar yielding, concrete peak strength being reached, or both.

Since only the reinforcements are optimized in the linear approach, the only alternative to mitigate bending failure in CLS is to provide an excessive amount of steel area in order to avoid steel yielding and keep the neutral axis between $0.6283d$ and h. Following NBR 6118 (ABNT, 2023), this configuration relates to cross-sections in domains 4 or 4a, in which steel capacity is not fully explored and concrete failure happens in a brittle fashion.

However, a nonlinear approach allows to address resisting mechanism that go beyond flexural capacity, thus making use of the load-bearing capacity that is still available after cross section plastification (as discussed in Chapter 2). Top rebars characterize the most relevant rebar layer in both cases, since they must resist to greater CLS bending moments in linear analysis and are subjected to greater rebar strains in the nonlinear approach.

As top reinforcements found via nonlinear approach are smaller, ductile plastification is allowed at the beam ends opposed to the lost column. Hence, the thorough usage of confined concrete beyond softening and of steel rebars up to their ultimate capacity is endorsed.

Figures 4.3 and 4.4 shows that $\sum C_{ef}$ for CLS bending failures is equivalent to C_M before reinforcement against plastification is justifiable. When comparing to Figures 4.3 and 4.8, it is noticed that allowing plastification is convenient in terms of C_M and C_{ef}.

Even when considering conservative dynamic effects and expensive reference costs from the pandemic period, APM design is ~35% cheaper along the 2nd stage. Besides, relying on ultimate material capacity justifies rebar strengthening against progressive collapse for smaller threats of column loss. As shown in Table 4.7 and Figure 4.10, the cost of increasing ~0.30% in ρ_B^* and ρ_T^* (~ 150 €) starts to compensates $C_{ef\ CL,SRCA}$ around $0.01C_M$ (~ 150 €).

4.2.2 Analysis of the total expected cost function

Level surfaces are appropriate to verify the behavior of C_{TE} with the given design variables along P_{LD}. In order to allow this visualization in 2D plots, 4 design variables at a time are set to their average optimal values ($\boldsymbol{d}^*$) for each P_{LD}, while the remaining variable is gradually increased from its lower to upper bound, as shown in Figure 4.13.

Figure 4.13 – Behavior of C_{TE} for each design variable and each P_{LD}.

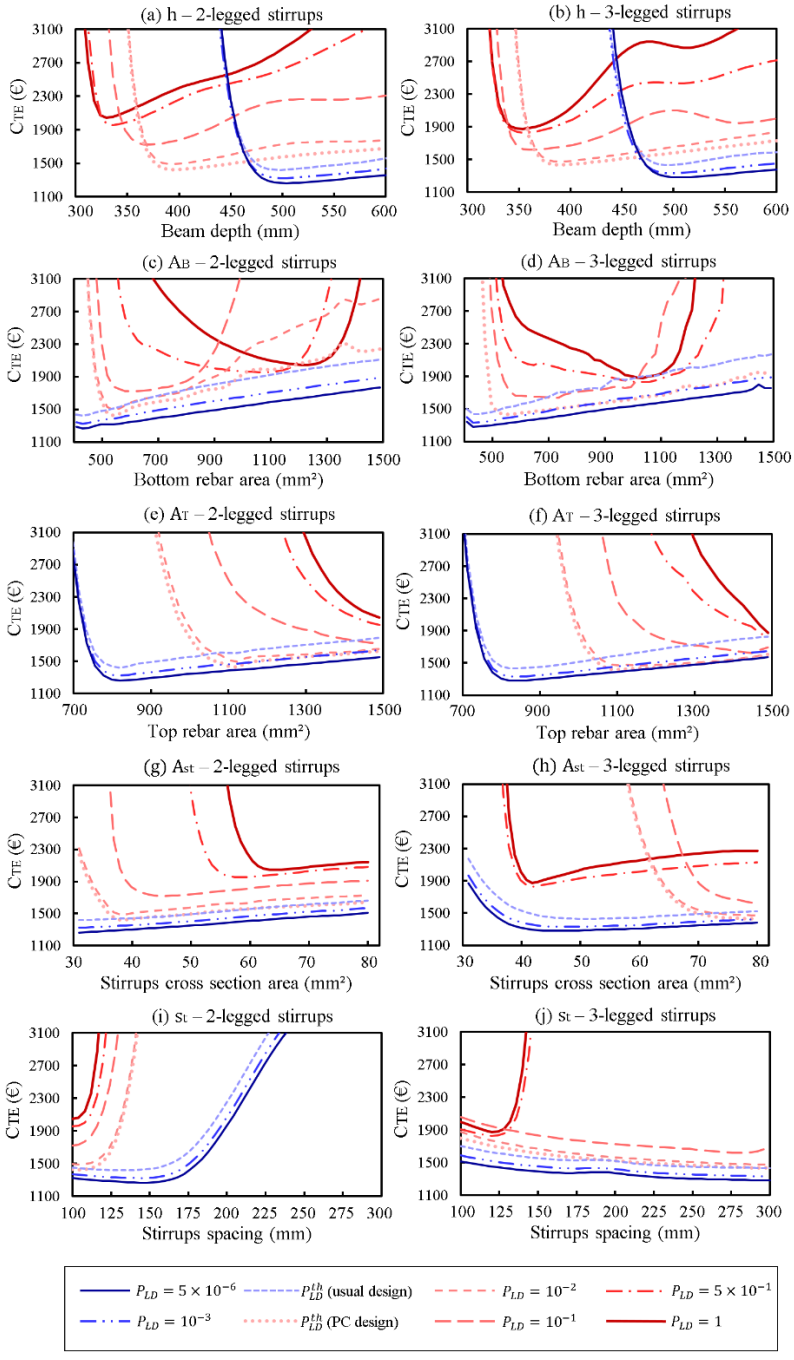

Source: own authorship.

For $P_{LD} < P_{LD}^{th}$, values of h and A_T below optimal lead to a very steep slope of C_{TE} due to greater C_{ef} and smaller safety margins against NLC failure modes of serviceability (displacements), bending, and shear. This is also true for A_{st} below optimum (3 legs) and s_t above optimum (2 legs), as they produce decreasing safety against shear resistance. If h, A_B, A_T and A_{st} are above their optimal values (and s_t is below it), a seemingly linear behavior is noticeable. This indicates overly conservative design solutions, where manufacturing cost is added with no corresponding reduction in the expected cost of failure.

Two curves (identified as A and B) are shown for P_{LD}^{th}, each representing one of the two optimal solutions shown in Figure 4.7. Although the level curves of conventional design (curve A) reflect the 1st stage behavior, the level curve B shows a slightly steeper slope for h and A_B above optimal. As $P_{LD} \rightarrow 1$, these slopes become more and more steeper. This behavior is motivated by a greater peak strength promoted at CAA, which increases the peak shear force at CAA with no corresponding increase in shear resistance.

Even though symmetric rebars are favorable at CA, the benefits in terms of C_{ef} reduction for SRCA (and also SRST) does not compensate its increase for shear failure. However, as $P_{LD} \rightarrow 1$, the need for greater ductility at CA leads to a more symmetric rebar setup, but with an even more reduced beam depth and increased transverse reinforcement to attenuate the increased CAA peak strength.

4.2.3 Assessment of guideline-conforming conventional design solution

Load and Resistance Factor Design (LRFD) according to ACI 318-19 (ACI, 2019) guidelines is used herein to validate the optimal configurations for NLC (i.e., for small P_{LD}):

$$\phi R_n \geq 1.2D_n + 1.6L_n \tag{4.7}$$

where ϕ is the strength reduction factor set to 0.9 for beam bending and 0.75 for shear failure verification; and R_n is the resistance parameter of interest, such as resisting shear strength. Bending and shear resistance (M_R and V_R, respectively) are estimated according to ACI 318-19 (ACI, 2019). Hence, Eq. (4.7) simplifies to:

$$0.9M_R \geq M_S \text{ for bending failure} \tag{4.8a}$$

$$0.75V_R \geq V_{S,I} \text{ for shear failure} \tag{4.8b}$$

Table 4.9 shows the validation of the optimal designs according to ACI 318-19 (ACI, 2019). All optimal design solutions meet the guideline provisions for bending failure. Demand Capacity Ratio (DCR) is very close to 1 in all cases, showing that the optimization ensured a accepable safety level against all ultimate failure modes. This reflects an adequate choice for the cost factors: $k = 30$ for bending was enough to keep DCR slightly smaller than 1 ($\beta^*_{I,BM} \approx$ 3.6 and $\beta^*_{I,BE} \approx 3.4$), while $k = 60$ for shear led to a DCR slightly over 1, even with $\beta^*_{I,SH}$ being the highest safety margin for NLC (β~3.8 for the optima with 2 and 3 legs).

Table 4.9. DCR complying with ACI 318-19 (ACI, 2019) guidelines.

Failure mode	Parameter	Optimal (2 legs)	Optimal (3 legs)
Bending at midspan	$0.9M_R$ (kNm)	91.84	93.93
	M_S (kNm)	87.70	88.35
	DCR	0.95	0.94
Bending at beam ends	$0.9M_R$ (kNm)	171.14	174.88
	M_S (kNm)	163.38	165.45
	DCR	0.95	0.95
Shear failure	$0.75V_R$ (kN)	157.40	163.44
	$V_{S,I}$ (kN)	166.50	166.50
	DCR	1.06	1.02

Source: own authorship.

In order for shear failure DCR to be exactly 1, V_R should be 222 kN. By keeping the same A^*_{st}, this is achieved by considering $s_t = 125.1$ mm for 2 legged stirrups, and $s_t = 284.8$ mm for 3 legs. Considering s_t values below optimum to satisfy Eq. (4.8b) leads to greater reliability indexes and smaller C_{ef} for shear failure. Anyway, the reduction in C_{ef} does not compensate the increase in C_M (and C_{TE}) due to the addition of more stirrups to the beam. Hence, a more conservative design is required to satisfy Eq. (4.8b) in this example.

4.2.4 Assessment of guideline-conforming progressive collapse design solution

The LRFD approach according to GSA guidelines (2016) is adopted herein to validate the optimal configurations for progressive collapse (i.e., for large P_{LD}). Those guidelines assume the following load combination for nonlinear static analysis:

$$\phi R_n \geq \Omega_N(1.2D_n + 0.5L_n) \tag{4.9}$$

where Ω_N is the dynamic increase factor, assumed as 2 in this study (worst case scenario).

Steel rupture is regarded by comparing the applied load $q_{S,CL} = \Omega_N[1.2(\gamma_C hb + D_n) + 0.5L_n]$ to the ultimate loads $q_{CL,SRCA}$ and $q_{CL,CAA}$, which are obtained via limit state surrogates. Since this failure mode depends on a material property (ε_{su}), no strength factor ϕ is required by GSA guidelines (2016). As for shear failure, the same strength reduction factor ϕ and equation used for NLC is used. Hence, Eq. (4.9) simplifies to Eq. (4.10), with DCRs being shown in Table 4.10, with $q_{CL,ULT} = \max[q_{CL,SRCA}, q_{CL,CAA}]$:

$$q_{CL,ULT} \geq q_{S,CL} \text{ for steel rupture} \tag{4.10a}$$

$$0.75V_R \geq V_{S,CL} \text{ for shear failure} \tag{4.10b}$$

Table 4.10. DCR factors for CLS following GSA guidelines (2016).

Failure mode	Parameter	Optimal (2-legs)		Optimal (3-legs)	
		$P_{LD} \gtrsim P_{LD}^{th}$	$P_{LD} > 10^{-1}$	$P_{LD} \gtrsim P_{LD}^{th}$	$P_{LD} > 10^{-1}$
Steel rupture	$q_{CL,CAA}$ (kN/m)	25.34	26.63	24.41	27.16
	$q_{CL,SRCA}$ (kN/m)	78.69	114.32	82.30	109.71
	$q_{S,CL}$ (kN/m)	77.38	76.26	77.33	76.67
	DCR	0.98	0.67	0.94	0.70
Shear failure	$0.75V_R$ (kN)	153.29	177.11	162.04	177.71
	$V_{S,CL}$ (kN)	152.04	159.78	146.46	156.96
	DCR	0.99	0.90	0.90	0.88

Source: own authorship.

All optimal design solutions satisfy the GSA (2016) provisions, showing DCR ≈ 1 for shear failure and steel rupture for $P_{LD} \gtrsim P_{LD}^{th}$. Despite all DCRs for shear failure being very close to unity, none of them is above 1. This means that the minimum safety margin against shear failure provided by the optimization algorithm is enough to satisfy GSA provisions, without any adaptation to make the design more conservative. The advantages of stirrups with 3 legs also rely on smaller DCR for shear failure during CLS (mainly if $P_{LD} \gtrsim P_{LD}^{th}$) in comparison with the optimal solutions with 2 legs.

DCRs very close to unity for steel rupture and $P_{LD} \gtrsim P_{LD}^{th}$ reflect a minimum safety margin against SRCA in order to reduce its C_{ef} no more than necessary, as this margin grows at larger rates for conventional design until P_{LD}^{th} (Figure 4.10). However, as P_{LD} increases to unity, this DCR approaches 0.70, even though Figure 4.9 shows that $\beta_{CL,SRCA}^{*}$ is approximately equal to 3 under $P_{LD} > P_{LD}^{th}$ (always the smaller reliability index under CLS). As shown in Table 4.8, for P_{LD} values slightly greater than the threshold, the unconditional probability of steel rupture is around 1.70×10^{-1} for 2-legged stirrups and 6.39×10^{-2} for 3-legged stirrups. As P_{LD} increases till unity, the unconditional probability of steel rupture reduces to 1.56×10^{-3} for 2-legged stirrups and 1.27×10^{-3} for 3-legged stirrups. Hence, the much higher unconditional probability for $P_{LD} \gtrsim P_{LD}^{th}$ is the reason behind the greater DCR from Eq. (4.10a), even though the conditional $\beta_{CL,SRCA}^{*}$ is approximately equal to 3 over the entire CLS design. This difference arises from the discretionary column removal of current guidelines, whereas in this study column loss is considered as an event conditioned on severity of hazard intensity (P_{LD}).

In addition, the DCR related to steel rupture decreases as P_{LD} increases, dropping from ~1.0 to ~0.7. This outcome shows that the greater the benefit of considering CLS in design, the larger the safety margin becomes, in terms of the demand-capacity relationship, for the beam to bridge over a lost column. This happens because as $P_{LD} \rightarrow 1$ the unconditional probability of steel rupture decreases until it becomes equivalent to its conditional probability, which the optimization algorithm always keeps around 1.35×10^{-3} ($\beta \approx 3.00$). Thus, the DCR associated with steel rupture as $P_{LD} \rightarrow 1$ is roughly the same over both optimal solutions in Table 4.10, being DCR ≈ 0.7 for $\Omega_N = 2.0$. This is also due to the ultimate load $q_{CL,SRCA}$ being around 110 kN and $q_{S,CL}$ being similar for both optimal solutions. Hence, a similar $\beta_{CL,SRCA}^{*} \approx 3.00$ over all optimal solutions led to a similar ductility level for all of them, despite all detailing differences.

Increased robustness as APM designs show better cost-benefit is also observed in terms of $q_{CL,CAA}$ and $q_{CL,SRCA}$, which are always greater for higher values of P_{LD}. Thus, $q_{CL,SRCA}$ is always 2 to 4 times greater than $q_{CL,CAA}$, evidencing the algorithm´s effort to avoid steel rupture during the instability stage and fully enhance CA capacity. Despite the ultimate load $q_{CL,SRCA}$ assuming high values (especially for $P_{LD} \rightarrow 1$), $q_{CL,CAA}$ being considerably smaller reflects a lack of benefits (in terms of C_{TE} reduction) from increasing CAA capacity, as propensity to premature rebar rupture is increased.

It is worth mentioning that these optimal configurations relate to a RC beam with perfect horizontal restraint, with no impact to the lateral supports due to increased axial forces under CAA and CA. Further examples addressing this feature show a distinct behavior.

Yet, additional failure modes under CLS, such as excessive cracking, rebar yielding, concrete spalling and crushing, and vertical drift, could add advantages to keeping higher values for $q_{CL,CAA}$. Hence, implementing a performance-based approach to the risk optimization shown in this study would allow many more insights.

When comparing DCR values of this example to those found previously for an analytical framework, it becomes once again evident that a fully nonlinear approach is significantly more suitable to address CLS failure modes in a risk-based optimization scope. Besides ensuring cheaper designs in terms of C_M and C_{TE} even when conservatively addressing dynamic effects and relying on more expensive reference costs to compose C_M, the realistic approach for column loss scenarios leads to better results in terms of DCR.

4.3 RC FRAME UNDER MULTIPLE COLUMN LOSS SCENARIOS

In this example, the entire RC frame tested by Yu and Tan (2013) is the object of study, not just the double-span beam above the lost column as shown in section 4.2. Progressive collapse may now advance vertically (upward propagation due to beam rebar failure) or horizontally (lateral propagation due to the column failure). Hence, the studied structure advances from a simple RC beam to a 2D RC frame system under multiple column loss scenarios, which is significantly more complex and much closer to a realistic situation.

This example addresses updated analysis in the conference papers from Ribeiro et al. (2022; 2023) published in XLIII CILAMCE and XLIV CILAMCE. The first study addresses a reduced RC frame (4 bays, 2 stories, beam length of 4 m) under middle column loss, low ductility rebars ($\varepsilon_{su} = 0.13$), and ultimate load capacity estimated via uniform pushdown analysis. The later addresses the same RC frame, but with greater ductility rebars ($\varepsilon_{su} = 0.20$) and addressing middle and exterior column loss. These results were obtained for a smaller RC frame due to the computational burden not being fully solved by the time they were obtained. At the time, structural analysis was still performed on a self-made algorithm. Yielding of compressed column rebars was still challenging, and ordinary kriging became impractical as the number of outputs increased for RC frame systems.

As shown in section 3.3 and 3.4, OpenSees greatly improved structural analysis efficiency, and IDW allowed metamodeling multiple outputs faster than kriging and accurately enough. This allowed both studies to be performed once again for a more realistic RC frame and taking into consideration precious feedback at both conferences.

Hence, results shown herein address multiple scenarios of column loss, lateral collapse propagation due to adjacent column failure, bay pushdown analysis, better representation of dynamic effects due to sudden column loss, and reconstruction of the entire pseudo-static pushdown curve and related internal forces via metamodeling. These updated and improved results are in a manuscript to be submitted to Engineering Structures.

As shown in Figure 4.6, the first-floor column height has 4.00 m, while the remaining floors have height of 3.30 m. All columns at ground floor are subjected to a local damage probability P_{LD}. Unidirectional floor slabs are considered; hence the perimeter frame gets floor loadings from one side only. It should me mentioned that if an inner frame was being optimized, two floor loads would be added to the beams, so greater optimal reinforcements would be expected for both intact and column loss scenarios. However, real life occurrences of progressive collapse due to terrorist attacks, for instance, shows that facade columns at the ground floor are usually more prone to sudden loss.

For the studied frame, pushdown analysis for middle column loss rarely shows the snap-through behavior that is always observed for the RC beam subassemblage, and when it does, is significantly less prominent (Figure 4.14). Besides, ultimate capacity at CA is shown to be reduced when the entire system is addressed, which is aligned to the observed behaviors in the validation examples of RC beams and frames in Section 3.4.2.

Figure 4.14 – Typical static pushdown curves for the RC frame (a) and the RC beam subassemblage (b) estimated for the same 200 sample points.

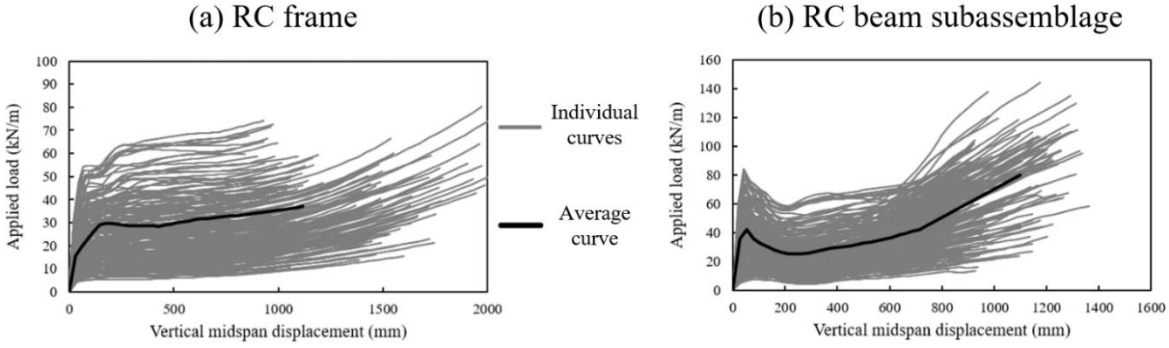

Source: own authorship.

Beam sensitivity analysis reveals a distinct behavior for some relevant variables (Figure 4.15). While a reduced beam depth increases the ultimate load capacity in a RC beam subassemblage, the opposite is observed for the RC frame system. This major difference relies on the horizontal drift at the adjacent columns, since they lack a perfect horizontal confinement for the beams when the entire RC frame is addressed.

Figure 4.15 – Beam sensitivity analysis comparison.

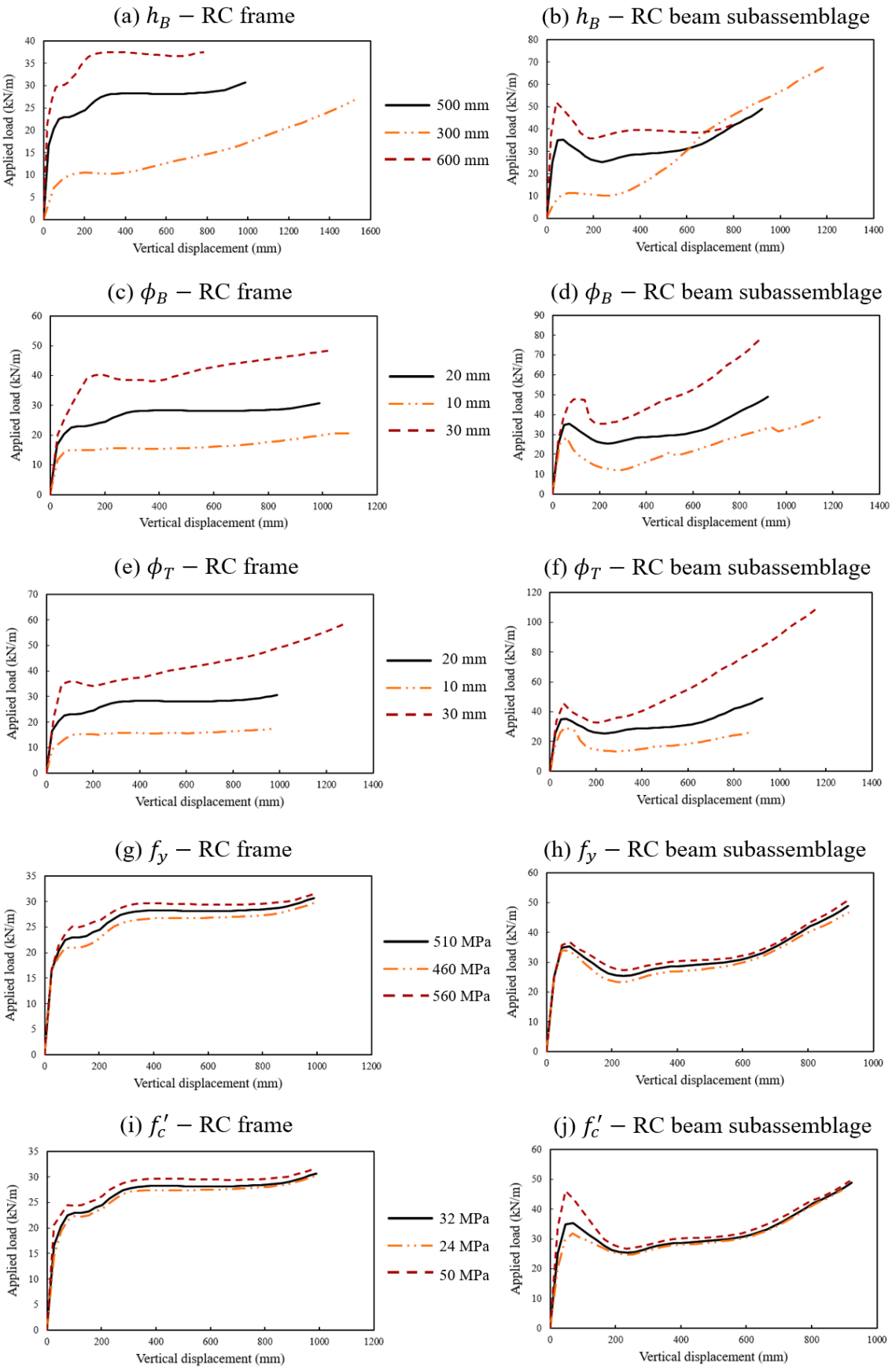

Source: own authorship.

In view of this, significant changes in the optimal risk-based design are expected for the frame system in comparison to the beam subassemblage. Additionally, concrete strength has a reduced role in the pushdown development when the RC frame system is adopted, since the increase in CAA capacity observed in the beam subassemblage model is not present.

Once again,total expected cost C_{TE} addresses manufacturing costs and the expected costs of all failure modes of the intact structure and each column loss scenario. Since the frame is symmetric, the loss of the exterior (CL1 and CL7), penultimate (CL2 and CL6) and antepenultimate columns (CL3 and CL5) are considered twice in C_{TE}. Additional life-cycle costs could be included in the objective function, but only those related to construction and loss are used in order to solely address the consequences of progressive collapse, as done in Beck et al. (2020; 2022), Ribeiro et al. (2023), and the previous examples.

$$C_{TE}(\boldsymbol{X}, \boldsymbol{d}) = C_M + \sum_{i=1}^{NIF} k_i P_{fi} C_{MAi} + \sum_{k=1}^{NCL} \sum_{j=1}^{NCLF} k_j P_{fj} C_{MAj} P_{LDkj} \tag{4.11}$$

Based on Beck et al. (2022), C_{MA} refers to the construction cost of the damaged area by a given failure mode. In the previous examples, $C_M = C_{MA}$ since only a RC beam subassemblage is addressed, so this distinction was not necessary. Design variables are the beam depth h_B, beam rebar diameter (bottom ϕ_B and top ϕ_T layers), beam stirrup spacing s_t, column size h_C (square column), and diameter of column reinforcement ϕ_C. As mentioned in section 3.2, design variables that can be represented as deterministic are addressed as random variables with low uncertainty in order to allow the usage of WASM for reliability analysis.

Since multiple columns are subject to sudden loss, P_{LD} is addressed in two different manners: a) P_{LD} relates to a specific column at a time, so the optimal risk-based design for each scenario is studied individually; b) P_{LD} relates to the loss of any supporting element, so each column is under a probability $P_{LDcol} = P_{LD}/(\text{number of columns})$ simultaneously. This allows to address how each scenario influences over the optimal design, and how they compete with each other in terms of reinforcement allocation when all of them are possible to occur.

In this first RC frame example, two distinct strategies are adopted for progressive collapse reinforcement: one regarding the regions of the frame to be strengthened (total or partial reinforcement), and the second regarding the amount of ductility provided by the longitudinal rebars (in terms of ε_{su}). Additional strategies, such as including structural fuses, will be addressed in future studies.

Probability of occurrence of each failure mode is estimated by metamodeling via IDW, which relies on 2000 design support points with probabilities computed via WASM (as shown in section 3.2). Table 4.11 shows the limit state functions, consequence factor k for all failure modes, and the extent of the final damaged area affected by each failure mode (in red).

Table 4.11 – Failure modes depiction.

Case	Failure mode	k	Limit state function	Damaged area
Intact structure (I)	Large deflection	5	$g_{I,SE}(\boldsymbol{x}) = \delta_{lim} - \delta(q_I)$	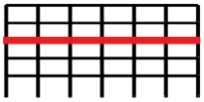
	Bending failure at midspan	30	$g_{I,BM}(\boldsymbol{x}) = M_{RM} - M_M(q_I)$	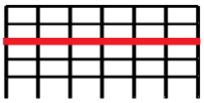
	Bending failure at beam ends	30	$g_{I,BE}(\boldsymbol{x}) = M_{RE} - M_E(q_I)$	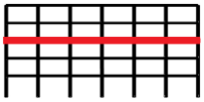
	Shear failure	60	$g_{I,SH}(\boldsymbol{x}) = V_R - V(q_I)$	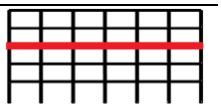
	Column failure	60	$g_{I,COL}(\boldsymbol{x}) = R(N_R, M_R) - S(N_{SI}, M_{SI})$	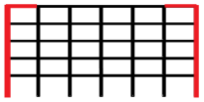
Column loss (CL_i)	Rebar rupture	40	$g_{CL_i,SR}(\boldsymbol{x}) = q_{CL_i,SR} - \tilde{q}_{CL}$	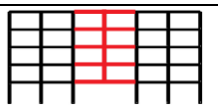
	Shear failure	60	$g_{CL_i,SH}(\boldsymbol{x}) = V_R - V(\tilde{q}_{CL})$	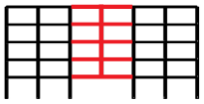
	Column failure	80	$g_{CL_i,COL}(\boldsymbol{x}) = R(N_R, M_R) - S(\tilde{N}_{SCLi}, \tilde{M}_{SCLi})$	

Source: own authorship.

Beam failure at the intact scenario is considered to damage only one continuous beam, since it is unlikely that live load reaches its 50-year extreme value in all stories simultaneously. Column failure at the intact scenario is considered only at the top corner due to the greater bending moments and low compressive forces in these regions (Section 3.4.2). Even with a eccentricity of 20 mm, column failure did not occur at the base of an inner column.

Middle column loss scenario is chosen just to illustrate the damaged areas in Table 4.11, but the actual frame portion to be damaged depends on which column is suddenly lost. Beam failure in column loss scenarios leads to an upward vertical propagation of progressive collapse, while failure of the adjacent columns results in one stage of horizontal propagation followed the immediate upward propagation of an increased portion of the frame (BECK et al. 2022). Depiction of Figure 4.18 justifies the adopted damaged frame area for this failure mode.

Table 4.12 shows the adopted uncertainty modelling for reliability analysis at the design support points, as well as the sampling domain $\mathcal{S}$ and design domain $\boldsymbol{\mathcal{D}}$. Boundary values for $\boldsymbol{\mathcal{S}}$ are chosen in terms of $\boldsymbol{\mu} \pm 2\boldsymbol{\sigma}$ for each random variable, since values beyond $2\boldsymbol{\sigma}$ have a reduced weight contribution and can be neglected without compromising the necessary efficiency for estimating the probabilities. Thus, lower and upper bounds for $\mathcal{S}$ for the random design variables are chosen in terms of $\boldsymbol{\mu}_{min}(\boldsymbol{\mathcal{D}}) - 2\boldsymbol{\sigma}$ and $\boldsymbol{\mu}_{max}(\boldsymbol{\mathcal{D}}) + 2\boldsymbol{\sigma}$, respectively.

Since the diameter for each rebar is optimized in this example, a fixed number of 3 rebars at each beam layer and 8 rebars for the square columns is adopted, as shown in Figure 4.16. For this example, with 6 random design variables and 8 random variables, 10 million sample points created via LHS are enough to ensure probability convergence for each failure mode of 2000 design support points. Each sample point created via LHS has its limit states evaluated as shown in Table 4.13, with the most relevant internal forces and ultimate load capacity at CA estimated via IDW metamodeling. This initial metamodeling stage relies on 2000 limit state support points, which are created via LHS and serves as input for structural analysis using OpenSees for both intact structure scenario and each column loss scenario.

Figure 4.16 – Cross-sections to be optimized in the RC frame.

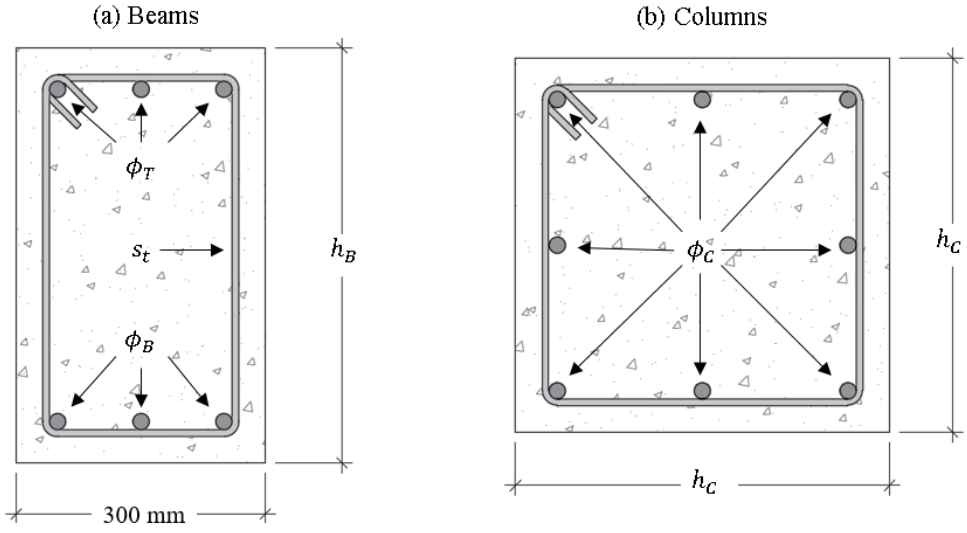

Source: own authorship.

Table 4.12 - Uncertainty modeling.

Category	RV	Distribution	Mean	Standard deviation	Coefficient of variation
Geometry	Beam depth (h_B)	Normal	To be optimized*	1 mm	-
	Bottom rebar diameter (ϕ_B)	Normal	To be optimized*	-	0.05
	Top rebar diameter (ϕ_T)	Normal	To be optimized*	-	0.05
	Stirrup spacing (s_t)	Normal	To be optimized*	-	0.05 (assumed)
	Column size (h_C)	Normal	To be optimized*	1 mm	-
	Column rebar diameter (ϕ_C)	Normal	To be optimized*	-	0.05
Material	Concrete strength (f_c')	Lognormal	32 MPa	-	0.12
	Rebar yield strength (f_y)	Normal	510 MPa	-	0.05
	Concrete unit weight (γ_c)	Normal	25 kN/m³	-	0.05 (assumed)
	Ultimate steel strain (ε_{su})	Normal	0.13 (1st case) 0.20 (2nd case)	-	0.14
Loads	Dead load (D)	Normal	$1.05D_n$	-	0.10
	50-year live load (L_{50})	Gumbel	$1.00L_n$	-	0.25
	Arbitrary point in time live load (L_{apt})	Gamma	$0.25L_n$	-	0.55
Analysis	Model error (M_E)	Lognormal	1.101	0.187	-

Source: Ellingwood and Galambos (1982), JCSS (2001), Real, Campos Filho and Maestrini (2003), Wisniewski et al. (2012), Santiago (2018), Santiago and Beck (2018), Parisi et al. (2018), Costa and Beck (2024a; 2024b).

Each beam span is discretized in 5 fiber displacement-based finite elements (3 Gauss-Lobatto integration points in each), being 3 finite elements for the beam itself and 1 at each beam end to represent the joint region. Praxedes (2020) shows the efficiency of this approach in terms of minimal refinement level and agreement with experimental static pushdown curves, although the beam-column joints are not explicitly modelled.

Corrotational transformation is used for all beam and column elements to account for the expected large geometrical nonlinearities. In order to avoid convergence issues along the entire sampling domain $\mathcal{S}$, the cross-section layering consists of 200 fibers for the confined concrete and 10 fibers for each face of unconfined concrete cover. Static bay pushdown analysis is performed with a displacement-based integrator using Kylov-Newton method to solve the nonlinear problem (tolerance of 10^{-5}). An initial increment size of 1 mm is adopted, but an adaptive algorithm is used to enhance or decrease the step depending on the lack or need of convergence improvement, respectively.

Since in bay pushdown analysis only the beam spans adjacent to the lost column have an increasing load applied, two load steps are adopted: a) nominal dead and live load are applied over all beam spans, as well as the self-weight of each structural member on itself; b) if beam rebar rupture does not occur on the first stage (possible for weak beam configurations), an increasing load is applied over the beam spans of interest until rebar rupture is verified.

The modified Park-Kent model (Park et al. 1982) is used as reference to estimate the confined and unconfined concrete behavior in compression, and the multilinear model from fib Model Code (2012) is the reference for concrete in tension. As shown in Figure 4.17, all main parameters from both models are used as inputs for the "concretewBeta" model available in OpenSees. Some parameters shown in Figure 4.17a, such as K, ε_{20u} and ε_{20c} are outputs from the reference concrete model (Park et al. 1982), relying on cross-section geometry, f_c' and stirrup detailing to be inferred.

Although commonly used for RC truss modelling, concretewBeta is able to satisfactorily represent softening and residual stresses both in tension and compression. Residual stress of tensile concrete is negligible in the applications of this study, but assuming a residual value of $0.01 f_{ctm}$ is enough to avoid major convergence issues from singular stiffness matrixes.

Rebar behavior is represented by the "ReinforcingSteel" model available in OpenSees, which realistically encompasses the linear elastic region, the yield plateau, strain hardening, and strain softening which are expected for typical steel reinforcements (Figure 4.17b).

Usual bilinear models are not used due a fixed value of hardening modulus of elasticity E_{sh} being adopted, which leads to load x displacement discrepancies and unrealistic rebar stresses for advanced stages of CA. As shown in section 3.3, this realistic rebar model results in close agreement with experimental data.

Figure 4.17 – Constitutive models and parameter values for concrete (a) and rebars (b).

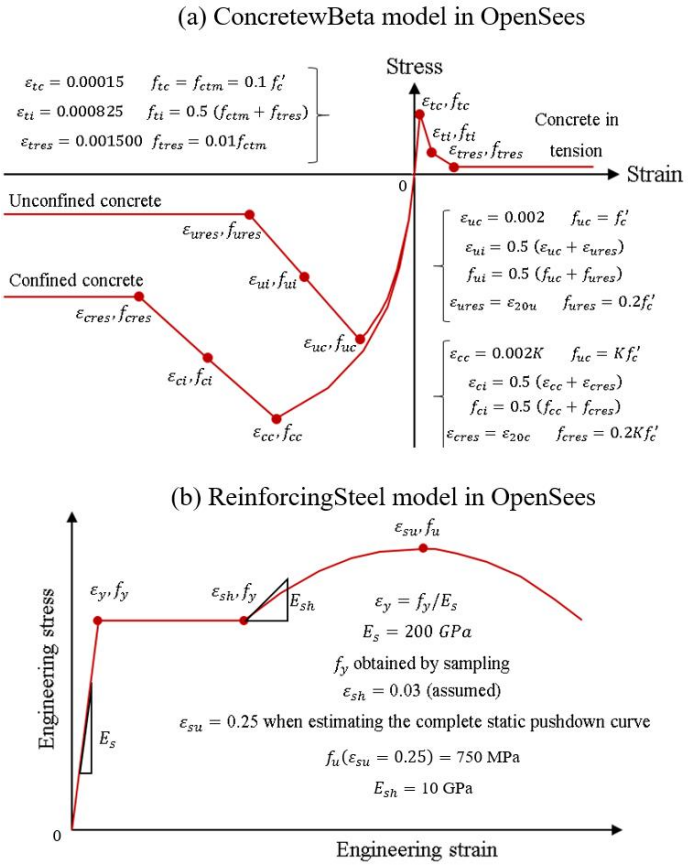

Source: own authorship.

Material nonlinear behavior is not considered in column discretization in order to avoid sudden breaks in the pushdown curve due to compressive rebar yielding and column buckling, as mentioned in section 3.3. This ensures a smooth and continuous force vs displacement curve, enabling metamodeling strategies to be efficiently used in order to proceed to reliability analysis.

As mentioned in section 3.5, satisfactory dispersion curves were not obtained even with 30 thousand limit state support points when explicitly addressing column failure. Therefore, one finite element with linear material behavior is assumed for columns in structural analysis, which still ensures a realistic evolution of axial forces and bending moments until the resisting envelope of the column is reached (as shown in section 3.4.2).

This simplified approach allows the internal forces to go beyond the cross section resisting envelope without a sudden force redistribution to keep further increments within the column resisting limit. Besides, this allows to estimate the frame load capacity at CA even though premature column failure may happen before it, ensuring a smooth behavior for all the probabilities of failure across the design domain $\boldsymbol{\mathcal{D}}$.

Herein, assuming a structural configuration prone to premature shear and/or column failures still relies on an estimated pushdown curve that increases until ultimate beam capacity at CA is reached. Although this is the only solution found to efficiently enable metamodeling strategies, reliability analysis, and ultimately the risk-based optimization, the estimated pushdown curve may differ from the realistic behavior if a premature failure occurs. However, this is not an issue for the proposed risk-based approach.

Beam shear and column internal forces realistically increase until their resisting limits are reached. As long as the internal forces are within their limits, the pushdown curve is realistic. Besides, when addressing the expected costs of failure, premature failure modes have greater penalization factors when compared to the ductile beam failure at CA. Hence, optimal risk-based design solutions are expected to not be prone to premature failure modes.

Based on Beck et al. (2020; 2022) and Ribeiro et al. (2023), the multipliers k reflect the severity of a given failure mode in terms of the construction cost of the area affected by the given failure mode C_{MA}.Values range accordingly to the analysis by Marchand and Stevens (2015), which compares the cost of construction to the cost of collapse of the Alfred P. Murrah Federal Building, World Trade Center and Pentagon. Hence, less severe failure modes, such as serviceability failure in terms of allowable displacements and bending failure (cross-section plastification by rebar yielding and/or concrete softening) have smaller values of k, while brittle shear and column failures have greater values.

As done in the previous example, rebar rupture in CA is considered the less severe failure mode for the column loss scenarios. Great displacements appear prior to rebar failure at CA, allowing enough time for building evacuation, so it is expected that the frame reaches this last line of defense against redistribution-type progressive collapse if it is unavoidable.

Identifying critical failure sequences to simplify the problem is fundamental (Rodrigues da Silva et al. 2024). Brittle shear for the column loss scenarios interrupts the full development of CA in the double span beams (or cantilever beam for an external column loss scenario), triggering a premature upward collapse propagation. Thus, Figure 4.18 shows how the failure of the columns adjacent to the lost one (due to a hazard and expressed in terms of P_{LD}) triggers a lateral propagation of collapse.

Figure 4.18 – Illustration of horizontal collapse progression due to column failure.

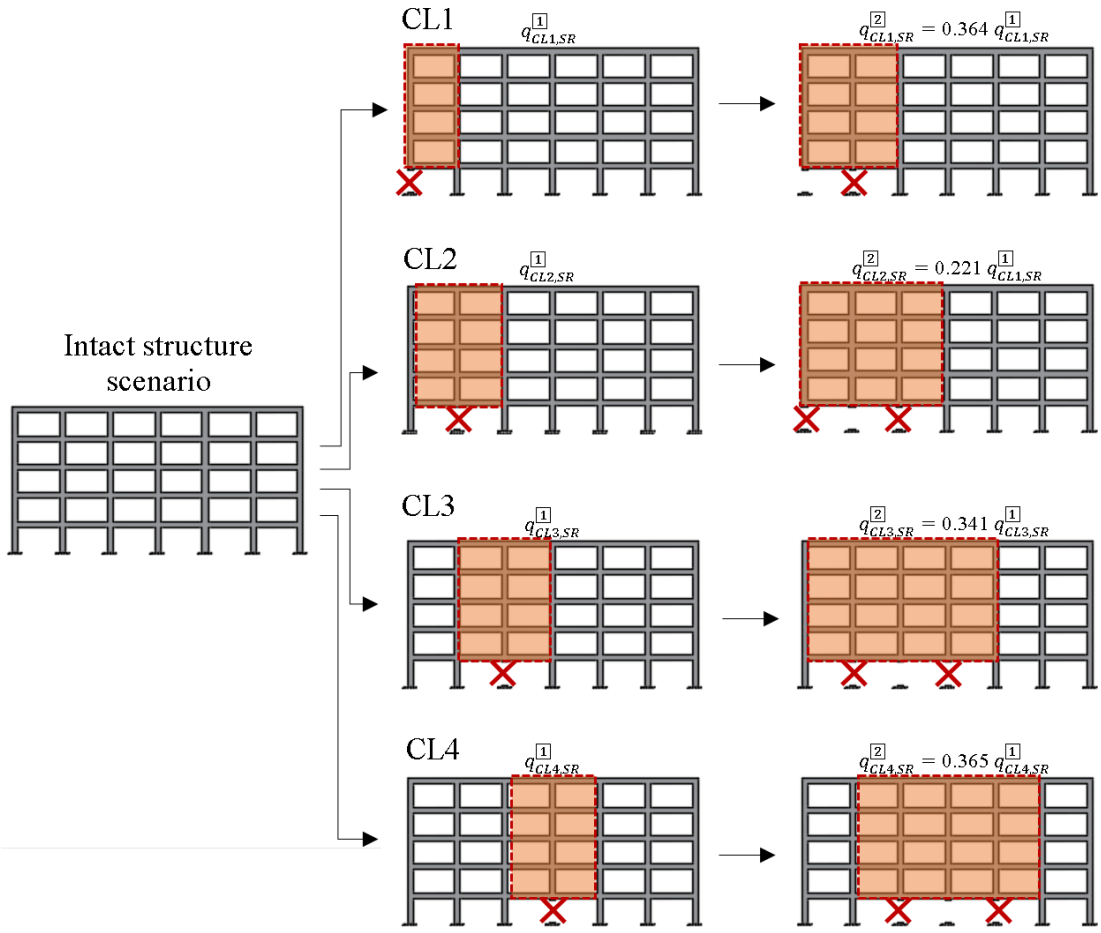

Source: own authorship.

When the first set of adjacent columns reach failure, beam span length increases above the updated number of lost columns, which in turn causes greater bending moments and axial forces for the remaining columns, mainly for the new set of adjacent columns. Since herein all columns have the same cross-section, failure of the initial set of adjacent columns unavoidably propagates the failure to the new set of adjacent columns, and failure propagates laterally until the increased beam span above reaches its new ultimate load-bearing capacity. Hence, adjacent column failure at a column loss scenario triggers a horizontal collapse propagation that advances until the upward propagation is unavoidable, resulting in a significantly increased extension of the damaged area and justifying the choice of greater k value for it.

Reliability analysis for the design support points reveals probabilities of beam failure due to rebar rupture greater than 0.99 when the first set of adjacent columns is removed, and equal to 1.00 for the upcoming stages. Therefore, only the 1st and 2nd stages (enclosed by a dashed dark red line in Figure 4.18) are actually addressed for adjacent column failure in the missing column loss scenarios.

4.3.1 Optimal design solutions

In order to address how the amount of reinforcement ductility influences over the optimal design, two mean values of ultimate steel strain are considered for column loss scenarios: 0.13, as used in the reference frames of Yu and Tan (2013), and 0.20, as commonly used in studies of structural robustness.

For each case the optimal risk-based design is investigated for increasing values of P_{LD} for each column loss scenario individually, and then considering the loss of any column in the first floor. Firefly algorithm is used to solve the optimization problem, relying on 10 optimization runs for each P_{LD} value, 100 iterations per run, and 40 fireflies.

An initial extensive search with 10000 fireflies is done over $\boldsymbol{\mathcal{D}}$ to improve convergence around the global optima, so only the 40 most bright fireflies are kept in further iterations. It should be noticed that the auxiliary extensive search + iterations only take a few seconds. This is possible due to IDW metamodeling to estimate the reliability indexes accurately for each failure mode at any region of the design domain $\boldsymbol{\mathcal{D}}$.

Tables 4.14 to 4.18 shows the optimal risk-based results at each columns loss scenario for all strengthening strategies. Starting from P_{LD}^{min}, the optimal design for all column loss scenarios remains constant until a threshold P_{LD}^{th} value is reached. Optimal 1st stage beam design is similar to the one found previously for the RC beam subassemblage. The slightly increased beam depth of 576 mm is compensated by a reduction in the top rebar diameter to 19 mm and increase in stirrup spacing to 200 mm, leading to reinforcement ratios of 0.26% for bottom rebars, 0.49% for top rebars and 0.17% for stirrups.

By comparing with the first example, allowing an upper bound of 600 mm for beam depth leads to a 1st stage design 1.8% more expensive in terms of beam manufacturing cost, but with greater overall resistance: 17% more for bending at midspan, 5% more for bending at beam ends, and 15% greater shear capacity. The advantages are more evident when addressing the second example (section 4.2), for which a 19% reduction in beam manufacturing costs leads to an overall increase of 25% for bending and shear capacities.

Hence, in terms of conventional scenarios under normal loading condition, ensuring greater moment of inertia by increasing beam depth seems to be the best approach for minimizing beam constructive costs and enhancing its resisting capacity. This is especially more evident when dealing with more expensive unitary construction costs.

Optimal column design seems to be indifferent to P_{LD} for all scenarios and reinforcement strategies, showing slight increases of a few mm in column size and up to 2 mm in column rebar diameter even for greater values of P_{LD}. Load combination of usual loading condition $q_I = 1.2D_n + 1.6L_n$ leads to approximately 63 kN/m for beam spans and 4.8 kN/m for column spans (D_n = 7.1 kN/m² and L_n = 4.8 kN/m²), so a total of 2000 kN is roughly expected at the foot of an inner column. This estimated demand is just 40% of the ultimate axial capacity of the optimal cross-section, and addressing a minimum eccentricity of 20 mm (IS, 2000) still keeps the axial load x bending moment demand in the column resisting envelope.

However, structural analysis shows that bending moments at the frame top corners have values ~5% of the axial demand at the foot of the inner columns. Thus, bending moments of roughly 100 kNm combined with negligible axial forces are expected at the top of corner columns. By addressing the column resisting envelope, column strength reduction factors ϕ ranging from 0.65 to 0.90 leads to an axial load x bending moment demand close to the resisting threshold. Hence, optimal 1st stage column design leads to Demand Capaciy Factors (DCRs) ranging from 1.18 ($\phi = 0.65$) to 0.85 ($\phi = 0.9$). Although leading to DCR > 1 for smaller ϕ values, the difference is small and column plastification in the frame top corner is not as severe as if it happens in the foot of a ground floor column (as discussed in Section 3.4.2).

Load combination for extraordinary loading condition is used with a DAF of 1.22 (common value after CAA). So, $q_{CL} = 1.22\ (1.2D_n + 0.5L_n)$ leads to 57 kN/m for the double span beams, 47 kN/m in the non-affected span beams and 4.8 kN/m for column spans, so a total of 2550 kN is roughly expected at the foot of the column adjacent to the lost one. Although this axial demand being 50% of the column axial capacity, optimal column design at the 2nd stage relies once again in the bending moment demand. As discussed in section 3.3, beams require enough axial restraint in order to Catenary Action (CA) to be developed, and herein this is provided by the RC columns. As shown in Figure 4.15a, the pushdown curves may reach vertical drifts ranging from ~2 h_B to ~4h_B, related to significant axial tensile. These enhanced axial forces due to CA cause severe bending moments in the adjacent columns, promoting their rebars to yield and compromising their lateral restraint capabilities. Hence, as opposed to the previous example, optimal design focuses on the CAA mechanism (greater beam depths).

The threshold value that defines a positive cost-effect in strengthening depends on the frame extent to be strengthened. It also depends on the amount of ductility provided, but in a smaller scale. Loss of the exterior column (CL1) is the only noticeable exception, with P_{LD}^{th} between 10^{-2} and 10^{-1} no matter what reinforcement decision is being adopted.

Table 4.14 – Optimal risk-based design for each individual scenario of column loss, low ductility rebars and whole frame strengthened.

Scenario	P_{LD}	h_B^* (mm)	ϕ_B^* (mm)	ϕ_T^* (mm)	s_t^* (mm)	h_C^* (mm)	ϕ_C^* (mm)	C^*_{TE} (€)	C_M^* (€)	C^*_{Beam} (€ / m)	C^*_{column} (€ / m)
External column loss (CL1)	$\leq 10^{-3}$	576	14	19	200	400	16	30741.33	30389.03	83.78	127.14
	10^{-2}	576	14	19	200	400	16	33287.39	30389.02	83.78	127.14
	10^{-1}	588	26	26	149	400	17	42412.93	40923.34	140.96	129.15
	1	598	25	28	134	400	17	44390.52	42354.93	147.17	131.75
Penult. column loss (CL2)	$\leq 10^{-3}$	576	14	19	200	400	16	30741.95	30389.03	83.78	127.14
	10^{-2}	576	14	19	200	400	16	34522.53	30389.02	83.78	127.14
	10^{-1}	590	26	26	148	400	17	41565.87	40996.14	141.25	129.32
	1	600	25	28	135	400	17	43230.63	42537.87	147.51	132.76
Antepenult. column loss (CL3)	$\leq 10^{-3}$	576	14	19	200	400	16	30743.50	30389.03	83.78	127.14
	10^{-2}	581	14	19	199	400	16	36942.24	30806.65	85.49	128.05
	10^{-1}	589	26	26	149	400	17	41361.58	40956.93	141.04	129.30
	1	600	25	28	139	400	17	42639.68	42306.72	147.13	131.42
Middle column loss (CL4)	$\leq 10^{-3}$	576	14	19	200	400	16	30744.28	30389.03	83.78	127.14
	10^{-2}	580	14	19	200	400	16	31584.05	30820.03	85.66	127.92
	10^{-1}	587	26	26	149	400	17	41202.75	40968.68	141.19	129.19
	1	600	25	28	135	406	17	42634.67	42513.72	147.33	132.79

Source: own authorship.

Table 4.15 – Optimal risk-based design for each column loss scenario, greater ductility rebars and whole frame strengthened

Scenario	P_{LD}	h_B^* (mm)	ϕ_B^* (mm)	ϕ_T^* (mm)	s_t^* (mm)	h_C^* (mm)	ϕ_C^* (mm)	C^*_{TE} (€)	C_M^* (€)	C^*_{Beam} (€ / m)	C^*_{column} (€ / m)
External column loss (CL1)	$\leq 10^{-3}$	576	14	19	200	401	16	30994.74	30389.03	83.78	127.14
	10^{-2}	576	14	19	200	401	16	33287.33	30389.02	83.78	127.14
	10^{-1}	597	20	26	151	412	16	39314.92	38250.37	125.15	130.59
	1	600	25	28	137	412	17	42885.04	42490.03	147.03	133.10
Penult. column loss (CL2)	$\leq 10^{-3}$	576	14	19	200	401	16	31118.25	30389.03	83.78	127.14
	10^{-2}	576	14	19	200	401	16	34522.48	30389.02	83.78	127.14
	10^{-1}	595	20	26	157	413	17	39413.46	38050.66	123.32	131.67
	1	600	25	28	138	413	17	42696.26	42338.31	146.86	132.08
Antepenult. column loss (CL3)	$\leq 10^{-3}$	576	14	19	200	401	16	31428.39	30389.03	83.78	127.14
	10^{-2}	584	14	19	199	400	17	36062.45	31214.29	85.58	131.31
	10^{-1}	600	20	26	157	408	17	39061.80	38257.98	124.16	132.14
	1	600	25	28	135	408	17	42592.19	42497.36	147.33	132.71
Middle column loss (CL4)	$\leq 10^{-3}$	576	14	19	200	401	16	31583.99	30389.03	83.78	127.14
	10^{-2}	581	14	19	200	401	17	36921.59	31376.24	86.40	131.44
	10^{-1}	597	20	26	153	406	17	39135.82	38330.48	125.18	131.21
	1	600	25	28	134	406	17	42634.67	42513.72	147.38	132.77

Source: own authorship.

Table 4.16 – Optimal risk-based design for each individual scenario of column loss, low ductility rebars and strengthening in the 2 first floors.

Scenario	P_{LD}	h_B^* (mm)	ϕ_B^* (mm)	ϕ_T^* (mm)	s_t^* (mm)	h_C^* (mm)	ϕ_C^* (mm)	C^*_{TE} (€)	C_M^* (€)	C^*_{Beam} (€ / m)	C^*_{column} (€ / m)
External column loss (CL1)	$\leq 10^{-3}$	576	14	19	200	401	16	31294.79	30388.91	83.78	127.14
	10^{-2}	576	14	19	200	400	16	33913.41	30392.91	83.78	127.18
	10^{-1}	600	25	28	135	400	17	43058.98	42443.77	146.84	132.99
	1	600	25	28	137	400	17	44768.34	42498.23	147.31	132.75
Penult. column loss (CL2)	$\leq 10^{-3}$	576	14	19	200	401	16	30685.62	30069.02	84.13	127.75
	10^{-2}	600	20	26	153	402	16	33836.69	33188.65	125.77	130.28
	10^{-1}	589	26	26	147	400	17	34820.34	34257.38	141.33	130.20
	1	600	25	28	134	401	17	35534.19	34832.16	147.04	132.59
Antepenult. column loss (CL3)	$\leq 10^{-3}$	576	14	19	200	401	16	30784.62	30174.30	84.52	129.35
	10^{-2}	591	21	26	151	405	17	33586.22	33088.29	124.58	129.96
	10^{-1}	590	26	26	148	400	17	34638.90	34247.30	141.13	129.29
	1	600	25	28	134	401	17	35149.26	34868.60	147.46	132.72
Middle column loss (CL4)	$\leq 10^{-3}$	576	14	19	200	401	16	31061.62	30112.47	84.71	129.23
	10^{-2}	600	20	26	153	401	16	33721.38	33142.14	125.73	130.34
	10^{-1}	590	26	26	148	401	17	34911.80	34250.85	146.49	132.60
	1	600	25	28	139	401	17	35142.90	34785.19	147.56	132.78

Source: own authorship.

Table 4.17 – Optimal risk-based design for each column loss scenario, greater ductility rebars and strengthening in the 2 first floors

Scenario	P_{LD}	h_B^* (mm)	ϕ_B^* (mm)	ϕ_T^* (mm)	s_t^* (mm)	h_C^* (mm)	ϕ_C^* (mm)	C^*_{TE} (€)	C_M^* (€)	C^*_{Beam} (€ / m)	C^*_{column} (€ / m)
External column loss (CL1)	$\leq 10^{-3}$	576	14	19	200	401	16	30568.72	30066.57	84.12	127.71
	10^{-2}	576	14	19	200	400	16	32913.38	30015.60	83.78	127.15
	10^{-1}	595	25	28	140	400	17	34865.69	34690.66	146.29	130.77
	1	600	25	28	135	400	17	35238.62	34853.04	147.24	132.73
Penult. column loss (CL2)	$\leq 10^{-3}$	576	14	19	200	401	16	30685.56	30069.01	84.13	127.75
	10^{-2}	600	19	27	138	400	17	33512.69	33204.41	125.36	131.21
	10^{-1}	600	20	26	153	401	16	34545.96	33192.13	125.82	130.27
	1	600	25	28	135	400	17	35150.65	34876.60	147.53	132.79
Antepenult. column loss (CL3)	$\leq 10^{-3}$	576	14	19	200	401	16	30784.51	30174.04	84.51	129.36
	10^{-2}	599	19	26	151	400	17	33238.40	33028.59	122.19	132.29
	10^{-1}	600	20	26	152	404	17	33993.89	33164.52	124.57	131.56
	1	600	25	28	138	400	17	34914.74	34852.43	147.19	132.79
Middle column loss (CL4)	$\leq 10^{-3}$	576	14	19	200	401	16	30852.53	30174.07	84.51	129.36
	10^{-2}	597	19	27	138	401	17	33443.74	33222.64	124.75	132.50
	10^{-1}	600	20	26	158	400	18	34007.25	33263.91	123.36	135.43
	1	596	25	28	134	402	17	34931.39	34736.58	147.36	130.14

Source: own authorship.

Table 4.18 – Optimal risk-based design addressing sudden loss at any ground floor column.

Scenario	P_{LD}	h_B^* (mm)	ϕ_B^* (mm)	ϕ_T^* (mm)	s_t^* (mm)	h_C^* (mm)	ϕ_C^* (mm)	C^*_{TE} (€)	C_M^* (€)	C^*_{Beam} (€ / m)	C^*_{column} (€ / m)
Entire frame strengthened Low ductility	$\leq 10^{-3}$	576	14	19	200	400	16	30740.11	30389.03	83.78	127.14
	10^{-2}	576	14	19	200	401	16	31238.16	30389.03	86.98	130.43
	10^{-1}	582	25	25	198	400	17	35372.65	31360.22	140.86	129.41
	1	589	25	28	152	401	17	41772.35	40935.29	146.78	131.48
Entire frame strengthened Greater ductility	$\leq 10^{-3}$	576	14	19	200	400	16	31238.11	30389.03	83.78	127.14
	10^{-2}	583	14	19	199	400	17	35183.22	31188.82	86.41	129.86
	10^{-1}	595	20	26	160	404	16	39427.41	37782.89	122.73	130.33
	1	600	25	28	136	400	17	42714.02	42486.48	147.25	132.73
Two floors strengthened Low ductility	$\leq 10^{-3}$	576	14	19	200	401	16	30705.37	30182.34	84.71	129.23
	10^{-2}	600	20	26	153	404	16	33839.96	33189.20	125.73	130.34
	10^{-1}	600	25	28	137	400	17	34909.86	34793.04	146.49	132.60
	1	600	25	28	135	400	17	35747.93	34878.20	147.56	132.78
Two floors strengthened Greater ductility	$\leq 10^{-3}$	576	14	19	200	401	16	30785.70	30098.34	84.68	127.54
	10^{-2}	600	18	27	140	400	17	33420.76	33135.32	122.98	133.33
	10^{-1}	595	20	26	156	400	17	34499.01	33108.15	124.40	130.65
	1	600	25	28	144	400	17	35007.08	34683.61	145.78	131.40

Source: own authorship.

As discussed in Section 3.3, 2D analysis shows that exterior column loss is the most demanding scenario. In fact, ultimate load-bearing capacity increases as the missing column scenario (ground floor) is located inner in the frame, reaching a maximum for middle column loss. Catenary Action (CA) effectiveness is shown to be enhanced as the amount of lateral frame confinement increases from both sides. Middle column loss has the greatest amount of remaining adjacent spans in each side, so the maximum mobilization of CA is achieved. The opposite is true for external column loss, as insufficient axial restraints makes the frame rely only on bending action and Vierendeel action. Therefore, greater costs of strengthening are expected for CL1 to provide a satisfactory load-bearing capacity, and this is shown to be justifiable only for larger threats for all the adopted reinforcement decisions.

When addressing only CL1, optimal 2nd stage beam design shows almost identical reinforcement ratios for both reinforcement strategies: 0.82% for bottom rebars, 1.03% for top rebars, and 0.25% for stirrups. However, the benefits of the strengthening strategies are shown in terms of C_{TE} and C_M. Greater ductility rebars provide an economy of ~1000€ in C_{TE} for both total and partial frame reinforcement, but it does not reduce C_M. However, partial frame strengthening reduces both C_M and C_{TE} in 19% when compared to total reinforcement, although it is only effective for loss in the first storey. The gap between optimal values of C_M and C_{TE} for CL1 ranges from 2000 € (low ductility rebars) to 1000 € (greater ductility rebars).

For a given setup of design parameters, ultimate capacity is expected to be greater for penultimate column loss (CL2) due to CA now being achievable. Yet, the same optimal 2nd stage beam design from CL1 is shown to be optimal for CL2. Greater ductility rebars still provide an economy of ~1000€ in C_{TE} for both total and partial frame reinforcement, and partial frame strengthening now reduces both C_M and C_{TE} in 17% when compared to whole frame reinforcing. Still, the gap between optimals C_M and C_{TE} is smaller for CL2, ranging from ~800€ (low ductility rebars) to ~300€ (greater ductility rebars). Since additional load-bearing capacity is possible due to CA, and C_M^* for CL1 and CL2 are equivalent, $\sum C_{ef}^*$ for CL2 is reduced.

Antepenultimate column has even greater lateral restraint, so an enhanced ultimate capacity is expected at CA. Yet, the same optimal 2nd stage beam design from CL1 and CL2 is found for CL3. Partial frame strengthening still reduces both C_M and C_{TE} by 17% when compared to a whole frame reinforcing, and the gap between optimal C_M and C_{TE} is ~200€ for both low ductility and greater ductility rebars. The economy of ~1000€ in C_{TE} previously found for greater ductility rebars is significantly reduced to ~200€. Hence, $\sum C_{ef}^*$ gets significantly reduced as the CA mechanism efficiency increases, even for low ductility rebars.

Optimal 2nd stage beam designs for middle column loss behave similarly to those from CL3. Partial frame strengthening reduces C_M and C_{TE} in 17%, and the gap between optimal C_M and C_{TE} is ~200€ independently on rebar ductility. Greater ductility rebars once again provide an economy of ~200€ in C_{TE}. Although the CA effectiveness for CL4 is greater than CL3, its effect in a risk-based approach is found to be equivalent to CL3.

Tables 4.14 to 4.18 show that the cost-benefit of reinforcement against progressive collapse is justifiable for lower threat probabilities as the CA effectiveness increases. As mentioned earlier, CL1 is the only scenario with P_{LD}^{th} ranging between 10^{-2} to 10^{-1} independently on the reinforcement strategy, which is due to a lower ultimate capacity resulting from a lack of CA mechanism. Penultimate column loss is the first scenario to allow CA to be developed, although not so efficiently. This leads to P_{LD}^{th} ranging between 10^{-2} to 10^{-1} when a more expensive total frame reinforcement is addressed, but this range reduces from 10^{-3} to 10^{-2} if the reinforcement is made just in the two first floors.

Antepenultimate and middle column loss show similar behaviors in this aspect, with P_{LD}^{th} ranging between 10^{-3} to 10^{-2} for all reinforcement strategies due to their extra enhanced CA capacity. However, optimal designs for $P_{LD} = 10^{-2}$ reveals just a small increase in beam depth (to account for shear capacity at CL3 and CL4) when the entire frame reinforcement is addressed. If partial frame strengthening is considered, optimal beam designs for $P_{LD} = 10^{-2}$ show already all characteristics of the optimal 2nd beam design: 0.82% for bottom rebars, 1.03% for top rebars, and 0.25% for stirrups.

As shown in the sensitivity analysis of Figure 4.15a and b, increasing h_B increases the ultimate load-bearing capacity at the expense of decreasing the overall frame ductility (in terms of large displacements) for a same amount of rebar ductility (in terms of ε_{su}). Hence, optimizing h_B while ensuring a thorough usage of confined concrete beyond softening and steel rebars up to their ultimate capacity is closely related to a multi-objective optimization problem, as shown in Figure 4.19. In terms of h_B, each static pushdown curve leads to a solution that fully utilizes the resisting capacity of each material, and the set of all solutions corresponds to a Pareto frontier in terms of ε_{su}.

This Pareto front explicitly shows a tradeoff between ultimate load-bearing capacity and overall frame ductility, as increasing one reduces the other. Thus, results shown herein demonstrate that the proposed risk-based optimization framework is able to efficiently address the best balance between this tradeoff by simultaneously addressing construction costs and expected costs of failure.

Figure 4.19 – Tradeoff between structural ultimate capacity and frame ductility.

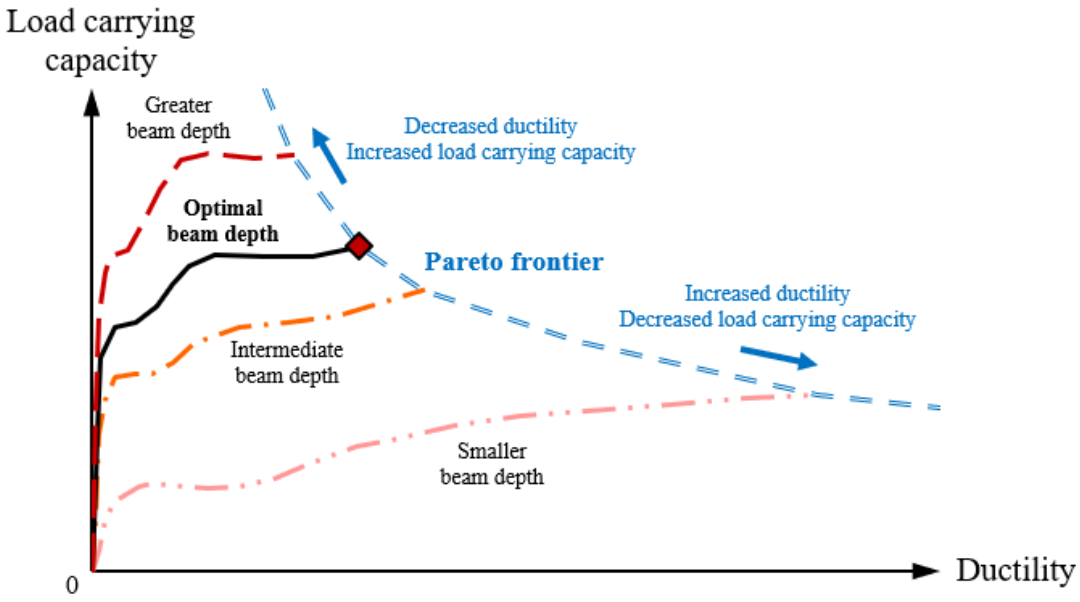

Source: own authorship.

In this example, $h_B^* = 600$ mm (upper bound for h_B in $\boldsymbol{\mathcal{D}}$) for all cases of individual column loss reflects a full preference of load carrying capacity in detriment of frame ductility. However, this result is valid specifically for the structure addressed in this example: a perimeter primary frame with 6 bays, 5 stories, beam spans of 6 m, column spans of 3.3 m (4 m at ground floor), and unusually high values for nominal dead load and live loads ($D_n = 7.1$ kN/m² and $L_n = 4.8$ kN/m²). Nonetheless, optimization constraints in terms of minimum ductility requirements could be adopted in order to ensure a minimal safety margin in terms of time for building evacuation.

Optimal beam designs with maximum load capacity and minimal vertical drifts, in terms of $h_B^* = 600$ mm, correspond to smaller tensile axial forces during CA stage, which in turn reduces the bending moments acting over the adjacent columns. Hence, beam depth is shown to be a highly relevant design variable due to its direct increase in resistance across 6 failure modes (serviceability in terms of allowable displacements, beam bending at its midspan and at its ends, shear failure in both intact and damaged scenarios, and steel rebar rupture) and its indirect reduction in moment demand when addressing column failure.

Reducing h_B^* in favor of more frame ductility would require additional longitudinal and transversal reinforcements, as well as possible greater dimensions for column cross sections, in order to achieve similar safety margins against all failure modes. This approach, however, is shown to have no cost-effectiveness in terms of the balance between C_M and $\sum C_{ef}$.

When P_{LD} relates to the sudden loss of any column at ground floor level, optimal 2nd stage beam designs still behave similarly to those found for individual column loss. Partial frame strengthening reduces C_M and C_{TE} in 16%, and the gap between optimal C_M and C_{TE} ranges from ~300€ (greater ductility rebars) to ~850€ (low ductility rebars). Nonetheless, greater ductility rebars provide a negligible economy in terms of just C_{TE}, as similarly found for the individual loss of the inner columns.

All reinforcement strategies lead to P_{LD}^{th} ranging from 10^{-3} to 10^{-2}, except for the case of low ductility rebars combined with whole frame strengthening (10^{-2} to 10^{-1}). However, it should be noticed that P_{LD} related to the sudden loss of any column implies, in this example, to an individual $P_{LDcol} = P_{LD}/\ 7$, with 7 being the number of columns subjected to local damage.

Hence, P_{LD} ranging from 5×10^{-6} to 1 for any column implies, in this example, that each column is subjected to P_{LDcol} ranging from ~7.14×10^{-7} to ~1.428×10^{-1}. This explains why the overall optimal behavior when addressing the loss of any column closely resembles optimal results for loss of inner columns. Since individual P_{LDcol} is able to reach a maximum of ~0.14, the greater gaps between C_M^* and C_{TE}^* observed for individual loss of CL1 and CL2 for $P_{LD} = 1$ are not obtained.

Figure 4.20 shows the behavior of the optimal conditional reliability indexes β^* with P_{LD} for NLC failure modes (intact structure) for the different strengthening strategies. Figures 4.21 and 4.22 shows β^* behavior with P_{LD} for the CLS failure modes addressing total and partial frame reinforcements, respectively. When assessing β^* for CLS, strong lines are related to the individual loss of the given column, while thinner transparent lines represent its loss when any column is subjected to P_{LD}.

Optimal 1st stage design is controlled by bending failure at the beam ends ($\beta_{I,BE}^* \approx$ 3.2) and by column failure at the top corner of the frame ($\beta_{I,CO}^* \approx 3.4$). As mentioned earlier, optimal 1st stage beam design is cheaper and more efficient, in terms of resisting capacity, than those found in the previous examples, and optimal column design leads to a DCR ranging from 0.85 to 1.13, depending on the strength reduction factor ϕ adopted.

After P_{LD}^{th}, $\beta_{I,BE}^*$ is the first safety margin to increase due to a gradual initial increase of h_B^*, followed by $\beta_{I,CO}^*$ and then the remaining failure modes. Besides, the reduction in P_{LD}^{th} for a partial frame reinforcement is once again noticeable.

Figure 4.20 - Behavior of β^* with P_{LD} for NLC.

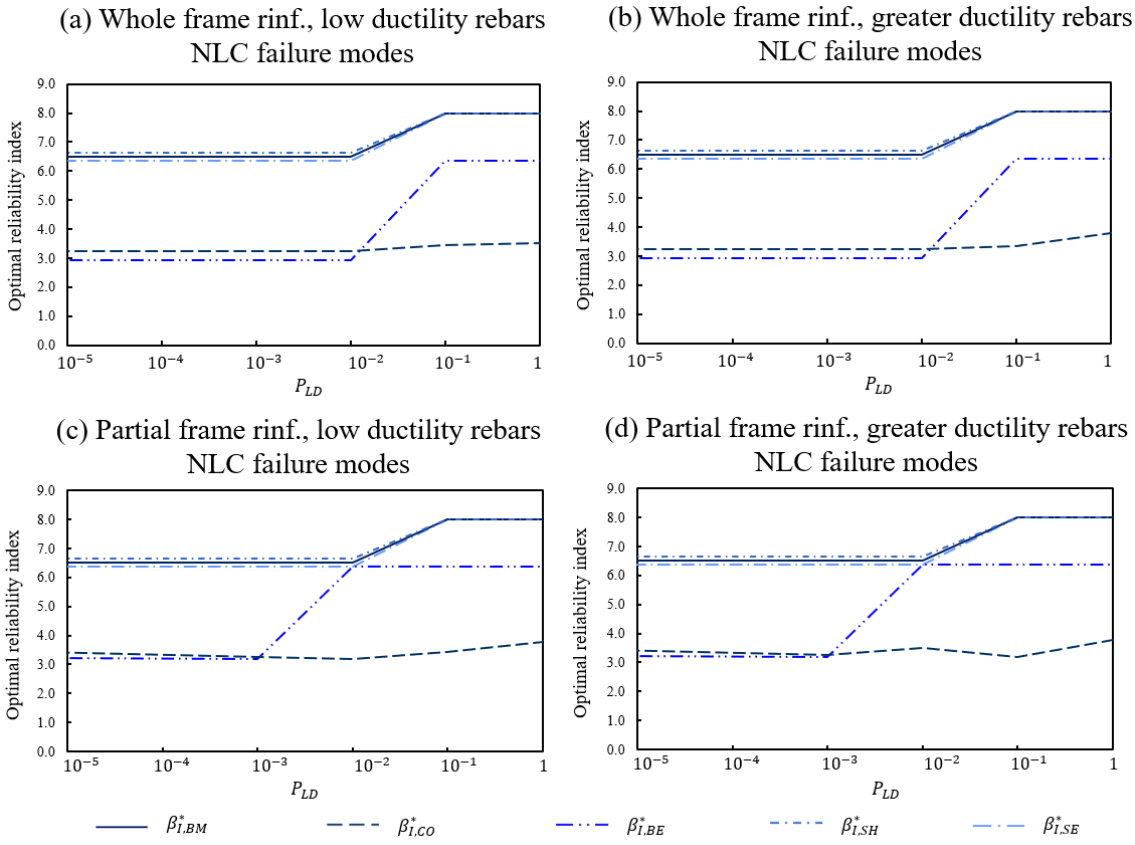

Source: own authorship.

For both partial and total frame reinforcements, optimal 2nd stage design is controlled either by steel rupture or by shear failure, depending on the strengthening strategy and P_{LD} value. Nonetheless, P_{LD}^{th} is characterized by $\beta^*_{CLi,SR}$ reaching a minimum of 2.33. For both partial and total frame strengthening, $P_{LD} = 10^{-1}$ is related to $\beta^*_{CLi,SH} < \beta^*_{CLi,SR}$ for low ductility rebars, while for greater ductility the opposite is observed.

Although no reduction in C_M is noticeable from using greater ductility rebars, their potential to provide greater decreases in $C_{ef\ CLi,SR}$ allows usage of slightly less longitudinal reinforcement while still providing satisfactory safety margins.

Symmetric rebars of 25 mm related to a slightly reduced h_B found for $P_{LD} = 10^{-1}$ and low ductility reinforcements enhance the beam's ultimate capacity, but this is more expansive and there is no correspondent increase in shear capacity. Hence, this option is shown to be justified only for low ductility rebars right after APM design becomes cost-effective, as an emergency response to increased expected costs of failure when P_{LD}^{th} is reached. Yet, for other alternatives and $P_{LD} > 10^{-1}$ there is a visible preference for $\phi_T > \phi_B$ and increased h_B, which is slightly cheaper and better suitable against larger strains in the top beam layer.

Figure 4.21 - Behavior of β^* with P_{LD} for each CLS (whole frame reinforcement).

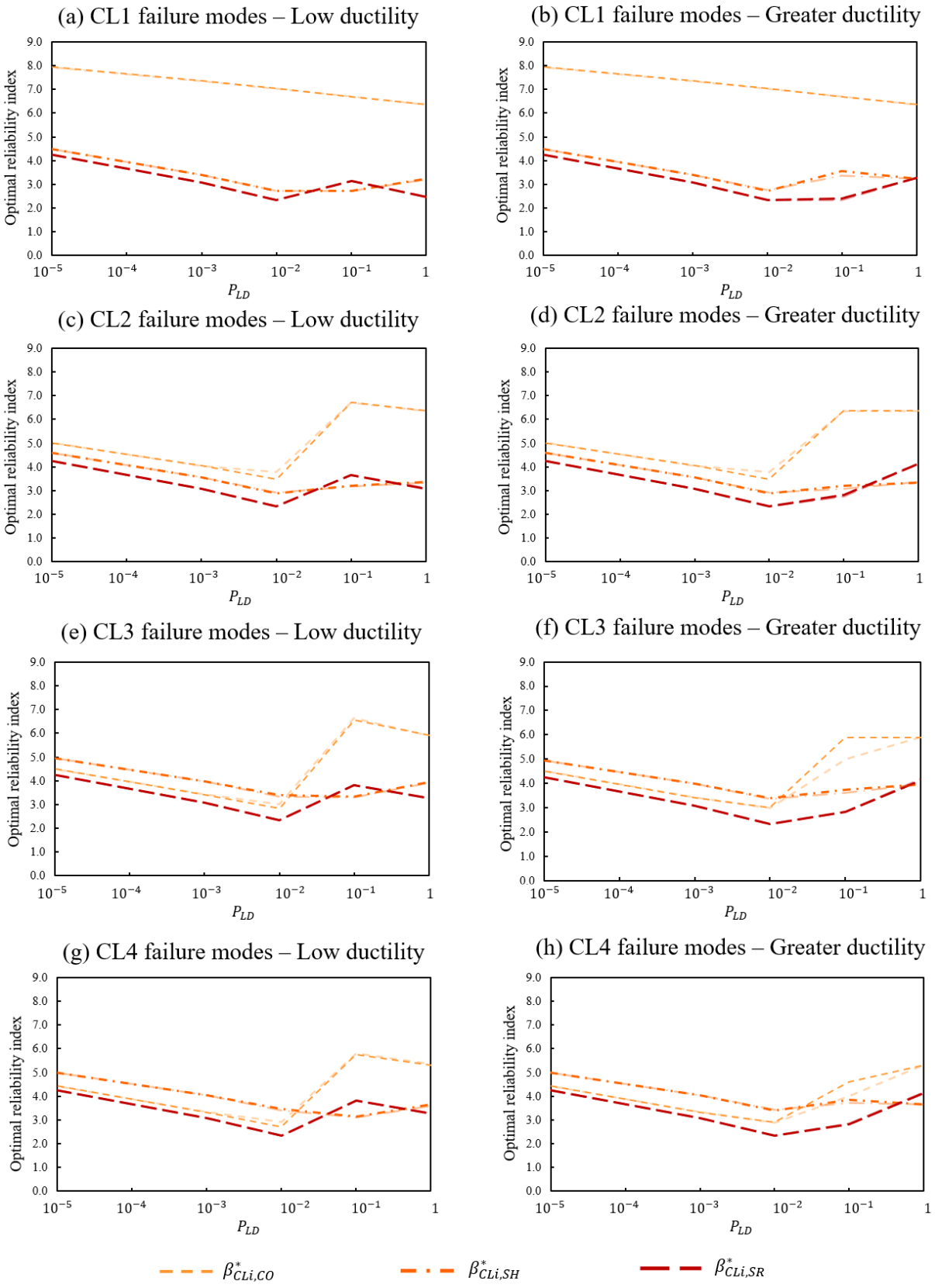

Source: own authorship.

Figure 4.22 - Behavior of β^* with P_{LD} for each CLS (partial frame reinforcement).

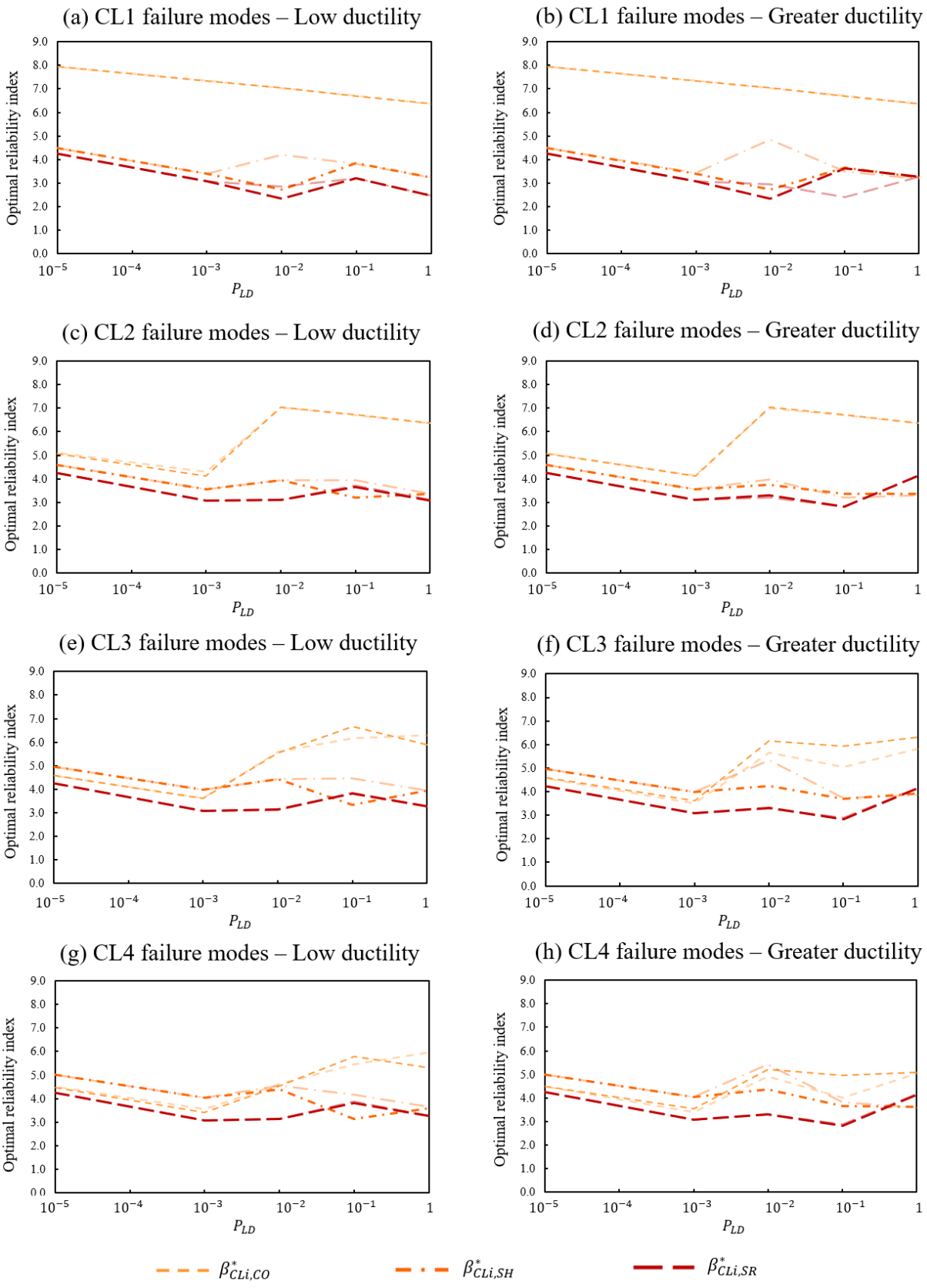

Source: own authorship.

Between adopting symmetric rebars plus additional stirrup ratio to ensure shear capacity, or using asymmetric rebars ($\rho_T \approx 1.7\rho_B$) with greater h_B and reduced s_t, the algorithm's preference relies on the amount of rebar ductility and threat probability. Therefore, symmetric rebar options related to slightly reduced beam depths are found to have the best cost-effectiveness when simultaneously dealing with individual column loss scenarios, providing low ductility reinforcements, and at the first part of the 2nd stage, right after P_{LD}^{th}.

Column safety margins for CLS shows a minimum of $\beta_{CLi,CO}^{*} \approx 4.0$ at P_{LD}^{th} and 6.0 for values beyond it, except for external column loss. Since in CL1 there is no development of catenary action, there are no enhanced bending moments acting over the adjacent column. Figure 4.21 reveals no significate difference between safety margins for individual column loss and those for the loss of any column when the entire frame is strengthened. However, Figure 4.22 shows that for a partial frame reinforcement, assuming loss of any column leads to the only case of the external column being reinforced for $P_{LD} < 10^{-2}$, and that symmetric rebars are not cost-effective at any range of P_{LD}, even when assuming low ductility rebars.

Optimal resistance factors γ_{CLi}^{*} are used to address the increase of each resisting parameter in terms of P_{LD} and each CLS in nondimensional terms:

$$\gamma_{CLi,fm}^{*} = \frac{R_{CLi,fm}^{*}(P_{LD})}{R_{CLi,fm}^{*}\left(P_{LD}^{min}\right)} \tag{4.12}$$

where CLi is the scenario being addressed; $R_{CLi,fm}^{*}\left(P_{LD,j}\right)$ relates to the optimal resisting capacity of any fm failure mode at CLi and the P_{LD} value of interest. Herein, γ_{CLi}^{*} relates to positive and negative beam bending, shear capacity, column axial capacity, and ultimate load capacity corresponding to steel rupture. Figure 4.23 shows the behavior of each $\gamma_{CLi,fm}^{*}$ as a function of P_{LD}.

Positive beam bending capacity is the resistance parameter with greater improvement at the 2nd stage ($\gamma_{CLi,BM}^{*} \approx 3.1$), and this is due to an increase in ρ_B^{*} from 0.31% to 0.82%. Although being one of the less relevant variables for the intact structure ($\beta_{I,BM}^{*} \approx 6.5$), ϕ_B plays a major role after P_{LD}^{th} by directly assisting to provide load-bearing capacity long after the plastification of the double span beam cross-sections. In line with the above, it is found that optimal load bearing capacity of rebar rupture in the 2nd stage increases up to $\gamma_{CLi,SR}^{*} \approx 2.25$, ensuring the beam being able to effectively achieve all resisting mechanisms, and that ductile steel rupture occurs in case of collapse being unavoidable (least worst failure mode).

Figure 4.23 - Behavior of γ^*_{CLi} with P_{LD}.

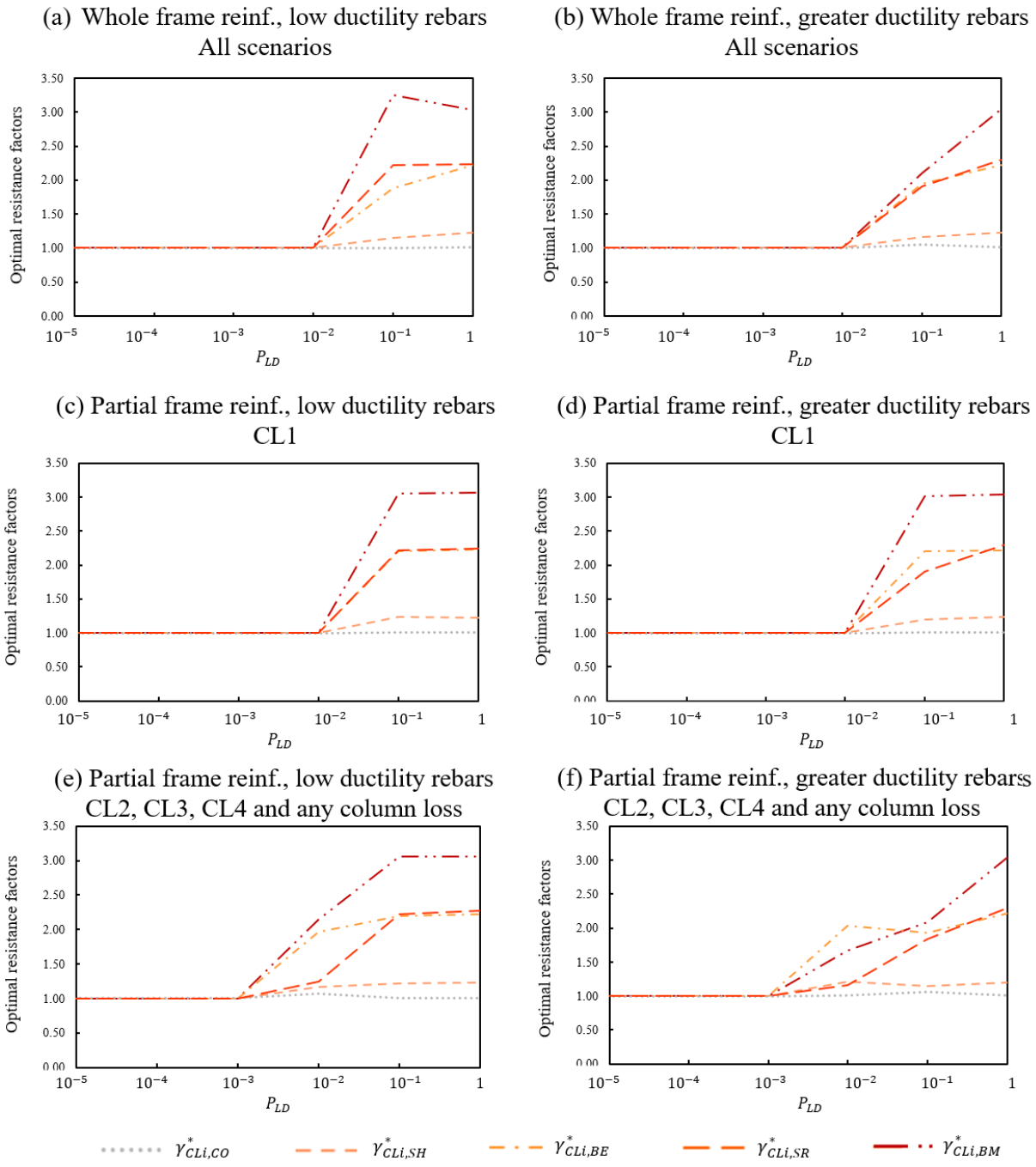

Source: own authorship.

Negative beam bending capacity also increase up to $\gamma^*_{CLi,BE} \approx 2.25$, but as a consequence of increasing rebar reinforcements being needed for enhancing the ultimate load capacity. Since shear capacity was already more than enough for the intact structure ($\beta^*_{I,SH} \approx 6.5$ even for minimal ρ^*_{st}), its increase in the 2nd stage is less noticeable compared to the previous ones ($\gamma^*_{CLi,SH} \approx 1.2$).

As previously discussed, optimal column design is guided by significant bending moments in the frame top corner (intact structure) or in the column adjacent to the lost one (damaged structure). Yet, the optimal configuration is coincidentally the same for both cases in this example, partially due to a reduced demand in column bending moments enabled by the increased optimal beam depth. Therefore, $\gamma^*_{CLi,CO} \approx 1.0$ along the entirety of the 2nd stage for all reinforcement strategies. Additionally, partial frame reinforcement allows γ^* factors to increase earlier in all scenarios except CL1, with only minor discrepancies observed when comparing low and greater ductility rebars.

4.4 ASPECT RATIO INFLUENCE

Based on Beck et al. (2022), this example solely focuses on investigating the influence of the frame aspect ratio over the optimal risk–based design. More specifically, it is investigated if the preference for optimal stronger beams in taller frames and weaker beams in lower frames, found by Beck et al. (2022), is also shown when addressing a nonlinear capacity model for progressive collapse simulation. This example addresses preview results from Ribeiro et al. (2024) published in ECCOMAS 2024 congress.

Five RC frames with distinct aspect ratios (number of bays x number of stories) are the objects of study. All frames have similar "tributary" area in terms of number of bays multiplied by the number of stories (Figure 4.24). Each frame has beam spans of 6.00 m and column spans of 3.00 m, and each one is subjected to 4 scenarios: intact structure, loss of exterior column at ground floor, loss of penultimate column at ground floor, and loss of middle column at ground floor. Each column loss scenario is treated individually, so local damage probability P_{LD} relates to the sudden loss of one column at a time.

Figure 4.24 – Studied RC frames and respective aspect ratios.

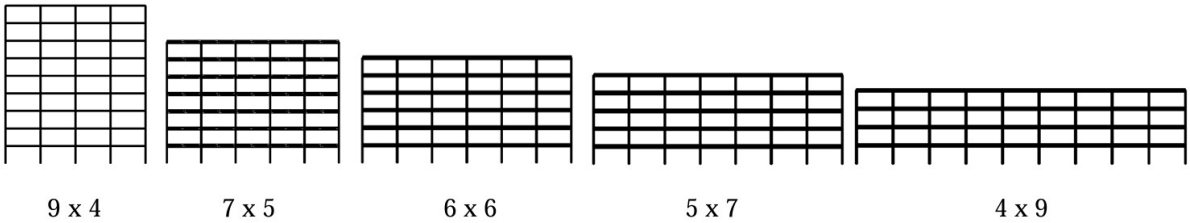

Source: own authorship.

Unlike the previous examples, the primary frames are extracted from the interior of the building, so unidirectional floor slabs lead to floor loadings from both sides. In view of this, more strengthening is expected at the columns when compared to a perimeter frame.

Although facade columns on the ground floor are more exposed for certain hazards, such as IEDs and vehicular impacts, it is herein assumed buildings with easy access at ground floor. Hence, admitting terrorist attacks as potential hazard, inner column spans at ground floor become potential targets. Additionally, performing a 2D analysis in a primary frame within the building allows (for future studies) a direct comparison when a 3D capacity model is adopted, addressing the influence of secondary beams and floor membrane action.

The total expected cost C_{TE} (Eq. 4.11) to be minimized (via Eq. 4.3) addresses manufactural costs and the expected costs of all failure modes. Additional life-cycle costs could be included in C_{TE}, but they are out of the scope of this manuscript.

As in the previous example, C_{MA} refers to the construction cost of the areas damaged by a given failure mode, which are once again assumed following Table 4.11 and Figure 4.18. As shown in Figure 4.25, design variables $\boldsymbol{d}$ are the beam depth h_B, diameter of beam reinforcement ϕ_B (symmetric bottom and top rebars), beam stirrup spacing s_t, column size h_C (square column), diameter of column reinforcement ϕ_C, and overall concrete strength f_c'. As mentioned in section 3.2, design variables that can be represented as deterministic are addressed as random variables with low uncertainty to allow reliability analysis with WASM.

Figure 4.25 – Adopted cross section detailing.

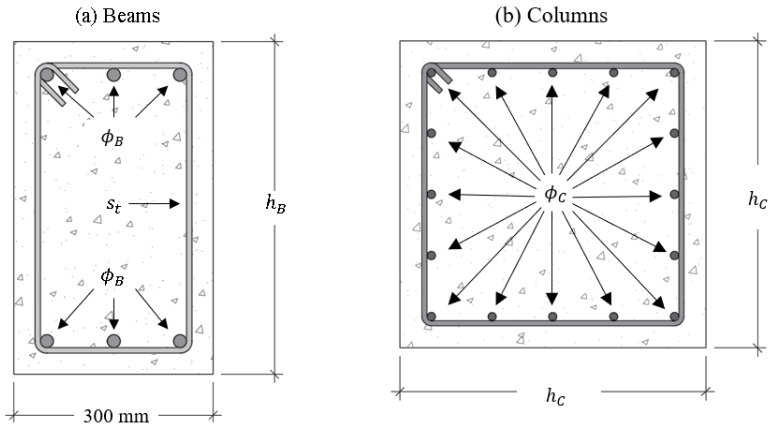

Source: own authorship.

Although f_c' has shown a minor contribution in terms of the frame pushdown behavior (Figure 4.15i), it is more relevant in terms of shear capacity and column capacity when addressing an inner primary frame, especially for taller frame configurations.

Symmetric beam reinforcements were shown, in the previous example, to be related to slightly reduced beam depths, enhancing ultimate capacity at the expense of requiring extra transversal reinforcement to address a non-corresponding increase in shear capacity. Yet, rebars are assumed symmetric to facilitate results comprehension given the greater complexity of addressing and comparing multiple frames.

Besides, a seemingly exaggerated number of 16 columns rebars is chosen to ensure that a unique detailing is able to cover all frames in all scenarios given the design domain $\boldsymbol{\mathcal{D}}$, which is favorable in terms of direct comparisons between distinct frames. Further results show that only lower frames (bellow 6 x 6) under Normal Loading Condition (NLC) could have smaller number of column rebars given the lower bounds in $\boldsymbol{\mathcal{D}}$ (300 mm for h_C and 12 mm for ϕ_C). Hence, 16 rebars is an adequate overall choice for inner primary RC frames.

Reinforcing the entire frame is the only progressive collapse mitigating strategy addressed, as the scope of this example relies in exclusively addressing aspect ratio influence. Based on Starossek and Haberland (2012), structural segmentation could be more appropriate for the horizontally aligned frames than an APM design, but this is avoided to allow an initial direct comparison between frames.

Partial frame reinforcement has shown significant advantages in terms of C_M and C_{TE} in the previous example and also in Beck et al. (2022; 2024). This goes in line with Praxedes and Yuan (2021; 2022), in which it was shown that the first floor requires the majority of reinforcements, followed by the second floor, to attain optimal robustness. This happens due to the double span beam above a lost column representing the critical path of failure due to CA behavior. However, Praxedes and Yuan (2022) also found some (optimal) beam strengthening beyond the (critical) first floors, with reduced reinforcements for upper floors.

In fact, static bay pushdown analysis for partially strengthened frames (with increasing load focused on the reinforced floors) reveals that Vierendeel Action develops differently if compared to a whole frame reinforcement, thus modifying the pushdown behavior. Hence, the optimal transition from full reinforcement (first floors) to smaller reinforcements (upper floors) seems to optimize the balance between axial compressive forces from Vierendeel Action (upper floors) to the tensile ones due to Catenary Action (lower floors).

Nevertheless, these differences are smaller for squared and horizontally aligned frames up to 5 stories. Hence, given the main scope of risk-based optimization, assuming pushdown curves equivalent to those found for whole frame strengthening is possible for such aspect ratios. These smaller differences for square-shaped frames also justify a partial frame strengthening being adopted in the previous RC frame example.

In the other hand, differences are greater for taller frames due to a significant number of floors contributing to Vierendeel Action, which in turn may lead to significantly increased bending moments in the first unreinforced column spans. Therefore, only total frame reinforcement is adopted in order to avoid unrealistic results for taller frames. Further investigations into these aspects will be addressed in future studies.

The probability of occurrence of each failure mode for each column loss scenario and each frame configuration is estimated via IDW, with each estimation relying on 2000 design support points and probabilities computed via WASM (Section 3.2). As in the previous example, Table 4.11 shows the limit state function, consequence factor k for all failure modes of each scenario, and the extent of the final damaged area affected by each failure mode.

The affected area for each failure mode is assumed similarly to the previous example. For inner primary frames, ground floor central column failures are also critical. Hence, for the (initially) intact frame, central column failure is also relevant. Beam failure in column loss scenarios leads to an upward vertical propagation of progressive collapse, while failure of the adjacent columns leads to one stage of horizontal propagation, followed by upward propagation of an increased portion of the frame. As shown in the previous example, a large beam span of 6.00 m leads to a single stage of lateral collapse propagation followed by the upward propagation of a larger portion of the frame. Further stages of lateral propagation can be more likely for beam spans ranging from 3.00 to 5.00 m.

Table 4.19 shows the uncertainty modelling for reliability analysis at the design support points. A sample with 10 million points created via LHS is enough to ensure probability convergence for each failure mode, for 2000 design support points, for each frame. Each sample point created via LHS has its limit states computed as shown in Table 4.11, with the most relevant internal forces and ultimate load capacity at CA estimated via IDW metamodeling. The parameters obtained via IDW refer to the static pushdown curve, so Energy Equivalence Method is used to obtain these parameters in terms of the Pseudo-static pushdown curve in order to address the dynamic effects. This initial metamodeling stage relies on 2000 limit state support points for each frame, which are created via LHS and then analyzed in OpenSees.

Discretization approach, material models and cost multipliers k are identical to those used in the previous example. Only large ductility rebars are assumed herein ($\varepsilon_{su} = 0.20$). As previously stated, material nonlinear behavior is not considered in column discretization in order to avoid sudden disruptions in the pushdown curve due to compressive rebar yielding and/or column buckling, especially for the taller frames (Section 3.4.2).

Table 4.19 - Uncertainty modeling.

Category	RV	Distribution	Mean	Standard deviation	Coefficient of variation
Geometry	Beam depth (h_B)	Normal	To be optimized*	1 mm	-
	Beam rebar diameter (ϕ_B)	Normal	To be optimized*	-	0.05
	Stirrup spacing (s_t)	Normal	To be optimized*	-	0.05 (assumed)
	Column size (h_C)	Normal	To be optimized*	1 mm	-
	Column rebar diameter (ϕ_C)	Normal	To be optimized*	-	0.05
Material	Concrete strength (f_c')	Lognormal	To be optimized*	-	0.12
	Rebar yield strength (f_y)	Normal	510 MPa	-	0.05
	Concrete unit weight (γ_c)	Normal	25 kN/m³	-	0.05 (assumed)
	Ultimate steel strain (ε_{su})	Normal	0.20	-	0.14
Loads	Dead load (D)	Normal	$1.05D_n$	-	0.10
	50-year live load (L_{50})	Gumbel	$1.00L_n$	-	0.25
	Arbitrary point in time live load (L_{apt})	Gamma	$0.25L_n$	-	0.55
Structural model	Model error (M_E)	Lognormal	1.101	0.187	-

Source: Ellingwood and Galambos (1982), JCSS (2001), Real, Campos Filho and Maestrini (2003), Wisniewski et al. (2012), Santiago (2018), Santiago and Beck (2018), Parisi et al. (2018), Costa and Beck (2024a; 2024b).

It should be mentioned that more common values are adopted in this example for the nominal dead load and live load: $D_n = 3$ kN/m² and $L_n = 2$ kN/m². These figures are aligned with the International Building Code (ICC, 2021) in regard to residential buildings.

Firefly algorithm is used to solve the optimization problem, relying on 10 optimization runs for each P_{LD} value, 100 iterations per run, and 40 fireflies. An initial extensive search with 10000 fireflies is done over the design domain $\boldsymbol{\mathcal{D}}$ in order to ensure convergence around the global optima, so only the 40 brighter fireflies are kept for the further iterations. It should be noticed that the computational burden required in this auxiliary extensive search is minimal (few seconds) due to IDW metamodeling for reliability analysis estimation.

4.4.1 Optimal design solutions

Tables 4.20 to 4.22 shows the optimal risk-based results for each frame configuration under each individual columns loss scenario. Optimal risk-based designs related to a Normal Loading Condition are constant from P_{LD}^{min} up to $P_{LD} \approx 10^{-3}$ for lower frames and 10^{-4} for taller frames, after which a threshold P_{LD}^{th} is identified in all scenarios for all frames. Since inner primary frames receive floor loadings from both sides, expected costs of column loss failures grow faster with P_{LD}. Hence, strengthening against progressive collapse becomes cost-effective earlier, in comparison to perimeter primary frames.

Overall concrete strength f_c' shows the same multipurpose characteristics of the beam depth h_B. Although it does not influence the pushdown behavior (Figure 4.15i), an increased f_c' directly provides greater resistance against 5 failure modes (serviceability, negative and positive beam bending, shear failure and column failure). Therefore, ensuring $f_c'^{*}$ at its upper bound in $\boldsymbol{\mathcal{D}}$ (45 MPa) for all frames in all scenarios is shown to be the choice of best cost-effectiveness. Increasing f_c' allows a simultaneous reduction in longitudinal and transversal reinforcements in order to attain similar desirable safety margins.

Optimal 1st stage beam design is similar to previous results: beam depth up to its upper bound, rebar ratio of 0.42%, and stirrup ratio of 0.17%. Load combination $q_I = 1.2D_n + 1.6L_n$ leads to roughly 64 kN/m over the beam spans. Hence, DCRs are obtained as follows: 1.03 for bending at the beam ends ($\phi = 0.9$); 0.52 for bending at the midspan ($\phi = 0.9$); and 0.82 for shear failure ($\phi = 0.75$). Since symmetric rebars are adopted, more than enough safety is shown against midspan bending. As reducing DCR for negative bending implies a sufficient reduction in the positive bending DCR, $\phi_B = 18$ mm is shown to make the optimal balance.

Optimal column designs are no longer constant with P_{LD}. Besides, optimal 1st stage column design shows an increased capacity for taller frames, as expected. Combination for usual loading condition $q_I = 1.2D_n + 1.6L_n$ leads to roughly 64 kN/m in the beam spans (6 m) and 4.8 kN/m for column spans (3 m). Therefore, at the foot of inner columns it is roughly expected 1550 kN for the lowest frame (4 x 9); 2000 kN for the lower intermediate frame (5 x 7); 2330 kN for the squared frame (6 x 6); 2800 kN for the taller intermediate frame (7 x 5); and 3600 kN for the tallest frame (9 x 4). These expected axial demands correspond to 0.36, 0.48, 0.56, 0.52 and 0.59 of the respective optimal axial column capacities, and a minimum eccentricity of 20 mm still keeps each axial load x moment demand inside the column resisting envelope. The top corner of each frame presents negligible axial forces and bending moments of ~0.05 of its greatest axial demand. By comparing these demands with the columns optimal resisting envelopes, DCRs ranging from 1.2 (taller frame) to 0.77 (lower frame) are obtained.

Hence, lower safety margins are allowed for column failure as the frame height increases, reaching DCR > 1 at the frame top corner ($\phi = 0.9$, as demand is mainly flexural) and ~0.91at the ground floor ($\phi = 0.65$) for the tallest frame configuration. As the column cost/meter increases for taller frames, cost-effectiveness of avoiding column plastification reduces for the intact structure, especially at the top corner of the frames.

As in the previous example, optimal 2nd stage beam design is similar for all frames and all column loss scenarios, with beam depth equal to its upper bound, maximum concrete strength, rebar ratios up to 1.03%, and stirrup ratio up to 0.50%. By addressing DAF = 1.22 (common value between CAA and CA in pseudo-static pushdown curves), load combination for extraordinary loading condition $q_{CL} = 1.25(1.2D_n + 0.5L_n)$ leads to roughly 64 kN/m over the beam spans ($D_n = 3$kN/m² and $L_n = 2$kN/m²). Ultimate load-carrying capacity (in terms of static pushdown analysis) is found via IDW metamodeling for each frame at each column loss scenario, leading to the DCR factors for rebar rupture shown in Table 4.23. Since DCR relates to a material property, no strength reduction factor ϕ is used.

Overall DCR factors are ~0.9, indicating a rebar rupture safety margin of ~10% for all frames for all column loss scenarios. In terms of optimal conditional reliability index, rebar rupture is related to $\beta^*_{CLi,SR} \approx 3.9$ for all frames in all scenarios (as shown in Figure 4.26). Although previous examples of perimeter primary frames have shown $\beta^*_{CLi,SR}$ ranging from 2.32 to 3.20, the greater expected load for an inner frame and imposed use of symmetric beam rebars result in a slightly larger safety margin against rebar rupture. This also reflects an increase of ~18% in the beam cost/meter after reaching the APM-strengthening threshold.

Table 4.20 – Optimal risk-based design addressing sudden loss of the external ground floor column (ECL).

Frame ($n_{stor} \times n_{bays}$)	P_{LD}	h_B^* (mm)	ϕ_B^* (mm)	s_t^* (mm)	$f_c'^*$ (MPa)	h_C^* (mm)	ϕ_C^* (mm)	C_{TE}^* (€)	C_M^* (€)	C_{Beam}^* (€ / m)	C_{column}^* (€ / m)
Lower (4 x 9)	$\leq 10^{-3}$	600	18	200	45	300	12	32801.41	32708.88	92.38	106.29
	10^{-2}	585	27	66	45	310	12	50985.57	50794.08	169.93	117.41
	10^{-1}	579	28	74	45	310	12	51456.25	51377.28	172.63	117.41
Lower intermediate (5 x 7)	$\leq 10^{-3}$	600	18	200	45	300	12	32567.64	32154.60	92.38	106.29
	10^{-2}	595	28	62	45	314	12	50975.33	50649.30	178.61	109.51
	10^{-1}	597	28	60	45	330	14	54257.57	54050.10	182.17	131.62
Square (6 x 6)	$\leq 10^{-4}$	600	18	200	45	300	12	33785.22	33346.62	92.38	106.29
	10^{-2}	590	28	67	45	363	12	53785.37	53534.34	177.15	121.19
	10^{-1}	599	28	60	45	363	13	55997.45	55774.44	182.37	130.02
Taller intermediate (7 x 5)	$\leq 10^{-4}$	600	18	200	45	350	12	34375.57	34271.58	92.38	118.03
	10^{-2}	594	28	67	45	427	13	55978.78	55715.94	177.54	146.29
	10^{-1}	594	27	60	45	427	13	56157.77	55928.04	178.55	146.29
Taller (9 x 4)	$\leq 10^{-4}$	600	18	200	45	375	12	36975.76	36714.33	92.38	124.15
	10^{-2}	598	28	81	45	439	12	56823.73	56517.75	171.50	144.25
	10^{-1}	598	28	69	45	439	13	58787.46	58549.50	177.65	149.46

Source: own authorship.

Table 4.21 – Optimal risk-based design addressing sudden loss of the penultimate ground floor column (PCL).

Frame ($n_{stor} \times n_{bays}$)	P_{LD}	h_B^* (mm)	ϕ_B^* (mm)	s_t^* (mm)	$f_c'^*$ (MPa)	h_C^* (mm)	ϕ_C^* (mm)	C_{TE}^* (€)	C_M^* (€)	C_{Beam}^* (€ / m)	C_{column}^* (€ / m)
Lower (4 x 9)	$\leq 10^{-3}$	599	18	200	45	300	12	33076.68	32708.88	92.38	106.29
	10^{-2}	593	28	73	45	354	13	54614.52	53008.80	174.40	127.82
	10^{-1}	590	27	65	45	449	12	64986.27	53919.36	170.01	143.31
Lower intermediate (5 x 7)	$\leq 10^{-3}$	600	18	200	45	300	12	32862.40	32154.60	92.38	106.29
	10^{-2}	595	28	73	45	366	13	53047.75	52355.10	174.59	130.76
	10^{-1}	591	27	63	45	454	13	57234.38	53431.80	171.30	145.49
Square (6 x 6)	$\leq 10^{-4}$	600	18	199	45	300	12	33398.56	33346.62	92.38	106.29
	10^{-2}	595	28	77	45	425	12	54329.12	54184.86	170.98	136.93
	10^{-1}	597	28	69	45	456	12	60276.95	57273.84	175.79	153.20
Taller intermediate (7 x 5)	$\leq 10^{-4}$	600	18	200	45	350	12	35508.21	34271.58	92.38	118.03
	10^{-2}	596	28	78	45	442	12	54354.12	53851.98	171.58	141.43
	10^{-1}	596	28	63	45	470	13	58232.14	57498.00	179.09	157.85
Taller (9 x 4)	$\leq 10^{-4}$	600	18	199	45	375	12	36955.13	36714.33	92.38	124.15
	10^{-2}	596	27	66	45	456	13	57823.92	57732.21	171.01	154.03
	10^{-1}	595	28	67	45	480	13	61239.74	59211.54	173.74	160.62

Source: own authorship.

Table 4.22 – Optimal risk-based design addressing sudden loss of the middle ground floor column (MCL).

Frame ($n_{stor} \times n_{bays}$)	P_{LD}	h_B^* (mm)	ϕ_B^* (mm)	s_t^* (mm)	$f_c'^*$ (MPa)	h_C^* (mm)	ϕ_C^* (mm)	C_{TE}^* (€)	C_M^* (€)	C_{Beam}^* (€ / m)	C_{column}^* (€ / m)
Lower (4 x 9)	$\leq 10^{-3}$	600	18	200	45	300	12	32808.77	32708.88	92.38	106.29
	10^{-2}	597	27	79	45	353	15	57923.21	54877.44	172.19	147.37
	10^{-1}	597	28	71	45	421	14	65687.80	56469.84	175.74	154.25
Lower intermediate (5 x 7)	$\leq 10^{-3}$	600	18	200	45	300	12	32210.75	32154.60	92.38	106.29
	10^{-2}	594	28	81	45	403	13	53783.46	52428.60	171.14	137.41
	10^{-1}	600	28	66	45	405	14	60749.27	56522.10	178.69	158.31
Square (6 x 6)	$\leq 10^{-4}$	600	18	200	45	300	12	33353.43	33346.62	92.38	106.29
	10^{-2}	596	27	73	45	394	12	53258.59	52196.04	167.39	127.30
	10^{-1}	594	28	74	45	413	14	60161.73	57777.84	174.04	160.20
Taller intermediate (7 x 5)	$\leq 10^{-4}$	600	18	200	45	350	12	34508.48	34271.58	92.38	118.03
	10^{-2}	584	28	72	45	395	13	54123.66	53933.46	174.02	138.01
	10^{-1}	600	30	87	45	499	12	59779.25	59062.08	180.49	167.93
Taller (9 x 4)	$\leq 10^{-4}$	600	18	198	45	375	12	36872.02	36714.33	92.38	124.15
	10^{-2}	597	27	73	45	426	13	55994.15	55890.54	167.49	146.02
	10^{-1}	596	28	63	45	506	13	62094.55	61569.99	180.09	167.93

Source: own authorship.

Table 4.23 – Rebar rupture DCR factors for $\varepsilon_{su} = 0.20$ and APM design ($P_{LD} = 10^{-1}$).

Frame ($n_{stories} \times n_{bays}$)	Scenario	Ultimate capacity (kN/m)	DCR
Lower frame (4 x 9)	ECL	69.09	0.926
	PCL	71.11	0.900
	MCL	73.04	0.876
Lower intermediate frame (5 x 7)	ECL	69.29	0.924
	PCL	71.15	0.900
	MCL	73.22	0.874
Square frame (6 x 6)	ECL	69.30	0.924
	PCL	71.39	0.896
	MCL	73.28	0.873
Taller intermediate frame (7 x 5)	ECL	69.35	0.923
	PCL	71.45	0.896
	MCL	73.35	0.873
Taller frame (9 x 4)	ECL	69.57	0.920
	PCL	71.56	0.894
	MCL	73.48	0.871

Source: own authorship.

Table 4.23 also reveals a slight decrease in DCR factors for taller frames and scenarios of inner column loss, especially MCL. Larger safety margins for these cases are related to more efficient development of Catenary Action and Vierendeel Action, so a similar optimal 2nd stage beam design is able to attain slightly greater ultimate capacity values. This indirectly explains the reduction in the gap between C_M and C_{TE} for PCL and MCL as the frame height increases.

When addressing penultimate and middle column loss, lower frames have less stories available above the double span beam, so reduced axial forces related to Catenary Action and Vierendeel Action are able to develop. Although the impact on the optimal beam capacity is ~2%, it implies in a significantly reduced bending moment demand over the adjacent columns. This allows lower column safety margins, with $\beta^*_{CL1,CO}$ ranging from 3.0 (lower frame) to 3.5 (square frame), and consequently to greater gaps of $0.12C_M$ between C_M and C_{TE} for lower frames (Tables 4.21 and 4.22). As reinforcing the whole frame is the only strengthening decision, reinforcing all column spans only pays off when significant axial forces are developed in the double span beams.

Figure 4.26 - β^*_{CLi} with the aspect ratio for $P_{LD} = 10^{-1}$.

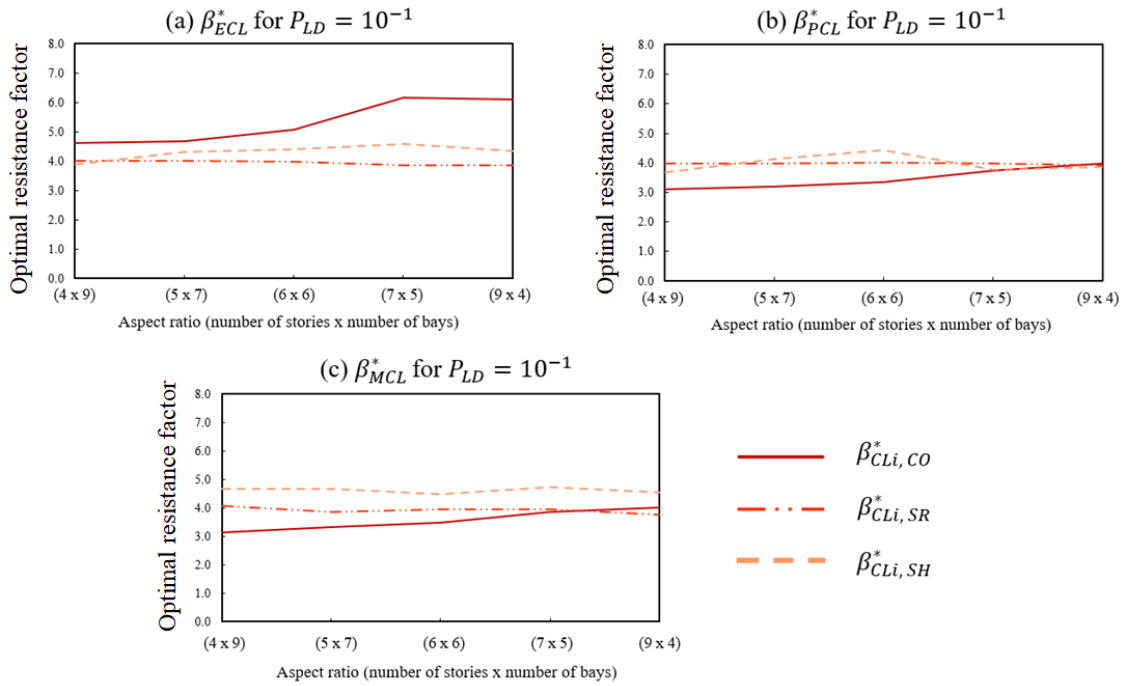

Source: own authorship.

On the other hand, Table 4.23 reveals that exterior column loss (ECL) has the greatest DCR for rebar rupture. Yet, this relates to the unconditional failure event, as Figure 4.26 shows a conditional $\beta^*_{CL1,SR} \approx 4.0$ for all aspect ratios. Since Catenary Action does not develop for ECL (as reflected by its greater DCRs), a reduced column reinforcement is able to ensure greater safety margin against horizontal collapse propagation ($\beta^*_{CL1,CO} \approx 4.5$ for smaller frames and 6.0 for taller frames). Hence, the gap between C_M and C_{TE} is negligible for ECL (~200 €).

Thus, it should be noticed that as the frame height increases, the frame has to become thinner in order to maintain the same tributary area. As the number of remaining columns decreases in damaged scenarios, the number of vertical loads and bending moments redistributed to each remaining column increases, particularly for the adjacent ones.

Although the column bending moments due to Vierendeel Action are not as large as those expected from Catenary Action, their relevance increases for taller frames. This also implies more strengthened optimal 2nd stage column designs, explaining why $\beta^*_{CL1,CO}$ for taller frames increases even in scenarios where Catenary Action does not develop.

Regarding shear forces, an expected load of 64 kN/m on the affected spans leads to approximately 384 kN. Optimal beam 2nd stage design leads to DCR factors up to ~0.99 ($\phi = 0.65$), demonstrating that the algorithm ensured a minimal amount of safety margin against shear failure.

When addressing the conditional failure event, Figure 4.26 shows $\beta^*_{CLi,SH}$ ranging between 4.0 and 4.6. As mentioned earlier, symmetric rebars provide greater ultimate load capacity without corresponding increase in shear capacity. Thus, maximizing beam depth and concrete strength to handle shear demands increases the cost per meter. Further reduction in stirrup spacing incurs additional strengthening costs that are not compensated by the reduction in expected costs of shear failure.

To address the increase in optimal beam resistance, Figure 4.27 shows the optimal resistance factors γ^*, defined at any P_{LD} in terms of optimal design at P_{LD}^{min} (Eq. 4.12) for bending and shear failure for each frame and each column loss scenario. Since rebars are symmetric, no distinction is made between positive or negative bending capacity.

Figure 4.27 – Behavior of beam γ^* with P_{LD} for each frame and CL scenario.

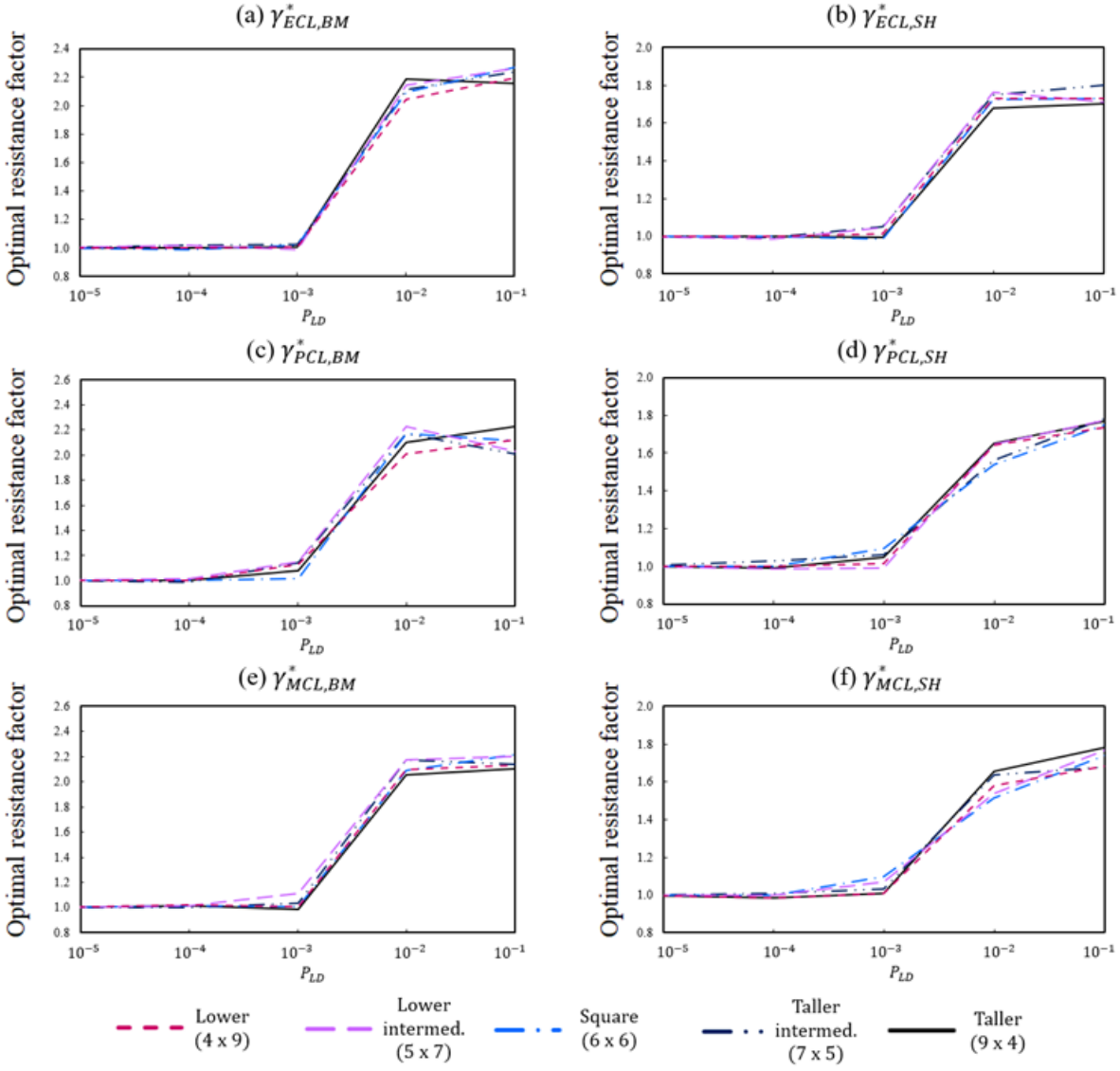

Source: own authorship.

Overall increase in optimal bending capacity is around 2.2 for $P_{LD} > P_{LD}^{th}$, whilst for shear capacity it is 1.8. Although lower frames have a smaller damaged area in case of upward collapse propagation due to beam failure, weaker beams are never shown to be justified, in contrast with Beck et al. (2022). In the mentioned study, a progressive collapse capacity model that neglects the bending moments over adjacent columns shows that stronger beams are only cost-effective for taller frames, where the upward collapse propagation is as severe as horizontal column collapse propagation. Additional comments related to seismic design (principle of weak beams – strong columns) are shown in Section 4.5.

However, realistic capacity models reveal that significant axial forces developed during Catenary and Vierendeel Actions have major impacts over adjacent columns. Besides weak beams having lower ultimate capacity, Vierendeel and Catenary Action develop earlier, leading to larger bending moment demands over the adjacent columns.

These additional flexural demands increase the propensity of column rebar yielding. In case of tensile column rebar yielding, full achievement of beam ultimate capacity is severely compromised, while compressive column rebar yielding also leads to a brittle and sudden column collapse (Section 3.4.2). This justifies the risk-based algorithm's preference for stronger beams independently of the frame configuration or column loss scenario.

To address the increase in optimal column resistance, Figure 4.28 shows the optimal column resistance factors γ^* (Eq. 4.12) in terms of axial capacity for each frame, for each CL scenario, and the whole range of P_{LD}. Axial capacity for lower frames increases by 90%, and for taller frames it increases 60%, but taller frames still have the greatest axial capacity. Hence, adopting optimal 1st stage design of each frame as reference can lead to misinterpretations in this regard. Therefore, optimal 1st stage column design for the lower frame is used as reference in Eq. 4.12, leading to γ^* for taller frames greater than 1 at P_{LD}^{min}.

Although beam reinforcement against progressive collapse happens for P_{LD} ranging between 10^{-3} to 10^{-2}, column reinforcement is cost-effective earlier for taller frames, even for exterior column loss scenario. Hence, taller frames have a threshold characterized just by column strengthening, reducing the C_{ef} related to greater axial forces in the adjacent beams.

The contrast between the aforementioned results and those from Beck et al. (2022) is better illustrated in Figure 4.29, w.r.t. $P_{LD} = 10^{-1}$. Optimal beam resistance factors are shown to be indifferent to the frame aspect ratio and column loss scenario, as stronger beams are required to avoid the magnified bending moments transmitted to the columns.

Figure 4.28 - Behavior of column γ^* with P_{LD} for each frame and scenario.

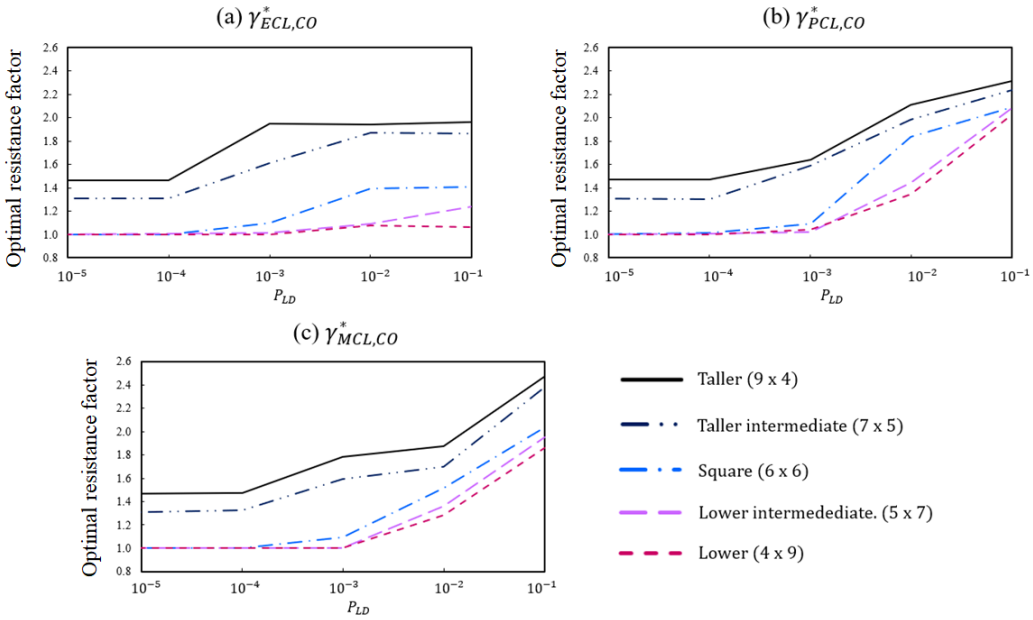

Source: own authorship.

Only optimal column axial resistance is shown to be sensitive to the frame aspect ratio, with increasing values being required for taller frames, which goes in line with Beck et al. (2022). Scenarios of inner column loss are related to column γ^* factors ranging from 2 (lower frames) to 2.5 (taller frames), while for external column loss it ranges from 1.0 to 1.8, respectively. Hence, scenarios where Catenary Action is able to develop show an increase in γ^*_{CO} of ~100% for lower frames, and ~40% for taller frames.

Figure 4.29 - Behavior of each γ^* with frame aspect ratio.

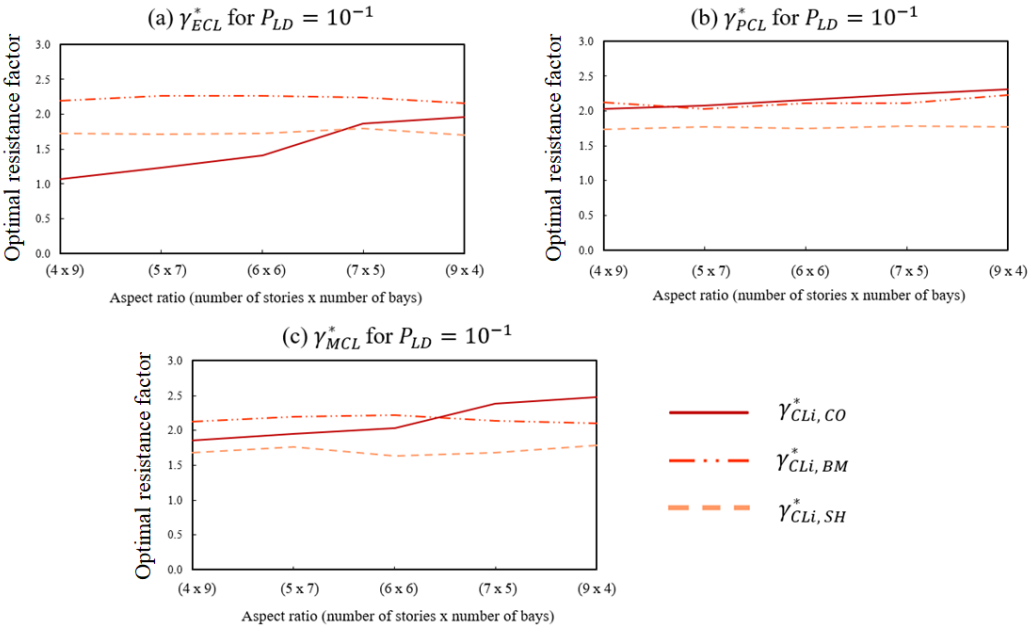

Source: own authorship.

4.5 COMMENTARY ON COLUMN STRENGHTENING FOR APM DESIGN

For the sake of brevity, figures and demonstrations in this section relate to optimal column results for the squared frame of the previous Section. Nonetheless, main conclusions drawn from this section are applicable to other frame configurations as well. It has been shown that ultimate beam capacity in terms of steel rupture, which is broadly regarded as the last resisting mechanism against progressive collapse, is strongly related to the flexural demand on the adjacent columns. Besides, Sections 4.1 and 4.2 show that an optimal risk-based design addressing the ultimate beam capacity is more cost-effective than relying solely on early resisting mechanisms e.g. Flexural Action. Further resisting mechanisms in the beam spans above a lost column rely on the development of axial compressive forces (Vierendeel and Compressive Arch Action) and tensile forces (Catenary Action), which depend on the available horizontal restraint. In this study, RC columns are the sole providers of this lateral confinement.

Catenary Action is the mechanism related to the greatest load-carrying capacity and overall frame ductility (in terms of large displacements until collapse). Scenarios of external column loss are unable to trigger this ultimate mechanism due to a lack of lateral restraint in both sides. Hence, load-carrying capacity relies on Flexural and Vierendeel Action, leading to minor impacts in the adjacent column in terms of flexural demand (Figure 4.30).

Figure 4.30 - Column failure assessment for ECL.

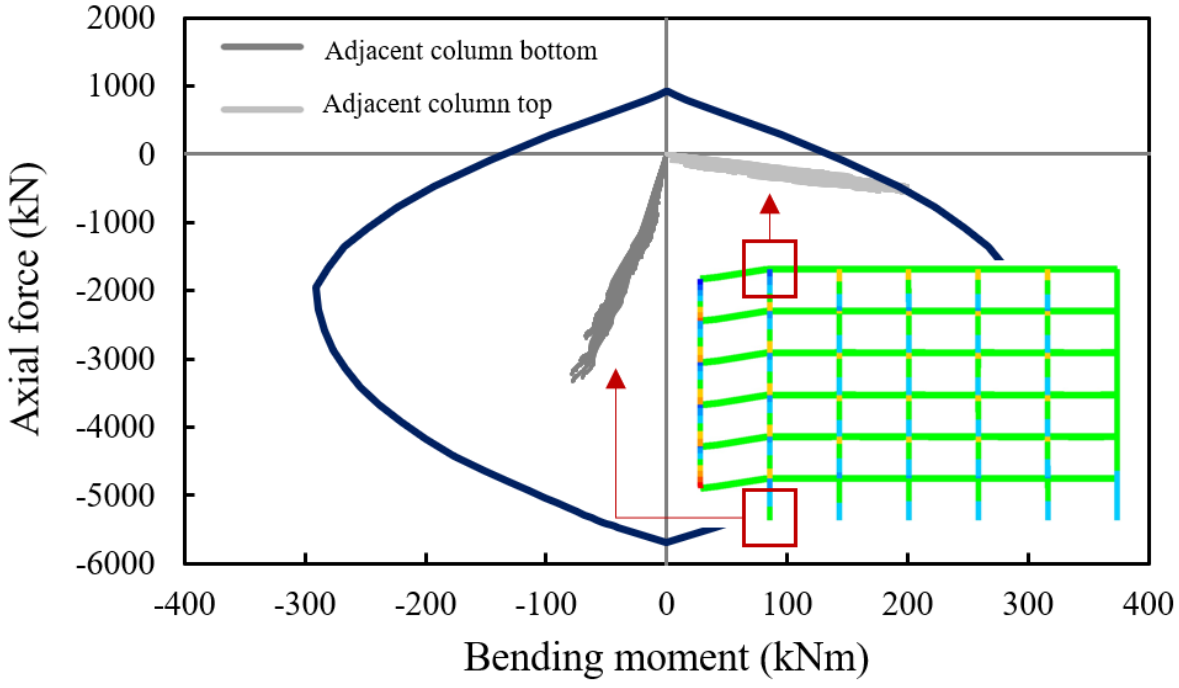

Source: own authorship.

Figure 4.30 shows the resisting envelope for the optimal 2nd stage column design for the square frame (6 x 6) and the expected force vs moment demands obtained by FE analysis for 200 sample points. Each FE analysis addresses the same square frame and the same optimal 2nd stage column design, but with random combination of beam design variables across the design space $\boldsymbol{\mathcal{D}}$. This allows to identify the effects that weak, intermediate and stronger beams have over the flexural column demand.

For all sample points the resisting envelope encompasses the main force vs moment demands of the adjacent columns. In this scenario, Vierendeel Action leads to compressive forces in the first floor, tensile forces in the last floor, and a gradual transition from lower to upper floors, ensuring equilibrium for the hanging frame span. These axial forces, which only develop due to the stiffness of the adjacent column, cause a flexural demand in it, with the frame being pushed inwards in the first floors and pulled outwards in the upper floors. As shown in Figure 4.30, a significant safety margin is observed for the force vs moment demand at the bottom of the adjacent column, which seems to be indifferent to the beam configuration.

However, greater bending moments at the top of the adjacent column can be observed for weaker beams, leading to smaller safety margins in this region. Nonetheless, this failure mode is related to column rebar yielding in tension, which has negligible impact over pushdown behavior, ultimate frame capacity, and structural robustness. Remaining floors in the hanging frame span have intermediate force vs moment demands, so they are omitted for clarification purposes. In addition, column tensile rebar yielding is common for the hanging column span, but with negligible implications.

Weak beams cause a major increase in column flexural demand for penultimate column loss, mainly at the outer-most adjacent column (Figure 4.31). Although some Catenary action is able to develop, the lateral restraint for the double-span beams is unbalanced, causing very distinct force vs moment demands over the adjacent columns.

Weak beams have lower Flexural, Compressive Arch and Catenary Action capacities, but can exhibit significantly larger vertical drifts (up to ~$4h_B$) until rebar rupture happens (Figures 4.14, 4.15 and 4.19). This inherently leads to the development of greater axial forces in Catenary Action, which produce larger bending moments ~370% on columns, which exceed the maximum bending capacity of the outermost column. This severely compromises the frame's pushdown behavior, leading to a premature collapse of a potentially larger portion of the frame. Despite domino–type progressive collapse not being addressed in this study, the propensity of its occurrence is visibly significant due to the overwhelming inward pull of the outer adjacent column.

Figure 4.31 - Column failure assessment for PCL

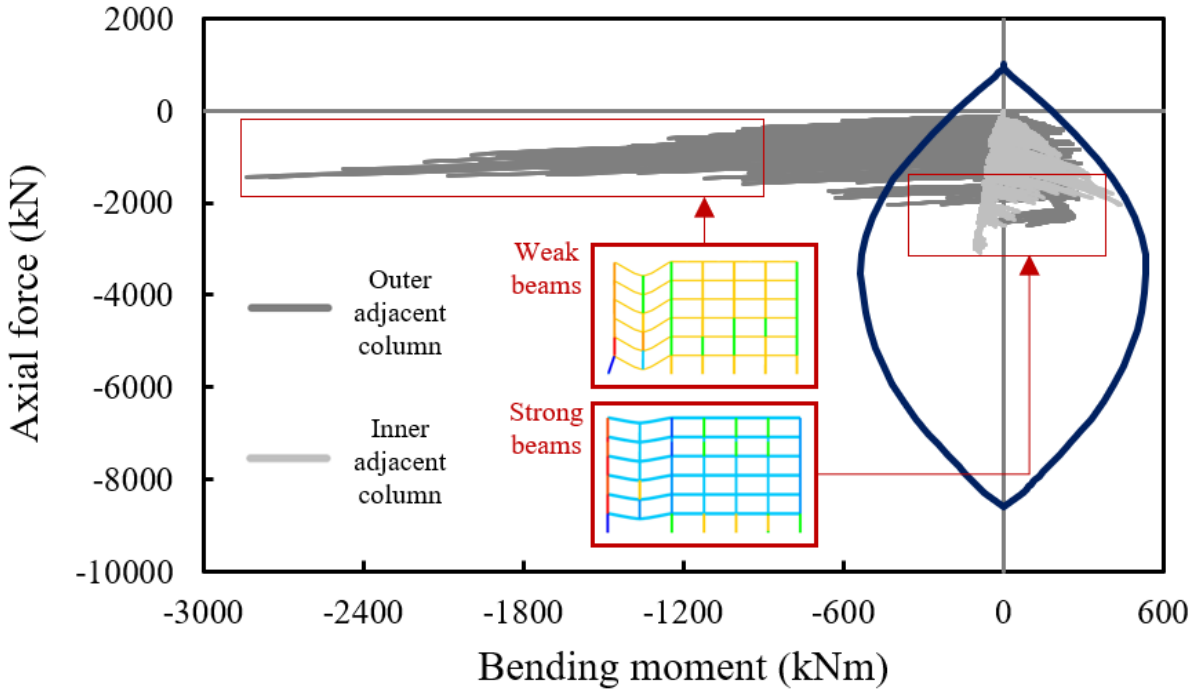

Source: own authorship.

Optimal 2nd stage column design is able to envelope all force vs bending demands of the inner-most adjacent column. For the outer adjacent columns, this only happens for the strongest beam configurations. Lower values of conditional $\beta^*_{CL2,CO} \approx 3.0$ (Figure 4.27b) are also justified by the aforementioned behavior. Column flexural demand is shown to be greater in the adjacent column related to lower capacity of lateral restraint. Hence, the outermost adjacent column should be prioritized when addressing structural strengthening for columns lost closer to facades or building corners.

Middle column loss leads to reduced values of flexural demand due to the balanced lateral restraints, but figures up to ~190% above the maximum flexural capacity are still possible for both adjacent columns (Figure 4.32). For middle column loss, both adjacent columns require strong beams. It should be mentioned that weak beam configurations can pull the entire frame inwards, potentially affecting the entire structure in case of adjacent column failure (domino-type collapse), rather than just the next adjacent span, as assumed in this study.

Despite middle column loss leading to smaller (yet relevant) flexural demands in adjacent columns, its potential to affect the entire frame through a zipper-type and domino-type collapses is greater compared to penultimate column loss. Zipper collapse for penultimate column loss, as assumed in this study, is also possible when addressing the inner most adjacent column, but with a reduced potential of inflicting the entire frame.

Figure 4.32 – Column failure assessment for MCL.

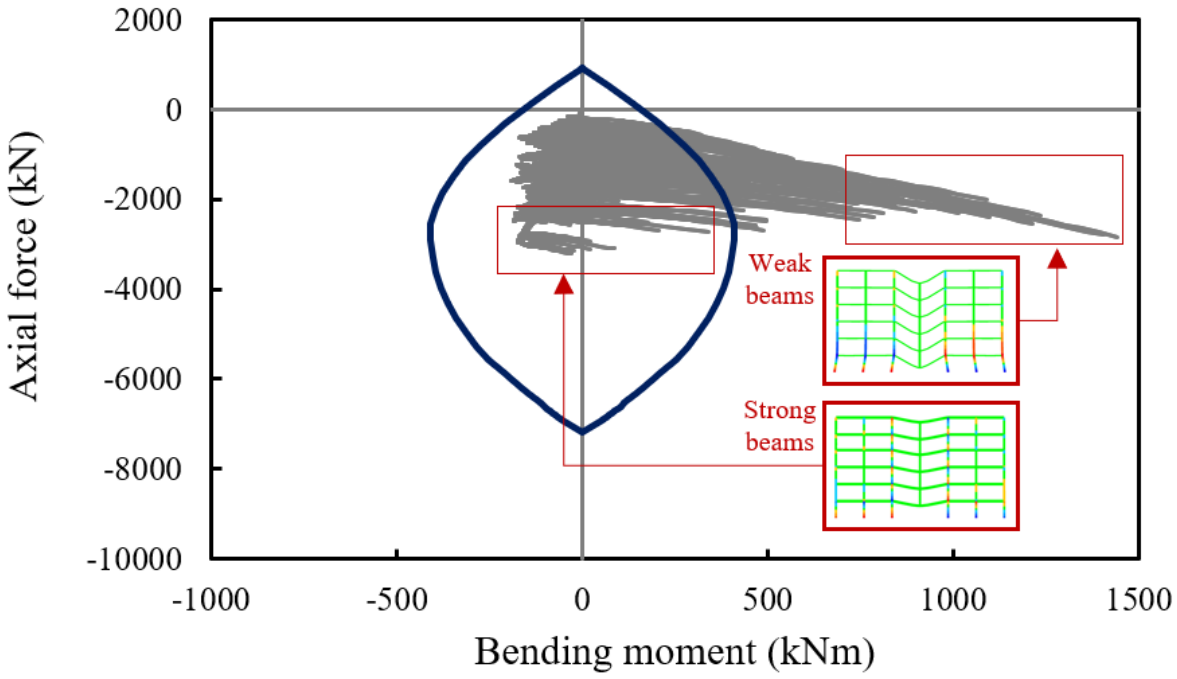

Source: own authorship.

All optimal 2nd stage column designs found for each frame and each scenario have one aspect in common: ultimate axial capacity at least twice the maximum expected axial demand. Since column failure in redistribution-type progressive collapse is solely attributed to increased flexural demands, Figure 4.33 shows that column cross-sections other than the classic square-shape could be better suited for APM design purposes.

Figure 4.33 – Column failure assessment for MCL under different cross-section configurations.

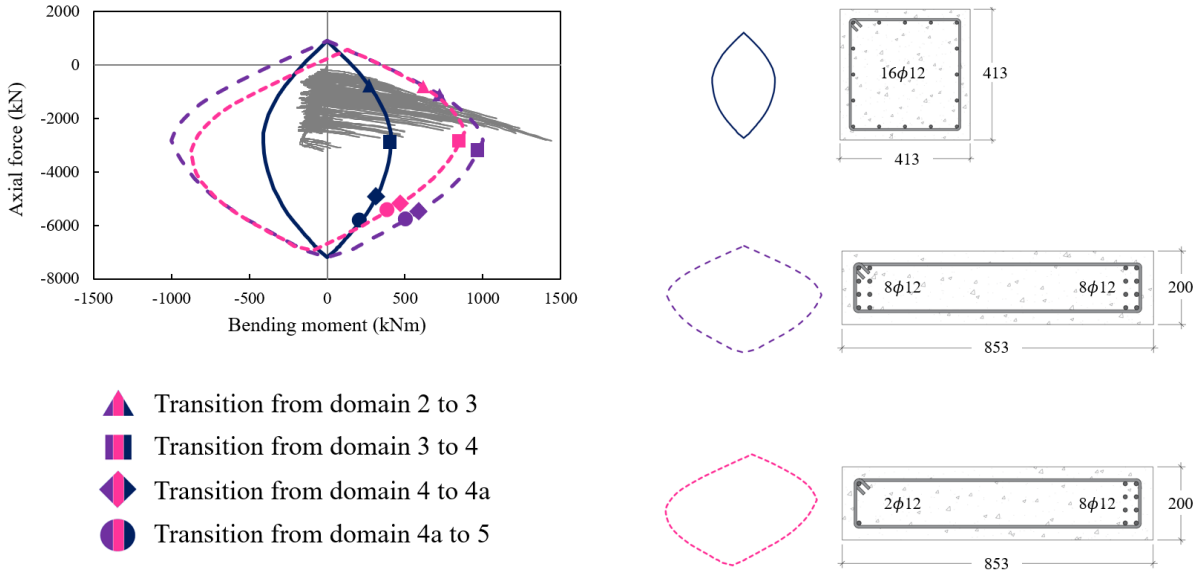

Source: own authorship.

In Figure 4.33, an illustrative rectangular cross-section with the same area and number of rebars are used, but with half of the rebars placed on each side (an unconventional arrangement adopted for clarity). This results in the same axial capacity, but the maximum flexural capacity is increased by approximately 150%. The new resisting envelope is able to accommodate greater bending demands, potentially providing more safety margins for weaker beams. Although the new rectangular section alters the axial vs bending demands, the previously calculated demands are maintained for clarity. In addition, removing ¾ of the rebars in the compressed side of the adjacent column seems to have a negligible negative effect in the tensioned side. This could lead to optimal strengthening solutions with APM design paying off at lower threat probabilities and possibly allowing weaker-intermediate beams to be used. Thus, optimal results found in Beck et al. (2022), in which weaker beams are justified for lower planar RC frames, could be valid for column sections better suited against flexural demands.

In terms of cross-section plastification, NBR 6118 (ABNT, 2023) introduces the concept of failure domains, which characterizes specific strain behaviors depending on how failure due to a nonlinear behavior onset occurs in a linear RC element. Line A corresponds to uniform tension, with all rebar layers equally yielding. Domain 1 corresponds to eccentric tension, with failure being characterized by rebar strain of 0.01. Domain 2 refers to under reinforced cross-sections, with flexural capacity being reached in terms of rebar yielding only, as concrete strains are below 0.0035. Domain 3 relates to well reinforced cross-sections, with flexural capacity being reached simultaneously with concrete strains of 0.0035 and rebar yielding. Domains 4 and 4a characterize over reinforced cross-sections, in which flexural capacity is reached in terms of concrete strains of 0.0035 and tensioned rebars still in linear behavior. While in domain 4 the neutral axis is within the concrete core, in domain 4a it is located in the concrete cover of the tensioned side. Domain 5 is the usual domain for column design, as it refers to eccentric compression, with its failure threshold defined in terms of the eccentricity. Line B relates to an idealized uniform compression.

By monitoring the neutral axis position in each coordinate of the column resisting envelope, the thresholds between each flexural domain can be identified. In Figure 4.33, the great majority of failure occurrences are related to the third domain: tensioned rebars yielding and concrete strains reaching the guideline threshold of 0.0035 in the compressed side. When considering a squared-shape section, some weak beam configurations lead to flexural capacity being reached in domain 2, which is very unexpected in column analysis. In this domain, the adjacent columns at ground floor have tensile demands significantly more critical than the compressive demands.

In view of this, a tradeoff between beam moment of inertia and column moment of inertia becomes apparent. RC beams in Sections 4.1 and 4.2 are related to adjacent columns with infinite moment of inertia, resulting in optimal 2nd stage beam designs with reduced moment of inertia. RC frame examples allows the simultaneous optimization of beams and columns, but squared cross-sections for the columns restricted the cost-effectiveness of greater moments of inertia for these elements. Hence, optimal 2nd stage designs relate to almost maximum beam moment of inertia and a significantly smaller column moments of inertia. As the depth of elements in a specific direction increases, the depth of elements in the perpendicular direction decreases to ensure a cost-effective solution.

An increase in column moment of inertia implies an increase in its flexural capacity. When addressing rectangular and squared cross sections of identical manufacturing costs, area and number of rebars, Figure 4.33 shows that the rectangular option withstands the majority of force vs moment demands due to its greater moment of inertia. Thus, increased column flexural capacity allows greater mobilization of beam Catenary Action, which in turn enhances the ultimate load-carrying capacity for (weaker) beams with reduced beam depth (Figure 4.15b). In this discussion, weaker beams refer to a reduced flexural capacity in these elements, even though their ultimate Catenary Action capacity is greatly improved when combined with columns of great flexural capacity. This goes in line with Long et al. (2021), who show that load capacity of frames under Catenary Action strongly depends on the moment capacity of the adjacent columns in order to provide strong restraints. This also goes in line with Yu and Tan (2013), whose experimental setups of great lateral restraint show that higher (beam) span-to-depth ratios enhances Catenary Action capacity, while smaller span-to-depth ratios improve Compressive Arch Action capacity in (as shown in Figure 4.15b).

Reduced column moments of inertia lead to a tradeoff between load-carrying capacity and overall frame ductility, as shown in Figure 4.19. Since lateral restraints are weaker, developed axial forces in Catenary Action exert larger horizontal drifts on the adjacent columns (weaker beams in Figures 4.31 and 4.32), resulting in larger vertical drifts being reached for reduced loads (Figure 4.15a). However, Figure 4.15b shows that there is no tradeoff when strong lateral restraints are available, as increased beam ductility due to Catenary Action also implies greater load-carrying capacity. Since column horizontal drift reduces for stronger lateral restraints, greater vertical forces are required to achieve larger vertical drifts.

The tradeoff between ultimate capacity and frame ductility (Figure 4.19) relates to a specific condition of low column moment of inertia. Hence, this tradeoff results from a much deeper tradeoff between beam and column moments of inertia, as shown in Figure 4.34.

For these plots, 2000 sample points for the square frame were run in OpenSees, with 3 rebars of 20 mm for both beam layers, 20 mm rebars in the columns, $f_c' = 45$ MPa, and $f_y = 510$ MPa. Rectangular cross-sections are assumed for beams and columns (width of 300 mm in both), with only beam and column depth varying.

Figure 4.34 – Ultimate frame capacity in terms of beam depth and column depth.

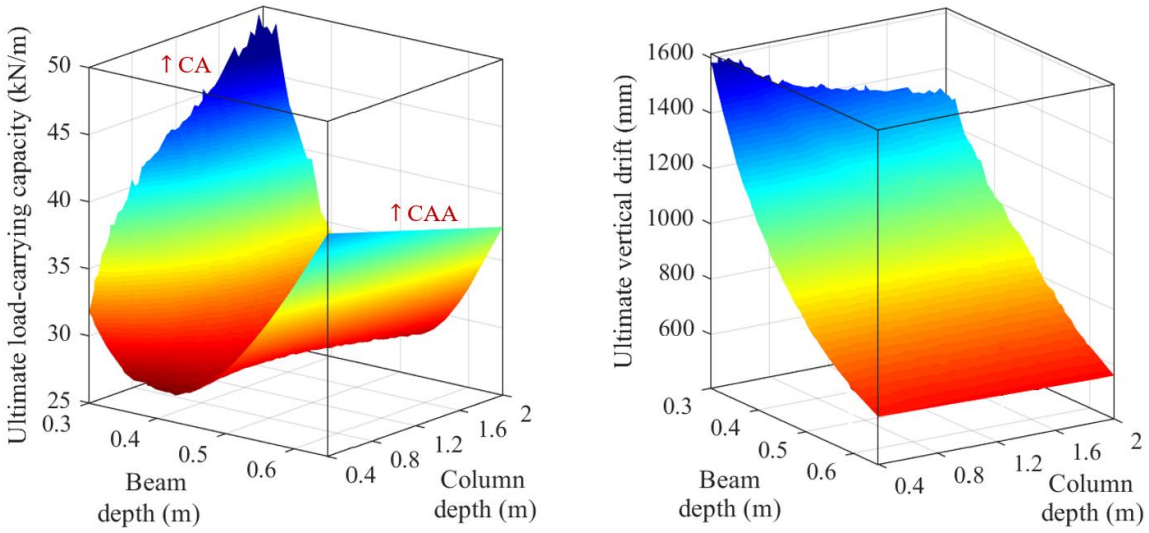

Source: own authorship.

Increased column flexural capacity decreases the Compressive Arch Action (CAA) capacity for strong beams and significantly increases the Catenary Action (CA) capacity for weaker beams. Column cross-sections closer to a squared shape leads to strong beams CAA capacity greater than weak beams CA capacity, resembling Figures 4.15a and 4.19. For a column depth twice its width, CAA and CA capacities for strong and weak beams, respectively, become equivalent. Increasing values of column depth leads to weak beams CA capacity up to ~39% greater than strong beams CAA capacity. Besides, greater column moment of inertia leads to simultaneously greater ductility and CA capacity for weaker beams, resembling the behavior in Figure 4.15b.

Intermediate beams are shown to be suboptimal in terms of post-flexural resisting mechanisms, as they are simultaneously unable to reach significant compressive forces during CAA and tensile forces during CA (Figure 4.35). This explains the significant gap between RC beam optimal results and RC frame optimal results found in this Chapter.

Ultimate capacity in frames of weak columns can only be attained via CAA, whereas stronger columns allows it either by CA and CAA. As weaker beams have reduced manufacturing costs, great overall cost-effectiveness is expected for them in future studies.

Figure 4.35 – Ultimate frame capacity in terms of CAA and CA.

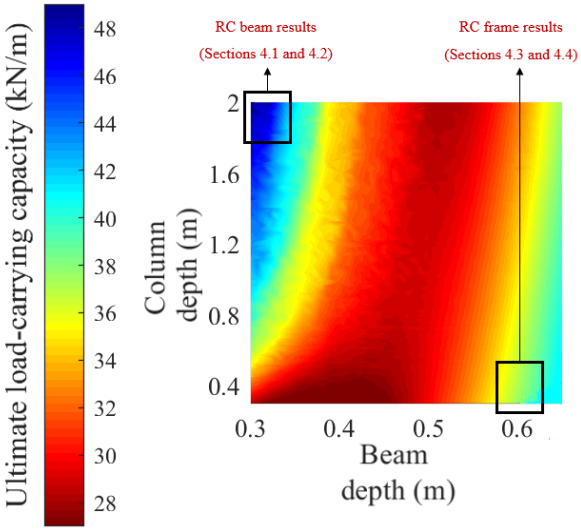

Source: own authorship.

Results in Section 4.2 have already shown a preference for weak beams when column moment of inertia is assumed infinite. However, increased shear capacity may lead to stronger beams being more cost-effective when assuming realistic values of strong columns.

Since the critical columns behave as beams in column loss scenarios, it would be appropriate to address reinforcement decisions that specifically target this aspect. Hence, greater cost-effectiveness is expected if columns of greater depth and smaller width were assumed in primary frames subjected to column loss scenarios. The same cannot be promptly expected for 3D frames, as enhanced bending moments are expected across both column cross-section axes. In such cases, the squared-shaped sections investigated in this study could be significantly more cost-effective, as well as L-shapes, T-shapes and a multitude of exotic possibilities which will be the object of study in future investigations e.g. H-shaped, polygonal, circular, trapezoidal, cross-shaped, and others. This thesis marks the end of a cycle, but not the end of this research.

CONCLUSIONS

This thesis addressed the optimal risk-based design of reinforced concrete frames under progressive collapse. Damage leading to loss of load-bearing elements in RC frames are low-probability high consequence events, with significant impacts in terms of disproportionate collapse consequences and in terms of strengthening costs. Herein, the Alternative Path Method has been addressed under accidental column loss scenarios, considering multiple strengthening options and distinct column loss scenarios in planar frame structures. The risk-based optimization looks for a proper point of balance between APM reinforcement costs, and expected costs of progressive collapse.

Cost-effectiveness of progressive collapse mitigation strategies in RC frames was found to strongly depend on threat probabilities and on the tradeoff between beam and column moments of inertia. By assuming squared cross-sections for the columns, it is not cost-effective to ensure great flexural capacity for these vertical members, so ultimate capacity solely relies on increasing the beam moment of inertia to promote the Compressive Arch Action mechanism, regardless on the frame aspect ratio. Yet, it is shown that beams with low moment of inertia (squared cross-sections) can be the most cost-effective APM solution if columns are assumed to have great flexural capacity to handle the increased bending moment demands caused on them due to Catenary Action in the beams.

In addition, primary design against hazards related to abnormal lateral loadings, such as tornados and earthquakes, follow well-stablished concepts of strong columns and weak beams (Macedo et al. 2024; Bosse et al. 2024; Rodrigues et al. 2024). Therefore, analysis shown in Section 4.5 evidences the possibility of optimal configurations simultaneously cost-effective for progressive collapse and abnormal lateral loadings, which is novel. Hence, optimal designs with weak beams (low moment of inertia) may be optimal for such multi-hazard exposition during the lifespan, as long as that adjacent columns have enough flexural capacity. Thus, strong columns with squared cross-sections are shown to not be cost-effective for column loss scenarios alone, they could be if earthquakes and/or tornados were also addressed. This will be investigated in future studies.

The previous paragraphs highlight the main findings of this study, focusing on the optimal balance between beam and column flexural capacities for progressive collapse mitigation and future investigations. However, additional conclusions were also drawn:

(a) A tradeoff between load-carrying capacity and overall frame ductility is observed when columns of squared-cross sections are assumed. As ultimate capacity relies in additional CAA capacity, optimal APM beam design is related to maximum beam depth and minimum ductility in terms of vertical drift. This might compromise the time needed for building evacuation, so the balance between risk-based cost-effectiveness of beam and column flexural capacities requires further investigations;

(b) Squared cross-section columns in perimeter frames show optimal APM design equivalent to optimal conventional design. Perimeter frames receive floor load contributions from one side only, so a reduced vertical beam demand results in a smaller force vs moment demand in the columns. This, combined with stronger beams, make the optimal conventional column design also cost-effective for APM design;

(c) Relying on the structure's entire plastic reserve up to beam rebar rupture was found to be the optimal approach to deal with progressive collapse threats, so nonlinear capacity models were key-factors to describe the resisting mechanisms beyond flexural capacity. Besides, metamodeling was fundamental to integrate all major pieces of the framework, although some difficulties were found for ordinary kriging;

(d) Literature findings were consistently related to cost-effective solutions. For instance: optimal beam designs with greater depth promote CAA (Alogla et al. 2016); large axial restraints lead to optimal beam designs with improved CAA and CA capacities (Long et al. 2021); optimal beam designs with reduced depth have improved CA capacity when assuming full lateral restraints (Alshaikh et al. 2020; Yu and Tan, 2013); greater optimal rebar reinforcements in APM designs were in favor of increasing the frame ultimate capacity (Abdelwahed, 2019); however, optimal over reinforced beams are related to slightly decreased flexural capacity and earlier mobilization of CA (Ren et al. 2016); top reinforcement ratio is always greater in optimal progressive collapse-resistant beam design (Long et al. 2021); strengthening the two first floors is shown to be a very cost-effective solution for low-rise frames (Praxedes and Yuan, 2022);

(e) Threshold probabilities above which partial frame reinforcement becomes cost-effective ranges between 2×10^{-5} to 2×10^{-4} per year in this work, whilst for Praxedes and Yuan (2022) it is among 2×10^{-7} and 2×10^{-6} per year. Yet, this is possibly related to their greater beam span lengths (7 m) and lower rebar yielding strength (413.7 MPa) on their frames, making them more susceptible to early collapse, even for lower values of dead and live loads;

(f) A transition in optimal solutions was observed, with optimal cross-sections changing from a configuration with best performance under normal loading condition to another with best performance against progressive collapse, characterizing the threshold local damage probability P_{LD}^{th}. It represents a break-even point between costs of strengthening and the reduction in expected costs of progressive collapse. When the abnormal load and threat are such that $P_{LD} < P_{LD}^{th}$, APM design for load bridging is not cost-effective. By contrast, APM design pays off under significant threat probabilities, with strengthening costs being compensated by a reduction in expected costs of failure;

(g) External column loss scenarios were shown to be the most critical due to neither CAA or CA being mobilized. As ultimate capacity solely relies on Vierendeel Action, reinforcing becomes expensive. This leads to APM design being cost-effective only for larger threat probabilities when addressing perimeter frames ($10^{-2} < P_{LD}^{th} < 10^{-1}$). For inner primary frames, P_{LD}^{th} for external column loss is in a similar range of inner column loss scenarios ($10^{-3} < P_{LD}^{th} < 10^{-2}$), but optimal APM design starts with significantly reduced safety margins against progressive collapse, especially for lower frames due to greater floor load contributions and less effective VA mechanism;

(h) Assuming the loss of any ground-floor column leads to optimal APM design being cost-effective for $10^{-3} < P_{LD}^{th} < 10^{-2}$ for all reinforcement strategies investigated. This relates to independent individual threat probabilities ranging from ~1.428×10^{-4} to ~1.428×10^{-3} for each of the seven columns of the investigated frame. Hence, passive measures that reduce the number of potential target columns for a given hazard can have better cost-benefit than addressing an APM design that simultaneously covers multiple scenarios of single column loss. Yet, this relates to a series system event, where local damage to any column either triggers progressive collapse or effectively engage resisting mechanisms (union of events). Assuming independence of events leads to a lower bound for P_{LD}^{th} ranging from ~1.428×10^{-4} to ~1.428×10^{-3}, whilst perfect dependency leads to $10^{-3} < P_{LD}^{th} < 10^{-2}$ as upper bound. Admitting a local damage event for any column implies in some dependency between columns, so the actual value for P_{LD}^{th} is between the aforementioned limits;

(i) Under prevalence of usual loading condition, the risk-based framework leads to a good balance between safety and construction cost, allocating material to provide just-enough safety against the most critical failure modes, namely bending at the beam ends and column failure;

(j) Increased ultimate capacity is ensured for $P_{LD} > P_{LD}^{th}$, with larger longitudinal and transversal reinforcement ratios, and concrete strength up to its upper bound. Optimal beam depth strongly depends on the lateral confinement: strong columns allow weak beams, whilst weak columns require strong beams. Yet, optimal APM design has increased safety margins against brittle shear, steel rupture before catenary action, and column failure, but also warranting a minimum safety margin against ductile steel failure in CA (i.e., the least bad failure mode);

(k) Inner primary frames of lower height have minimum safety margin against column failure after P_{LD}^{th}. As lower frames have less stories, reduced axial forces are developed in Vierendeel Action and Catenary Action (inner column loss scenarios). This implies a reduction in column flexural demand, allowing reduced safety margins for these vertical elements. Hence, when addressing the entire frame, reinforcing all column spans only pays off when significant axial forces are developed over the critical beams;

(l) The gap between optimal manufacturing cost and total expected costs reduces according to how efficiently Vierendeel and Catenary Actions can be mobilized. Hence, scenarios of inner column loss are related to the smallest expected costs of progressive collapse, whilst external and penultimate column loss scenarios have greater gaps due to lower safety margins e.g. greater expected costs of failure. Hence, this cost-gap is reduced for taller frames due to more efficient resisting mechanisms;

(m) Additional robustness against progressive collapse also provides satisfactory safety margins against all intact structure failure modes. Strong lateral restraint leads to increased safety against ultimate failure modes, and an adequate admissible safety margin against excessive midspan displacements (serviceability). Weaker columns result in optimal APM beam designs with greater depth, so safety against serviceability failure also increases;

(n) Beam cross-section depth and overall concrete strength are design variables able to ensure capacity against multiple failure modes. Consequently, the risk-based algorithm tends to favor high values for these parameters. However, it is shown that great depth (stronger) columns can lead to optimal low depth (weaker) beams due to their enhanced CA capacity, but always ensuring an admissible safety margin against serviceability and shear failure. Thus, concrete strength is a design variable with significant uncertainty, so higher values help to ensure sufficient column safety margin in case of non-compliant concrete (Magalhães, Real and da Silva Filho, 2016);

(o) By studying how the total expected costs change in terms of the optimal risk-based solution, two situations are noticeable. Conservative design relates to total expected costs slowly increasing, as resources are allocated with no corresponding decrease in expected costs of failure. Unsafe design has its total expected costs increasing in a very steep slope due to lacking capacity against one or more failure modes. Therefore, all optimal design solutions for a given P_{LD} reflect the best allocation of resources, balancing reinforcement costs with the reduction in expected costs of failure;

(p) Column axial capacity for optimal APM design increases according to frame height and column loss scenario, as greater flexural demands are expected for taller frames and inner column loss scenarios due to Vierendeel, Compressive Arch and Catenary Actions being more efficiently mobilized;

(q) Greater unitary reference costs lead to similar optimal designs both before and after P_{LD}^{th}. However, the increased overall manufacturing costs imply in slightly reduced reinforcements and safety margins against critical failure modes. Besides, cost-effectiveness of APM design becomes positive for slightly increased threat probabilities due to more expensive reference reinforcement costs. In comparison to expensive reference costs from the Covid-19 pandemic period, cheaper reference costs from 2024 lead to a ~19% reduction in beam manufacturing costs and overall increase of 25% for bending and shear capacities;

(r) Optimal design slightly changes in terms of the amount of ductility in the rebars, leading to optimal solutions of similar manufacturing cost. However, greater ductility rebars provide increased safety margins and smaller expected costs of failure;

(s) Symmetric rebar reinforcements related to slightly reduced beam depths enhance the ultimate capacity, but not with a corresponding increase in shear resistance. Hence, this option is shown to be cost-effective only when simultaneously meeting the following conditions: loss of a single column, low ductility rebars, and P_{LD} slightly above P_{LD}^{th}. This combination reflects a situation where more rebars are needed, due to their lower ductility, to manage a high probability of rebar rupture, for which the algorithm allows for a slight reduction in shear capacity to meet the more urgent need;

(t) Partially strengthening the first two floors reduces manufacturing and total expected costs in ~19% when compared to whole frame reinforcement. In addition, partial frame reinforcement makes APM design cost-effective for smaller threat probabilities. Yet, gas explosions at the upper floors, for instance, are not addressed by this solution;

(u) For $P_{LD} < P_{LD}^{th}$, an optimal setup with 2-legged stirrups is slightly cheaper than a setup with 3-legged stirrups, although the additional shear resistance due to a third stirrup leg is compensated by a reduction in stirrup diameter to meet a similar ρ_{st}. The advantages of the extra core confinement provided by slightly more expensive 3-legged stirrups become noticeable for $P_{LD} > P_{LD}^{th}$, reducing the total expected cost by approximately 10% in comparison with the 2-legged stirrup option, and slightly increasing P_{LD}^{th}. This slight advantage in the APM design relates to the extra confinement provided by an additional stirrup leg, which assists on the CAA capacity, reduces the propensity of rebar failure during snap-though instability, and slightly postpone the CA onset;

(v) ACI and GSA guideline provisions for conventional and progressive-collapse-resistant design are satisfied by the optimal solutions, and the few exceptions are related to Demand-Capacity Ratios (DCR) slightly greater than one. In these few cases, the risk-based algorithm does not show cost-effectiveness in providing greater reinforcements solely to meet the safety margin required by guidelines. Besides, slightly more conservative designs would be needed to ensure safety margins in these cases;

(w) Target reliability indexes cold be added to ensure that guideline provisions are always automatically met. Nevertheless, DCRs close to unity are a good indication that the optimal solutions are in agreement with expected real-life safety demands, indicating a good choice of cost multipliers k when computing expected cost of failure. Thus, DCR factors for rebar rupture reduces for taller frames under inner column loss, reflecting their greatest effectiveness in developing both VA and CA;

(x) As the cost-benefit of APM design grows, the optimal structure becomes more efficient at bridging over a lost column. If P_{LD} is slightly above P_{LD}^{th}, much higher unconditional probabilities of ductile steel failure led to greater DCRs, even though its optimal conditional reliability index is between 3.0 and 4.0;

(y) Resistance factors show that flexural capacity for optimal APM designs is at least twice than the flexural capacity for optimal conventional design. Ultimate capacity in terms of rebar rupture is also shown to become more than double, regardless of frame aspect ratio and column loss scenario, when square cross-sections are assumed for the columns.

Ongoing investigations are addressing all the main outcomes. As stated in the end of Chapter 4: this thesis marks the end of a cycle, but not the end of this research. In fact, this is just the beginning.

REFERENCES

ABDELWAHED, B. Beam-column joints reinforcement detailing adequacy in case of a corner column loss-numerical analysis. **Latin American Journal of Solids and Struct**, SciELO, v. 16, n. 7, p. e216, 2019. doi: 10.1590/1679-78255536.

ADAM, J. M.; PARISI, F.; SAGASETA, J.; LU, X. Research and practice on progressive collapse and robustness of building structures in the 21st century, **Engineering Structures**, Elsevier, v. 173, p. 122–149, 2018. doi: 10.1016/j.engstruct.2018.06.082.

AGARWAL J.; ENGLAND J. Recent developments in robustness and relation with risk. **Proceedings of the Institution of Civil Engineers - Structures and Buildings**, London: Thomas Telford Ltd, v. 161, n. 4, p. 183–188, 2008. ISSN 0965-0911. E-ISSN 1751-7702.

ALAM, M. I.; FAWZIA, S. Numerical studies on CFRP strengthened steel columns under transverse impact. **Composite Structures**, Elsevier, v. 120, p. 428–41, 2015. doi: 10.1016/j.compstruct.2014.10.022.

ALLEN, D. E.; SCHRIEVER, W. R. Progressive collapse, abnormal loads and building codes. **Proceedings ASCE National Meeting on Structural Engineering: 1972-04**, Cleveland, USA, 1972.

ALOGLA, K.; WEEKES, L.; AUGUSTHUS-NELSON, L. A new mitigation scheme to resist progressive collapse of RC structures. **Construction and Building Materials**, Elsevier, v. 125, p. 533–545, 2016. doi: 10.1016/j.conbuildmat.2016.08.084.

ALPER H E, YU S, STELLMAN S D, BRACKBILL R M. Injury, intense dust exposure, and chronic disease among survivors of the World Trade Center terrorist attacks of September 11, 2001. **Injury Epidemiology**, BMC, v. 4:17, p.1-10, 2017. doi: 10.1186/s40621-017-0115-x.

ALSHAIKH, I. M.; BAKAR, B. A.; ALWESABI, E. A.; AKIL, H. M. Experimental investigation of the progressive collapse of reinforced concrete structures: An overview. **Structures**, Elsevier, v. 25, p. 881–900, 2020. doi: 10.1016/j.istruc.2020.03.018.

AMERICAN CONCRETE INSTITUTE (ACI). **ACI 318-05**: Building code requirements for structural concrete. Detroit, Michigan, 2005. 430 p.

AMERICAN CONCRETE INSTITUTE (ACI). **ACI 318-19**: Building code requirements for structural concrete. Detroit, Michigan, 2019. 624 p. ISBN-10: 1641950560. ISBN-13:978-1641950565.

AMERICAN SOCIETY OF CIVIL ENGINEERS (ASCE). **ASCE/SEI 7-22**: Minimum design loads and associated criteria for buildings and other structures. Reston, Virginia, 2022. 975 p. ISBN (print):9780784415788. ISBN (PDF):9780784483497.

AMERICAN SOCIETY OF CIVIL ENGINEERS (ASCE). **ASCE/SEI 41-23**: Seismic Evaluation and Retrofit of Existing Buildings. Reston, Virginia, 2023. ISBN (PRINT):9780784416112. ISBN (PDF):9780784484760

ARCGIS PRO. How IDW works. **ArcGIS PRO documentation**, 2024. Available in: https://pro.arcgis.com/en/pro-app/latest/tool-reference/3d-analyst/kriging.htm. Access in: 15 aug. 2024.

ARSHIAN, A. H.; MORGENTHAL G. Three-dimensional progressive collapse analysis of reinforced concrete frame structures subjected to sequential column removal. **Engineering Structures**, Elsevier, v. 132, p. 87-97, 2017. doi: 10.1016/j.engstruct.2016.11.018.

ARSHIAN, A. H.; MORGENTHAL, G.; NARAYANAN, S. Influence of modelling strategies on uncertainty propagation in the alternate path mechanism of reinforced concrete framed structures. **Engineering Structures**, Elsevier, v. 110, p. 36-47, 2015. doi: 10.1016/j.engstruct. 2015.11.019.

ASSOCIAÇÃO BRASILEIRA DE NORMAS TÉCNICAS, **ABNT NBR 6118**: Projeto de Estruturas de Concreto. Rio de Janeiro, 2023. 238 p.

AOUES, Y.; CHATEAUNEUF, A. Benchmark study of numerical methods for reliability-based design optimization. **Structural and Multidisciplinary Optimization**, Springer, v. 41, p. 277-294, 2010. doi: 10.1007/s00158-009-0412-2.

BAO, Y.; MAIN, J. A.; NOH, S.-Y. Evaluation of structural robustness against column loss: methodology and application to RC frame buildings. **Journal of Structural Engineering**, ASCE, v. 143, n. 8, p. 04017066, 2017. doi: 10.1061/%28ASCE%29ST.1943-541X.0001795.

BAUMGARDT, G. R.; REAL, M. V.; TEIXEIRA, P. R. F.; SANTOS, E. D.; SILVEIRA, T.; ISOLDI, L. A. Computational model verification and numerical analysis of plate buckling due to combined loading. **Ciência e Natura**, UFSM, v. 45, p. e75137, 2023.

BAŽANT, Z. P.; ZHOU, Y. Why did the world trade center collapse? – Simple analysis. **Journal of Engineering Mechanics**, ASCE, v. 128, n. 1, p. 2-6, 2002. doi: 10.1061/(ASCE)0733-9399(2002)128:3(369).

BECK, A. T. **StRAnD**: structural risk analysis and design. São Carlos: EESC-USP, 2007.

BECK, A. T. **Confiabilidade e segurança das estruturas**. 1. ed. Rio de Janeiro: Elsevier, 2019. ISBN 978-85-352-8688-5.

BECK, A. T. Optimal design of hyperstatic redundant structural systems: fundamentals. **Engineering Structures**, Elsevier, v. 219, p. 110542, 2020. doi: 10.1016/j.engstruct.2020.1105 42.

BECK, A. T.; GOMES, W. J. S. A comparison of deterministic, reliability-based and risk-based structural optimization under uncertainty. **Probabilistic Engineering Mechanics**, Elsevier, v. 28, p. 18–29, 2012.

BECK, A. T.; GOMES, W. J. S.; LOPEZ, R. H.; MIGUEL, L. F. F. A comparison between robust and risk-based optimization under uncertainty. **Structural and Multidisciplinary Optimization**, Springer, v. 52, p. 479-492, 2015. doi: 10.1007/s00158-015-1253-9.

BECK, A. T.; RIBEIRO, L. d. R.; COSTA, L. G. L.; STEWART, M. G. Comparison of risk-based robustness indices in progressive collapse analysis of building structures. **Structures**, Elsevier, v. 57, p. 105295, 2023. doi: 10.1016/j.istruc.2023.105295.

BECK, A. T.; RIBEIRO, L. d. R.; VALDEBENITO, M. Risk-based cost-benefit analysis of frame structures considering progressive collapse under column removal scenarios. **Engineering Structures**, Elsevier, v. 225, p. 111295, 2020. doi: 10.1016/j.engstruct.2020.111295.

BECK, A. T.; RIBEIRO, L. d. R.; VALDEBENITO, M.; JENSEN, H. A. Risk-Based Design of Regular Plane Frames Subject to Damage by Abnormal Events: A Conceptual Study, **Journal of Structural Engineering**, ASCE, v. 148, n. 1, p. 04021229, 2022. doi: 10.1061/(ASCE)ST.1943-541X.0003196.

BECK, A. T.; STEWART, M. G. Risk-based cost-benefit analysis of structural strengthening to mitigate disproportionate collapse of buildings under abnormal blast loading. **Structures**, Elsevier, v. 57, p. 105103, 2023. doi: 10.1016/j.istruc.2023.105103.

BECK, A. T.; TESSARI, R. K.; KROETZ, H. M. System reliability-based design optimization and risk-based optimization: a benchmark example considering progressive collapse. **Engineering Optimization**, Taylor & Francis, v. 51, p. 1000-1012, 2019. doi: 10.1080/0305215X.2018.1502760.

BECK, A. T.; VERZENHASSI, C. C. Risk Optimization of a Steel Frame Communications Tower Subject to Tornado Winds, **Latin American Journal of Solids and Structures**, SciELO, v. 5, p. 187-203, 2008.

BEHNAM, B.; SHOJAEI, F.; RONAGH, H. R. Seismic progressive-failure analysis of tall steel structures under beam-removal scenarios. **Frontiers of Structural and Civil Engineering**, Springer, v. 13, n. 4, p. 904–17, 2019. doi: 10.1007/s11709-019-0525-7.

BENNETT, R. M. Formulations for probability of progressive collapse. **Structural Safety**, Elsevier, v. 5, n. 1, p. 66–77, 1988. doi: 10.1016/0167-4730(88)90006-9.

BEYER, H-G.; SENDHOFF, B. Robust optimization – A comprehensive survey. **Computer Methods in Applied Mechanics and Engineering**, Elsevier, v. 196, p. 3190-3218, 2007. doi: 10.1016/j.cma.2007.03.003.

BOSSE, R M.; FLÓREZ-LÓPEZ, J.; GIDRÃO, G. M.S.; RODRIGUES, I. D.; BECK, A. T. Collapse mechanisms and fragility curves based on Lumped Damage Mechanics for RC frames subjected to earthquakes. **Engineering Structures**, Elsevier, v. 311, p. 118115, 2024. doi: 10.1016/j.engstruct.2024.118115.

BRETT, C.; LU, Y. Assessment of robustness of structures: current state of research. **Frontiers of Structural and Civil Engineering**, Springer, v. 7, n. 4, p. 356–68, 2013. doi: 10.1007/s11709-013-0220-z.

BRITISH STANDARDS INSTITUTION (BSI). **CP 110-1**: Code of Practice for the Structural Use of Concrete. Design, materials and workmanship. London, UK, 1972.

BRODING, W. C.; DIEDERICH, F. W.; PARKER, B. P. Structural optimization and design based on a reliability design criterion. **Journal of Spacecraft**, ARC, v. 1, p. 56–61, 2012. doi: 10.2514/3.27592.

BRUNESI, E.; NASCIMBENE, R.; PARISI, F.; AUGENTI, N. Progressive collapse fragility of reinforced concrete framed structures through incremental dynamic analysis. **Engineering Structures**, Elsevier, v. 104, p. 65-79, 2015.

BRUNESI, E.; PARISI, F. Progressive collapse fragility models of European reinforced concrete framed buildings based on pushdown analysis. **Engineering Structures**, Elsevier, v. 152, p. 579-596, 2017.

BUCHAN, P.; CHEN, J. F. Blast resistance of FRP composites and polymer strengthened concrete and masonry structures–A state-of-the-art review. **Composites Part B: Engineering**, Elsevier, v. 38, n. 5–6, p. 509–22, 2007.

BYFIELD, M.; MUDALIGE, W.; MORISON, C.; STODDART, E. A review of progressive collapse research and regulations. **Proceedings of the Institution of Civil Engineers: Structures and Buildings**, Elsevier, v. 167, n. SB8, p. 447–456, 2014.

CAREDDA, G.; MAKOOND, N.; BUITRAGO, M.; SAGASETA, J.; CHRYSSANTHOPOULOS, M.; ADAM, J.M. Learning from the progressive collapse of buildings. **Developments in the Built Environment**, Elsevier, v. 15, p. 100194, 2023.

CARNEIRO, J. C. C. B. **Dispositivo para proteção de pilares em prédios: absorção de impactos contra colapso progressivo**. 2024. 137 p. Dissertation (Master's in Civil Engineering) – São Carlos School of Engineering, University of São Paulo, São Carlos, 2024.

CHAI, J.; SHEN, S.; DING, W.; ZHU, H.; CARTER, J. Numerical investigation of the failure of a building in Shanghai, China. **Computer and Geotechnics**, v. 55, p. 482-493, 2014.

CODA, H. B.; PACCOLA, R. R. A total-Lagrangian position-based FEM applied to physical and geometrical nonlinear dynamics of plane frames including semi-rigid connections and progressive collapse. **Finite Elements in Analysis and Design**, v. 91, p. 1–15, 2014.

COMITÉ EURO-INTERNATIONAL DU BÉTON. CEB-FIP. **Model Code 2010**: Final Draft. Bulletin D'information, CEB, Lausanne, 2011.

COSTA, L.G.L.; BECK, A.T. Probabilistic evaluation of design live loads for Brazilian light-duty vehicle parking garages, **Revista IBRACON de Estruturas e Materiais**, SciELO, v. 17, n. 2, p. e17209, 2024.

COSTA, L. G. L.; BECK, A. T. A critical review of probabilistic live load models for buildings: Models, surveys, Eurocode statistics and reliability-based calibration. **Structural Safety**, Elsevier, v. 106, p. 102411, 2024.

DA SILVA, L. A. R; TORII, A.J.; BECK, A. T. Hyperstatic and redundancy thresholds in truss topology optimization considering progressive collapse due to aleatory and epistemic uncertainties. **Probabilistic Engineering Mechanics**, v. 71, p. 103384, 2023.

DA SILVA, L. A. R; TORII, A. J.; Beck, A. T. System-reliability-based sizing and shape optimization of trusses considering millions of failure sequences. **Structural Safety**, Elsevier, v. 108, p. 102448, 2024.

DANESHVAR, H.; OOSTERHOF, S.A.; DRIVER, R.G. Arching followed by catenary response of steel shear connections in disproportionate collapse. **Canadian Journal of Civil Engineering**, Canadian Science Publishing, v. 47, n. 8, p. 908–20, 2020.

DE BIAGI, V.; CHIAIA, B. M. Damage tolerance in parallel systems. **International Journal of Damage Mechanics**, SAGE Journals, v. 25, n. 7, p. 1040–59, 2016.

DEPARTMENT OF DEFENSE (DoD). **UFC 4-023-03**: Design of buildings to resist progressive collapse. Washington, DC, 2009.

DIMAS, T. d. S. **Análise de estruturas de edifícios sujeitas a ações acidentais**. 2014. 132 p. Dissertation (Master's in Civil Engineering) – NOVA University Lisbon, Lisbon, 2014.

DING, L.; CHEN, J.; CASPEELE, R. Determination of dynamic collapse limit states using the energy-based method for multi-story RC frames subjected to column removal scenarios, **Engineering Structures**, Elsevier, v. 311, p. 118170, 2024.

DOS ANJOS, F. F. C. **Avaliação das Armaduras contra o Colapso Progressivo em Estruturas de Concreto Armado**. Projeto de Graduação (Graduação – Engenharia Civil), 2016 – Escola Politécnica da Universidade Federal do Rio de Janeiro, RJ, 2016.

DU, X.; CHEN, W. Sequential Optimization and Reliability Assessment Method for Efficient Probabilistic Design. **Journal of Mechanical Design**, ASME, v. 126, n. 2, p. 225–233, 2004.

DUBOURG, V. **Adaptive surrogate models for reliability analysis and reliability-based design optimization**. 2011. 309 p. Thesis (PhD in Mechanical Engineering) – Université Blaise Pascal, Clermont Ferrand, France, 2011.

EAGAR, T.W., MUSSO, C. Why did the world trade center collapse? Science, engineering, and speculation. **The Journal of the Minerals, Metals & Materials Society**, Springer, v. 53, p. 8–11, 2001.

ENGLAND, J.; AGARWAL, J.; BLOCKLEY, D. The vulnerability of structures to unforeseen events. **Computers and Structures**, v. 86, n. 10, p. 1042–51, 2008.

ELKADY, N.; NELSON, A. L.; WEEKES, L.; MAKOOND, N.; BUITRAGO, M. Progressive collapse: Past, present, future and beyond. **Structures**, Elsevier, v. 62, p. 106131, 2024.

ELLINGWOOD, B. R. Mitigating Risk Form Abnormal Loads and Progressive Collapse. **Journal of Performance of Constructed Facilities**, ASCE, 20 (4), p.315-323, 2006.

ELLINGWOOD, B.; GALAMBOS, T. V. Probability-based criteria for structural design. **Structural Safety**, Elsevier, v. 1, n. 1, p. 15–26, 1982.

ELLINGWOOD, B, LEYENDECKER, E. V. Approaches for design against progressive collapse. **Journal of the Structural Division**, ASCE, v. 104, n. 3, p. 413–23, 1978.

ENEVOLDSEN, I.; SØRENSEN, J. Reliability-based optimization in structural engineering. **Structural Safety**, Elsevier, v. 15, p. 169–196, 1994.

EUROPEAN COMMITTEE FOR STANDARTIZATION, **EUROCODE 1: Actions on structures – Part 1-7**: General actions — accidental actions. CEN, EN 1991, Brussels, Belgium, 2006. 66 p.

EUROPEAN COMMITTEE FOR STANDARTIZATION, **EUROCODE 2, Design of Concrete Structures – Part 1-1**: General Rules and Rules for Buildings. CEN, EN 1992, Brussels, Belgium, 2004.

EZODDIN, A.; KHEYRODDIN, A.; GHOLHAKI, M. Experimental and numerical investigation on the seismic retrofit of RC frames with linked column frame systems. **Journal of Building Engineering**, Elsevier, v. 44, p. 102956, 2021.

FAN, W.; SHEN, D.; ZHANG, Z.; HUANG, X.; SHAO, X. A novel UHPFRC-based protective structure for bridge columns against vehicle collisions: Experiment, simulation, and optimization. **Engineering Structures**, Elsevier, v. 207, p. 110247, 2020.

FANG, C.; IZZUDDIN, B.; ELGHAZOULI, A.; NETHERCOT, D. Simplified energy-based robustness assessment for steel-composite car parks under vehicle fire. **Engineering Structures**, Elsevier, v. 49, p. 719–32, 2013.

FASCETTI, A.; KUNNATH, S. K.; NISTICO, N. Robustness evaluation of RC frame buildings to progressive collapse. **Engineering Structures**, Elsevier, v. 86, p. 242-249, 2015.

FELIPE, T. R. C. **Novo Método para a Avaliação do Risco de Colapso Progressivo em Edifícios de Alvenaria Estrutural**. 2017. 150 p. Dissertation (Master's in Civil Engineering) – São Carlos School of Engineering, University of São Paulo, São Carlos, 2017.

FELIPE, T. R. C.; HAACH, V. G.; BECK, A. T. Systematic reliability-based approach to progressive collapse. **Journal of Risk and Uncertainty in Engineering Systems**, v. 4, n. 4, p. 1-9, 2018.

FELIPE, T. R. C.; LEONEL, E. D.; HAACH, V. G.; BECK, A. T. A comprehensive ductile damage model for 3D truss structures. **International Journal of Non-Linear Mechanics**, v. 112, p. 13-24, 2019.

FEMA 277. **The Oklahoma City bombing: improving building performance through multi hazard mitigation**. Washington (DC): Building Performance Assessment Team, Federal Emergency Management Agency, 1996.

FENG, P.; QIANG, H.; QIN, W.; GAO, M. A novel kinked rebar configuration for simultaneously improving the seismic performance and progressive collapse resistance of RC frame structures. **Engineering Structures**, Elsevier, v. 147, p. 752–67, 2017.

FREDDI, F.; CIMAN, L.; TONDINI, N. Retrofit of existing steel structures against progressive collapse through roof-truss. **Journal of Constructional Steel Research,** Elsevier, v. 188, p. 107037, 2022.

FU, G.; FRANGOPOL, D. M. Balancing weight, system reliability and redundancy in a multiobjective optimization framework. **Structural Safety**, Elsevier, v. 7, n. 2-4, p. 165–175, 1990.

GALAL, K.; EL-SAWY, T. Effect of retrofit strategies on mitigating progressive collapse of steel frame structures. **Journal of Constructional Steel Research,** Elsevier, v. 66, n. 4, p. 520–31, 2010.

GALAL, M.A., BANDYOPADHYAY, M.; BANIK, A. K. Dual effect of axial tension force developed in catenary action during progressive collapse of 3D composite semi-rigid jointed frames. **Structures**, Elsevier, v. 19, p. 507–19, 2019.

GALDINO, B. C. P.; MELO, G. S. S. A. Post punching shear pattern and progressive collapse of flat slab building. **Revista Ibracon de Estruturas e Materiais**, SciELO, v. 16, p. 16312-16319, 2023.

GARDNER, N.; HUH, J.; CHUNG, L. Lessons from the Sampoong department store collapse. **Cement and Concrete Composites**, Elsevier, v. 24, n. 6, p. 523–529, 2002.

GARG, S.; AGRAWAL, V.; NAGAR, R. Case study on strengthening methods for progressive collapse resistance of RC flat slab buildings. **Structures**, Elsevier, v. 29, p. 1709–22, 2021.

GARG, S.; AGRAWAL, V.; NAGAR, R. Sustainability assessment of methods to prevent progressive collapse of RC flat slab buildings. **Procedia CIRP**, Elsevier, v. 98, p. 25–30, 2021.

GARG, S.; AGRAWAL, V.; NAGAR, R. Progressive collapse behaviour of reinforced concrete flat slab buildings subject to column failures in different stories. **Materials Today: Proceedings,** Elsevier, v. 43, p. 1031–7, 2021.

GEDAM, B. A. Fire resistance design method for reinforced concrete beams to evaluate fire-resistance rating. **Structures**, Elsevier, v. 33, p. 855–77, 2021.

GERASIMIDIS, S.; BANIOTOPOULOS, C. Progressive collapse mitigation of 2D steel moment frames: assessing the effect of different strengthening schemes. **Stahlbau,** Wiley, v. 84, n. 5, p. 324–331, 2015.

GERNAY, T.; GAMBA, A. Progressive collapse triggered by fire induced column loss: Detrimental effect of thermal forces. **Engineering Structures**, Elsevier, v. 172, p. 483–496, 2018.

GOMES, W. J. S.; BECK, A. T. Global structural optimization considering expected consequences of failure and using ANN surrogates. **Computers & Structures**, Elsevier, v. 126, p. 56-68, 2013. doi: 10.1016/j.compstruc.2012.10.013.

GOMES, W. J. S.; BECK, A. T.; LOPEZ, R. H.; MIGUEL, L. F. F. A probabilistic metric for comparing metaheuristic optimization algorithms. **Structural Safety**, Elsevier, v. 70, p. 59-70, 2018. doi: 10.1016/j.strusafe.2017.10.006.

GRIFFITHS, H.; PUGSLEY, A.; SAUNDERS, O. **Report of the Inquiry into the Collapse of Flats at Ronan Point, Canning Town**. Her Majesty's Stationery Office, London, 1968.

GROSS, J. L.; MCGUIRE, W. Progressive collapse resistant design. **Journal of Structural Engineering,** ASCE, v. 109, n. 1, p. 1-15, 1983.

GENERAL SERVICES ADMINISTRATION (GSA). **General Services Administration Alternate Path Analysis & Design Guidelines for Progressive Collapse Resistance**. Washington DC, 2013.

GENERAL SERVICES ADMINISTRATION (GSA). **General Services Administration Alternate Path Analysis & Design Guidelines for Progressive Collapse Resistance**. Washington DC, 2016. 203 p.

INTERNATIONAL CODE COUNCIL (ICC). **International Building Code**. 2021.

HANIFEHZADEH, M.; ARYAN, H.; GENCTURK, B.; AKYNIYAZOV, D. Structural response of steel jacket-UHPC retrofitted reinforced concrete columns under blast loading. **Materials**, MDPI, v. 14, n. 6, p. 1521, 2021.

HARTMANN D.; BREIDT, M.; NGUYEN, V.; STANGENBERG, F.; HÖHLER, S. Structural collapse simulation under consideration of uncertainty – Fundamental concept and results. **Computers & Structures**, Elsevier, v. 86, p. 2064-2078, 2008.

HENDRY, A. W. Summary of research and design philosophy for bearing wall structures. **Journal Proceedings**, Farmington Hills, v. 76, n. 33, p. 723–737, 1979. doi: 10.14359/6966.

HORR, A.; SAFI, M. Multi-layered energy absorber frames for tall buildings under high-speed impact. **The Structural Design of Tall and Special Buildings,** Wiley, v. 12, n. 5, p. 423–450, 2003.

IZADI, I. T.; RANJBARAN, A. Investigation on a mitigation scheme to resist the progressive collapse of reinforced concrete buildings. **Frontiers of Structural and Civil Engineering,** Springer, v. 6, n. 4, p. 421–30, 2012.

IZZUDDIN, B. A.; VLASSIS; A. G.; ELGHAZOULI, A. Y.; NETHERCOT, D. A. Progressive collapse of multi-storey buildings due to sudden column loss - Part I: simplified assessment framework. **Engineering Structures**, Elsevier, v. 30, n. 5, p. 1308-1318, 2008.

JENKINS, J. A.; SEITZ, T. B.; PRZEMIENIECKI, J. S. Large deflections of diamond-shaped frames. **International Journal of Solids and Structures**, Elsevier, v. 2, n. 4, p. 591- 600, IN1-IN2, 601-603, 1966.

JIANG J, L.I. G-Q.; USMANI, A. Effect of bracing systems on fire-induced progressive collapse of steel structures using OpenSees. **Fire Technology**, Springer, v. 51, n. 5, p. 1249–1273, 2015.

JIANG, J.; LI, G-q. Mitigation of fire-induced progressive collapse of steel framed structures using bracing systems. **Advanced Steel Construction**, Springer, v. 15, n. 2, p. 192–202, 2019.

JIANG, J.; LU, Y.; DAI, X.; LI, G-Q.; CHEN, W.; YE, J. Disproportionate collapse of steel-framed gravity buildings under travelling fires. **Engineering Structures**, Elsevier, v. 245, p. 112799, 2021. doi: 10.1016/j.engstruct.2021.112799.

JOANNI, A.; RACKWITZ, R. Cost benefit optimization for maintained structures by a renewal model. **Reliability Engineering and System Safety**, Elsevier, v. 93, p. 489–499, 2008.

JOINT COMMITTEE ON STRUCTURAL SAFETY (JCSS). **Probabilistic Model Code**: Part 2: Load models. 2001. 73 p. Available in: https://www.jcss-lc.org/publications/jcsspmc/part_ii.pdf. Access in: 14 aug. 2024.

JOINT COMMITTEE ON STRUCTURAL SAFETY (JCSS). **Probabilistic Model Code**: Part 3: Material properties. 2002. 41 p. Available in: https://www.jcss-lc.org/publications/jcsspmc/part_iii.pdf. Access in: 14 aug. 2024.

KABALA, R. E. Design of minimal-weight structures given reliability and cost. **Journal of Aerospace Sciences**, ARC, v. 29, p. 355–356, 1962.

KADHIM, M. M.; WU, Z.; CUNNINGHAM, L. S. Loading rate effects on CFRP strengthened steel square hollow sections under lateral impact. **Engineering Structures**, Elsevier, v. 171, p. 874–82, 2018.

KAYMAZ, I. Application of kriging method to Structural Reliability problems. **Structural Safety**, Elsevier, v. 27, p. 133-151, 2005.

KAZEMI-MOGHADDAM, A.; SASANI, M. Progressive collapse evaluation of Murrah Federal Building following sudden loss of column G20. **Engineering Structures**, Elsevier, v. 89, p. 162-171, 2015.

KHANDELWAL, K.; EL-TAWIL, S.; SADEK, F. Progressive collapse analysis of seismically designed steel braced frames. **Journal of Constructional Steel Research,** Elsevier, v. 65, n. 3, p. 699–708, 2009.

KHANDELWAL, K.; EL-TAWIL, S. Pushdown resistance as a measure of robustness in progressive collapse analysis. **Engineering Structures**, Elsevier, v. 33, p. 2653-2661, 2011.

KHOEI, A. S; REZA, A.; MAALEK, S.; GHARIGHORAN, A. Assessment of Design and Retrofitting Solutions on the Progressive Collapse of Hongqi Bridge, **Shock and Vibration**, Wiley, v. 2020, p. 4932721, 2020.

KHOURY, G. Compressive strength of concrete at high temperatures: a reassessment. Magazine of concrete Research, Thomas Telford Ltd, v. 44, n. 161, p. 291–309, 1992.

KIAKOJOURI, F., DE BIAGI, V., CHIAIA, B., SHEIDAII, M. R. Progressive collapse of framed building structures: Current knowledge and future prospects. **Engineering Structures**, Elsevier, v. 206, p. 110061, 2020.

KIAKOJOURI F, F.; SHEIDAII, M. R.; DE BIAGI, V.; CHIAIA, B. Progressive collapse of structures: A discussion on annotated nomenclature. **Structures**, Elsevier, v. 29, p. 1417–1423, 2021. doi: 10.1016/j.istruc.2020.12.006.

KIAKOJOURI, F.; DE BIAGI, V.; CHIAIA, B.; SHEIDAII, M. R. Strengthening and retrofitting techniques to mitigate progressive collapse: A critical review and future research agenda. **Engineering Structures**, Elsevier, v. 262, p. 114274, 2022.

KIM, S. H.; BOUKOUVALA, F. Machine learning-based surrogate modeling for data-driven optimization: a comparison of subset selection for regression techniques. **Optimization Letters**, Springer, v. 14, p. 989-1010, 2020. doi: 10.1007/s11590-019-01428-7.

KIM, J.; CHOI, H.; MIN, K-W. Use of rotational friction dampers to enhance seismic and progressive collapse resisting capacity of structures. **The Structural Design of Tall and Special Buildings,** Wiley, v. 20, n. 4, p. 515–537, 2011.

KIM, J.; HONG, S. Progressive collapse performance of irregular buildings. **The Structural Design of Tall and Special Buildings,** Wiley, v. 20, n. 6, p. 721–734, 2011.

KIM, J.; JUNG, M-K. Progressive collapse resisting capacity of tilted building structures. **The Structural Design of Tall and Special Buildings,** Wiley, v. 22, n. 18, p. 1359–1375, 2013.

KIM, J.; LEE, S.; MIN, K-W. Design of MR dampers to prevent progressive collapse of moment frames. **Structural Engineering and Mechanics,** Techno Press, v. 52, n. 2, p. 291–306, 2014.

KISI, K.; SULBARAN, T. Construction Cost and Schedule Impacts Due to COVID-19. **Journal of Legal Affairs and Dispute Resolution in Engineering and Construction**, ASCE, v. 14, n. 4, 2008.

KLEINMANN, N. L.; SPALL, J. C.; NAIMAN, D.C. Simulation-based optimization with stochastic approximation using common random numbers. **Management Science**, Informs, v. 45, n. 11, p. 1570—1578, 1999.

KOTSOVINOS, P.; USMANI, A.; The World Trade Center 9/11 Disaster and Progressive Collapse of Tall Buildings. **Fire Technology**, Springer, v. 49, p. 741-765, 2013.

KROETZ, H. M. **Otimização estrutural sob incertezas: métodos e aplicações**. 2019. 143 p. Thesis (PhD – Engenharia de Estruturas) – Escola de Engenharia de São Carlos, Universidade de São Paulo, São Carlos, São Paulo, 2019.

KROETZ, H. M.; TESSARI, R. K.; BECK, A. T. Performance of global metamodeling techniques in solution of structural reliability problems. **Advances in Engineering Software**, Elsevier, v. 114, p. 394–404, 2017. doi: 10.1016/j.advengsoft.2017.08.001.

KROETZ, H. M.; MOUSTAPHA, M.; BECK, A.T.; SUDRET, B. A Two-Level Kriging-Based Approach with Active Learning for Solving Time-Variant Risk Optimization Problems. **Reliability Engineering & System Safety**, Elsevier, v. 103, p. 107033, 2020. doi: 10.1016/j.ress.2020.107033.

KUNNATH, S. K.; BAO, Y.; EL-TAWIL, S. Advances in computational simulation of gravity induced disproportionate collapse of RC frame buildings. **Journal of Structural Engineering**, ASCE,144(2), 03117003. 2018.

LALKOVSKI, N.; STAROSSEK, U. Pancake-type collapse-preventing downward progression. *In*: IABSE symposium report, Madrid, Spain, 2014. **International Association for Bridge and Structural Engineering**; v. 102, n. 20, p. 1642–1649, 2014. doi: 10.2749/222137814814068148.

LA MALVA, K. J.; BARNETT, J. R.; DUSENBERRY, D. O.; Failure Analysis of the World Trade Center 5 Building. **Journal of Fire Protection Engineering**, SAGE Journals, v 19, p. 261-274, 2009.

LEW, H. S.; BAO, Y.; PUJOL, S.; SOZEN, M. A. Experimental study of reinforced concrete assemblies under Column removal scenario. **ACI Structural Journal**, Farmington Hills, v. 111, n. 4, p. 881-892, 2014.

LEYENDECKER, E. V.; FATTAL, S. G.; **Investigation of the Skyline Plaza Collapse in Fairfax County, Virginia. Dept. of Commerce**, National Bureau of Standards, Institute for Applied Technology, Center for Building Technology, U.S. Govt. Printing Office, Washington, DC, 1973.

LI, Y.; LU, X.; GUAN, H.; REN, P.; QIAN, L. Probability-based progressive collapse-resistant assessment for reinforced concrete frame structures. **Advances in Structural Engineering,** Sage Journals, v. 19, n. 11, p. 1723–1735, 2016.

LIANG, J.; MOURELATOS, Z. P.; NIKOLAIDIS, E. A Single-Loop Approach for System Reliability-Based Design Optimization. **Journal of Mechanical Design**, ASME v. 129, n. 12, p. 1215–1224, 2007.

LIANG, J.; MOURELATOS, Z. P.; TU, J. A Single-Loop Method for Reliability-Based Design Optimization. **Proceedings of ASME Design Engineering Technical Conferences**, ASME, 2004.

LIN, K.; LU, X.; LI, Y.; ZHUO, W.; GUAN, H. A novel structural detailing for the improvement of seismic and progressive collapse performances of RC frames. **Earthquake Engineering & Structural Dynamics,** Wiley, v. 48, n. 13, p. 1451–70, 2019.

LONG, X.; WANG, S.; HUANG, X-J.; LI, C.; KANG, S-B. Progressive collapse resistance of exterior reinforced concrete frames and simplified method for catenary action. **Engineering Structures**, Elsevier, v. 249, p. 113316, 2021.

LOPEZ, R. H.; BECK, A. T. Reliability-based design optimization strategies based on FORM: a review. **Journal of the Brazilian Society of Mechanical Sciences and Engineering,** Springer, v. 34, n. 4, p. 506-514, 2012.

LU, Z.; RONG, K.; ZHOU, Z.; DU, J. Experimental study on performance of frame structure strengthened with foamed aluminum under debris flow impact. **Journal of Performance of Constructed Facilities,** ASCE, v. 34, n. 2, p. 04020011, 2020.

LUIZ, C. B. **Otimização Topológica de Treliças Hiperestáticas Considerando Incertezas**. 2020. 120 p. Dissertation (Master's in Civil Engineering) – São Carlos School of Engineering, University of São Paulo, São Carlos, 2020.

MA, Q.; REJAB, M.; SIREGAR, J.; GUAN, Z. A review of the recent trends on core structures and impact response of sandwich panels. **Journal of Composite Materials,** Sage Journals, v. 55, n. 18, p. 2513–2555, 2021.

MACEDO, F. C. **Projeto baseado em desempenho de linhas de transmissão sujeitas a ações de tornados**. 2023. 101 p. Dissertation (Master's in Civil Engineering) – São Carlos School of Engineering, University of São Paulo, São Carlos, 2023.

MAGALHÃES, F. C.; REAL, M. V.; DA SILVA FILHO, L. C. P. The problem of non-compliant concrete and its influence on the reliability of reinforced concrete columns. **Materials and Structures**, Springer, v. 49, p. 1485-1497, 2016.

MAGHROON, F.; IZADINIA, M.; SOLHJOEI, N.; ABADI, E. I. Z. Effects of earthquake components on seismic progressive collapse potential of steel frames. **Iranian Journal of Science and Technology, Transactions of Civil Engineering,** Springer, v. 46, p. 3555–3569 2022.

MARCHAND, K. E.; STEVENS, D. J. Progressive collapse criteria and design approaches improvement. **Journal of Performance of Constructed Facilities, ASCE,** v. 29, n. 5, p. B4015004, 2015.

MATTIASSON, K. Numerical results from large deflection beam and frame problems analysed by means of elliptic integrals. **International Journal for Numerical Methods in Engineering**, Wiley, v. 17, n. 1, p. 145–153, 1981.

MATTOS, L. E. G. **Dispositivo para Proteção de Pilares em Prédios: Impactos e Incêndios**. 2024. 190 p. Dissertation (Master's in Civil Engineering) – São Carlos School of Engineering, University of São Paulo, São Carlos, 2024.

MAXWELL, J. C. **The scientific papers of James Clerk Maxwell**. Dover Publications, INC. New York, 1869.

MAZARS, J.; HAMON, F.; GRANGE, S. A new 3D damage model for concrete under monotonic, cyclic and dynamic loadings. **Materials and Structures**, Springer, v. 48, p. 3779-3793, 2015.

MCKAY, M. D., BECKMAN, R. J., CONOVER, W. J. Comparison of Three Methods for Selecting Values of Input Variables in the Analysis of Output from a Computer Code. **Technometrics**, Taylor & Francis, v. 21, n. 2, p. 239–245, 1979.

MCKENNA, F. T. **Object-Oriented Finite Element Programming: Frameworks for Analysis, Algorithms and Parallel Computing**. 1997. Thesis (PhD in Civil Engineering), University of California, Berkeley, USA, 1997.

MCKENNA, F. T.; SCOTT, M. H.; FENVES, G. L. Nonlinear finite-element analysis software architecture using object composition. **Journal of Computing in Civil Engineering**, ASCE, v. 24, n. 1, p. 95-107, 2010.

MELCHERS, R. E.; BECK, A. T. **Structural Reliability**: Analysis and Prediction. 3. ed. Hoboken, NJ: John Wiley & Sons, 2018. 506 p. doi: 10.1002/9781119266105. ISBN 9781119265993

MELO, G. S. S. A.; REGAN, P. E. Post-punching resistance of connections between flat slabs and interior columns. **Magazine of Concrete Research**, ICE, v. 50, n. 4, p. 319-327, 1998.

MURUGAN, V.; SRINIVASAN, S. K. Influence of cover thickness in structural frames exposed to fire and service loads. **Environmental Science and Pollution Research,** Springer, v. 29, p. 85955–85968, 2021.

MUSAVI-Z, M.; SHEIDAII, M. R. Effect of seismic resistance capacity of moment frames on progressive collapse response of concentrically braced dual systems. **Asian Journal of Civil Engineering,** Springer, v. 22, n. 1, p. 23–31, 2021.

NAJI, A.; OMMETALAB, M. R. Horizontal bracing to enhance progressive collapse resistance of steel moment frames. **The Structural Design of Tall and Special Buildings,** Wiley, v. 28, n. 5, p. e1563, 2019.

NATIONAL INSTITUTE OF STANDARD AND TECHNOLOGY (NIST). **NISTIR 7396**: Best practices for reducing the potential for progressive collapse in buildings, technology administration. Gaithersburg, MD, 2007.

NATIONAL SEPTEMBER 11 MEMORIAL & MUSEUM. On Independence Day, 2,983 flags wave on the Memorial's bronze parapets. **9/11 Museum & Memorial**. 2017. Available in: https://911memorial.org/connect/blog/independence-day-2983-flags-wave-memorials-bronze-parapets. Acess in: 14 aug. 2024.

NATIONAL INSTITUTE OF STANDARD AND TECHNOLOGY (NIST). **Final report on the collapse of the world trade center towers**. Principal Findings, 2005. 302 p.

NGUYEN, T. H.; SONG J.; PAULINO G. H. Single-Loop System Reliability-Based Design Optimization Using Matrix-Based System Reliability Method: Theory and Applications. **ASME Journal of Mechanical Design**, ASME, v. 132, p. 011005-1-11, 2010.

OKASHA, N. Improved weighted average simulation approach for solving reliability-based analysis and design optimization problems. **Structural Safety,** Elsevier, v. 60, p. 47—55, 2016.

OLIVEIRA, D. R. C.; MELO, G. S. S. A.; REGAN, P. E. Punching resistance of RC slabs with rectangular columns. **Magazine of Concrete Research**, ICE, v. 56, n.3, p. 123-138, 2004.

PANG, B.; WANG, F.; YANG, J.; NYUNN, S.; AZIM, I. Performance of slabs in reinforced concrete structures to resist progressive collapse. **Structures**, Elsevier, v. 33, p. 4843–56, 2021.

PARISI, F. Blast fragility and performance-based pressure-impulse diagrams of European reinforced concrete columns. **Engineering Structures**, Elsevier, v. 103, p. 285-297, 2015.

PARISI, F.; AUGENTI, N. Influence of seismic design criteria on blast resistance of RC framed buildings: A case study. **Engineering Structures**, Elsevier, v. 44, p. 78-93, 2012.

PARISI, F.; SCALVENZI, M.; BRUNESI, E. Performance limit states for progressive collapse analysis of reinforced concrete framed buildings. **Structural Concrete**, Wiley, v. 20, p. 68-84, 2019.

PARK, R.; PRIESTLEY, M. J. N.; GILL, W. D. Ductility of square-confined concrete columns. **Journal of Structural Engineering**, ASCE, v. 108, n. ST4, p. 929-950, 1982.

PATE-CORNELL, E. Quantitative safety goals for risk management of industrial facilities. **Structural Safety**, Elsevier, v. 13, n. 3, p. 145–157, 1987.

PEARSON, C.; DELATTE, N.; Ronan Point Apartment Tower Collapse and its Effect on Building Codes. **Journal of Performance of Constructed Facilities**, ASCE, v. 19 n. 2, p. 172-177, 2005.

PEREIRA, E. M. V.; ANDRADE, R. B.; LEITÃO, F. F.; CAROBENO, C. L.; SIQUEIRA, G. H. Seismic risk evaluation of non-ductile low-rise RC buildings in Brazil: Time-based and intensity-based assessments considering different performance metrics. **Journal of Building Engineering**, Elsevier, v. 88, p. 109147, 2024.

PRAXEDES, C. S. N. **Robustness-based optimal progressive collapse design of RC frame structures**. 2020. 207 p. Thesis (PhD – Civil Engineering) – Ryerson University, Toronto, Ontario, Canada, 2020.

PRAXEDES, C. S. N., YUAN, X.-X. A novel robustness assessment methodology for reinforced concrete frames under progressive collapse threats. **Journal of Structural Engineering**, ASCE, v. 147, n. 8, p. 04021119, 2021.

PRAXEDES, C. S. N.; YUAN X.-X.; HE, X-H-C. A novel robustness index for progressive collapse analysis of structures considering the full risk spectrum of damage evolution. **Structure and Infrastructure Engineering,** Taylor & Francis, v. 18, n. 4, p. 1-19, 2021.

PRAXEDES, C. S. N., YUAN, X.-X. 2022. Robustness-oriented optimal design for reinforced concrete frames considering the large uncertainty of progressive collapse threats. **Structural Safety,** Elsevier, v. 94, p. 102139, 2022.

QIAN, K.; LAN, X.; LI, Z.; FU, F. Effects of steel braces on robustness of steel frames against progressive collapse. **Journal of Structural Engineering**, ASCE, v. 147, n. 11, p. 04021180, 2021.

QIAN, K.; WENG, Y.-H.; LI, B. Improving behavior of reinforced concrete frames to resist progressive collapse through steel bracings. **Journal of Structural Engineering**, ASCE, v. 145, n. 2, p. 04018248, 2019.

QIANG, H.; YANG, J.; FENG, P.; QIN, W. Kinked rebar configurations for improving the progressive collapse behaviours of RC frames under middle column removal scenarios. **Engineering Structures**, Elsevier, v. 211, p. 110425, 2020.

QIU, L.; LIN, F.; WU, K.; GU, X. Progressive collapse resistance of RC T-beam cable subassemblages under a middle-column-removal scenario. **Journal of Building Engineering**, Elsevier, v. 42, p. 102814, 2021.

RACKWITZ, R.; FIESSLER, B. Structural reliability under combined load sequences. **Computers & Structures**, Elsevier, v. 9, p. 489-494, 1978.

RASHKI, M.; MIRI, M.; MOGHADDAM, M. A. A new efficient Simulation method to approximate the probability of failure and most probable point. **Structural Safety**, Elsevier, v. 39, p. 22-29, 2012.

RASHKI, M.; MIRI, M.; MOGHADDAM, M. A. Closure to "A new efficient Simulation method to approximate the probability of failure and most probable point". **Structural Safety**, Elsevier, v. 46, p. 15-16, 2014.

REAL, M. V.; CAMPOS FILHO, Américo; MAESTRINI, S. R. Response variability in reinforced concrete structures with uncertain geometrical and material properties. **Nuclear Engineering and Design**, Elsevier, v. 226, n.3, p. 205-220, 2003.

REN, P.; LI, Y.; LU, X.; GUAN, H.; ZHOU, Y. Experimental investigation of progressive collapse resistance of one-way reinforced concrete beam–slab substructures under a middle-column-removal scenario. **Engineering Structures**, Elsevier, v. 118, p. 28–40, 2016.

REZVANI, F. H.; BEHNAM, B.; RONAGH, H. R.; ALAM, M. S. Failure progression resistance of a generic steel moment-resisting frame under beam-removal scenarios. **International Journal of Structural Integrity,** Emerald, 2017.

RIBEIRO, L. d. R.; BECK, A. T. Structural optimization of a continuous reinforced concrete beam considering risks and progressive collapse. *In*: XLI Ibero-Latin American Congress on Computational Methods and Engineering (XLI CILAMCE), 2020, Foz do Iguaçú, Brazil. **Proceedings of XLI Ibero-Latin American Congress on Computational Methods and Engineering**, Belo Horizonte: ABMEC, 2020.

RIBEIRO, L. d. R.; BECK, A. T. Risk optimization of RC beam under column loss scenario. *In*: XLII Ibero-Latin-American Congress on Computational Methods in Engineering (XLII CILAMCE), 2021, Rio de Janeiro, Brazil. **Proceedings of the joint XLII Ibero-Latin-American Congress on Computational Methods in Engineering and III Pan-American Congress on Computational Mechanics**, Belo Horizonte: ABMEC, 2021. v. 1.

RIBEIRO, L. d. R.; BECK, A. T.; PARISI, F. Risk optimization of a RC frame under column loss scenario. *In*: XLIII Ibero-Latin-American Congress on Computational Methods in Engineering (CILAMCE 2022), 2022, Foz do Iguaçu, Brazil. **Proceedings of the XLIII Ibero-Latin-American Congress on Computational Methods in Engineering**. Belo Horizonte: ABMEC, 2022. v. 1.

RIBEIRO, L. d. R.; BECK, A. T.; PARISI, F. Comparison of the optimal risk-based design of planar RC frames with different aspect-ratios under progressive collapse. *In*: 9th European Congress on Computational Methods in Applied Sciences and Engineering (ECCOMAS 2024), 2024, Lisbon, Portugal. **Proceedings of the 9th European Congress on Computational Methods in Applied Sciences and Engineering**. Barcelona: CIMNE Congress Bureau, 2024.

RIBEIRO, L. d. R.; KROETZ, H. M.; PARISI, F.; BECK, A. T. Optimal risk-based design of a RC frame under different column loss scenarios. *In*: XLIV Ibero-Latin American Congress on Computational Methods in Engineering (CILAMCE 2023), 2023, Porto, Portugal. **Proceedings of the XLIV Ibero-Latin American Congress on Computational Methods in Engineering**. Belo Horizonte: ABMEC, 2023. v. 1.

RIBEIRO, L d R; KROETZ, H M; PARISI, F; BECK, A T. Optimal risk-based design of reinforced concrete beams against progressive collapse. **Engineering Structures**, Elsevier, v. 300, p. 117158, 2024.

RODRIGUES, I. D; CAVALCANTE, G. H. F; PEREIRA, E. M. V; VIEIRA JÚNIOR, L. C. M; LIEL, A.; SIQUEIRA, G. H. Seismic fragility assessment of a RC frame considering concentrated and distributed plasticity modelling. **Revista Ibracon de Estruturas e Materiais**, SciELO, v. 17, p. e15110, 2024.

SAAD, L.; AISSANI A.; CHATEAUNEUF A.; RAPHAEL W. Reliability-based optimization of direct and indirect LCC of RC bridge elements under coupled fatigue-corrosion deterioration processes. **Engineering Failure Analysis,** Elsevier, v. 59, p. 570–587, 2016.

SALMASI, A.; SHEIDAII, M. R.; TARIVERDILO, S. Performance of fully restrained welded beam-column connections subjected to column loss. **International Journal of Steel Structures,** Springer, v. 21, p. 1370–1382, 2021.

SAGIROGLU, S. **Analytical and experimental evaluation of progressive collapse resistance of reinforced concrete structures**. 2012. 433 p. Thesis (PhD in Structural Engineering) – Northeastern University, Boston, Massachusetts, USA, 2012.

SANTIAGO, W. C. **Calibração baseada em confiabilidade dos coeficientes parciais de segurança das principais normas brasileiras de projeto estrutural**. 2019. 181 p. Thesis (PhD in Civil Engineering) – São Carlos School of Engineering, University of São Paulo, São Carlos, 2019. Available in: https://teses.usp.br. Access in: 14 aug. 2024.

SANTIAGO, W. C. et al. Reliability-based calibration of main Brazilian structural design codes. **Latin American Journal of Solids and Structures**, SciELO, v. 17, n. 1, p. 1–28, 2020. doi: 10.1590/1679-78255754.

SANTOS, J. B.; SOUZA, R. M.; MELO, G. S. S. A.; GOMES, R. B. Punching Resistance of Flat Slabs with Openings Adjacent to the Columns. **ACI Structural Journal**, Farmington Hills, v. 119, p. 41-52, 2022.

SARTI, F.; PALERMO, A.; PAMPANIN, S. Fuse-type external replaceable dissipaters: Experimental program and numerical modeling. **Journal of Structural Engineering,** ASCE, v. 142, n. 12, p. 04016134, 2016.

SASANI, M.; BAZAN, M.; SAGIROGLU, S. Experimental and analytical progressive collapse evaluation of actual reinforced concrete structure. **ACI Structural Journal**, Farmington Hills, v. 104, n. 6, p. 731–739, 2007.

SCALVENZI, M; GARGIULO, S; FREDDI, F; PARISI, F. Impact of seismic retrofitting on progressive collapse resistance of RC frame structures. **Engineering Failure Analysis**, Elsevier, v. 131, p. 105840, 2022.

SCALVENZI, M; RAVASINI, S; BRUNESI, E; PARISI, F. Progressive collapse fragility of substandard and earthquake-resistant precast RC buildings. **Engineering Structures**, Elsevier, v. 275, p. 115242, 2023.

SCHELLHAMMER, J.; DELATTE, N.; BOSELA, P. A.; Another Look at the Collapse of Skyline Plaza at Bailey's Crossroads, Virginia. **Journal of Performance of Constructed Facilities**, ASCE, v. 27, n. 3, p. 354-361, 2013.

SHAN, S.; LI, S. Progressive collapse mechanisms of post-tensioned reinforced concrete frames considering effect of infill walls. **Engineering Structures**, Elsevier, v. 250, p. 113451, 2022.

SHAN, L.; PETRONE, F.; KUNNATH, S. Robustness of RC buildings to progressive collapse: Influence of building height. **Engineering Structures**, Elsevier, v. 183, p. 690–701, 2019.

SHEIKHOLESLAMI, R.; RAZAVI, S. Progressive Latin Hypercube Sampling: An efficient approach for robust sampling-based analysis of environmental models. **Environmental Modelling & Software**, Elsevier, v. 93, p. 109-126, 2017.

SHI, Y.; STEWART, M. G. Spatial reliability analysis of explosive blast load damage to reinforced concrete columns, **Structural Safety**, Elsevier, v. 53, p. 13–25, 2015.

SIMO, J. C.; HJELMSTAD, K. D.; TAYLOR, R. L. Numerical formulation of elasto-viscoplastic response of beams accounting for the effect of shear. **Computer methods in applied mechanics and engineering**, Elsevier, v.42, p.301-330, 1984.

SINGHAL, A.; KIREMIDJIAN, A.S. Method for Probabilistic Evaluation of Seismic Structural Damage, **Journal of Structural Engineering**, ASCE, v. 122, n. 12, p. 1459-1467, 1996.

SIQUEIRA, G. H.; SANDA, A. S.; PAULTRE, P.; PADGETT, J. E. Fragility curves for isolated bridges in eastern Canada using experimental results. **Engineering Structures**, Elsevier, v. 74, p. 311-324, 2014.

SIQUEIRA, G. H.; TAVARES, D. H. ; PAULTRE, P. Seismic fragility of a highway bridge in Quebec retrofitted with natural rubber isolators. **Revista IBRACON de Estruturas e Materiais**, SciELO, v. 7, p. 534-547, 2014.

SOSSO, B.; ANDRADE, S. S.; VIEIRA JR., L. C. M.; BERKE, P. Z. Probabilistic modelling of the robustness of reinforced concrete frames accounting for material property variability using a layered beam finite element approach. **Engineering Failure Analysis**, Elsevier, v. 118, p. 104789, 2020.

SOUZA, E. G. **Colapso de edifício por ruptura das estacas**: estudo das causas e da recuperação. 2003. 115 p. Dissertation (Master's in Civil Engineering) – São Carlos School of Engineering, University of São Paulo, São Carlos, 2003.

STAROSSEK, U. Typology of progressive collapse. **Engineering Structures**, Elsevier, v. 29, n. 9, p. 2302–2307, 2007.

STAROSSEK, U. **Progressive collapse of structures**. 2nd ed. ICE Publishing; 2017.

STAROSSEK, U.; HABERLAND, M. Disproportionate collapse: Terminology and procedures. **Journal of Performance of Constructed Facilities**, ASCE, v. 24, n. 6, p. 519–528, 2010.

STEWART, M. G. Risk of progressive collapse of buildings from terrorist attacks: are the benefits of protection worth the cost? **Journal of Performance of Constructed Facilities**, ASCE, v. 31, n. 2, p. 04016093, 2017.

STEWART, M.G., MELCHERS, R.E. **Probabilistic risk assessment of engineering systems**. London: Chapman & Hall; 1997.

SUN, R.; HUANG, Z.; BURGESS, I. W. The collapse behaviour of braced steel frames exposed to fire. **Journal of Constructional Steel Research,** Elsevier, v. 72, p. 130–142, 2012.

SU, Y.; TIAN, Y.; SONG, X. Progressive collapse resistance of axially-restrained frame beams. **ACI Structural Journal**, Farmington Hills, v. 106, n. 5, p. 600, 2009.

TANG, B. Orthogonal Array-Based Latin Hypercubes. **Journal of the American Statistical Association**, Taylor & Francis, v. 88, n. 424, p. 1392–1397, 1993.

TAVAKOLI, H. R.; HASANI, A. H. Effect of earthquake characteristics on seismic progressive collapse potential in steel moment resisting frame. **Earthquake Engineering & Structural Dynamics,** Wiley, v. 12, n. 4, p. 529–541, 2017.

THAI, D.-K.; PHAM, T.-H.; NGUYEN, D.-L. Damage assessment of reinforced concrete columns retrofitted by steel jacket under blast loading. **The Structural Design of Tall and Special Buildings**, Wiley, v. 29, n. 1, p. e1676, 2020.

TU, J.; CHOI K. K.; PARK Y. H. A New Study on Reliability-Based Design Optimization. **Journal of Mechanical Design**, ASME, v. 121, n. 4, p. 557–564, 1999.

USMANI, A. S.; CHUNG, Y.; TORERO, J. L. How did the WTC towers collapse: a new theory. **Fire Safety Journal**, Elsevier, v. 38, n. 6, p. 501–533, 2003.

USMANI, A.; JIANG, Y.; JIANG, J.; JIANG, L.; WELCH. S. Adapting OpenSees to simulate bridge structures in fire. In: International Conference on Bridge Maintenance, Safety and Management (IABMAS 2012), Stresa, Italy, 2012. **Proceedings of the Sixth International Conference on Bridge Maintenance, Safety and Management**, p. 1580-1584, 2012.

USMANI, A. S; ZHANG, J.; JIANG, J.; JIANG, Y.; KOTSOVINOS, P.; ZHANG, J.; MAY, I. Using OpenSees for structures in fire. *In*: International Conference on Structures in Fire, SiF'10, East Lensing, USA, 2010. **Proceedings of the 6th International Conference on Structures in Fire – SiF'10**, p. 919-926, 2010.

VAPPER, M.; LASN, K. Blast protection of concrete columns with thin strips of GFRP overlay. **Structures**, Elsevier, v. 25, p. 491–499, 2020.

VATANI OSKOUEI, A.; KIAKOJOURI, F. Non-linear dynamic analysis of steel hollow I-core sandwich panel under air blast loading. **Civil Engineering Infrastructures Journal**, University of Tehran, v. 48, n. 2, p. 323–344, 2015.

VROUWENVELDER, T. Treatment of risk and reliability in the Eurocodes. **Proceedings of the Institution of Civil Engineers: Structures and Buildings**, Elsevier, v. 161, n. 4, p. 209-214, 2008. ISSN 0965-0911. E-ISSN 1751-7702. doi: 10.1680/stbu.2008.161.4.209.
WANG, Y.; ZHANG, R.; LIU, S.; ZHAI, X.; ZHI, X. Energy absorption behaviour of an aluminium foam-filled circular-triangular nested tube energy absorber under impact loading. **Structures**, Elsevier, v. 34, p. 95–104, 2021.

WEN, Y.; KANG, Y. Minimum building life-cycle cost design criteria ii: Applications. **Journal of Structural Engineering**, ASCE, v. 127, n. 3, p. 330–337, 2001.

WISNIEWSKI, D.; CRUZ, P. J. S.; HENRIQUES, A. A.; SIMÕES, R. A. D. Probabilistic models for mechanical properties of concrete, reinforcing steel and pre-stressing steel. **Structure and Infrastructure Engineering**, Taylor & Francis, v. 8, n. 2, p. 111–23. doi: 10.1080/15732470903363164.

XU, G. Q.; ELLINGWOOD, B. R. An energy-based partial pushdown analysis procedure for assessment of disproportionate collapse potential. **Journal of Constructional Steel Research**, Elsevier, v. 67, n. 3, p. 547-555, 2011.

XU, S.; LIU, Z.; LI, J.; YANG, Y.; WU, C. Dynamic behaviors of reinforced NSC and UHPC columns protected by aluminum foam layer against low-velocity impact. **Journal of Building Engineering**, Elsevier, v.34, p. 101910, 2021.

XU, G. Q.; ELLINGWOOD, B. R. An energy-based partial pushdown analysis procedure for assessment of disproportionate collapse potential. **Journal of Constructional Steel Research**, Elsevier, v. 67, n. 3, p. 547-555, 2011.

XUE, B.; LE, J. L. Simplified energy-based analysis of collapse risk of reinforced concrete buildings. **Structural Safety**, Elsevier, v. 63, p. 47-58, 2016.

YANG, X. S. **Nature-Inspired Metaheuristic Algorithms**. UK: Luniver Press, 2008.

YANG, L.; SUI, L.; DONG, Y.; LI, X.; ZI, F.; ZHANG, Z. Quasi-static and dynamic behavior of sandwich panels with multilayer gradient lattice cores. **Composite Structures**, Elsevier, v. 255, p. 112970, 2021.

YANG, R.; ZHANG, J. Numerical simulation of various materials for the impact protection of a reinforced concrete slab. **Strength of Materials**, Springer, v. 53, n. 1, p. 145–153, 2021.

YANG, X.-J.; LIN, F.; GU, X.-L. Experimental study on a novel method to improve progressive collapse resistance of RC frames using locally debonded rebars. **Journal of Building Engineering**, Elsevier, v. 41, p. 102428, 2021.

YANKELEVSKY, D. Z.; KARINSKI, Y. S.; BRODSKY, A.; FELDGUN, V. R Evaluation of punching shear design criteria to prevent progressive collapse of RC flat slabs. **International Journal of Protective Structures**, SAGE Journals, v. 12, n. 2, p. 174–205, 2021.

YARLAGADDA, T.; HAJILOO, H.; JIANG, L.; GREEN, M.; USMANI, A. Preliminary modelling of Plasco tower collapse. **International Journal of High-Rise Buildings**, KoreaScience, v. 7, n. 4, p. 397–408, 2018. doi: 10.21022/IJHRB.2018.7.4.397.

YE, K. Q. Orthogonal Column Latin Hypercubes and Their Application in Computer Experiments. **Journal of the American Statistical Association**, Taylor & Francis, v. 93, n. 444, p. 1430–1439, 1998.

YI, W.-J.; HE, Q.-F.; XIAO, Y.; KUNNATH, S. K. Experimental study on progressive collapse resistant behavior of reinforced concrete frame structures. **ACI Structural Journal**, Farmington Hills, v. 105, n. 4, p. 433-439, 2008.

YOUN, B. D.; CHOI K. K.; PARK Y. H. Hybrid Analysis Method for Reliability-Based Design Optimization. **Journal of Mechanical Design**, ASME, v. 125, p. 221–232, 2003.

YOUPO, S.; YING, T.; XIAOSHENG, S. Progressive collapse resistance of axially restrained frame beams, **ACI Structural Journal**, Farmington Hills, v. 106, n. 5, p. 600-607, 2009.

YU, X. H.; LU, D. G.; QIAN, K.; LI, B. Uncertainty and sensitivity analysis of reinforced concrete frame structures subjected to column loss. **Journal of Performance of Constructed Facilities**, ASCE, v. 31, n. 1, p. 04016069, 2017.

YU, J.; GAN, Y.-P.; JI, J. Behavior and design of reinforced concrete frames retrofitted with steel bracing against progressive collapse. **The Structural Design of Tall and Special Buildings**, Wiley, v. 29, n. 12, p. e1771, 2020.

YU, J.; TAN, K. H. Experimental and numerical investigation on progressive collapse resistance of reinforced concrete beam Column sub-assemblies. **Engineering Structures**, Elsevier, v. 55, p. 90-106, 2013.

YU, J.; TAN, K. H. Structural Behavior of RC Beam-Column Subassemblages under a Middle Column Removal Scenario. **Journal of Structural Engineering**, ASCE, v. 139, n. 2, p. 233-250, 2013.

YUAN-BIN, M. O.; YAN-ZHUI, M. A.; QIAO-YAN, Z. Optimal choice of parameters for firefly algorithm. **Proceedings of Fourth International Conference of Digital Manufacturing & Automation**, 2013. doi: 10.1109/ICDMA.2013.210.

ZAHRAI, S. M.; EZODDIN, A. Cap truss and steel strut to resist progressive collapse in RC frame structures. **Steel and Composite Structures**, Techno Press, v. 26, n. 5, p. 635–47, 2018.

ZHANG, Y.; DER KIUREGHIAN, A. **Finite element reliability methods for inelastic structures**. Report UCB/SEMM-97/05. Department of Civil and Environmental Engineering, University of California, Berkeley, 1997.

ZHOU, Y.; YANG, J.; WANG, Z.; HWANG, H.-J.; HUANG, Y.; DENG, L. Static load test on the progressive collapse resistance of precast concrete frame substructure during and after high temperature. **Journal of Structural Engineering**, ASCE, v. 147, n. 8, p. 04021110, 2021.

ZHOU, Q.; YU, T. Use of high-efficiency energy absorbing device to arrest progressive collapse of tall building. **Journal of Engineering Mechanics**, ASCE, v. 130, n. 10, p. 1177–1187, 2004.


PPG
SET


EESC • USP